TURBULENT MIXING OF GAS STREAMS

A theoretical and experimental investigation of the effects of free-stream turbulence on the development of plane mixing layers

by

S. J. Peerless

A thesis submitted for the degree
of Doctor of Philosophy
in the Faculty of Engineering
of the University of London

Department of Mechanical Engineering
Imperial College

February, 1971

ABSTRACT

The turbulence level in two parallel streams of fluid has been shown to have a marked effect on the development of the plane mixing layer between them; the effect has been investigated both experimentally and theoretically.

In the experiments, an increase in the free-stream turbulence intensity was found to produce an increase of roughly the same size right through the layer; in addition, the rate of growth of the layer increased. The increase was proportionately greater as the ratio of the stream velocities approached unity.

The Patankar-Spalding finite-difference method has been used to solve the governing differential equations. The computations have been carried out using several different ways of relating turbulent shear stress to local flow conditions - the Prandtl mixing-length hypothesis, two different extensions of that hypothesis, and a version of the Kolmogorov model of turbulence.

The predictions based on the unmodified mixing-length hypothesis differed widely from the experimental results, confirming expectations of its inadequacy for representing flow phenomena of this type.

Both modifications of the mixing-length shear law improved the agreement between predicted and observed flows, but at the expense of increased empiricism, in the form of either one or two experimentally-determined constants.

The Kolmogorov model in the form used was found to predict qualitatively the effect of free stream turbulence and to give reasonably close agreement with the measurements, but further development leading to increased accuracy appears possible in this case.

PREFACE

The work which forms the basis for this thesis was originally envisaged as a comparatively small part of a more general ingestigation of mixing layer flows, initiated by myself in 1965. This in turn was an offshoot from a mainly theoretical investigation of film cooling which had for several years been carried out as a joint enterprise by the Ministry of Technology and Imperial College. In the early stages it was assumed that the effect of free-stream turbulence on mixing-layer development would be fairly small, but that, in any case, in view of the theoretical difficulties, any attempt to incorporate it into flow predictions would necessarily have a mainly empirical basis.

Fortunately, by the time that the experimental work was beginning to show the full importance of the stream turbulence effect, the Patankar-Spalding method appeared on the scene. It brought a considerable degree of freedom to carry out numerical experiments by computer as part of a search for improved models of turbulent motion. It was therefore decided, in the autumn of 1966, to devote a considerable part of the whole research effort to a combined theoretical and experimental investigation of the effect for uniform density, plane mixing layer flows.

The initial aim was to find conceptually simple extensions of the Prandtl mixing-length hypothesis which would provide reasonable agreement with the experimental results, particularly for the spreading rate of the mixing layer.

By the time that this objective had been achieved, considerable development of more sophisticated models of turbulence had taken place, and several were available "off the shelf" for incorporation into the finite-difference programme. Although the experimental work had been designed specifically for comparison with mixing-length predictions, it was decided to extend the investigation to one of the new models. Kolmogorov's was chosen because it was, historically, the first of the new wave, and because it appeared to have received less attention than the others.

In carrying out this work I have received help and support from many sources, and wish to make grateful acknowledgement for it:

To Dr. S.V. Patankar, and Professor D.B. Spalding, without whose achievement this present work could hardly have been done at all. To Professor Spalding, again, for acting as my supervisor, and in particular, for his usual rigorous but helpful correction of the drafts of this thesis.

To that excellent technician, Mr. Oscar Vis, for constructing and commissioning complicated apparatus with patience and skill.

To Mr. (now Dr.) S.C. Kacker, for undertaking the frequency-spectrum measurements reported in section 5.9.

To Mr. F.A. Bell for his help in installing the heavier parts of the experimental equipment.

To Mr. P. Dale, for patient guidance in my early attempts at computing.

To the Ministry of Technology (now Aviation Supply) for providing the necessary funds to support this research, and to their technical representative, Dr. M.G. Hall, of the Royal Aircraft Establishment, for his interest in the work.

To Miss Tessa Reveley for her quick and skilful typing.

S. J. Peerless

Dept. of Mechanical Engineering
Imperial College,
London, S.W.7

CONTENTS

Page

ABSTRACT 2

PREFACE 4

1. INTRODUCTION

1.1 The purpose and scope of the present work 12

1.2 Some general aspects of the theoretical problem 15

1.3 Related published work 20

1.4 Presentation of material in this thesis 25

Figure 1.1 facing 12

" 1.2 " 19

" 1.3 " 22

2. THE TURBULENCE MODELS

2.1 General descriptions of the models 28

2.2 Modification of the mixing-length hypothesis 30

2.3 Other features of the modified mixing-length predictions 34

2.4 The k-z model 36

2.5 Boundary conditions for the k-z model 39

2.6 The relationship between the k-z and mixing-length models 41

Figure 2.1 facing 33

3. ANALYTICAL ASPECTS OF THE SOLUTION PROCEDURE

3.1 Introduction 44

3.2 The analytical basis of the finite-difference method 46

3.3 Determination of the slip coefficients 51

3.4 Calculation of entrainment rate 53

Figure 3.1 facing 46

" 3.2 " 49

" 3.3 " 49

4. THE FINITE-DIFFERENCE PREDICTIONS

4.1 Introduction 56

4.2 Adaptation of the basic programmes 58

4.3 Results of the asymptotic mixing-length solutions 60

4.4 Comparison with the exact analytical solutions 64

4.5 More realistic mixing-length predictions 66

4.6 The idealised k-z calculations 67

4.7 The effects of varying the constants 71

4.8 Strategy for determining the k-z constants 78

4.9 Predictions of the total flow 80

Table 4.1 facing 63

" 4.2 " 64

" 4.3 " 66

" 4.4 " 74

" 4.5 " 75

" 4.6, 4.7 " 76

" 4.8 " 77

" 4.9 " 78

Figure 4.7 " 69

" 4.9 " 71

" 4.14 " 81

5. EXPERIMENTAL WORK

5.1 General description of the wind-tunnel 84

5.2 The working section and traversing gear 85

5.3 The method for increasing free-stream turbulence 91

5.4 Instrumentation 93

5.5 Scope of experimental results 94

5.6 The effect of stream turbulence on spreading rate 97

5.7 The turbulence-intensity and velocity profiles 98

5.8 Free-stream energy-frequency spectra 100

5.9 Conditions in the working section 103

5.10 The choice of working-section dimensions and limitation of the velocity ratio 108

Table 5.1 facing 96

" 5.2 " 100

" 5.3 " 106

Figure 5.1 " 84

" 5.2 " 86

" 5.3 " 88

" 5.4 " 90

" 5.5 " 91

" 5.6 " 93

" 5.23 " 103

6. COMPARISON OF EXPERIMENTAL RESULTS AND PREDICTIONS

6.1 Introduction 111

6.2 Comparison with the mixing-length predictions: spreading rate 115

6.3 Comparison with the mixing-length predictions: velocity and turbulence-intensity profiles 120

6.4 The k-z predictions with uniform Pr_{eff} 121

6.5 Variation of the effective Prandtl numbers 124

6.6 The effect of varying C_μ and C_D 125

6.7 Further changes in the coefficients 127

Table 6.1 facing 118

" 6.2 " 120

" 6.3 " 123

" 6.4 " 127

" 6.5 " 130

Figure 6.2 " 115

7. CONCLUDING DISCUSSION

7.1 Introduction 131

7.2 The physical situation 131

7.3 The mixing-length model 134

7.4 The k-z model 136

7.5 Suggestions for future work 139

8. STATEMENT OF PRINCIPAL CONCLUSIONS 142

REFERENCES 145

PRINCIPAL NOTATION 148

GRAPHS OF RESULTS 152-190

APPENDIX A: Some details of the finite-difference solution programmes 194

Programme listings: NEWMOD 214
NEWMOD-F (MAIN section) 225
LAYER 229
LAYER-3 (" ") 246

APPENDIX B: The Tollmien-Kuethe solutions 257

APPENDIX C: Experimental data processing 269

APPENDIX D: Copy of reference 2 278

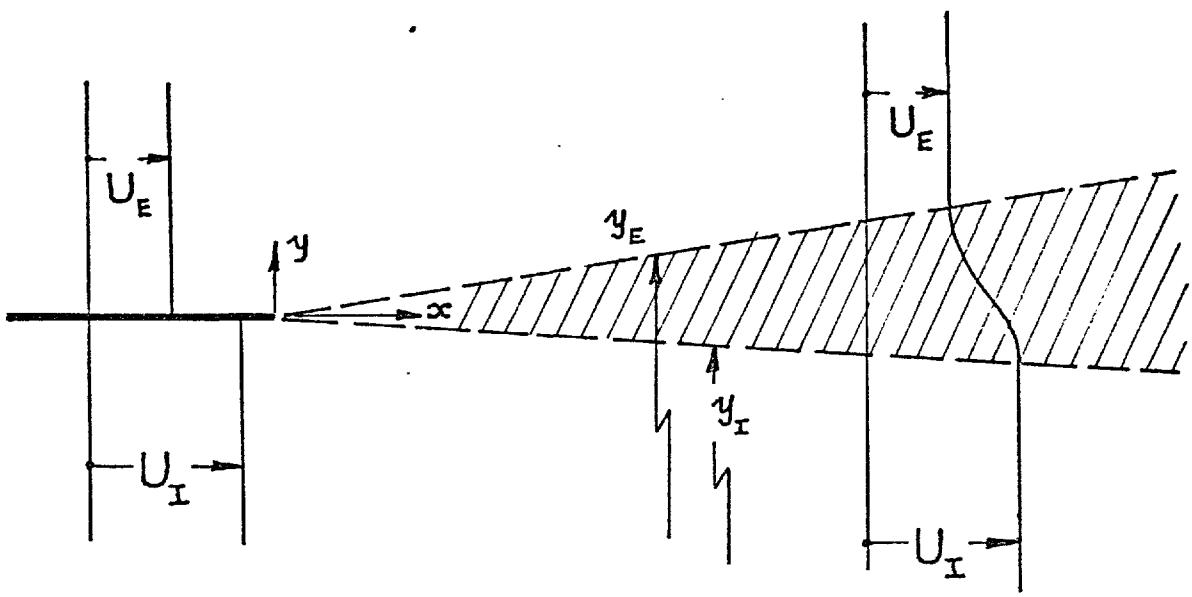


Figure 1.1

General diagram for plane mixing-layer flow.

1. INTRODUCTION

1.1 The purpose and scope of the present work.

The investigation herein reported is centred on the flow situation illustrated in figure 1.1 - the plane, uniform-density, turbulent mixing layer between nominally parallel and uniform streams of a single fluid.

It has seemed probable for a considerable time that the behaviour of such flows is affected to a significant extent by the levels of turbulence in the adjacent free streams. This tentative conclusion is supported by the unexplained differences which exist between mixing-layer measurements from various sources (of which some examples are presented in the literature survey in section 1.3); however, until very recently, only indirect experimental evidence was available, and existing theoretical methods were unable to predict such an effect.

The principal objects of the present investigation were, therefore:-

a) To establish experimentally the importance of free-stream turbulence as a factor influencing the development of plane mixing layers, and to obtain quantitative results within reasonable ranges of the stream velocity ratio U_E/U_I, and of the turbulence intensities in the free streams.

b) To search for simple analytical models of turbulent motion which would enable predictions to be made with an accuracy appropriate to engineering applications.

The experiments were carried out with low-speed streams of air at atmospheric pressure and temperature. For practical reasons (which are explained in section 5.10) the velocity ratio was restricted to the range 0.4 to about 0.8. A system of oscillating grids was designed for the purpose of agitating the air streams; these produced relative turbulence intensities up to about 10%. Without them the turbulence intensity was less than 1%.

Examination of the measurements taken by a pitot tube and a single hot wire anemometer traversed across the air stream showed that the grids caused large increases in the rate of spread of the mixing layer for all velocity ratios in the range of the tests; in addition, they raised the level of turbulence right through the layer.

The first phase of the theoretical investigation was based on the Prandtl mixing-length hypothesis (reference 1). This is inherently incapable of predicting any effect produced by change of free-stream turbulence, but it was hoped that an analytically simple modification of the basic hypothesis could be found which would achieve

the desired result. Two such extensions were formulated, one containing a single new empirical constant, and the other, two such constants. Numerical predictions of mixing layer flow were made for comparison with the experimental results so that the best values of these constants could be obtained. Predictions based on the original Prandtl shear law were also carried out, to provide a basis for comparison.

It was found that both of the modified versions could give considerably closer agreement with experiment than the simple mixing-length hypothesis. In particular, the version with two extra constants produced satisfactory predictions not only of the growth rates for high and low free-stream turbulence, but also of the turbulence intensity distributions within the layer.

Further predictions were then made using a version of the turbulence model proposed by Kolmogorov (reference 2), in which the turbulent component of effective viscosity is related to the local values of k, the kinetic energy of the fluctuating part of the motion, and z, a characteristic frequency. For convenience it will be referred to here as the 'k-z' model.

By virtue of its greater complexity, such a model is inherently capable of describing the flow in greater detail than the simpler ones previously used. However, its accuracy was rather less than that achieved with the best of the mixing-length variants. The investigation

was concluded with a limited attempt to determine the most promising lines for further development of the Kolmogorov model.

All the flow predictions were carried out by the Patankar-Spalding finite-difference method for the solution of the boundary-layer equations (references 3 and 4).

1.2 Some general aspects of the theoretical problem.

From the foregoing description of the present investigation it will be apparent that it is concerned mainly with the time-mean component of the flow; the fluctuating component is considered only to the extent required to provide information for solving the equations describing the time-mean flow. The primary concern, for uniform-density fluid, is the solution of the familiar momentum equation for boundary-layer flow:-

$$U\frac{\partial U}{\partial x} + V\frac{\partial U}{\partial y} = \frac{1}{\rho}\frac{\partial \tau}{\partial y} \qquad (1.2\text{-}1)$$

where U and V are the time-mean velocity components in the x and y directions, ρ is the fluid density, and τ is the local shear stress (acting in the x direction on a plane of constant y).

The shear stress, τ, is taken to be related to the local transverse velocity gradient by the usual law of Newtonian form:

$$\tau = \mu_{eff} \frac{\partial U}{\partial y} \qquad (1.2\text{-}2)$$

ant it is in the means for connecting the effective viscosity, μ_{eff}, to the local flow conditions that the differences between the various models of turbulence arise.

It is assumed, as is usual in analysis of free turbulent flows, that the contribution to μ_{eff} from the fluctuating part of the motion is much larger than the laminar component, which can then be neglected.

An important point which arises in the theoretical predictions of flows with free boundaries concerns the behaviour of the effective viscosity at these boundaries and the extent of the field covered by the solution. It can conveniently be illustrated by reference to the two most widely used expressions for effective viscosity:-

1. The Prandtl mixing-length hypothesis

$$\mu_{eff} = \rho l^2 \frac{\partial U}{\partial y} \qquad (1.2\text{-}3)$$

in which the mixing-length, l, is usually taken as proportional to the width of the layer, thus

$$\ell = (y_E - y_I) \qquad (1.2\text{-}4)$$

or to some other representative transverse dimension y_{nom}, say.

2. The constant-effective viscosity hypothesis

$$\mu_{eff} = \text{constant} \times \rho y_{nom}(U_E - U_I) \ , \qquad (1.2\text{-}5)$$

also originated by Prandtl.

For the present purpose the most important difference between these two hypotheses lies in the width of the fields of the solutions that they produce. Solutions based on the mixing-length hypothesis yield mixing layers of finite width, and at each boundary the values of $\frac{\partial U}{\partial y}$ and μ_{eff} are zero. In solutions obtained with the second expression the free-stream velocity is approached asymptotically on either side of the layer, and the boundaries y_E and y_I are at $\pm\infty$. At first sight this might seem to imply a serious limitation on the kinds of effective viscosity formulation that can be used in finite-difference solutions, which necessarily involve grids of finite width, and to require that μ_{eff} be zero at each grid boundary. Fortunately this is not so, and any effective-viscosity hypothesis likely to be of practical interest can be incorporated in the solution; by appropriate control of the grid width the essential part of the velocity profile can be predicted to any desired degree of accuracy.

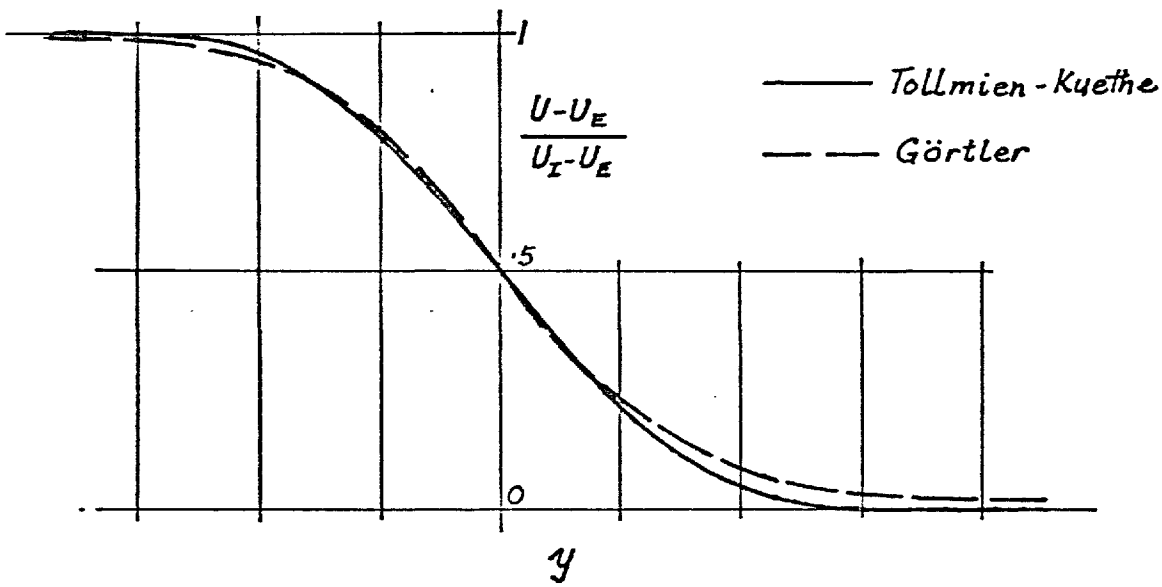


Figure 1.2

Comparison of the standard exact solutions.

It is, in fact, necessary to use a finite-difference method for investigations of the present kind because of the freedom which such methods give in the choice of shear law and of boundary conditions.

Since the mixing-length model forms one of the starting points for the search for a better one, it is of interest to note some of the main features of solutions which it yields for mixing-layer flow at uniform density and pressure. A solution was first obtained by Tollmien (reference 5), for $U_E/U_I = 0$, and later extended to other velocity ratios by Kuethe (reference 6). Tollmien devised a transformation which allowed the partial differential equation (1.2-1) to be reduced to an ordinary differential equation. The solution describes a wedge-shaped flow field in which all surfaces of constant U/U_I are planes passing through the apex of the wedge, and in which the velocity profiles at all values of x have the same shape. The analytical details of the Tollmien-Kuethe solution are presented in appendix B.

An analytical solution for the same flow conditions, but using the constant-effective-viscosity hypothesis, was obtained by Gortler (reference 7). The velocity profiles predicted by the two different shear laws are compared in figure 1.2. The rounding of the Gortler profile, which is the result of the higher effective viscosity at the edges of the layer, can easily be seen.

1.3 Related published work.

The whole class of free turbulent flows - mixing layer, jets, and wakes - has attracted a good deal of attention from both applied mathematicians and experimentalists. Apart from their intrinsic importance the attraction of such flows follows from their basic simplicity, since the absence of solid surfaces provides situations in which molecular transport processes can be ignored, and "pure" turbulent motion studied in isolation.

Nevertheless, very little published work has been concerned directly with the topic of the present investigation. No theoretical predictions of the influence of external turbulence on free turbulent flows appear in the literature; until very recently no way round the analytical difficulties had been found.

On the experimental side, only two attempts to examine the turbulence effect have been reported. Using apparatus in the form of a simple air-to-air injector, Curtet and Ricou (reference 8) carried out two series of measurements, with approximately 1% and 5% turbulence in the secondary air stream at entry to the mixing section. They found that the increase in the initial turbulence level brought about a significant increase in the rate of spread of the primary air stream, and a marked increase in the general level of turbulence in the mixing zone. In a much more recent series of

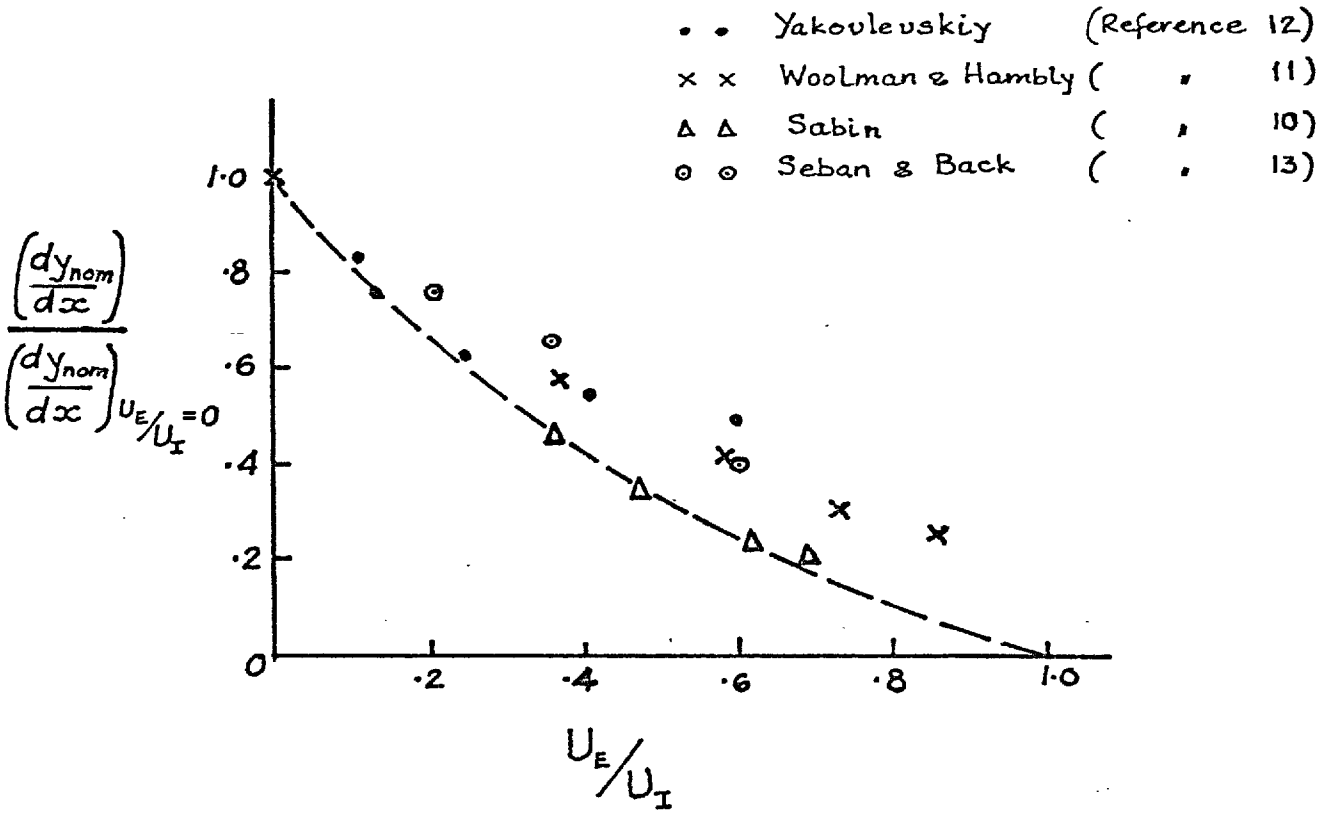


Figure 1.3

Typical experimental results for plane mixing layers.

measurements, Patel (reference 9) found that an increase of 30% in the spreading rate of the plane mixing layer between a moving air stream and a stationary atmosphere was caused by a change in the turbulence level of the moving stream from 0.6% to 1.4%.

An interesting comparison can be made between the experimental results of Sabin (reference 10), Woolman (reference 11), Yakovlevskiy (reference 12), and Seban and Back (reference 13), although none of them was consciously concerned with the effects of free-stream turbulence, and indeed no turbulence measurements were reported by them. Their results are presented in figure 1.3, in the form of graphs showing how the spreading rate of the plane mixing layer varies with the ratio of free-stream velocities (U_E/U_I in present notation); to eliminate differences of presentation, the ordinates are normalised by dividing by the spreading rate for zero velocity ratio. Also shown in this figure, are the predicted spreading rates based on the Prandtl mixing-length hypothesis.

Setting aside the unlikely possibility that the difference shown by this figure are the result of experimental error alone, we see that the Prandtl shear law provides a good model of the flow in Sabin's case, but not for the other two. Commenting on these results, the present author (reference 14) pointed out that as Sabin's work was performed in an open water channel, it

was likely that the stream turbulence levels were low; on the other hand Woolman's measurements were carried out on the discharge side of two air supply fans, and as no attempt was made to reduce the turbulence levels, it is likely that these were fairly high. Abramovich (reference 15) commenting on Yakovlevskiy's results, implicitly drew the same inference in this case also, but supposed the level of free-stream turbulence to be significant only if it exceeds the level within the mixing layer.

The remainder of the literature pertaining to turbulent mixing layers lies largely outside the scope of the present investigation. Various solutions extending the work of Tollmien, Kuethe and Gortler to more general flow conditions (compressibility, streamwise pressure gradient, non-uniform temperature, etc.) have been obtained. A good deal of experimental work has been carried out in parallel with these solutions, but most of it has been confined to the zero-velocity-ratio case.

The general situation can be conveniently studied in the review papers of Halleen (reference 16) and Sforza et al. (reference 17). The first of these was written in 1964; Halleen's graph for non-zero velocity ratio contains only the data of Sabin (reference 10), and of Seban and Back (reference 10) already referred to, which is included in figure 1.3 of this thesis. For $U_E/U_I = 0$, values of spreading rates differing by over 20% are

quoted from various sources, including Liepmann and Laufer (reference 18) who appear to have been the first to design apparatus specifically for plane mixing-layer measurements.

Several years later Sforza was able to comment, with considerable justification that "In spite of the fervor and industry with which this class of flow fields has been investigated over the past forty-odd years, its mystery appears curiously undiluted". The publication of other experimental and analytical studies, for example by Baker (reference 19) and Watt (reference 20) has not significantly improved the situation.

Quite recently the availability of rapid digital computers has led to the development of finite-difference methods for the numerical solution of differential equations. The consequent relaxation of the previous analytical constraints has given a considerable impluse to the search for new and more accurately descriptive models of turbulent motion. Two examples of work in this category are the papers by Lee and Harsha (reference 21) and Rodi and Spalding (reference 22). In the first of these, the turbulent shear stress is related to the local turbulence kinetic energy, k; in the second, it is also related to a dimension characterising the local scale of the turbulence. Reference 22 includes a discussion of a number of different models of turbulence which can now be used because of the freedom conferred by numerical solution procedures.

1.4 Presentation of material in this thesis.

The turbulence models and the experimental observations are the main components of the present investigation; the ultimate goal is the comparison of the experimental results with predictions based on the different models, and the conclusions that follow from that comparison.

The characters of the models are established in chapter 2; section 2 of that chapter shows the two extensions of the simple Prandtl mixing-length expression for effective viscosity by which it is proposed to account for the effect of free-stream turbulence on mixing-layer development. The differential equations for k and z are presented in section 2.4, together with the shear law relating these quantities to the effective viscosity; the following section examines the boundary conditions required to satisfy the k and z equations. The final section of the chapter shows how, in some circumstances, the basic mixing-length hypothesis and the k-z model can be related to one another.

Chapter 3 is concerned with some analytical aspects of the method used for solving the differential equations, including a brief general description of its operation, and details of the treatment of free boundaries.

Chapter 4 describes the adaptation of the computer programmes of references 3 and 4 to the present problem. This adaptation has been carried out in two stages.

Initially, flow predictions were made for idealised mixing-layers in order to obtain clear ideas about the character of each turbulence model, and to ensure correct operation of the programmes - in particular, to check the accuracy of the solution procedure. The results of these predictions are presented and discussed. The second stage of calculation required further development of the programmes to obtain more realistic predictions which could be compared directly with the experimental results. These developments are described in chapter 4 but the comparison itself is deferred until chapter 6.

The intervening chapter deals with the experimental work. Descriptions of the apparatus and measurements are followed, in sections 5.5 to 5.7, by a presentation of the experimental results.

Section 5.9 is a detailed discussion of the actual flow conditions in the measurement section of the apparatus; this section, and section 6.1, between them constitute an examination of the extent to which comparison of theoretical and experimental results is valid. The remainder of chapter 6 covers the actual comparison. The main purpose here is to discover how well the predictions can be made to match the experimental observations, by appropriate choice of the numerical coefficients contained in the models. In the case of the k-z model, the possibility of improving the agreement with experiment by further refinement of the model is considered.

Chapter 6 is thus the culmination of the thesis; it is followed by a short concluding chapter which rounds off the present work and makes suggestions for further developments in the same field.

Details of the computational side of the work are contained in the appendices. These include, in addition to the most important points of the main finite-difference programmes, the extra programmes written to process the experimental observations, and to recalculate the Tollmien-Kuethe mixing-layer solutions.

The main parts of the work are thus seen to be contained in chapter 2, the second half of chapter 5, and chapter 6. The intervening sections, and the appendices, are concerned with the supporting material. On the first reading, the reader should find that, by passing from section 2.5 to section 5.5, he will be able to extract the essence of the work with the minimum effort.

Tables of values are contained in the body of the text at the point of first reference. Explanatory diagrams, and photographs of experimental apparatus are also inserted in the text, where they most conveniently support its development.

Graphs of experimental and predicted results are arranged in a block at the end of the main text, and thus provide a collected graphical display of the products of the investigation.

2. THE TURBULENCE MODELS

2.1 General descriptions of the models.

The Boussinesq concept of effective viscosity in turbulent flow, embodied in equation 1.2-2, is incorporated in both of the turbulence models used in the present work. Also, following the usual practice, the effective viscosity is equated directly to its turbulence component, ignoring the contribution to the shear stress which is produced by molecular diffusion.

The mixing-length hypothesis. The way in which the simple mixing-length hypothesis models turbulent motion by supposing that the intermolecular exchanges, envisaged in the kinetic theory of gaseous behaviour, are repeated on a macroscopic scale, is now well known, and the resulting effective-viscosity expression, equation 1.2-3, is well established. The shear laws used here are extensions of the basic law; in each one an addition is made to the mixing-length effective viscosity. The extra term is proportional to the relative turbulence intensity in the free streams outside the mixing layer. Thus, in effect, free-stream turbulence is assumed to increase the mixing length, whose value may now vary with transverse position, instead of being independent of y as in the basic hypothesis.

These modifications of the mixing-length model are presented in section 2.2.

The Kolmogorov model. Kolmogorov recognised that in turbulent motion the scale of the fluctuations covers a wide range. The size of the largest eddies is represented by the mixing-length; the scale of the smallest ones (the "internal scale", or "microscale") is such that the moleular viscosity of the fluid is effective in dissipating the kinetic energy of the eddies. He argued that the character of the motion is largely determined by the internal scale and the corresponding rate of dissipation. By assuming that at this end of the size range all turbulence is effectively homogeneous and isotropic, Kolmogorov was able to make use of detailed analyses of such motion carried out by Taylor, von Karman, and others. The analysis is outside the scope of the present work, but a detailed treatment is given by Hinze (chapter 3 of reference 23). The set of three differential equations derived by Kolmogorov is displayed in reference 2, which is reproduced, for convenience, as appendix D; the dependent variables in these equations are, respectively, the time-mean velocity, the turbulence kinetic energy, and a "characteristic frequency"; they apply to all uniform-density turbulent flows. After being reduced to the parabolic form appropriate to steady flow of boundary-layer type, these equations can be solved by the finite-difference method of references 3 and 4.

Before proceeding to examine these differential equations in detail (in section 2.4) it is worth noting

two important features of the model. Kolmogorov's proposal is a scalar description of turbulent motion, in that it does not differentiate between the components, in different directions, of the fluctuations of velocity. Consequently it is not possible to use it to predict the size of the velocity fluctuations in any particular direction, or the corresponding relative turbulence intensity.

The second point concerns the characteristic frequency. This is a hypothetical quantity, since in no real flow will the fluctuations all be associated with a single frequency. In this sense it resembles the "equivalent sand-grain roughness dimension" used to represent the size and shape of the irregularities of a rough surface.

2.2 Modification of the mixing-length hypothesis.

As previously mentioned, the two mixing-length variants used in this investigation are based on the Prandtl hypothesis, for which the effective viscosity is given by the expression:

$$\mu_{eff} = \rho \ell^2 \left| \frac{\partial U}{\partial y} \right| \qquad (2.2\text{-}1)$$

It is reasonable to assume that the effect of free-stream turbulence will appear near the edges of the mixing-layer, if at all. This requires that the modification of 2.2-1 take the form of an additional term, rather

than a multiplying factor; the latter would leave μ_{eff} unchanged, with the value zero, at the boundaries of the layer. We therefore write:

$$\mu_{eff} = \rho \ell^2 \left| \frac{\partial U}{\partial y} \right| + \mu_{eff,add} \qquad (2.2\text{-}2)$$

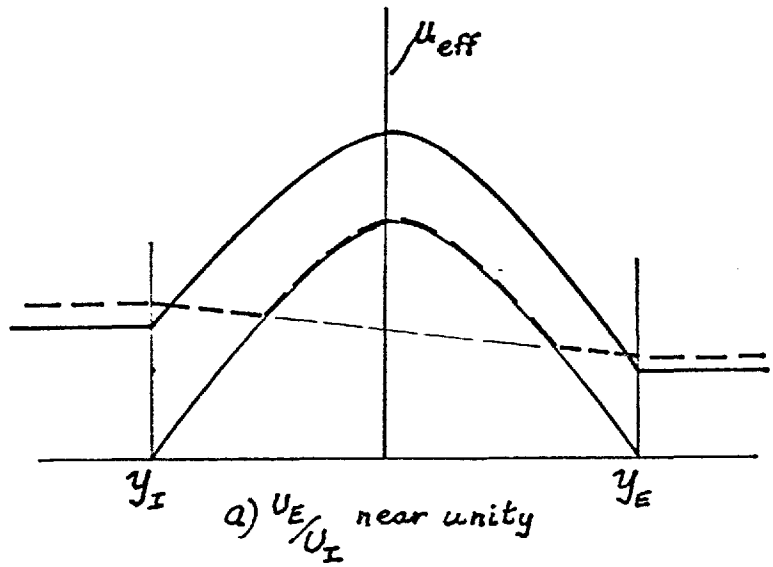
and assume, in the first place, that the extra term has the form:

$$\mu_{eff,add} = A \rho \ell u_{r,IE} \qquad (2.2\text{-}3)$$

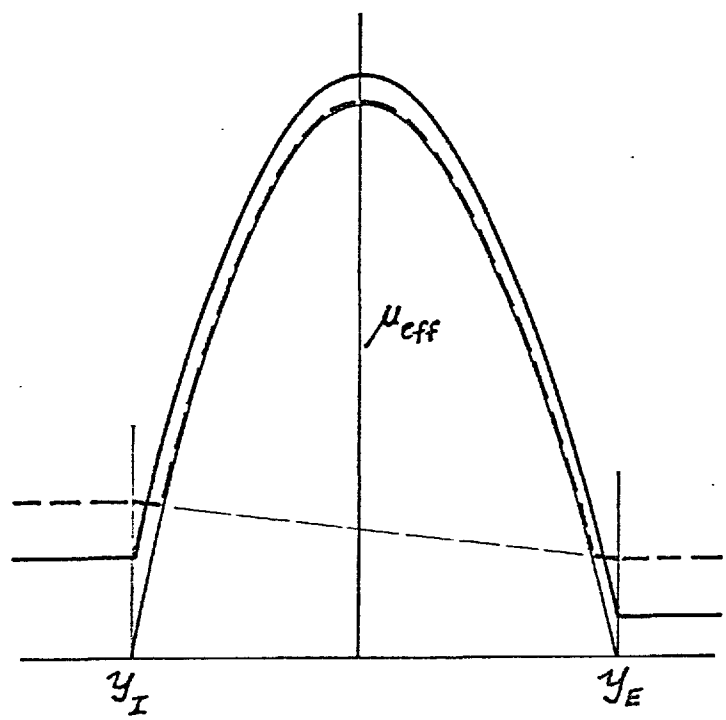
where u_r represents the velocity fluctuations (to be consistent with later usage in the k-z model, u_r is taken to be the root-mean-square value of the fluctuating component of velocity, irrespective of direction), and the subscript IE denotes that the free-stream value of u_r is to be used.

A little thought indicates that some modification of the new expression will be required. In the first place, it is necessary to cater for cases in which the turbulence intensities in the two streams are unequal. Secondly, the available experimental evidence suggests that the increase in effective viscosity should be related to the relative, rather than the absolute, intensities in the two free streams.

The final modification proposed for equation 2.2-3 arises from the need to deal with a range of values of the



a) U_E/U_I near unity



b) U_E/U_I near zero

Figure 2.1

——— MU1
— — — MU2
——— Prandtl

Proposed modification of the Prandtl mixing-length effective viscosity.

stream velocity ratio, U_E/U_I. It is known that the inherent turbulence level in a mixing layer decreases as U_E/U_I approaches unity; it is reasonable to suppose that a given level of free-stream turbulence will have a proportionately larger effect when U_E is close to U_I than when it is relatively small. A multiplying factor, $(B+U_E/U_I)$ say, would have the required effect.

These three changes can be brought about by writing the complete μ_{eff} expression as follows:

$$\mu_{eff} = \rho l^2 \left|\frac{\partial U}{\partial y}\right| + A_1 \rho l U (B + \frac{U_E}{U_I})[(\frac{u_r}{U})_I (\frac{y_E - y}{y_E - y_I}) + (\frac{u_r}{U})_E (\frac{y - y_I}{y_E - y_I})] \qquad (2.2\text{-}4)$$

However, an alternative method, which would have roughly the same effect, would be to regard $\mu_{eff,add}$ not as an addition right through the layer, but as a lower limit to μ_{eff}, thus:

$$\mu_{eff} = \text{the greater of} \begin{cases} \rho l^2 \frac{\partial U}{\partial y} \\ A_2 \rho l U[(\frac{u_r}{U})_I (\frac{y_E - y}{y_E - y_I}) + (\frac{u_r}{U})_E (\frac{y - y_I}{y_E - y_I})] \end{cases} \qquad (2.2\text{-}5)$$

These two formulations for μ_{eff} will be referred to as MU1 and MU2 respectively, for convenience; note that suffixes have been added to distinguish the A's. They are compared graphically in figure 2.1, with each other and with the basic mixing length expression; in drawing these diagrams the effect of the different μ_{eff} formulations on the shape of the velocity profile has been ignored, for simplicity.

One important difference between the two new shear laws can be seen at this stage. With MU1 the distribution curve for μ_{eff} will always have a maximum value near the middle of the mixing layer, whatever the values of $(\frac{u_r}{U})_I$, $(\frac{u_r}{U})_E$, A_1 and B. In the second proposal, on the other hand, the basic mixing-length contribution to μ_{eff} can be submerged if $(\frac{u_r}{U})_I$, $(\frac{u_r}{U})_E$ and A_2 are large enough.

Further progress, in particular the determination of suitable values for A_1, B and A_2, requires comparison of predicted and experimental results. This process is carried out in chapter 6.

2.3 Other features of the modified mixing-length predictions.

Although the expression for μ_{eff} has been made more complicated, the procedure for flow prediction with the mixing-length models remains essentially unchanged. The momentum equation remains the only differential equation to be solved, and no change is required in the boundary conditions for it; the only constraint is that, since there is no pressure gradient, U_E and U_I must be uniform throughout their respective streams. The free stream values of relative turbulence intensity, may, in contrast, be varied independently both of x and of each other.

One important choice, concerns the basis for calculation of the Prandtl mixing length, ℓ. The present work follows the usual practice of taking ℓ proportional to a characteristic transverse dimension of the mixing layer. Several such dimensions appear in the literature:

$$y_{nom} \equiv y_{0.1} - y_{0.9} \tag{2.3-1}$$

$$y_{ms} \equiv (U_E - U_I)/(\frac{\partial U}{\partial y})_{0.5} \tag{2.3-2}$$

$$\theta \equiv \int_I^E \frac{U - U_E}{U_I - U_E}(1 - \frac{U - U_E}{U_I - U_E})dy \tag{2.3-3}$$

In the definitions of the "nominal thickness", y_{nom}, and the "mean-slope thickness", y_{ms}, the subscripts denote the value of the velocity-difference ratio $(U-U_E)/(U_I-U_E)$ defining the point referred to. The "momentum thickness", θ, is seen to be defined, relative to the slow stream, in the same way as the momentum thickness of a wall boundary layer (perhaps the name "relative momentum thickness" would be a better one).

Any of these three dimensions (or indeed, yet another) can be used. Each has disadvantages, but it can reasonably be claimed that θ is more characteristic of the whole velocity profile than the others; it also has the practical advantage that its value will be less affected by measurement errors for individual experimental points than either y_{nom} or y_{ms}.

Whichever dimension is used, it is, of course, necessary to associate with it the appropriate value of the proportionality constant; throughout the present work the momentum thickness has been taken as the basis for calculating ℓ, thus:

$$\ell = \lambda.\theta \qquad (2.3\text{-}4)$$

After comparison of predicted and measured spreading rates, the best value of λ was found to be 0.50(see section 6.2).

2.4 The k-z model.

The solution of the momentum equation, 1.2-1, coupled with the general shear law, 1.2-2,requires additional information about the behaviour of the effective viscosity μ_{eff}. In the Kolmogorov model, μ_{eff} is related to the turbulence kinetic energy, k, and the characteristic frequency, z, thus:-

$$\mu_{eff} = C_{\mu}\rho k/z \qquad (2.4\text{-}1)$$

wher C_{μ} is a constant.

This relation is implied by the form of the diffusion term in Kolmogorov's momentum equation (see equation 1 of appendix D, but note the use of different symbols); in writing equation 2.4-1 the laminar contribution to the effective viscosity is ignored, as usual.

Provided that z can be regarded as a hypothetical quantity, C_{μ} may be set equal to unity, and this is the

normal practice in the present work and elsewhere; at a later stage, when measured frequencies are supplied as input conditions for some of the flow predictions, the possibility of a different value for C_μ has to be considered.

After some modification, described below, Kolmogorov's equations for turbulence energy and frequency may be written in the forms appropriate to steady flow of boundary-layer type thus:-

$$U\frac{\partial k}{\partial x} + V\frac{\partial k}{\partial y} = \frac{1}{\rho}\frac{\partial}{\partial y}\left(\frac{\mu_{eff}}{Pr_{eff,k}}.\frac{\partial k}{\partial y}\right) + \frac{\mu_{eff}}{\rho}\left(\frac{\partial U}{\partial y}\right)^2 - C_D k z \qquad (2.4\text{-}2)$$

$$U\frac{\partial z}{\partial x} + V\frac{\partial z}{\partial y} = \frac{1}{\rho}\frac{\partial}{\partial y}\left(\frac{\mu_{eff}}{Pr_{eff,z}}.\frac{\partial z}{\partial y}\right) + C_1\frac{\mu_{eff}}{\rho z}\left(\frac{\partial^2 U}{\partial y^2}\right)^2 - C_2 z^2 + C_3\left(\frac{\partial U}{\partial y}\right)^2 \qquad (2.4\text{-}3)$$

where C_D, C_1, C_2 and C_3 are constants, and $Pr_{eff,k}$ and $Pr_{eff,z}$ are the effective Prandtl numbers.

These equations now follow the general pattern for boundary-layer equations. The first three terms in each describe the convection and transverse diffusion of the dependent variable, and the remaining ones allow for generation and dissipation. The dissipation terms for z (containing C_1 and C_3) are additions proposed by Spalding (reference 24), on the basis of experience with a closely similar turbulence model (the "k-w" model, briefly described in section A.8). Equations 2.4-2 and 2.4-3 also contain a rather different disposition of the constants from that in the original proposal, and do not

make use of the numerical values obtained by Kolmogorov for some of them. The purpose here is to allow greater freedom in the alignment of predicted and experimental results.

It may be added here that although the coefficients C_D, C_1, C_2 and C_3 and also $Pr_{eff,k}$ and $Pr_{eff,z}$, are at present assumed to be constants, the possibility that some of these would be better treated as functions of local flow conditions should not be excluded. Some suggestions on this point are made in the closing stages of this work (sections 6.5 and 7.4).

The solution of the U, k and z equations (equations 1.2-1, 2.4-2 and 2.4-3) together with equations 1.2-2 and 2.4-1, completely describes the distribution of these quantities throughout the field of the solution. A more comprehensive result is thus obtained than with the mixing length model, although not without cost, since the more complicated model naturally requires more computing time. The application of the finite-difference method of reference 4 to the solution of the equations for the k-z model is described in chapter 4.

From the predicted distribution of the turbulence energy, k, it is desirable to calculated values of the turbulence intensity for comparison with the measurements of this quantity. Since k represents the total turbulence energy while the measurements comprised only the x-components of the fluctuating velocity, an assumption must

be made in relating the two. In the absence of information about the distribution of k it is necessary to assume the turbulence to be isotropic, so that the predicted x-component of the intensity is equal to the mean value, u_r given by the expression:

$$u_r = \left(\frac{2k}{3}\right)^{\frac{1}{2}} \quad ; \qquad (2.4\text{-}4)$$

the corresponding relative intensity is:

$$\frac{u_r}{U} = \left(\frac{2k}{3}\right)^{\frac{1}{2}} \quad . \qquad (2.4\text{-}5)$$

The validity of comparison between this predicted value of relative turbulence intensity and the experimental value is examined in section 6.1.

2.5 Boundary conditions for the k-z model.

Since the momentum equation remains unchanged, the boundary conditions required by it are the same as for the mixing-length hypothesis, i.e., that U_E and U_I are independent of x, the streamwise pressure gradient being zero.

The addition of differential equations for k and z imposes additional conditions on the free streams. Outside the mixing layer $\frac{\partial}{\partial y}$ is zero, and so the two equations, 2.4-2 and 2.4-3, reduce to:

$$U\frac{dk}{dx} + C_D kz = 0 \quad , \tag{2.5-1}$$

and

$$U\frac{dz}{dx} + C_2 z^2 = 0 \quad . \tag{2.5-2}$$

Apart from k = 0 and z = 0, the simplest expressions which satisfy these equations are, for the I stream,

$$k = k_{ref,I}\left(\frac{x}{x_{ref}}\right)^{-C_2/C_D} \tag{2.5-3}$$

and

$$z = U_I/C_2 x \tag{2.5-4}$$

where the suffix "ref" indicates a set of reference conditions. These expressions imply that at $x = 0$, i.e., at the hypothetical origin of the layer, where its width is also zero, both k and z are infinite.

Equations 2.5-3 and 2.5-4 lead to the following expressions for the x-wise variation of μ_{eff} and $(\frac{u_r}{U})$ in the free streams:

$$\mu_{eff,I} = \frac{\rho C_2 k_{ref,I}}{U_I} x^{1-C_2/C_D} x_{ref}^{C_2/C_D} \tag{2.5-5}$$

and

$$\left(\frac{u_r}{U}\right)_I = \frac{1}{U_I}\left[\frac{2k_{ref,I}}{3}\left(\frac{x}{x_{ref}}\right)^{-C_2/C_D}\right]^{\frac{1}{2}} \tag{2.5-6}$$

Expressions similar to 2.5-3,4,5 and 6 hold for the E stream.

A partial verification of equations 2.5-3 and 2.5-6 can be found in the results of measurements of the streamwise decay of artifically generated turbulence. For example, Batchelor and Townsend (reference 25) found that isotropic turbulence downstream of cylindrical rods decayed in accordance with the rule:

$$\left(\frac{U}{u_r}\right)^2 \propto r \qquad (2.5\text{-}7)$$

which agrees with the form of equation 2.5-6 if C_2 and C_D are equal. It will be seen later, however, that there is reason to doubt that either equation 2.5-6 or 2.5-7 exactly describes conditions in the free-stream regions of the flows measured in this investigation.

2.6 The relationship between the k-z and mixing-length models.

In general it is impossible to find simple relationships between similar quantities predicted by the k-z and mixing-length models. For example, a characteristic length for the turbulent motion can be defined, for the k-z model, by:

$$\ell_s \equiv k^{\frac{1}{2}}/z \quad , \qquad (2.6\text{-}1)$$

but ℓ_s differs from the Prandtl mixing-length ℓ and there is no general and simple connection between the two.

A simple relation can, however, be found when a particular condition is satisfied - that the generation and dissipation rates of turbulence energy are in balance, for then the last two terms in equal 2.4-1 cancel one another, so that:

$$\frac{k}{z}\left(\frac{\partial U}{\partial y}\right)^2 - C_D kz = 0 \qquad (2.6\text{-}1)$$

$$z = C_D^{-\frac{1}{2}} \frac{\partial U}{\partial y} \qquad (2.6\text{-}2)$$

Combination of this equation with 2.4-1 and 2.6-1 leads to the following expression for the turbulence effective viscosity:

$$\mu_{eff} = C_\mu C_D^{-\frac{1}{2}} \rho \ell_s^2 \frac{\partial U}{\partial y} \qquad (2.6\text{-}3)$$

This is similar in form to the corresponding expression for the mixing-length model, equation 1.2-2; the comparison shows that:

$$\ell^2 = \frac{u_{eff}}{\rho \frac{\partial U}{\partial y}} = C_u C_D^{-\frac{1}{2}} \ell_s^2 = C_\mu C_D^{-\frac{1}{2}} k/z^2 \qquad (2.6\text{-}4)$$

and finally we have:

$$k = \left(\ell \frac{\partial U}{\partial y}\right)^2 / C_D^{\frac{1}{2}} C_\mu \qquad (2.6\text{-}5)$$

Apart from showing more clearly than before how the two turbulence models are related, these equations have direct utility. In the absence of more precise information about k and z, 2.6-2 and 2.6-5 can be used to establish approximate profiles of these quantities, for example, as part of the initial conditions at the beginning of the flow prediction. This device has, in fact, been used in some of the k-z computations described in Chapter 4.

3. ANALYTICAL ASPECTS OF THE SOLUTION PROCEDURE

3.1 Introduction.

A complete exposition of the Patankar-Spalding finite-difference method is given in references 3 and 4, but for the reader's convenience some aspects of it, which are of particular importance in the prediction of free turbulent flows, are described in this chapter.

The function of the method is to solve the (parabolic) partial differential equations which represent the behaviour of steady two-dimensional boundary-layer flows. Any number of such equations can be dealt with simultaneously; and in addition to accommodating a wide variety of fluid variables, the procedure can be used for both plane and axi-symmetric geometries. However, for its application to the present problem, its main virtue is the freedom it affords in the choice of effective viscosity formulation.

The following section shows how the general method is applied in the solution of the momentum equation for plane, isobaric flow. The special treatment required at free flow boundaries, and the way in which the rates of entrainment from the free streams into the mixing layer are calculated, are presented in the remainder of the chapter.

The general form of solution of the differential equations for k and z is precisely similar to that for the momentum equation, and is not described here. These equations do differ from the momentum equation in one important

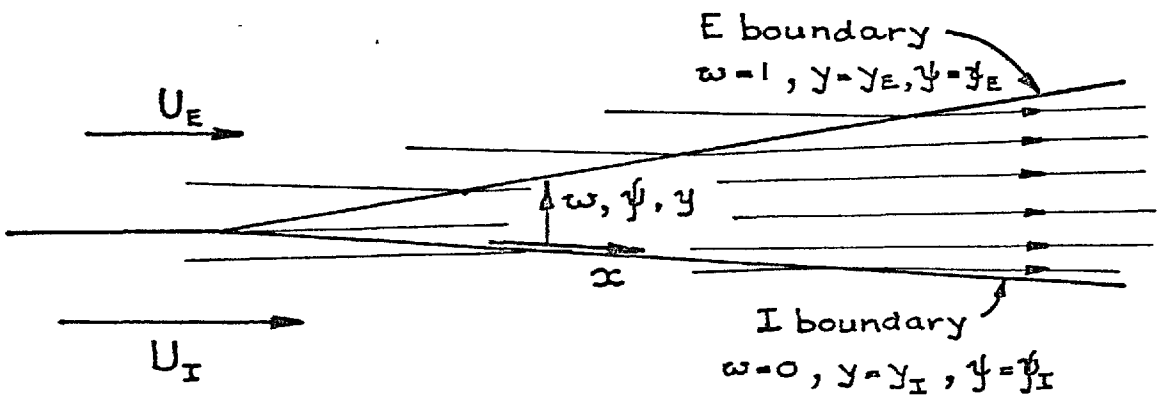


Figure 3.1

Analytical coordinate system

respect - they contain "source" terms which represent generation or dissipation of the dependent variable. The way in which these terms are dealt with is shown in appendix A.6.

3.2 The analytical basis of the finite-difference method.

The appropriate co-ordinate system for plane flow is indicated in figure 3.1. The stream function ψ is defined in the usual way:

$$\frac{\partial \psi}{\partial x} = -\rho V \quad , \quad \frac{\partial \psi}{\partial y} = \rho U \qquad (3.2\text{-}1)$$

and then converted into non-dimensional form:

$$\omega \equiv \frac{\psi - \psi_I}{\psi_E - \psi_I} \qquad (3.2\text{-}2)$$

The suffixes I and E refer to the limits of the field of the solution; at these boundaries ω always has the values zero and unity respectively.

The computations are carried out with x and ω as the independent variables; in terms of these, the solution field is a rectangular grid formed of lines of constant ω (in the flow direction) intersected by transverse lines of constant x. The physical width of the grid $(y_E - y_I)$ is made to increase with x so that it always conforms closely to the width of the boundary layer itself, i.e.

so that it always includes all the significant variations of the dependent variables. This is achieved by ensuring that the width of the grid increases to accommodate all the fluid entrained from the free streams into the layer. The way in which the entrainment rates, $\dot{m}''_I$ and m''_E are determined, is shown in section 3.4.

To recast the basic differential equations in the form required, with x and ω as independent variables, they are first re-derived in the x-ψ (von Mises) co-ordinate system. The momentum equation takes the form:

$$\frac{\partial U}{\partial x} = \frac{\partial}{\partial \psi}(\tau) \qquad (3.2\text{-}3)$$

This is, in effect, the same as equation 1.2-1, the term in V having disappeared because the streamwise distance, x, is now measured along individual streamlines instead of along a predetermined axis, as before.

The transformation of equation 3.2-3 to the x-ω plane, coupled with the introduction of the effective viscosity relation 1.2-2, leads to:

$$\frac{\partial U}{\partial x} + (a+b\omega)\frac{\partial U}{\partial \omega} = \frac{\partial}{\partial \omega}\left(c\frac{\partial U}{\partial \omega}\right) \quad , \qquad (3.2\text{-}4)$$

in which

$$a \equiv \dot{m}''_I/(\psi_E - \psi_I) \quad , \qquad (3.2\text{-}5)$$

$$b \equiv (\dot{m}''_E - \dot{m}''_I)/(\psi_E - \psi_I) \quad , \qquad (3.2\text{-}6)$$

and

$$c \equiv \rho U \mu_{eff}/(\psi_E - \psi_I)^2 \quad . \qquad (3.2\text{-}7)$$

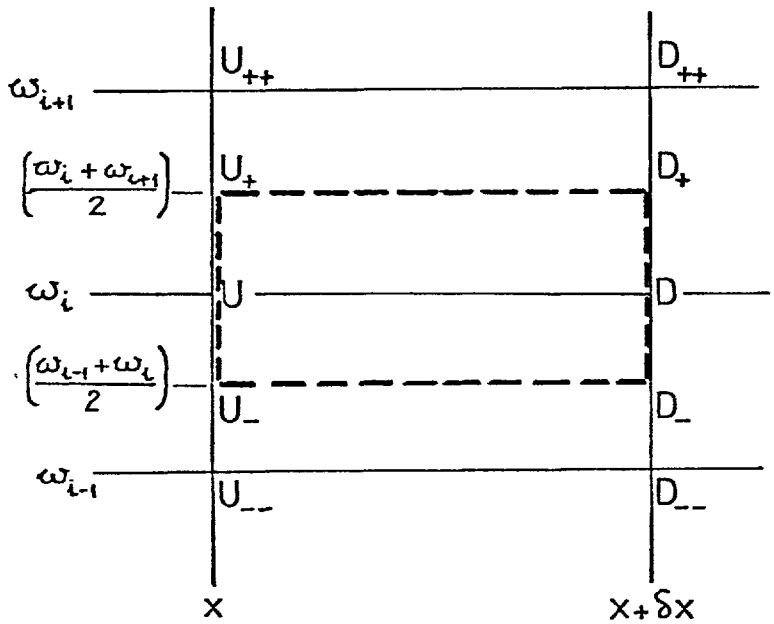


Figure 3.2

Unit control volume for finite-difference analysis.

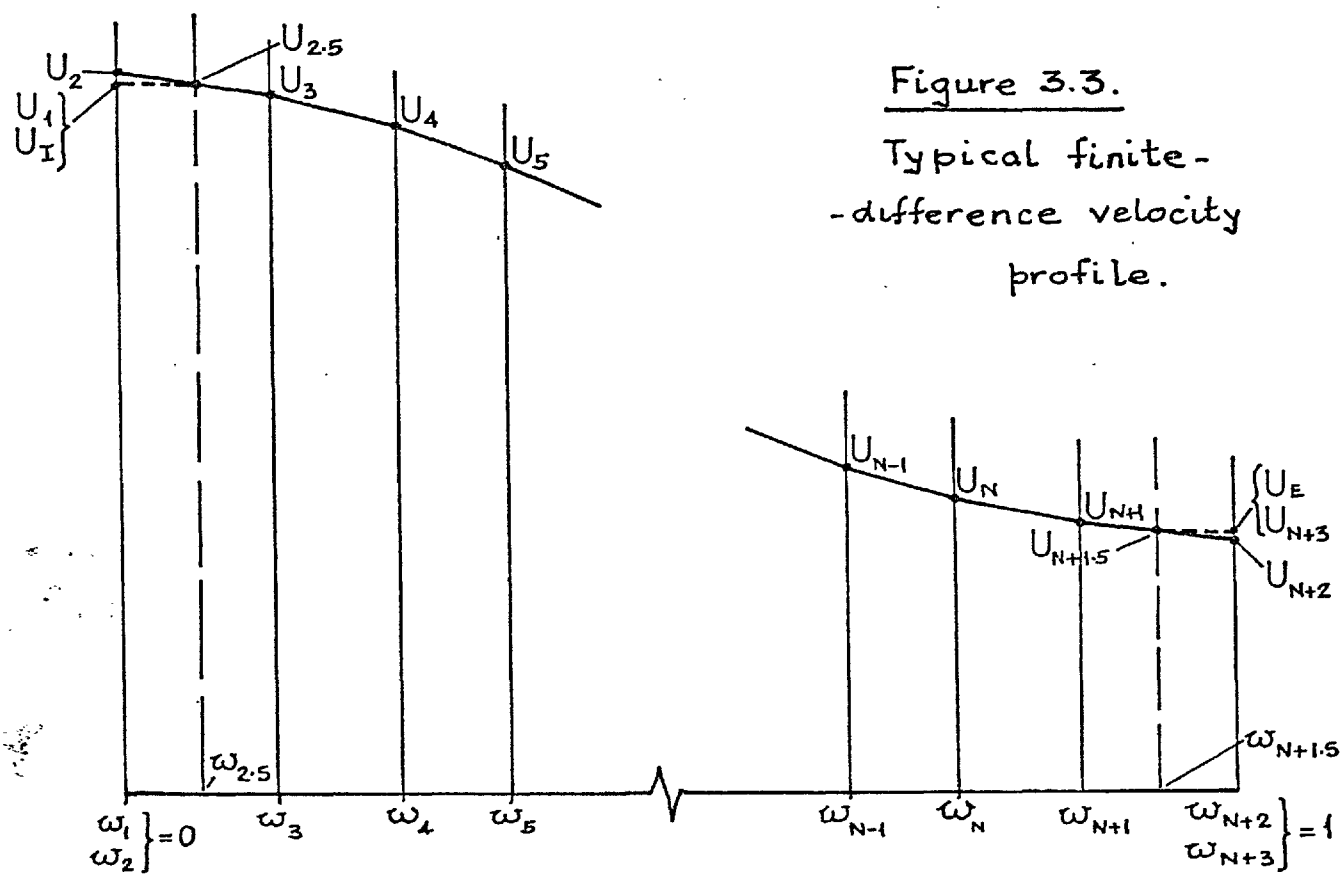


Figure 3.3.

Typical finite-difference velocity profile.

The computation has the object of determining the values of velocity U at all the intersections of the grid lines within the layer. It follows a step-by-step "marching integration" process; the known values at any transverse grid line, together with the known boundary values U_I and U_E, are used to obtain the values of U at the next station downstream ($x+\delta x$). The basic unit in the formulation of the finite-difference equations, by which this procedure is effected, is the elementary control volume shown in figure 3.2. The result of integrating equation 3.2-4 across this region is expressed in the form:

$$U_D = A.U_{D++} + B.U_{D--} + C \qquad (3.2\text{-}8)$$

in which the coefficients A, B and C depend only on the known upstream values (U_{U++}, U_U, U_{U--}, $\dot{m}''_I$, $\dot{m}''_E$, and μ_{eff}); the significance of the subscripts is shown in the diagram.

In the construction of each such equation the velocity is taken to vary linearly with ω in the intervals between grid-lines; in each x- interval, the valueis taken to be uniform along any one ω grid-line and equal to that at the downstream point, D. One equation of this type is formed for each internal ω grid-line, each equation covering two half-intervals of ω, one on each side of the line.

At the I and E boundaries, departures from this practice are required. If the boundaries are free, as in the present problem, then a linear U-ω relationship

through the actual boundary value U_I or U_E is clearly unsatisfactory, because the velocity gradient at either edge of the layer must be zero. To overcome this difficulty, fictitious values of velocity are introduced at each boundary; the finite-difference equation for the boundary is based on a linear variation between this fictitious value and that for the adjacent grid-line, as indicated in Fig. 3.3. The principles underlying the calculation of these "slip" velocities are described in the following section.

The total number of finite-difference equations formed is equal to the number of grid-lines (including the I and E boundaries). They are solved by a simple process of successive substitution, and yield the values of velocity at all D points. The entrainment rates $\dot{m}''_I$ and $\dot{m}''_E$ are then calculated for the newly-determined velocity distribution at $(x + \delta x)$; these also are assumed uniform within each x-interval. This enables the increase in mass flow rate within the layer to be obtained, and consequently the physical position (y co-ordinate) of each grid point. The distribution of velocity at the downstream station is thus fully determined, and the whole sequence of operations can begin again for the next step in the x-direction.

The initial station chosen for the computation procedure must have a non-zero width, and the condition of the stream at all points in this station must be specified.

3.3 Determination of the slip coefficients.

The starting point for the calculation of the coefficients A, B, and C for the half-intervals next to the I and E boundaries of the layer, is the momentum equation (3.2-4). Following the general practice, this equation is integrated over the half-interval in question. The following derivation applies particularly to the I boundary; an essentially similar one holds for the E boundary. The appropriate limits are $\omega_1 (=0)$ and $\omega_{2.5}$; it should be noted that the suffix 2 is reserved for slip values (of U and other dependent variables) at the I boundary, as indicated in Fig. 3.3. Equation (2.4-1) becomes:

$$\frac{d}{dx}\int_1^{2.5} U\, d\omega + \int_1^{2.5} (a+b\omega)\frac{\partial U}{\partial \omega} d\omega - \left[c\frac{\partial U}{\partial \omega}\right]_1^{2.5} = 0 \qquad (3.3\text{-}1)$$

After multiplication by $\frac{(\psi_{2.5}-\psi_1)}{(\rho U\omega)_{2.5}}$, and the insertion of the condition $(\frac{\partial U}{\partial \omega})_1 = 0$ (the free-boundary condition), this may be written as:

$$Y\delta x\frac{d}{dx}\int_1^{2.5} \frac{U}{\omega_{2.5}} d\omega + \int_1^{2.5} (M+2M'\frac{\omega}{\omega_{2.5}})\frac{\partial U}{\partial \omega} d\omega - V\omega_{2.5}(\frac{\partial U}{\partial \omega})_{2.5} = 0 \qquad (3.3\text{-}2)$$

where

$$\left.\begin{aligned} Y &\equiv (\psi_{2.5}-\psi_1)/\delta x(\rho U)_{2.5} \quad , \\ M &\equiv \frac{\dot{m}''_I}{(\rho U)_{2.5}} \quad , \\ M' &\equiv \frac{(\dot{m}''_E-\dot{m}''_I)\omega_{2.5}}{2(\rho U)_{2.5}} \quad , \end{aligned}\right\} \qquad (3.3\text{-}3)$$

and

$$V \equiv \frac{\mu_{eff\ 2.5}}{(\psi_{2.5}-\psi_1)}$$

Again in accordance with the general procedure, equation 3.3-2 is converted to finite-difference form; the first term involves both upstream and downstream values of U, denoted by suffixes U and D respectively, while the remainder are written in terms of downstream values only. In the present analysis, consideration of the special character of the outer half-interval leads to the following principle:-

In formulating the x-convection integral (in the first term), or the transverse gradient (in the third term), a linear U-ω profile between $(U_2, 0)$ and (U_3, ω_3) is assumed; when transverse convection through the I boundary is in question, the free stream value U_1 ($\equiv U_I$) is taken. The result is:

$$\frac{Y}{4}[(U_3+3U_2)_D-(U_3+3U_2)_U+\frac{M}{2}(U_2+U_3-2U_1)_D+\frac{M'}{2}(U_3-U_2)_D-\frac{V}{2}(U_3-U_2)_D = 0 \qquad (3.3\text{-}4)$$

where

$$\left.\begin{aligned} A_2 &\equiv \frac{V-M-M'-Y/2}{E} \\ B_2 &\equiv \frac{2M}{E} \\ C_2 &\equiv \frac{Y(3U_2+U_3)_U}{2E} \\ E &\equiv V + M - M' + 3Y/2 \end{aligned}\right\} \qquad (3.3\text{-}5)$$

3.4 Calculation of entrainment rate.

In order to calculate the rate of growth of a mixing layer, it is necessary to know the entrainment rates at the boundaries; at any value of x the rate of increase of the mass flow rate within the layer is the sum of the local rates of flow through the two boundary surfaces, I and E. The positions of these free boundaries are essentially arbitrary, but this does not cause any difficulty - it is necessary only to ensure that the entrainment-rate calculation is consistent with the definition of boundary position which is used. [Note that in the present co-ordinate system, the entrainment rates $\dot{m}''_I$ and $\dot{m}''_E$ normally have positive and negative values respectively.]

Two separate methods for the determination of $\dot{m}''_I$ and $\dot{m}''_E$ have been used in the present investigation. The first is a modification of that described in section 2.3 of reference 3, for cases, like the present one, in which the effective viscosity is not proportional to $\partial U/\partial y$, and therefore does not vanish at the free boundaries. It is based on the force-momentum equation (3.2-4), combined with an arbitrary specification of a point through which the velocity profile is desired to pass. In the present author's analysis, equation (3.2-4) is written in the following form applying specifically to grid-line 4 (this is the line nearest to the I boundary which is convenient for the present purpose):-

$$(a+b\omega)_4 = \left[\frac{\frac{\partial}{\partial\omega}(c\frac{\partial U}{\partial\omega})}{\frac{\partial U}{\partial\omega}}\right]_4 - \frac{(\frac{\partial U}{\partial x})_4}{(\frac{\partial U}{\partial\omega})_4} \qquad (3.4\text{-}1)$$

At any step in the computation process, the only quantity on the right-hand side of equation 3.4-1 which cannot be evaluated from upstream values is $(\frac{\partial U}{\partial x})_4$. Initially this was obtained from the equation:

$$(\frac{\partial U}{\partial x})_4 = \frac{\tilde{U}_4 - U_4}{x_D - x_U} \qquad (3.4\text{-}2)$$

where $\tilde{U}_4$ is an arbitrarily-chosen value close to U_I. This enables equation 3.4-1 and the corresponding equation for the N^{th} grid line to be solved simultaneously for a and b, and hence for $\dot{m}''_I$ and $\dot{m}''_E$. The arrangement is easily seen to be a device for controlling the growth rate of the grid so that transverse gradient $\frac{\partial U}{\partial\omega}$ is neither too small nor too large in the vicinity of the I and E boundaries, and undesirable truncation or extension of the velocity profile is avoided.

In practice, it was found necessary to vary $(U_I-\tilde{U}_4)$ and $(\tilde{U}_N-U_E)$ to suit the computational conditions, otherwise excessively large values of $\dot{m}''_I$ and $\dot{m}''_E$ resulted. This refinement is examined in detail in Appendix A.10.

This method for calculating entrainment rate was used for most of the mixing-length predictions. For the remainder , and for all the k-z computations, the simpler method of reference[4] was employed; it is described below.

Where direct comparison of results using the two alternatives was possible, the differences were found to be negligible.

The second method for calculation of entrainment rate recognises more directly the arbitrary nature of this quantity. Since an arbitrary decision has to be made at some stage, the analysis is best made as simple as possible. A statement fixing the relative magnitude of any two of the quantities Y, M and V also fixes the relative magnitudes of U_1, U_2 and U_3, by virtue of their connection with the coefficients A_2, B_2, and C_2. One very simple example is:

$$M = V \quad , \tag{3.4-3}$$

which implies, as the entrainment "law":

$$\dot{m}''_I = \frac{(\rho U)_{2.5}\, \mu_{eff\ 2.5}}{(\psi_{2.5} - \psi_1)} \tag{3.4-4}$$

The effect on A_2, B_2, and C_2 depends mainly on the number of grid lines (N + 1) and on the step length δx. When both are large (i.e. when the grid rectangles have a high length/width aspect ratio), A_2,B_2 and C_2 are close to zero, unity, and zero respectively; U_2 is then close to U_1 - a satisfactory state of affairs.

In this case also a device to limit undesirably large entrainment was found to be necessary; when $\dot{m}''_I$ is too big, (U_1-U_3) becomes unnecessarily small, and the velocity profile develops a long and wasteful "tail". A simple correction is made by varying $\mu_{eff,2.5}$ or $\dot{m}''_I$ so that (U_1-U_3) maintains a small, arbitrarily-specified size.

4. THE FINITE-DIFFERENCE PREDICTIONS

4.1 Introduction.

At this stage it is possible to describe the flow predictions themselves. They were made by the method of references 3 and 4. Their purpose was to determine how well the effects of free-stream turbulence on mixing layer development could be reproduced by the turbulence models presented in chapter 2.

The first group of predictions made with each model were of idealised mixing-layer flows, starting from simple arbitrary initial profiles, and with the simplest possible boundary conditions. In the mixing-length calculations, the relative turbulence intensity had the same value throughout both free streams during each prediction, and the predicted velocity profiles became similar in shape for large values of x; these are referred to here as the symptotic solutions. In the parallel calculations with the k-z model asymptotic solutions were not obtained, since (except for the special case in which the boundary values of k and z are zero) k and z must vary with x in the free streams.

Further details of these idealised predictions are presented in this chapter, and their results examined. The main object in carrying out this part of the work was to obtain general information about the character of the analytical turbulence models. Their results are

not intended to be compared directly with the experimental observations, because they do not take into account several significant features of the real flows.

The most important of these is the existence of an outer mixing layer between each free stream region and the surrounding atmosphere. This point is illustrated in figure 5.23 in conjunction with the description of the real flows, in section 5.9. As a result of the presence of the outer mixing layers, the boundary conditions for the middle one were less simple than has been assumed in the idealised predictions.

Two other departures from ideal conditions were

a) the wake produced by the dividing wall between the two streams, and

b) the spatial non-uniformity of velocity and turbulence intensity in the streams entering the working section.

It was possible to approach the real flows more closely, but to different degrees, and in different ways for the two models. The details of these more realistic flow predictions are given in sections 4.5 and 4.9 for the mixing-length and k-z predictions respectively. The comparison of the results with those of the experiments, is deferred to chapter 6, after the description of the experimental work itself.

The computer programmes used for these various sets of calculations were identified by the following code names:

Idealised predictions, mixing-length basis: NEWMOD

Realistic " " " " : NEWMOD-F

Idealised " k-ż basis : LAYER

Realistic " " " : LAYER-3

The main modifications made in deriving these programmes from the basic ones of references 3 and 4 are described briefly in the following section.

Listings of the programmes are displayed in appendix A, preceded by a description of the main computational details. Appendix A also contains an examination of the effect of varying the main computational parameters, such as the number of streamwise grid lines, the size of the forward step, and the arbitrary velocity difference appearing in the entrainment control sequence.

4.2 Adaptation of the basic programmes.

In applying the basic programmes to the present investigation, various modifications were made. The most important of these arose in the incorporation of the new turbulence models. Others arose from the particular nature of the problem; for example, unless it was inconvenient to do so, sections not required for uniform density, plane, free turbulent flow predictions were discarded.

Some of the specific changes made in deriving the NEWMOD programme were:

1) The restatement of the effective-viscosity sequence, in accordance with equations 2.2-4 and 2.2-5.
2) The introduction of the momentum thickness as the basis for calculation of the mixing length, as described in section 2.3.
3) The change of entrainment-rate calculation to that described in the first part of section 2.4.

Only minor differences exist between the NEWMOD and NEWMOD-F programmes (see section 4.5).

The main changes made in the basic programme of reference 4, to produce LAYER were:

4) The incorporation of the turbulence kinetic energy, k, and the charateristic frequency, z, as the second and third primary dependent variables.
5) The modification of the boundary conditions in accordance with the analysis of section 2.5.

The particular function carried out by the LAYER-3 programme, and the additional changes required, are described in section 4.9.

All the programmes contained a final sequence in which the output values from the finite-difference procedure were processed for convenient comparison with other solutions and with the experimental results. The most important common features of these sequences were the calculations of the following quantities:

The representative widths, y_{nom} and y_{ms} (defined in section 2.3)

The velocity difference ratio, $(U-U_E)/(U_I-U_E)$

The non-dimensional transverse co-ordinate y^*/θ, where y^* is cross-stream distance measured from the position at which $U = (U_I+U_E)/2$

The velocity profile shape factors y_{nom}/θ and y_{ms}/θ,

The shape factor for the turbulence intensity profile, η/θ (defined in section 4.7).

4.3 Results of the asymptotic mixing-length solutions.

The asymptotic solutions have been obtained for velocity ratios over the whole range from 0 to 1, and for free-stream relative turbulence intensities, $(\frac{u_r}{U})_I$ and $(\frac{u_r}{U})_E$, of 0, 0.05, 0.1, and 0.2. In all cases presented the values of these last two quantities are equal, and independent of x. The calculations have been carried out with both the MU1 and MU2 effective-viscosity formulations. The main results are shown graphically in figures 4.1 to 4.6; for these calculations the values of λ, A_1, A_2 and B were those found to give "best" agreement with experimental results, as shown in section 6.2, i.e., $\lambda = 0.50$, $A_1 = 1.05$, $A_2 = 2.0$, $B_2 = 0.50$.

It is immediately clear from the first four graphs that there are considerable differences between the results

from the MU1 and MU2 versions, in the way that the spreading rate $d\theta/dx$ varies with U_E/U_I and $(u_r/U)_{IE}$. The difference is most easily seen by comparing the straight lines of figure 4.3 with the roughly hyperbolic shapes of figure 4.4. With the MU1 formulation, any increase in $(\frac{u_r}{U})_{IE}$ always produces a proportionate increase in $d\theta/dx$; with MU2, the effect of an increase is negligible when $(u_r/U)_{IE}$ is small, particularly at low velocity ratios.

As might be expected, the differences between the results for the two shear laws are even more striking when the predicted distributions of relative turbulence intensity are compared, as in figure 4.5. With the MU2 version, the result anticipated in section 2.2 occurs - the simple mixing-length component of μ_{eff} is swamped by the additional quantity $\mu_{eff,add}$; also, because $A_2 = 2$, the predicted increase in $\frac{u_r}{U}$ is twice the free stream value, so that a large discontinuity exists at each edge of the layer. Much better matching occurs with MU1, for which the predicted value of $\frac{u_r}{U}$ at each edge of the layer can easily be seen to be $A_1(B+U_E/U_I)$ times as great as that in the adjacent free stream. With $A_1 = 1.05$ and $B = 0.5$, exact matching is obtained when $U_E/U_I = 0.45$.

The corresponding differences in velocity distribution are much smaller, as figure 4.6 shows - so small that they are probably more clearly indicated by the values of the velocity profile shape factors y_{nom}/θ and y_{ms}/θ listed in

TABLE 4.1 : Mixing-length predictions : profile shape factors, and spreading rates

U_E/U_I	$\left(\frac{u_r}{U}\right)_{IE}$	MU1			MU2		
		$\frac{y_{nom}}{\theta}$	$\frac{y_{ms}}{\theta}$	$\frac{d\theta}{dx}$	$\frac{y_{nom}}{\theta}$	$\frac{y_{ms}}{\theta}$	$\frac{d\theta}{dx}$
0.4	0	4.73	5.17	.0111	4.73	5.17	.0111
	.05	4.67	4.95	.0187	4.54	4.42	.0156
	.10	4.63	4.84	.0261	4.54	4.48	.0309
0.6	0	4.72	5.17	.0064	4.72	5.17	.0064
	.05	4.62	4.82	.0158	4.54	4.43	.0158
	.10	4.60	4.70	.0250	4.54	4.43	.0316
0.8	0	4.72	5.18	.0029	4.73	5.18	.0029
	.05	4.58	4.65	.0139	4.54	4.42	.0160
	.10	4.56	4.55	.0248	4.52	4.41	.0320

TABLE 4.2 : Comparison of finite-difference (NEWMOD) results with exact solution (KUESOL)

	$U_E/U_I = 0.4$				$U_E/U_I = 0.8$			
	NEWMOD		KUESOL		NEWMOD		KUESOL	
$\frac{y^*}{\theta}$	VDR	$\frac{\theta}{U_I}\frac{\partial U}{\partial y}$ ×100	VDR	$\frac{\theta}{U_I}\frac{\partial U}{\partial y}$ ×100	VDR	$\frac{\theta}{U_I}\frac{\partial U}{\partial y}$ ×100	VDR	$\frac{\theta}{U_I}\frac{\partial U}{\partial y}$ ×100
-3.6	.999	0.4	.999	0.8	.998	0.32	.997	0.49
-3.2	.986	3.4	.985	3.3	.980	1.23	.980	1.21
-2.8	.956	5.5	.956	5.5	.949	1.86	.949	1.85
-2.4	.914	7.3	.913	7.3	.907	2.41	.906	2.40
-2.0	.860	8.8	.859	8.8	.854	2.87	.854	2.86
-1.6	.797	10.0	.797	9.9	.793	3.24	.793	3.23
-1.2	.728	10.8	.728	10.8	.725	3.53	.725	3.51
-0.8	.654	11.4	.654	11.3	.653	3.72	.653	3.71
-0.4	.578	11.6	.577	11.6	.577	3.84	.577	3.83
0	.500	11.6	.500	11.6	.500	3.87	.500	3.86
0.4	.423	11.4	.423	11.4	.423	3.82	.423	3.81
0.8	.349	10.9	.349	10.9	.348	3.69	.348	3.68
1.2	.278	10.2	.279	10.2	.276	3.48	.277	3.47
1.6	.213	9.3	.214	9.3	.210	3.19	.210	3.18
2.0	.155	8.3	.155	8.2	.150	2.82	.150	2.81
2.4	.104	7.0	.104	7.0	.098	2.38	.098	2.37
2.8	.062	5.6	.062	5.6	.055	1.87	.056	1.86
3.2	.030	4.0	.030	4.0	.024	1.28	.024	1.27
3.6	.009	2.3	.009	2.3	.005	0.60	.005	0.61
4.0	.000	0.3	.000	0.4	.000	0.00		

Table 4.1 for velocity ratios 0.4, 0.6, and 0.8; this table also contains values of the spreading rate $d\theta/dx$ for these velocity ratios.

One important conclusion which can immediately be drawn from these collected results is that the shape of the velocity profile is the least satisfactory feature on which to base conclusions about the form of the shear law. An investigation relying solely on the comparison of predicted and measured velocity profiles cannot be expected to yield reliable information about the effective viscosity.

4.4 Comparison with the exact analytical solutions.

When the constant A_1 or A_2 is set at zero, both the MU1 and MU2 shear laws reduce to the original Prandtl mixing-length version. The asymptotic solutions so obtained may be compared directly with exact analytical solutions of the boundary-layer equations, in particular, those of Tollmien (reference 5) and Kuèthe (reference 6).

To obtain more accurate results for the analytical solutions than those normally available, these have been re-calculated, using a short digital-computer programme called KUESOL; details of both the analysis and the programme are given in Appendix B.

Results from the KUESOL programme are listed with the corresponding finite-difference results in Table 4.2. The agreement can be seen to be very close everywhere.

TABLE 4.3 : Boundary conditions for NEWMOD-F predictions

No. of grid bars	Velocity ratio U_E/U_I	Station 1			Station 2			Station 3			Station 4		
		x (cm)	$\left(\frac{u_r}{U}\right)_I$	$\left(\frac{u_r}{U}\right)_E$	x (cm)	$\left(\frac{u_r}{U}\right)_I$	$\left(\frac{u_r}{U}\right)_E$	x (cm)	$\left(\frac{u_r}{U}\right)_I$	$\left(\frac{u_r}{U}\right)_E$	x (cm)	$\left(\frac{u_r}{U}\right)_I$	$\left(\frac{u_r}{U}\right)_E$
5	·41	10	·069	·087	15	·051	·080	20	·044	·100			
5	·59	10	·076	·083	15	·053	·064	20	·046	·066			
5	·83	10	·088	·084	15	·063	·062	20	·047	·053			
4	·40	10	·090	·104	15	·065	·085	20	·053	·096			
4	·60	10	·082	·091	15	·062	·068	20	·051	·064			
4	·83	10	·083	·083	15	·059	·063	20	·047	·053			
—	·40	5·0	·006	·010	10	·006	·016	15	·009	·031	20	·014	·052
—	·60	10	·006	·009	15	·008	·014	20	·011	·024			
—	·79	10	·006	·008	15	·008	·012	20	·010	·015	25	·015	·021

4.5 More realistic mixing-length predictions.

The starting-point for these calculations is provided by the experimental velocity profile derived from the readings for the upstream traverse station. In the prediction of the downstream development of the central mixing layer, the velocity in each free-stream was taken as constant, and the turbulence intensity varied with x in accordance with the values observed at the traverse stations.

In this way, except for the free-stream velocity variations, all the 'real' features of the actual flows mentioned in the previous section were taken into account, albeit in a rather elementary manner, necessitated by the nature of the mixing-length hypothesis and the extent of the experimental information. The observed x-wise velocity variations could not have been included without implying the existence of a spurious streamwise pressure gradient. A practical difficulty arising from the transverse variation of velocity was that of assigning precise values of U_I and U_E. The way in which the points marking the I and E boundaries of the layer were located in the data-processing programme is explained in Appendix C.

The values of velocity ratio U_E/U_I, and of the relative turbulence intensities at the I and E boundaries at positions corresponding to the traverse stations, are set out in Table 4.3; this table is similar to Table 5.1, which gives the actual running conditions in the test section.

The modifications required in the NEWMOD programme were slight and involved no further change in its basic operation; they were confined to the main section of the programme, and largely concerned with the alignment of the predictions with the experimental measuring stations.

A more detailed description of the programme (NEWMOD-F) and a listing of its main section, are given in appendix A.4. The way in which the values of the constants λ , A, and B were determined, and the corresponding flow predictions, are described in section 6.2.

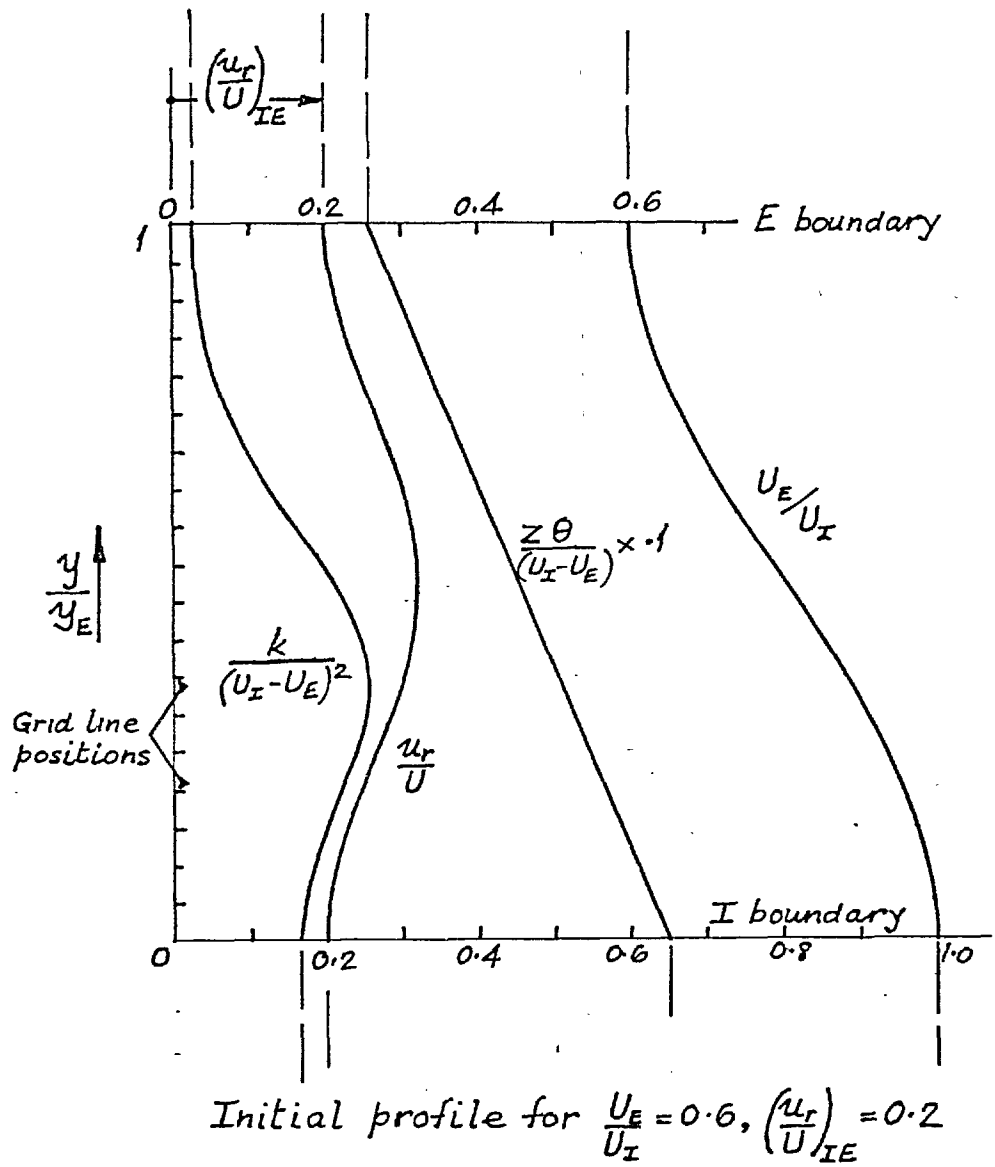
4.6 The idealised k-z calculations.

With the k-z model, k and z must vary with x along the edges of the mixing layer, as explained in section 2.5. Similarity of the velocity profiles is achieved only when k and z are both zero at the boundaries. Apart from this special case, the simplest solutions are obtained when:

a) the velocities U_E and U_I are uniform, and

b) the relative turbulence intensities $(\frac{u_r}{U})_I$ and $(\frac{u_r}{U})_E$ are equal at any value of x.

A considerable number of calculations with boundary conditions of this type have been carried out, with the object of determining the general effects of varying the effective Prandtl numbers, $Pr_{eff,k}$ and $Pr_{eff,z}$, and the constants C_1, C_2, C_3 and C_D, on the main features of the



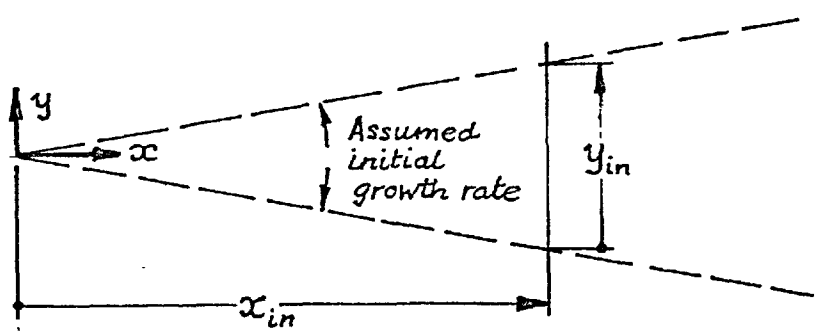


Figure 4.7 : Initial conditions for idealised k-z predictions (LAYER programme)

mixing layer, as a preliminary to the more realistic predictions described in the final section of this chapter.

The starting conditions used for the present calculations are indicated by figure 4.7. Details of these and other features of the predictions are contained in section A.5. The work was arranged to give solutions for values of the free-stream turbulence intensities in the range .01 to 0.20.

Some preliminary information about the values of the constants was available from previous work with the closely similar "k-w" turbulence model. (The relation between the two models is shown in section A.8). During the present calculations, they were varied within the following ranges:

$Pr_{eff,k}$ and $Pr_{eff,z}$	0.4 to 1.0
C_D	.08 to .12
C_1	0.0 to 6.0
C_2	.08 to .10
C_3	.50 to .65

Collected results, in the form of graphs of spreading rate $d\theta/dx$, and profile shape factor η/θ, plotted against $(\frac{u_r}{U})_{IE}$ with U_E/U_I as parameter, are shown in figure 4.8; the values used for the constants were in the middle of each range, and are listed on the figure.

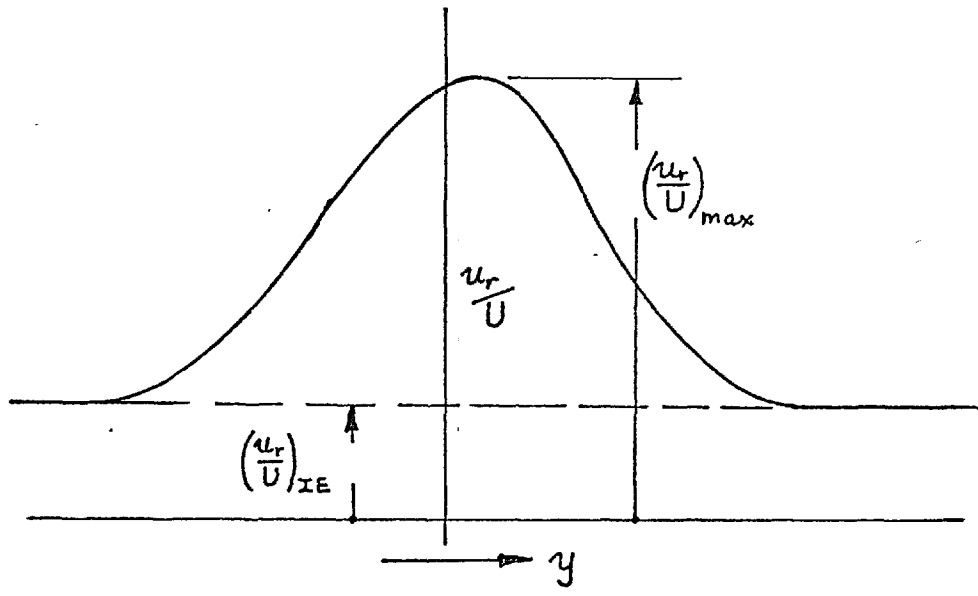


Figure 4.9.

Definition diagram for η

It is interesting to note at this stage that the shape of the upper graph appears to be a compromise between the corresponding figures for the modified-mixing-length calculations (figures 4.3 and 4.4). The general shape of the new graph is similar to that for the MU2 shear law, but the slope of the lines for high values of $(\frac{u_r}{U})_{IE}$ is nearer to that for the MU1 version.

4.7 The effects of varying the constants.

For a given set of boundary conditions, the angle of spread of the mixing layer and the predicted variations of U, k and z within it, depend on the values assigned to the constants. Significant features of the flow which can conveniently be used to judge the effects of varying these values are:

a) The growth rate of the layer, for example $d\theta/dx$.

b) The shape of the velocity profile as indicated by the ratios of pairs of representative transverse dimensions, e.g. y_{ms}/θ.

c) The shape of the distribution of k or u_r/U; for our purpose the latter is more convenient since it allows direct comparison with experiment. An appropriate quantity is η, the "excess relative turbulence intensity thickness", defined as:

$$\eta \equiv \frac{\int_I^E [\frac{u_r}{U} - (\frac{u_r}{U})_{IE}]dy}{(\frac{u_r}{U})_{max} - (\frac{u_r}{U})_{IE}} \quad , \qquad (4.7\text{-}1)$$

the significance of the suffixes being indicated by diagram figure 4.9; the ratio η/θ forms a shape factor for the turbulence intensity profile.

A similar treatment of the z-profile would not be possible, as z is not necessarily an experimentally-observable quantity.

Examination of the exploratory solutions leads to the following qualitative conclusions about the effects of varying the constants:

1) The profile shape factors η/θ and y_{ms}/θ are affected most by variation of $Pr_{eff,k}$, and relatively little by changes in the other constants.
2) The spreading rate $d\theta/dx$ is controlled mainly by C_2 and C_3, while C_D also has a small effect; the influence of C_1, and of the effective Prandtl numbers for k and z, is practically negligible.

A quantitative basis for these conclusions is provided by the calculation of the appropriate influence coefficients. The influence coefficient $i_{p,q}$ indicates the effect of variation of quantity p on quantity q and is defined as:

$$i_{p,q} \equiv \frac{p}{q}\frac{dq}{dp} \qquad (4.7\text{-}2)$$

or, in finite-difference form:

$$i_{p,q} \equiv \frac{p_{mean}}{q_{mean}} \times \frac{\Delta q}{\Delta p} \qquad (4.7\text{-}3)$$

TABLE 4.4 : Influence coefficients : Variation of $\frac{d\theta}{dx}$, $\frac{y_{nom}}{\theta}$ and $\frac{\eta}{\theta}$ with $Pr_{eff,k}$.

$C_D = 0.1$, $C_1 = 3.0$, $C_2 = 0.1$, $C_3 = 0.56$

$\left(\frac{u_r}{U}\right)_{IE} = .06$, $Pr_{eff,k} = 0.4$ to 1.0.

$Pr_{eff,z}$	U_E/U_I	$i_{Pr_{eff,k}, \frac{d\theta}{dx}}$	$i_{Pr_{eff,k}, \frac{y_{nom}}{\theta}}$	$i_{Pr_{eff,k}, \eta/\theta}$
0.4	0.4	.019	.015	.33
	0.6	.069	.009	.31
	0.8	.009	.008	.37
0.7	0.4	.023	.024	.32
	0.6	.074	.011	.32
	0.8	.017	.010	.37
1.0	0.4	.028	.027	.33
	0.6	.078	.010	.32
	0.8	.017	.010	.37

TABLE 4.5 : Influence coefficients : Variation of $\frac{d\theta}{dx}$, $\frac{y_{nom}}{\theta}$ and $\frac{\eta}{\theta}$ with $Pr_{eff,z}$

$C_D = 0.1$, $C_1 = 3.0$, $C_2 = 0.1$, $C_3 = 0.56$

$\left(\frac{ur}{U}\right)_{IE} = .06$, $Pr_{eff,z} = 0.4$ to 1.0

$Pr_{eff,k}$	U_E/U_I	$i_{Pr_{eff,z}, \frac{d\theta}{dx}}$	$i_{Pr_{eff,z}, \frac{y_{nom}}{\theta}}$	$i_{Pr_{eff,z}, \eta/\theta}$
0.4	0.4	−.005	−.010	.050
	0.6	−.024	−.003	.023
	0.8	−.001	−.003	.014
0.7	0.4	.004	−.004	.035
	0.6	−.019	−.003	.018
	0.8	−.002	−.001	.015
1.0	0.4	.006	.001	.024
	0.6	−.016	−.001	.015
	0.8	−.002	.000	.015

TABLE 4.6: Influence coefficients: Variation of $\frac{d\theta}{dx}$, $\frac{y_{nom}}{\theta}$, $\frac{y_{ms}}{\theta}$ and $\frac{\eta}{\theta}$ with C_D

$C_1 = 3.0$, $C_2 = 0.1$, $C_3 = 0.56$, $Pr_{eff,k} = Pr_{eff,z} = 0.7$, $C_D = .09$ to $.11$

$\left(\frac{u_r}{U}\right)_{IE}$	U_E/U_I	$i_{C_D, \frac{d\theta}{dx}}$	$i_{C_D, \frac{y_{nom}}{\theta}}$	$i_{C_D, \frac{y_{ms}}{\theta}}$	$i_{C_D, \eta/\theta}$
.08	0.4	-.58	.010	.009	-.040
	0.6	-.45	.000	.007	.047
	0.8	-.33	.010	.016	.172
.01	0.6	-1.28	.020	.015	0.13

TABLE 4.7: Influence coefficients: Variation of $\frac{d\theta}{dx}$, $\frac{y_{nom}}{\theta}$ and $\frac{\eta}{\theta}$ with C_1

$\left(\frac{u_r}{U}\right)_{IE} = .06$, $\frac{U_E}{U_I} = 0.6$, $C_D = 0.1$, $Pr_{eff,k} = Pr_{eff,z} = 0.7$

$C_1 = 0$ to 6.0

C_2	C_3	$i_{C_1, \frac{d\theta}{dx}}$	$i_{C_1, \frac{y_{nom}}{\theta}}$	$i_{C_1, \eta/\theta}$
.08	.51	-.018	-.0001	-.005
.08	.61	-.017	-.0001	-.005
.12	.51	-.034	-.0007	-.008
.12	.61	-.035	-.0007	-.008

TABLE 4.8 : Influence coefficients : Variation of $\frac{d\theta}{dx}$, $\frac{y_{nom}}{\theta}$, $\frac{y_{ms}}{\theta}$ and $\frac{\eta}{\theta}$ with C_2

$\left(\frac{u_r}{U}\right)_{IE} = \cdot 08$, $C_D = 0.1$, $C_1 = 3.0$, $Pr_{eff,k} = Pr_{eff,z} = 0.7$

$C_2 = \cdot 085$ to $\cdot 095$

C_3	U_E/U_I	$i_{C_2, \frac{d\theta}{dx}}$	$i_{C_2, \frac{y_{nom}}{\theta}}$	$i_{C_2, \frac{y_{ms}}{\theta}}$	$i_{C_2, \eta/\theta}$
0.5	0.4	1.20	-.007	-.049	.009
	0.6	1.13	-.001	-.044	.063
	0.8	0.97	-.014	-.040	.022
0.55	0.4	1.12	-.009	-.038	-.083
	0.6	1.01	-.001	-.037	-.087
	0.8	0.97	-.013	-.034	-.079
0.6	0.4	1.15	-.012	-.042	-.146
	0.6	1.01	-.003	-.039	-.152
	0.8	0.87	-.016	-.035	-.179

TABLE 4.9 : Influence coefficients : Variation of $\frac{d\theta}{dx}$, $\frac{y_{nom}}{\theta}$, $\frac{y_{ms}}{\theta}$ and $\frac{\eta}{\theta}$ with C_3

$\left(\frac{u_r}{U}\right)_{IE} = \cdot 08$, $C_D = 0.1$, $C_1 = 3.0$, $Pr_{eff,k} = Pr_{eff,z} = 0.7$

$C_3 = 0.5$ to 0.6

C_2	U_E/U_I	$i_{C_3, \frac{d\theta}{dx}}$	$i_{C_3, \frac{y_{nom}}{\theta}}$	$i_{C_3, \frac{y_{ms}}{\theta}}$	$i_{C_3, \frac{\eta}{\theta}}$
	0.4	-·357	-·004	-·040	·005
·085	0.6	-·170	-·001	-·030	·012
	0.8	-·051	-·001	-·012	·017
	0.4	-·366	-·005	-·048	·002
·09	0.6	-·200	-·002	-·036	·011
	0.8	-·053	-·004	-·013	·017
	0.4	-·439	-·008	-·055	·002
·095	0.6	-·211	-·002	-·042	·008
	0.8	-·058	-·006	-·016	·016

In tables 4.4 to 4.9 are tabulated the values of the influence coefficients which express the effects of all the constants on the shape factors and the spreading rate. The more significant of these influences are also displayed graphically in figures 4.10, 4.11 and 4.12.

4.8 Strategy for determining the main k-z constants.

Between the constants ($Pr_{eff,k}$, $Pr_{eff,z}$, C_D, C_1, C_2, C_3), the boundary conditions (U_E/U_I, x_{in}, $(\frac{u_r}{U})_{IE}$), and the output quantities ($d\theta/dx$, y_{nom}/θ, y_{ms}/θ, η/θ) there exists a complicated set of interdependencies. However, the results displayed in the previous section show that some of the constants are more important than others, notably $Pr_{eff,k}$, C_D, C_2 and C_3. Further consideration leads to the following strategy for determining, at least tentatively, values for these:

a) The predicted value of η/θ is strongly dependent on $Pr_{eff,k}$, and is hardly affected by any of the other constants. The best value for $Pr_{eff,k}$ can therefore be readily determined from a comparison of predicted and experimental values for η/θ. These are shown in figures 4.10 and 11, and in Table 5.2* respectively. The comparison indicates that the best value for $Pr_{eff,k}$ is close to 0.7.

---

*Facing page 100.

b) The next most significant effect is a double one - the combined influence of C_2 and C_3 on $d\theta/dx$. Unfortunately, the real flow conditions were too complicated to allow direct comparison with the idealised k-z predictions; a move which <u>can</u> be made instead, is to compare the k-z predictions for zero free-stream turbulence with the corresponding mixing-length results. In figure 4.13 are shown the variations of $(\frac{d\theta}{dx})_{asym}$ with C_2 and C_3, for velocity ratios 0.4, 0.6, and 0.8. Also indicated are the single values of $(\frac{d\theta}{dx})_{asym}$ predicted by the mixing-length analysis (with A = 0). To obtain these same values with the k-z model, it would be necessary for C_3 to vary with C_2 approximately in accordance with the following equations:-

$$\left.\begin{aligned} U_E/U_I = 0.4 \;&:\; C_3 = 8.5C_2 - .156 \\ " \quad = 0.6 \;&:\; C_3 = 8.4C_2 - .148 \\ " \quad = 0.8 \;&:\; C_3 = 8.3C_2 - .144 \end{aligned}\right\} \quad (4.8\text{-}1)$$

The closeness of these three equations indicates the degree of agreement between the k-z and mixing-length models for this range of conditions. For the present purpose they can be replaced by the single equation

$$C_3 = 8.4C_2 - .150 \qquad (4.8\text{-}2)$$

Any attempt to abstract more precise information from the comparison would be unjustified, as it would place undue weight on the accuracy of the mixing-length predictions, and ignore the effect of possible adjustments of the other constants in the k-z model.

It is worth remembering at this point that the mixing-length results do receive some support from the experimental work of Sabin (see figure 1.3, and the accompanying discussion in section 1.3).

c) Knowledge of $Pr_{eff,k}$, and of the relation between C_2 and C_3 provided by equation 4.8-2 will limit the amount of further work required to determine the full set of constants. By paying particular attention to the results for high stream turbulence, one may hope, for example, to determine the best pair of values of C_2 and C_3 fairly easily and quickly.

4.9 Predictions of the total flow.

One obvious way to allow for interactions, between the central mixing layer and the outer ones on either side of it, is to apply the finite-difference procedure to the whole stream of moving fluid. Of the two turbulence models used in this investigation, the k-z model is clearly more suited to this particular task, as it is inherently able to predict the expected streamwise decay of turbulence in the free-stream regions. The LAYER-3 programme version was developed for these "overall" predictions.

In view of the greater complexity of the k-z calculations, and the fact that the experimental measurements did not extend right across the whole stream, it was decided that these predictions should start from a semi-idealised set of starting profiles supposed located at the

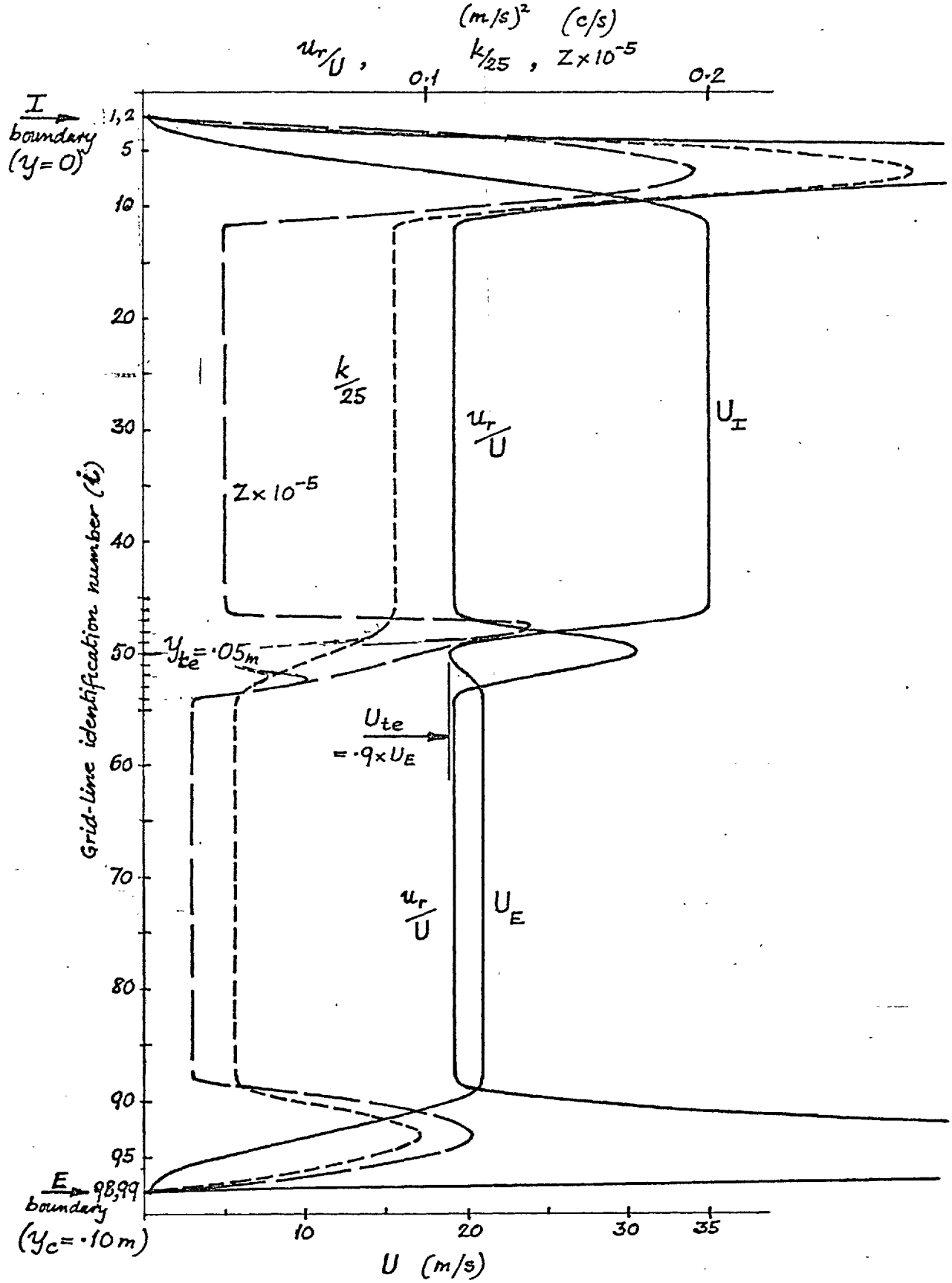


Figure 4.14 : Initial conditions for k-z predictions with LAYER-3 programme [for $\frac{U_E}{U_I} = 0.6$, $\left(\frac{u_r}{U}\right)_{IE} = 0.11$]

upstream end of the working section. These starting conditions are indicated by figure 4.14 and described in detail in appendix A.7. The velocity was assumed to be uniform across each free stream, and to vary sinusoidally in the central wake region and the two outer mixing layers. In the calculation of the initial values of k and z, use was made of the approximate expressions derived in section 2.6 by comparison with the mixing-length hypothesis. The parameters defining the central wake were chosen, by trial and error, to give general agreement between predicted and measured conditions at the first measuring station.

For the high turbulence cases (those simulating experimental runs with the turbulence grids in operation) the initial value of z in the free streams was calculated to coincide with the preferred frequency of the velocity fluctuations deduced from the energy spectrum, as described in section 5.8. For the low-turbulence cases the value 100 c/s was arbitrarily chosen.

Since, in these predictions, the central mixing layer formed only part of the whole stream, a large number of grid-lines was desirable; the chosen value of N was 96. The number of grid intervals spanned by the central mixing layer varied during the course of each prediction, and was usually between 15 and 30. The limits of the velocity and turbulence-intensity layers did not normally coincide; the limits of these layers

were located by separate sequences and the calculations of θ, η, etc., were carried out between the respective limits instead of across the whole stream, as was previously done.

Comparison of the results of early predictions, obtained with LAYER-3, and the experimental results, led to some further modifications of the model. These are described and discussed in section 6.3 et seq.

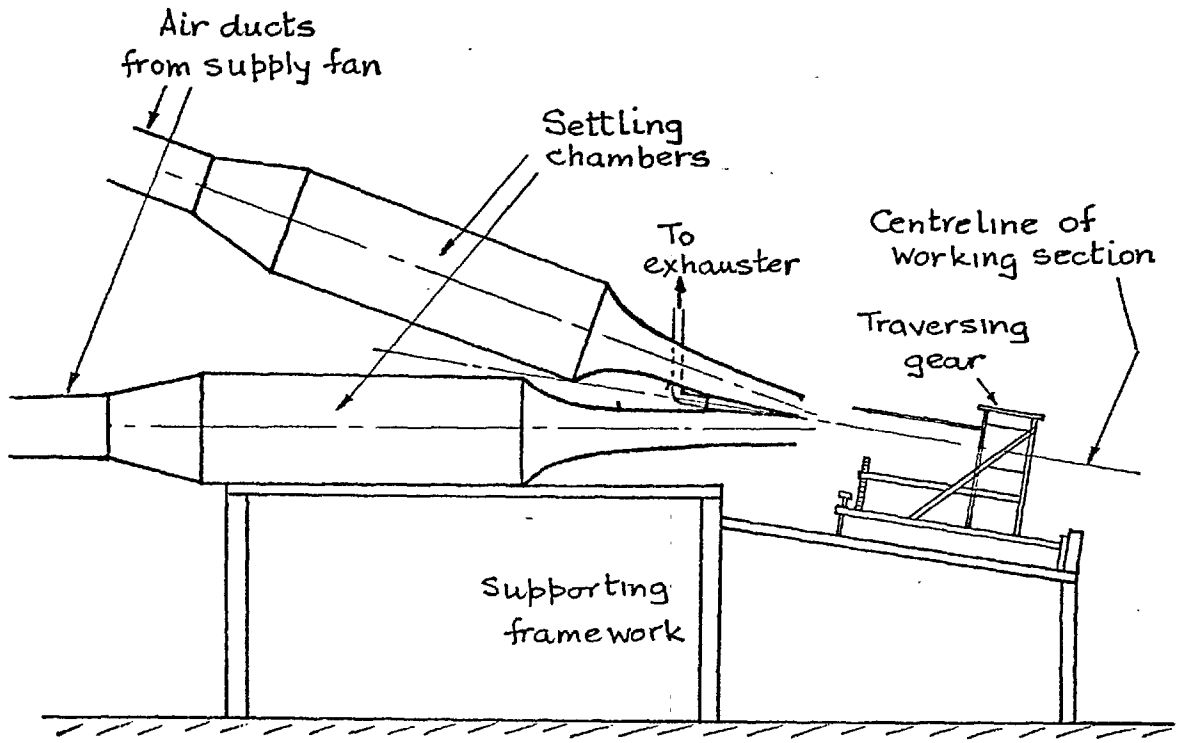


Figure 5.1 Diagram of apparatus.

5. EXPERIMENTAL WORK

5.1 General description of the wind-tunnel.

The general form of the apparatus used for the experimental work is shown by Fig. 5.1. The working section was immediately downstream of the junction of two nearly parallel ducts, and open to the atmosphere.

Each duct had a large settling chamber fitted with phosphor-bronze wire mesh screens to smooth the flow. From the outlet of each chamber a smoothly-faired "Perspex" contraction lead the air to the working section. The adjacent walls of the ducts were combined to form a sharp trailing edge. Upstream of this edge the inner walls of the ducts were made of porous phosphor-bronze sheet and formed a common suction box, connected by 2-inch pipework to a small vane-type exhauster. This arrangement allowed the boundary layers on the inner walls to be sucked away, so making the velocity at the beginning of the mixing region more uniform.

The air supplies for the two ducts were obtained from a centrifugal fan, which had a simple-flow-splitting flap incorporated in the outlet, so that the air delivered could be divided between the two ducts in any desired proportions. The whole of the fan and motor assembly was enclosed by filter cloth supported by a light metal framework, in order to reduce dust-contamination of the hot-wire anemometers used in the working section.

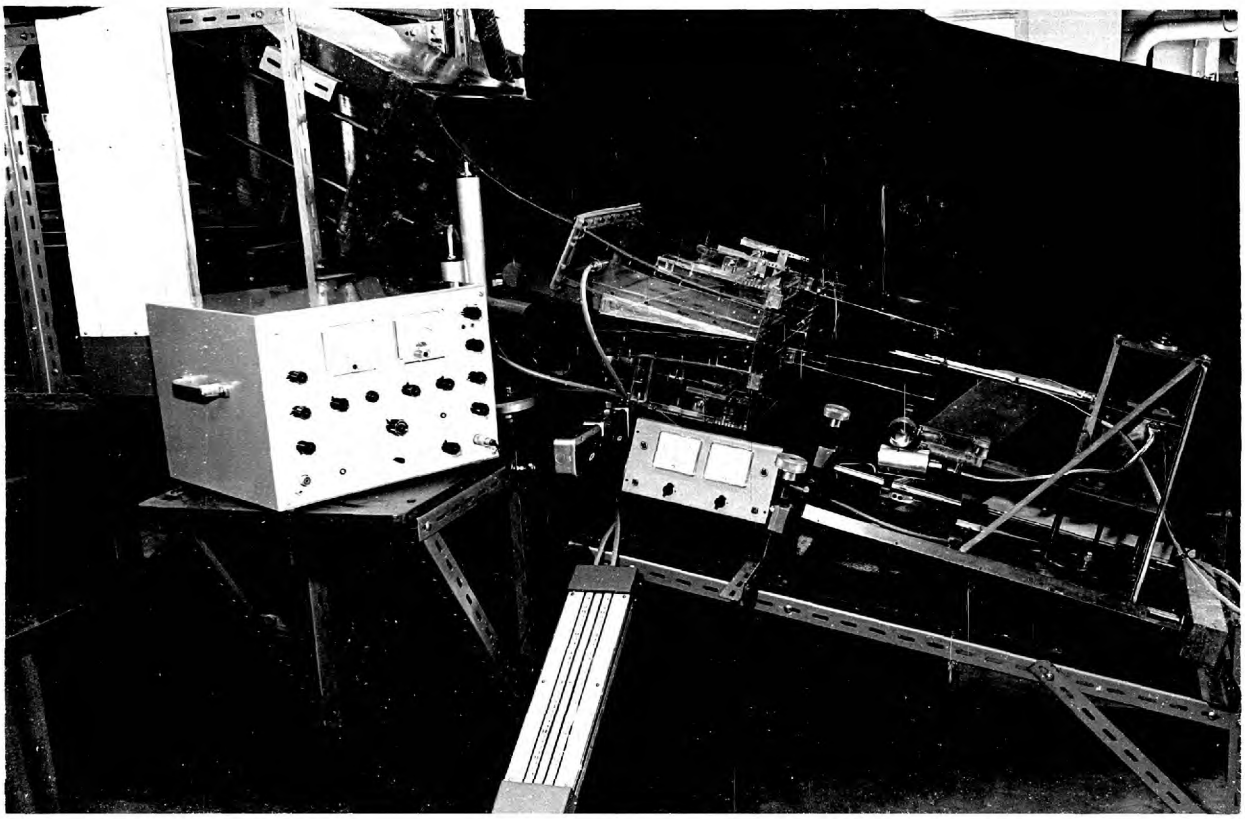


Figure 5.2

The two settling chambers and ducts were mounted rigidly on a bench, one above the other. For convenience the lower one was horizontal. The connecting ductwork was so shaped that the two air streams approached each other at a small angle (approximately 8.5^{o}), and the general direction of the mixed airstream was inclined downwards at about 15^{o} to the horizontal. The observations were carried out with air speeds between 33 m/s and 39 m/s in the faster stream, and speeds down to about 14 m/s in the slower stream depending on the velocity ratio required. The temperature in the working section differed only slightly from the ambient value, while the pressure was, of course, exactly atmospheric.

The apparatus was installed on a gallery in a medium-sized laboratory and discharged into a space of about 1000 m^3. Fig. 5.2 is a photograph of the apparatus, excluding the fan and the ductwork joining it to the settling chambers.

5.2 The working section and traversing gear.

The top and bottom duct walls were cut off level with the trailing edge of the common inner wall, while deep side walls extended downstream a distance of about 30 cm. (Note that the nearer side wall has been omitted from the photographs of the apparatus for clarity).

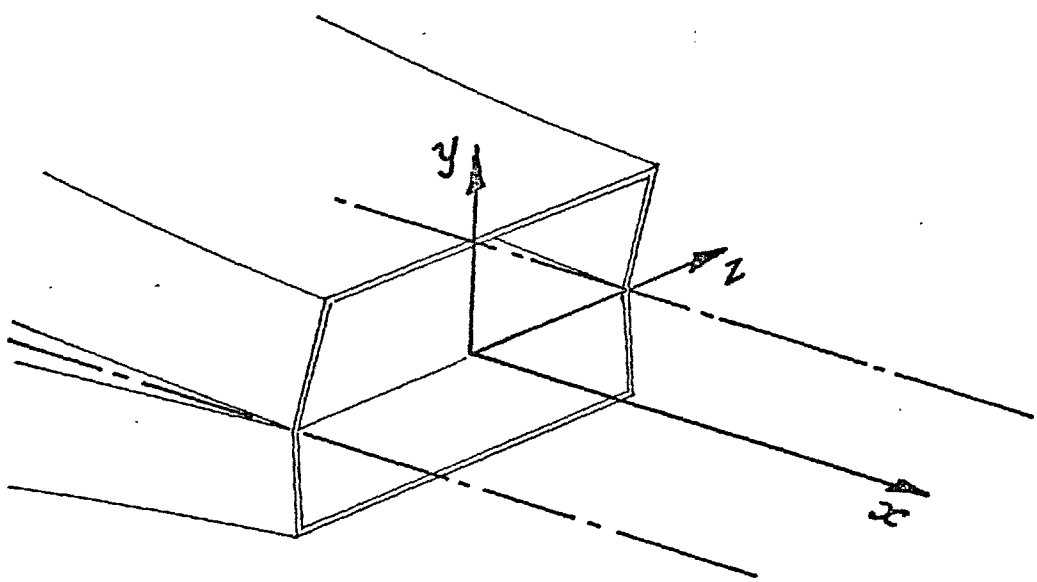


Figure 5.3

Coordinate system in working section.

These provided some protection from draughts, but their main purpose was to prevent the formation of mixing regions at the sides of the working section. The outlet of each duct measured 30 cm. by 5 cm.

Fig. 5.3 indicates the orthogonal co-ordinate system used to specify position within the working section.

The traversing gear was made mainly from heavy gauge stainless steel tubing and brass angle plate and bar. The base frame, which rested on a sloping extension of the main bench, incorporated two steel support tubes aligned in the x-direction. The main frame slid along these tubes and could be locked in any desired position by thumb-screws. The sensing instruments (hot-wire anemometer, pitot tube, and thermometer) were carried on an arm projecting forward from the instrument carriage, which moved up and down two steel tubes aligned in the y-direction and rigidly supported in the main frame; motion of this carriage was produced by a lead screw (20 threads per inch) chain-driven from a small hand-wheel.

The main frame was a rigid, triangulated structure, and the method for supporting the instrument carriage in the main frame, and the latter on the base frame, was kinematically correct. In order to reduce position error still further, the scale for measuring the y-position of the instruments was mounted almost vertically beneath them.

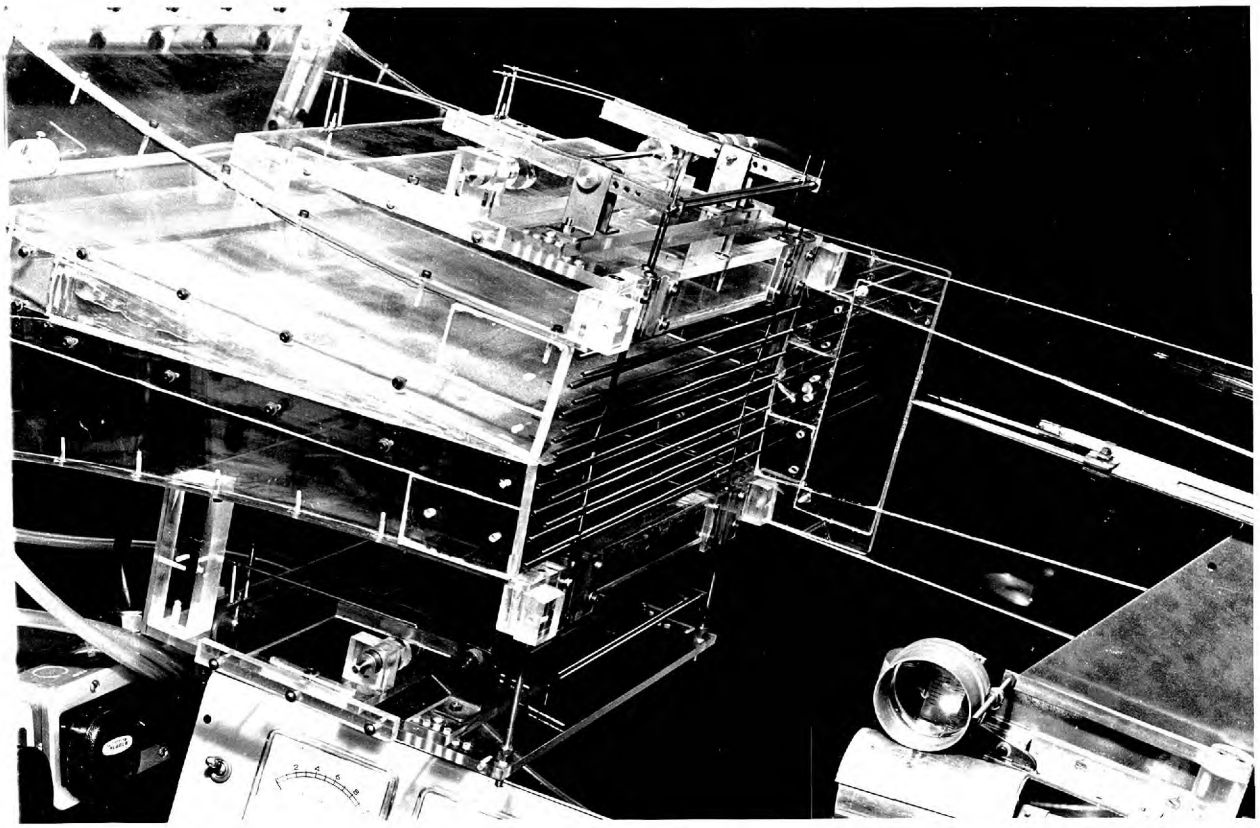


Figure 5.4

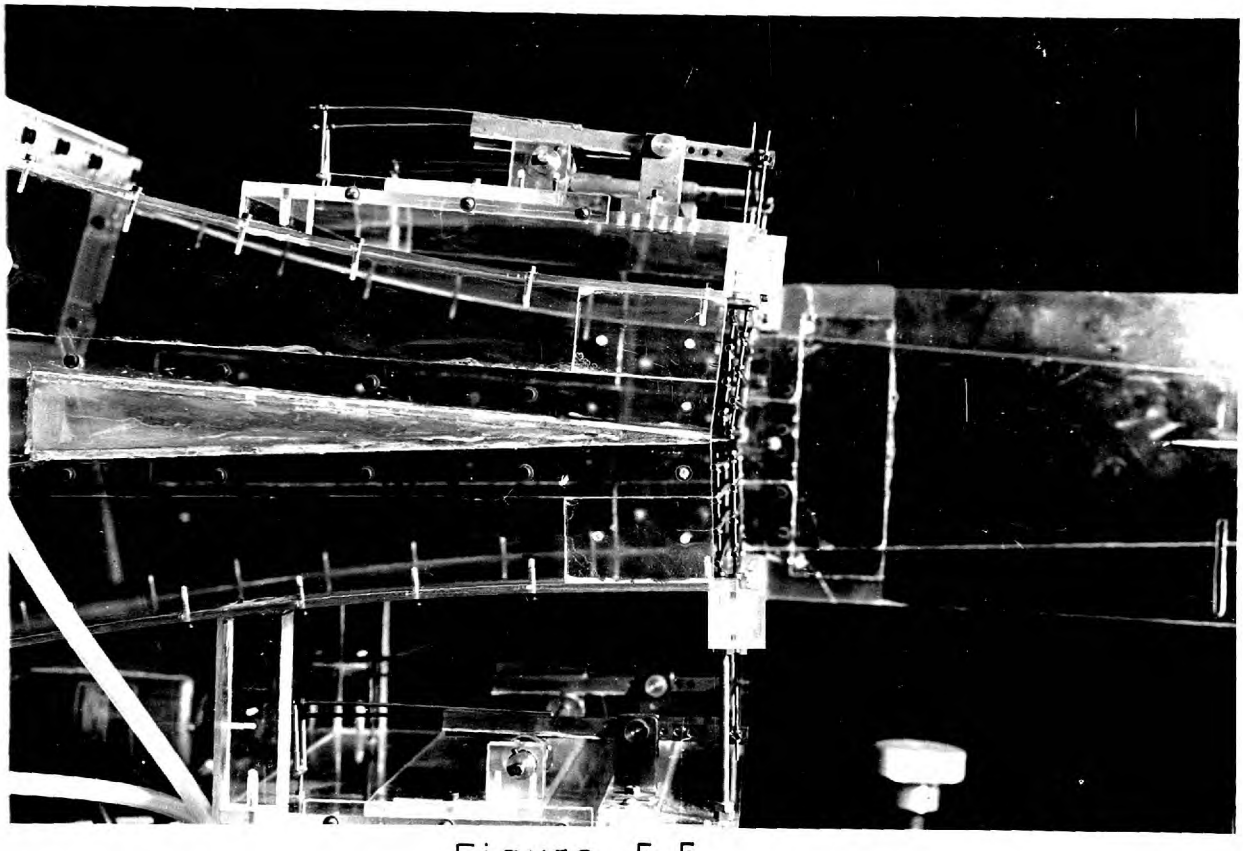


Figure 5.5

Normally the readings of stream conditions were taken in the central, vertical plane of the flow, involving measurement of x and y co-ordinates only. When required however (for checks on the two-dimensionality of the flow), readings at other values of z could be obtained by simply pushing the base frame sideways into the required position.

5.3 The method for increasing free-stream turbulence.

The air streams at the outlets of the ducts had turbulence intensities of about 0.6%. When required, higher intensities were produced by the oscillating grid systems illustrated in the photographs, Figs. 5.4 and 5.5. Each airstream had its own independent grid system. Each system comprised a pair of grids which had an oscillatory motion across the stream (in the y direction), the motions being half a cycle out of phase, so that at any instant the two grids in each pair were moving in opposite senses. The grids consisted of four or five small stainless steel tubes (3 mm. outside diameter) held together by 10 B.A. nuts on two threaded rods. Each grid was operated by a pair of cam-operated rocker arms, with adjustable fulcrum positions, the motive power being provided through a flexible drive shaft from a variable-speed electric motor.

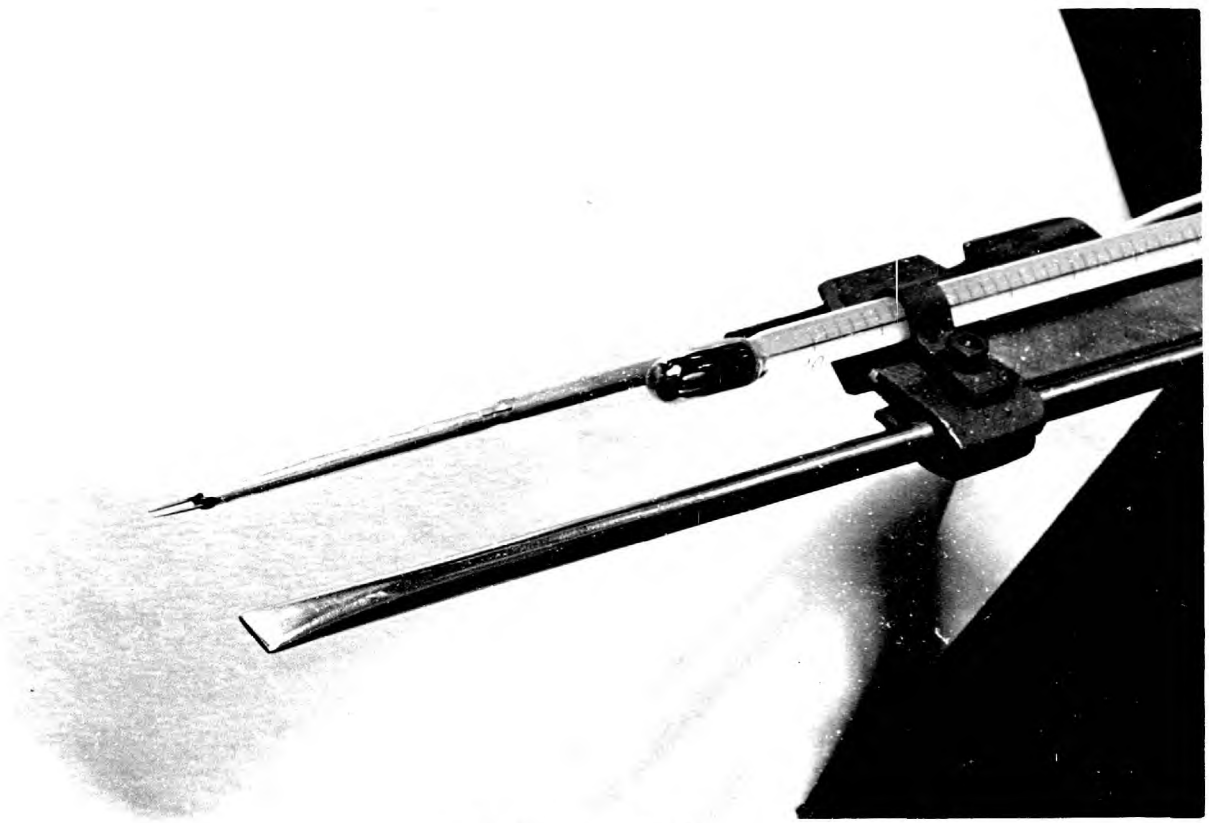


Figure 5.6

The spacings and mean positions of the tubes in each gridwere adjusted by trial and error to give what was judged to be the most uniform distributions of velocity and turbulence intensity obtainable at the beginning of the measuring section.

5.4 Instrumentation.

Apart from a few subsidiary observations, the measurements required in this series of experiments were of velocity and turbulence-intensity distribution throughout the mixing region and the adjacent free streams. These measurements were obtained by using the pitot tube and hot wire probe shown in Fig. 5.6.

The pitot tube was specially made for this rig, from stainless steel tube of 3.5 mm and 4.7 mm inside and outside diameters, flattened at the forward end to produce an opening 5.8 mm (z dimension) by 0.38 mm (y dimension). The front of the probe was rounded off by hand to a smooth profile. This pitot tube was calibrated in a separate wind-tunnel against a standard N.P.L. elliptic profile tube. The disagreement between the two was found to be nowhere more than 0.5% of indicated velocity, within the range of the main experiments. In use the pitot tube was connected to a T.E.M. micromanometer filled with water and graduated in intervals of 0.2 mm.

The hot-wire probe used was a DISA miniature type (55A25), having a tungsten wire of length 1.2 mm and diameter .005 mm. The probe was always used with the wire aligned in the z-direction. It was connected to a standard DISA electronic box (Type 55D01) and operated in accordance with the manufacturers instruction manual.

Other instruments used in the performance of normal tests were:-

A mercury-in-glass thermometer, mounted on the arm carrying the pitot tube and hot-wire probe.

Pitot tubes fixed in each of the duct contractions, and connected to sloping manometer, to allow the constancy of the flow rates to be checked; one of these can be seen in the top left-hand corner of Fig. 5.4.

A Hasler hand tachometer for measuring the speed of the camshaft driving the oscillating grids.

A Fortin barometer.

5.5 Scope of experimental results.

Nine different combinations of flow conditions were observed; for each of three velocity ratios, approximately 0.4, 0.6, and 0.8, the apparatus was run without the turbulence grids, and with these grids in operation, first with four bars in each, and then with five bars. Pitot and hot-wire traverses were made at

Table 5.1 : Experimental Conditions.

RUN NUMBER	No of grid bars	Traverse station				
		$x = 5$ cm	$x = 10$ cm	$x = 15$ cm	$x = 20$ cm	$x = 25$ cm
		U_I $\left(\frac{u_r}{U}\right)_I$	U_I $\left(\frac{u_r}{U}\right)_I$	U_I $\left(\frac{u_r}{U}\right)_I$	U_I $\left(\frac{u_r}{U}\right)_I$	U_I $\left(\frac{u_r}{U}\right)_I$
		U_E $\left(\frac{u_r}{U}\right)_E$	U_E $\left(\frac{u_r}{U}\right)_E$	U_E $\left(\frac{u_r}{U}\right)_E$	U_E $\left(\frac{u_r}{U}\right)_E$	U_E $\left(\frac{u_r}{U}\right)_E$
		U_I/U_E	U_I/U_E	U_I/U_E	U_I/U_E	U_I/U_E
5/57	5		35.9 .069 13.9 .087 0.39	35.1 .052 14.0 .080 0.40	34.8 .044 14.0 .100 0.40	
4/48	4		36.9 .090 14.8 .103 0.40	36.2 .065 14.8 .085 0.41	36.0 .053 14.6 .096 0.41	
0/58	0	38.3 .005 15.1 .010 0.40	38.4 .006 15.3 .016 0.40	38.4 .009 15.3 .031 0.40	38.3 .014 15.3 .052 0.40	
5/54	5		34.7 .075 20.6 .083 0.60	33.8 .053 20.4 .063 0.60	33.7 .046 20.2 .065 0.60	
4/49	4		35.9 .082 21.2 .091 0.59	35.2 .061 20.9 .068 0.59	35.0 .051 20.8 .064 0.59	
0/59	0		36.6 .0055 21.8 .009 0.60	36.5 .0075 21.8 .013 0.60	36.5 .011 21.8 .023 0.60	
5/53	5		32.7 .083 27.0 .084 0.83	32.3 .058 26.7 .061 0.83	32.0 .047 26.6 .053 0.83	
4/47	4		33.2 .083 27.6 .083 0.83	33.0 .058 27.3 .063 0.83	32.8 .047 27.1 .053 0.83	
0/60	0		34.5 .006 27.2 .008 0.79	34.7 .0075 27.5 .012 0.79	34.6 .010 27.5 .015 0.79	34.6 .015 27.6 .021 0.80

Velocities quoted in metres/second.

distances of 10 cm, 15 cm, and 20 cm downstream from the trailing edge of the common duct wall; an extra traverse was carried out in two runs where it appeared that useful additional results would be obtained.

The complete set of running conditions is listed in Table 5.1. The values of U_I and U_E given here are the velocities for the points taken as the outer limits of the velocity mixing layer. A routine for locating these points is contained in the data-processing programme (see appendix C) the final selection of these points is, ultimately and necessarily, a somewhat subjective process. The relative turbulence intensities quoted are the smoothed minimum values in each free stream, and occur at short distances outside the velocity mixing layer.

The experimental results are presented graphically in three sets of figures, 5.7 to 5.9, 5.10 to 5.18, and 5.19 to 5.21. Each of figures 5.7 to 5.9 consists of three diagrams drawn for one of the three velocity ratios. In the lower one the momentum thickness θ, is plotted against streamwise distance x, thus showing the growth of the layer with each of the three grid arrangements. The upper diagrams show the three distributions of velocity difference ratio and relative turbulence intensity for the middle traverse station (x = 15 cm).

Figures 5.10 to 5.18 display the three main velocity-ratio profiles for each of the nine runs. The positions of the points taken as the edges of the velocity mixing layer are indicated by short bars labelled I and E, and the values of the stream velocities U_I and U_E are also marked on the diagrams. In preparation for later comparison and discussion, some velocity profiles predicted by the finite-difference method have been added at x = 20 cm.

Figures 5.19 to 5.21 show the observed profiles of relative turbulence intensity.

5.6 The effect of stream turbulence level on spreading rate.

The lower graphs in figures 5.7 to 5.9 show quite clearly that for each velocity ratio the increased turbulence produced by the grids causes an increase in the rate of spread of the mixing layer; the prime objective of the experimental investigation has thus been achieved. Further examination shows also that the increase in the spreading rate is proportionately greatest for the highest velocity ratio.

These graphs, read in conjunction with Table 5.1, also show that the results for four-bar and five-bar grids are not very different, and that such differences as do occur at not entirely consistent. At U_E/U_I of 0.4 and 0.6, increasing the number of grid bars decreases the stream turbulence intensity and the value of θ at

x = 10 cm, but has little effect on $d\theta/dx$; for U_E/U_I = 0.8, on the other hand, the extra bar has an insignificant effect on the turbulence levels but reduces the spreading rate

5.7 The turbulence-intensity and velocity profiles.

The middle graphs in figures 5.7 to 5.9 demonstrate another marked change produced by the grids, one which was not originally expected. When the free-stream turbulence level is increased, the intensity increases right through the layer as well. For U_E/U_I = 0.8, the increase is practically independent of y, but for the lower ratios appears to be even larger at the centre than at the edges of the layer.

In contrast, the effect of the grids on the shape of the velocity profile is very small indeed; any consistent differences which may exist are masked by the experimental scatter. In addition, near the edges of the layer, where the differences caused by stream turbulence would be expected to be greatest, there is the extra masking effect of local irregularities in the free-stream velocity distribution.

These comparisons have been made at the middle of the measurement section, at x = 15 cm. The choice of this station is a compromise between two conflicting desires - on one hand to be sure that the mixing layer

Table 5.2: Experimentally-derived values of profile shape factors at $x = 15$ cm.

Run Number	Approx. Velocity Ratio U_E/U_I	No. of grid bars	$\frac{y_{nom}}{\theta}$	$\frac{y_{ms}}{\theta}$	$\frac{\eta}{\theta}$
5/57	0.4	5	4.6	4.8	4.6
4/48		4			4.9
0/58		0			5.7
5/54	0.6	5	4.55	4.6	4.3
4/49		4			4.8
0/59		0			5.4
5/53	0.8	5	4.5	4.6	3.7
4/47		4			5.3
0/60		0			5.1

was fully established, on the other to avoid excessive distortion caused by interference from the outer mixing layers, which are discussed in sections 5.9 and 5.10.

Experimental values of the profile shape factors y_{nom}/θ, y_{ms}/θ and η/θ were determined, by measurement, from the velocity and relative turbulence intensity profiles of figures 5.7 to 5.9, in accordance with their definitions previously quoted (sections 2.3 and 4.7). They are listed in Table 5.2.

5.8 Free-stream energy-frequency spectra.

To gain some idea of the character of the turbulence generated by the grid system, a series of measurements were made with a single-wire anemometer (aligned in the z-direction as for the main observations), in conjunction with a Wayne-Kerr frequency analyser (operating with a constant band-width of 1 c/s). The results of measurements taken at four difference vertical positions across one of the duct outlets, a short distance (2.5 cm) downstream from the grid, are presented in the form of energy-frequency spectra in figure 5.22. E_f is twice the specific turbulence kinetic energy associated with frequency f, so that:

$$\int_0^\infty E_f df = u_z^2 \qquad (5.8\text{-}1)$$

where u_z is the root-mean-square value of the fluctuating

velocity component. The outstanding feature of these spectra is the single energy peak at a frequency of about 2400 c/s. Allowing for the logarithmic form of the graphs, they show that about 90% of the total turbulence kinetic energy in the stream was associated with a quite narrow band of frequency, between 2 kc/s and 3 kc/s. During these measurements, the grids were operating in the usual way, i.e. oscillating in transverse planes at a frequency of about 8.3 c/s.

Curves of similar shape, but indicating an even greater concentration of energy at the preferred frequency, were obtained from measurements taken when the grids were stationary; the preferred frequency was again about 2400 c/s.

The Reynolds number of the flow around the grid tubes, based on mean stream velocity U and tube diameter, d, was 6200; the corresponding value of the Strouhal number, fd/U, is 0.18 (from e.g. reference 26). This indicates a vortex-shedding frequency of 1950 c/s which differs from the observed preferred frequency by 18%. Since the difference is not accounted for by the transverse motion of the grids, it is presumably the result of the particular configuration of tubes, and of changes occurring in the structure of the disturbance between the grids and the measuring station. Whatever the cause, there is little doubt that the main source of turbulence within the free streams is the shedding of vortices from the grid tubes.

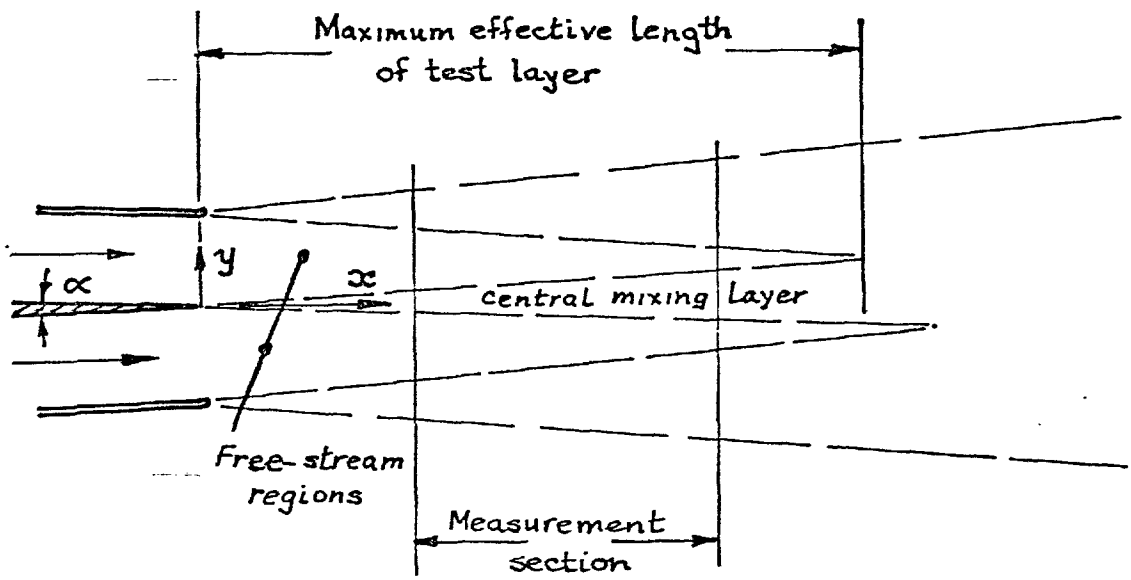


Figure 5.23

Inner and outer mixing layers.

5.9 Conditions in the working section.

Since the working section was open to the atmosphere of the top and bottom, there were altogether three mixing zones as indicated in figure 5.23; this was an important factor in the execution and interpretation of the measurements.

For the convenience of specification, and of comparison with the theoretical predictions, the flow in the working section should satisfy the following conditions:

1) Steady (in the time-mean sense)
2) Isothermal
3) Isobaric
4) Plane, two-dimensional
5) Uniform free-stream velocity
6) Free-stream turbulence independent of y (in each stream).

It can be expected, from the general nature of the apparatus, that the first three of these conditions, at least, are closely satisfied, and these expectations were confirmed by observation. Minor fluctuations of pitot manometer reading (usually up to about $\pm 1\%$), of the kind usually experienced with turbulent flow, were observed, but were normally damped out by an adjustable restriction in the tube connecting the pitot tube and manometer. The common source of air ensured that the two air streams were at essentially equal temperature; the only variations noted were the result of slow change of ambient temperature within the laboratory. No measurements of static pressure

were made, but in an open working section the only possible variation of time-mean pressure is a transverse one associated with curvature of the free streamlines; no allowance for such curvature was made in the present investigation.

To check the uniformity and two-dimensionality of the flow, pitot and hot-wire readings were taken at positions 2 cm and 4 cm on either side of the central plane of the working section, for each of two values of x and at three vertical stations - one in each free stream, and the third near the middle of the central mixing region; these readings were taken for two velocity ratios, both with and without the turbulence grids. Fig. 5.24 shows the observed velocity distributions; the ordinates of the points are values of the ratio of the local velocity, U, to the velocity at x = 10 cm, z = 0, in the faster free stream, $U_{I(10,0)}$. For precisely uniform two-dimensional plane flow each pair of curves, for x = 10 and 20 cm, would coincide in one straight horizontal line; in fact the upper and lower pairs in each case come very close to this condition, and indicate a very satisfactory degree of uniformity in the z direction within the free streams. This test is not, however, sensitive to transverse curvature of the flow (in the yz plane); the existence of such curvature is shown by the middle pairs of curves. The magnitude of this curvature can be estimated from the velocity

TABLE 5.3.

Velocity ratio U_E/U_I	Estimated cross-stream curvature (in z-direction)	
	Without grids (mm^{-1})	With grids (mm^{-1})
0.4	·002	·005
0·8	·0013	·0014

variation shown by these curves, and knowledge of the velocity gradient $\partial U/\partial y$, obtained from the standard traverses. Its value for the various flow conditions is given in Table 5.3. Clearly the departure from pure plane flow increases as the velocity ratio decreases, but even in the worst case it seems unlikely that any significant effect has been produced on, for example, the velocity profile shape.

A combination of factors prevented completely uniform conditions being achieved in the two free-stream regions:

a) The impossibility of obtaining uniform velocity and turbulence intensity at the outlet of each air duct. When the grids were not in position, the degree of non-uniformity was very small. With boundary-layer suction through both surfaces of the dividing wall, the momentum thickness of the residual wake at its trailing edge was about 0.8 mm.

With the grids in place, the variations were more marked. The profiles obtained were, nevertheless, considerably better than those achieved in earlier attempts with grids of fixed bars. Even when these fixed grids were so constructed that the spacing of the bars could be adjusted, it was found impossible to avoid general distortion of the velocity profile in addition to the inevitable ripple corresponding to the wakes of individual bars;

(similar distortions of the mean profile were reported by Baines and Peterson, reference 27, after tests on flow through various types of screen). The object in designing the oscillating grids was to spread the disturbance over the whole stream, and it was found to be relatively easy to adjust the relative positions of the bars in these grids to give acceptable profiles. Figure 5.25 compares typical velocity profiles produced at x = 5 cm by the various types of grid tried. The main experimental velocity profiles are shown in figures 5.10 to 5.18 inclusive.

b) The inherent turbulence-dissipation mechanism operating in the free streams downstream from the grids, and the interference from the adjacent mixing layers. From the measurements taken it is impossible to separate these two effects. The profiles all indicate regions of nearly-uniform velocity on either side of the central mixing layer. When the grids were operating, the irregularities in the free streams tended to smooth out and the general level of turbulence decreased with x. Without the grids, however, the turbulence intensity outside the mixing layer increased between the first and last measuring stations. The measured turbulence-intensity profiles are shown in figures 5.19 to 6.21; they indicate that

in all cases the turbulence layers spread more rapidly than the velocity layers, so that the free-stream regions are considerably less extensive than the velocity profiles alone suggest.

A final set of commissioning measurements were made with a yawmeter traversed over the central x-z plane of the working section. It was found that, within the area covered by the main traverse stations, the direction of the air stream did not differ by more than $\pm 2^{o}$ from the mean, so that pitot-tube errors arising from this source could be expected to be very small.

5.10 The choice of working-section dimensions and limitation of the velocity ratio.

The size and shape of the working section were the result of necessarily rather arbitrary decisions. The combined area of the air supply ducts follows from the available air flow rate (itself a somewhat arbitrary choice), and the decision to operate with mean air velocities of about 25 m/s to reduce doubts about the possible effects of stray air currents on the development of the flow. The aspect ratio of the ducts (6:1 for each duct, or 3:1 for the two together) was chosen in the expectation that this would sufficiently minimise end effects.

The position of the first traversing station (x = 10 cm) allows sufficient distance for the residual trailing-edge wake from the dividing wall to be completely eradicated, and for the ripple in the free stream velocity profile, produced by the grids, to have decreased to acceptable size. The distance between the first and last measuring stations (also 10 cm) allows sufficient distance to examine the development of the central mixing layer without serious interference from the outside mixing layers.

Because the spreading rate of the central layer varied with the stream velocity ratio U_E/U_I, so too did the maximum effective length of the working section. For the higher turbulence intensities, the free-stream region on the low-speed side, as indicated by the velocity profile, only just reached to x = 20 cm when the velocity ratio was 0.4, and this value was taken as the practical lower limit of U_E/U_I for the present apparatus. In establishing this limit, the turbulence intensity distribution may be ignored since in the corresponding theoretical calculations the turbulence intensity can either be specified arbitrarily as a boundary condition of the velocity layer (in the mixing-length predictions), or else does not appear specifically as input data (in the k-z predictions); on the other hand, in the absence of a streamwise pressure gradient, a uniform free stream velocity is an essential feature of the calculations.

Another reason for limiting the velocity ratio at the lower end concerns the impingement angle of the two streams (marked α in figure 5.23). Entrainment into the mixing layer requires a velocity component in the $\pm$ y direction; although the two streams are nominally parallel they should, therefore, be inclined at an angle, as was, in fact, the case in these experiments. The ideal impingement angle varies with both velocity ratio and stream turbulence, and could not be predicted in advance. It can, however, be shown qualitatively to remain small until U_E/U_I approaches zero, when it increases rapidly to 90^o.

Ideally the upper limit for U_E/U_I is unity. As this value is approached, however, the uncertainty in the values of U_E and U_I become increasingly serious, leading to proportionately large uncertainty in the value of (U_I-U_E) and hence of θ, y_{nom}, y_{ms}, etc. For this reason no readings were taken with U_E/U_I higher than 0.83.

6. COMPARISON OF EXPERIMENTAL RESULTS AND PREDICTIONS

6.1 Introduction.

It is now possible to compare the observations with the results of the calculations designed to reproduce them, i.e., with the output from the NEWMOD-F and LAYER-3 programmes. With the available measurements, the comparison can be based on the following properties:-

the θ-x distributions;

the velocity profile shape factors, y_{nom}/θ and y_{ms}/θ;

the turbulence profile shape factor, η/θ;

and a few less easily quantifiable features of the flow pattern.

Following the order of presentation in the previous chapters, the comparison is made first with the predictions obtained with the modified mixing-length programme. The results produced by LAYER-3 in its present form are then considered, and lead to a discussion of some ideas for further modification of the k-z model.

Before proceeding to undertake these comparisons, however, it is worth while considering the validity of the operation.

Concerning the comparison of measured and predicted time-mean velocities (and, of course, derived quantities such as the momentum thickness and velocity profile shape factors), there need be little doubt. The measurements were made exclusively by a pitot tube of fixed

direction, and because of the limitation of overall velocity ratio, the streamline direction varied by less than $\pm 2^{o}$ (as reported in section 5.9), and only negligible errors should be expected from this case. The present investigation is therefore free of the difficulties arising in the measurement of free flows in stationary surroundings, where the fluid direction varies through 90^{o} near the low-speed side of the layer. The error in time-mean velocity arising from the velocity fluctuations is also probably small, although there is some doubt about its actual mignitude (Hinze, section 2.11 of reference 23). On the theoretical side, a high degree of accuracy has been achieved by using an adequate number of grid-lines for the computations (see section 4.4 and appendix A.10). The measured and predicted values of velocity can, therefore be directly compared.

There is more doubt about the comparability of the relative turbulence intensity values. According to Hinze (section 2.6 of reference 23) again, the linear relationship implied by equation C.4-2, in the calculation of turbulence intensity, is acceptable for intensities up to 25% (the highest value achieved in the present investigation). However, the signal produced by a single hot wire aligned in the z-direction, although mainly connected with velocity fluctuations in the x-direction, is also affected by fluctuations in the y-direction, and so does not give a simple measure of the fluctuating

velocity field. The deviation from the true value of $\overline{u^2}$ depends on the relative sizes of $\overline{u^2}$ and $\overline{v^2}$, and also products of these x and y components, such as $\overline{uv^2}$, $\overline{u^2v^2}$ .... etc. Hinze shows that for the particular case of isotropic turbulence with normally-correlated u and v components having Gaussian distributions, the deviation is approximately +10% for $\frac{u}{U} = 0.2$. In the absence of detailed knowledge of the turbulence structure, no correction has been applied to the experimental values reported in this thesis; it seems likely, however, that the turbulence intensity profiles should be modified by a slight flattening of the central peaks, of the order of 10% for $\frac{u_r}{U} = 0.2$, with the correction proportional to $(\frac{u_r}{U})^2$. With this qualification (and others directly connected with the operational accuracy of the hot-wire equipment) the experimental values identified as $\frac{u_r}{U}$ on the graphs can be equated to the x-wise relative intensity component, $\frac{\overline{u^2}}{U}$.

A similar problem arises in the interpretation of the predicted values. The k-z model of turbulence does not differentiate between the components of the fluctuating motion in different directions, and the relative turbulence intensity calculated in accordance with equation 2.4-5 is the mean value; it can be compared directly with experimental values of $\frac{\overline{u^2}}{U}$ only if it is assumed that one-third of the turbulence kinetic energy is associated with the x-direction.

Measurements of $\overline{u^2}$, $\overline{v^2}$ and $\overline{w^2}$, (reported in reference 28) suggest that the proportion of total turbulence

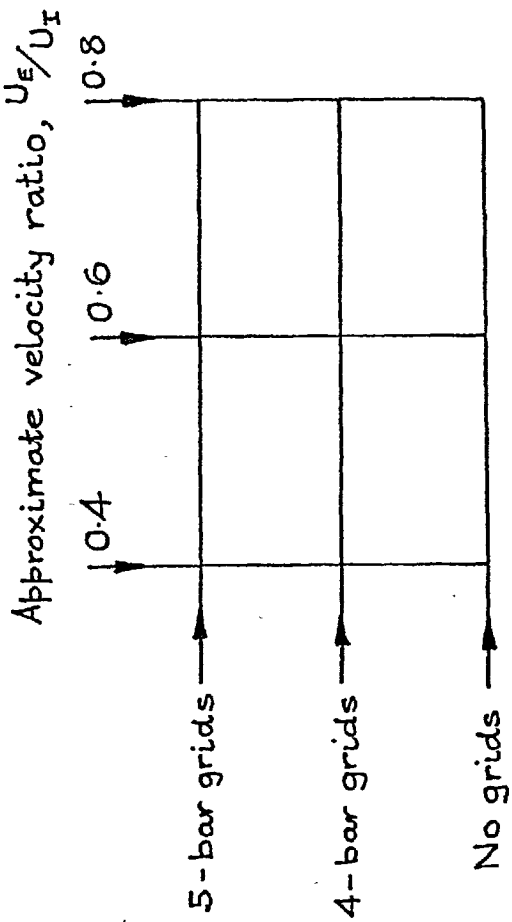


Figure 6.2

Disposition of graphs in Figures 6.1 and 6.2

kinetic energy associated with the x-direction varies between roughly $\frac{1}{4}$ and $\frac{1}{2}$, being lowest at the high speed edge, and highest at the low speed edge of a mixing layer. This suggests that errors of up to about $\pm$18% can arise from the use of equation 2.8-5 to predict the x-wise turbulence intensity. However, the results of reference 28 were obtained in the mixing layer between a stationary atmosphere and the potential core region of a plane jet with a fairly low turbulence level (about 1%). It would be unwise to use them to draw firm conclusions in the present investigation, particularly for the cases with high free-stream turbulence.

6.2 Comparison with the mixing-length predictions: spreading rate.

Figure 6.1 is an array of nine graphs, one for each of the experimental runs, arranged in accordance with the diagram opposite, figure 6.2. The points on the graphs indicate the value of momentum thickness obtained from:

a) the experimental velocity profiles;

b) the predicted velocity profiles using the NEWMOD-F programme (starting from the measured upstream velocity profile, as described in Appendix A·4) incorporating the MU1 effective viscosity formulation, with $\lambda = 0.5$, $A_1 = 1.05$, $B = 0.5$;

c) the velocity profiles predicted in the same way, but using the unmodified Prandtl mixing-length hypothesis, i.e., with A = 0.

The values of λ , A_1, and B used in the MU1 equation (equation 2.2-4) were, of course, originally unknown. The final values were chosen after a trial-and-error process requiring predictions to be carried out using several alternative sets. The following simple method for assessing the discrepancy between measurement and prediction was used:

The measured and predicted increases in θ between any two stations were expressed as a ratio

$$\frac{\Delta\theta_{pred}}{\Delta\theta_{exp}} = 1 + \varepsilon \qquad (6.2\text{-}1)$$

where ε indicates the relative size of the discrepancy. The value of ε was calculated between the upstream station and each downstream station for each run. The overall degree of fit between theory and experiment is expressed by the arithmetic mean, ε_m, and the root-mean-square value, ε_r, of the whole set of ε's.

Various combinations of λ , A_1, and B were tried until an acceptably small value of ε_m was obtained; it would, of course, be possible by further trial and error to find a set of constants for which ε_m was

TABLE 6.1 Values of prediction errors ε, ε_m and ε_r

Range of x (cm)	Prandtl			MU1			MU2		
	Approximate velocity ratio, U_E/U_I								
	0.4	0.6	0.8	0.4	0.6	0.8	0.4	0.6	0.8
	ε for 5-bar-grid runs :-								
10-15	-.48	-.57	-.67	-.00	+.22	-.33	-.05	+.36	+.65
10-20	-.51	-.64	-.82	-.09	-.04	-.21	-.11	+.03	+.48
	ε for 4-bar-grid runs :-								
10-15	-.42	+.60	-.89	+.20	+.18	+.19	+.29	+.35	-.01
10-20	-.46	-.60	-.86	+.06	+.12	+.11	+.12	+.25	+.08
	ε for no-grid runs :-								
10*-15*	-.06	-.20	-.32	+.05	+.02	-.04	-.05	-.21	-.28
10*-20*	-.09	-.13	-.39	+.06	+.13	-.02	-.08	-.13	-.32
10*-25*	-.21		-.37	+.05		-.01	-.20		-.22
* 5 cm less for $U_E/U_I \approx 0.4$									
ε_m	-.46			+.03			+.05		
ε_r	.52			.14			.27		

For Prandtl predictions, $A = 0$ (unmodified mixing length hypothesis)

For MU1 , , $A_1 = 1.05$, $B = 0.50$

" MU2 , $A_2 = 2.0$

$\lambda = 0.50$ throughout.

Predictions performed with NEWMOD-F programme.

zero, but for the present purpose it is sufficient that it is small compared with ε_r.

The same process was repeated with the MU2 shear expression, equations 2.2-5. The results shown in figure 6.3 are for $\lambda = 0.5$, $A_2 = 2.0$.

The values of ε for all three of the mixing-length laws are tabulated in Table 6.1 opposite; the corresponding values of ε_m and ε_r are also shown. The superiority of both the MU1 and MU2 modifications over the original Prandtl hypothesis is immediately obvious from this table, and from the graphs in figures 6.1 and 6.3.

Additional evidence of the superiority of the MU1 version is provided by figures 5.10 to 5.18, where the velocity profiles predicted for the last traverse station ($x = 20$ cm) have been drawn for direct comparison with the experimental profiles.

Further examination of the graphs of spreading rate and their associated discrepancy values leads to two further conclusions:

a) There are significant inconsistencies in the experimental values of θ; almost certainly the main factor here is the non-uniformity of free-stream velocity, and the resulting difficulty in the assignment of values to U_I and U_E.

b) The MU1 viscosity formulation produces closer agreement with the experimental results than MU2

TABLE 6.2 Values of shape factors $\frac{y_{nom}}{\theta}$, $\frac{y_{ms}}{\theta}$ and $\frac{\eta}{\theta}$ from mixing-length predictions and experimental results

Run No.	U_E/U_I (approx)	MU1 $\frac{y_{nom}}{\theta}$	MU1 $\frac{y_{ms}}{\theta}$	MU1 η/θ	Experiment $\frac{y_{nom}}{\theta}$	Experiment $\frac{y_{ms}}{\theta}$	Experiment η/θ	MU2 $\frac{y_{nom}}{\theta}$	MU2 $\frac{y_{ms}}{\theta}$
5/57	0.4	4.66	4.92	6.04	4.6	4.8	4.6	4.56	4.60
4/48		4.65	4.87	6.33			4.9	4.56	4.54
0/58		4.70	5.04	5.37			5.7	4.70	5.06
5/54	0.6	4.60	4.79	7.30	4.55	4.7	4.3	4.55	4.51
4/49		4.60	4.76	7.55			4.8	4.55	4.50
0/59		4.68	5.02	5.69			5.4	4.70	5.07
5/53	0.8	4.52	4.47	8.23	4.5	4.6	3.7	4.49	4.29
4/47		4.53	4.52	8.19			5.3	4.48	4.35
0/60		4.62	4.81	5.98			5.1	4.51	483

does, the difference between the ε_r's for the two models being considerably greater than the ε_m's. The most consistent feature of the comparison is that MU2 underestimates the effect of small levels of free-stream turbulence, while except at $U_E/U_I \approx 0.8$, MU1 overestimates the effect, but to a smaller extent. Although it isn't possible to draw the experimental equivalents of figures 4.3 and 4.4, the actual effect of varying $(u_r/U)_{IE}$ appears to be closer to the former than the latter.

6.3 Comparison with the mixing-length predictions: velocity and turbulence-intensity profiles.

As has been previously remarked, the velocity profiles alone do not provide much help in assessing the merits of the various shear laws. This point is well shown by the values of y_{nom}/θ and y_{ms}/θ listed in Table 6.2. The two sets of predicted values of y_{nom}/θ agree almost equally well with the experimental ones. The values of y_{ms}/θ for the MU1 version are closer to the measured ones than those for MU2, but when allowance is made for the inevitable uncertainty associated with the experimental results, the agreement of the MU2 values is probably also acceptable. Perhaps the most significant feature of this comparison is that the predicted changes in the shape factors with $(\frac{u_r}{U})_{IE}$ are barely, if at all, discernible in the experimental profiles (see figures 5.7, 5.8 and 5.9).

A quite different picture emerges when attention is turned to the distributions of relative turbulence intensity. As already indicated in section 4.3, the curves produced by the MU2 version are basically different in form from those for MU1 and also from the experimental ones, so much so that the concept of "excess relative turbulence intensity thickness" is inapplicable for the high stream turbulence cases. Figure 6.4 shows the two predicted profiles compared with the experimental one for a typical set of flow conditions. The defects of the MU1 version are relatively unimportant. The predicted height of the profile peak is too small, and there are discontinuities at the boundaries of the layer. In addition, as Table 6.2 shows, the predicted value of η/θ increases with the stream turbulence level, whereas the experimental one decreases.

6.4 The k-z predictions with uniform Pr_{eff}.

Two sets of results obtained with the LAYER-3 programme are presented in figures 6.5, 6.6, and 6.7. These computer runs were made as described in section 4.9 and appendix A.7, with the following values for the constants:

	C_μ	C_D	C_1	C_2	C_3	$Pr_{eff,k}$	$Pr_{eff,z}$
Run L3/1	1.0	0.1	3.0	.085	.56	0.7	0.7
Run L3/2	1.0	0.1	3.0	.0935	.63	0.7	0.7

TABLE 6.3. Shape factors for $x = 15$ cm in k-z predictions, Runs L3/1 and L3/2

U_E/U_I	Initial $\left(\frac{u_r}{U}\right)_{IE}$	L3/1 $\frac{y_{nom}}{\theta}$	L3/1 $\frac{y_{ms}}{\theta}$	L3/1 $\frac{\eta}{\theta}$	L3/2 $\frac{y_{nom}}{\theta}$	L3/2 $\frac{y_{ms}}{\theta}$	L3/2 $\frac{\eta}{\theta}$
0.4	·110	4.62	4.70	4.35	4.62	4.76	4.35
	·007	4.66	4.91	5.56	4.66	4.89	5.57
0.6	·110	4.61	4.67	3.96	4.61	4.66	4.01
	·007	4.70	5.19	5.58	4.71	5.19	5.62
0.8	·110	4.65	4.65	3.33	4.66	4.67	3.36
	·007	4.69	5.28	6.32	4.68	5.26	6.38

Predictions performed with programme LAYER-3

k-z constants :-

	C_μ	C_D	C_1	C_2	C_3	$Pr_{eff,k}$	$Pr_{eff,z}$
Run L3/1	1.0	0.1	3.0	·085	·56	0.7	0.7
" L3/2	1.0	0.1	3.0	·0935	·63	0.7	0.7

In the first run the constants were thus unchanged from the standard values used in the idealised computations reported in section 4.6; for the second run C_2 was increased by 10% and C_3 changed to remain in accord with equation 4.8-2.

In the graphs, the curves represent the experimental results and are transferred directly from figures 5.7, 5.8, and 5.9; the points represent a selection from the computer output values(usually alternate points on the profiles are omitted for clarity).

It can easily be seen from the θ-x curves that for both these sets of values for the constants the programme consistently underestimates the growth rate $d\theta/dx$, and also the increase in θ and $d\theta/dx$ caused by the increase in stream turbulence level, except perhaps at the highest velocity ratio. The turbulence-intensity profiles also help to suggest that in this form the model underestimates the effect of the increase, as in each case the hump in the profile is less prominent for the flow with high free-stream turbulence.

The effect of the change in the values of C_2 and C_3 is small compared with the departures from the experimental results. This is disappointing, because it indicates the failure of the simple strategy outlined in section 4.8, and shows that more radical changes in the constants, and possibly in the structure of the k-z model, are required.

The values of the shape factors obtained in these two runs are given in Table 6.3.

6.5 Variation of the effective Prandtl numbers.

In the general description of the flow in the measuring section of the apparatus (in section 5.9) it was noted that the measured turbulence-intensity layer was everywhere much wider than the time-mean velocity layer. An accompanying feature of the flows without the turbulence grids was that, in the regions of uniform U between the velocity mixing layers, which were originally regarded as the free streams, the minimum value of turbulence intensity increases with x, rather than decreasing in accordance with the analysis of section 2.5, and with the k-z results so far presented.

Probably the most plausible explanation for this phenomenon, and the one which requires the simplest modification to the analytical model to be put into effect, is that the lateral diffusion of turbulence kinetic energy occurs much more readily in the outer parts of the layer than in the middle, i.e., that the effective Prandtl number for k diminishes from the middle of the layer outwards.

The AUX subroutine of the LAYER-3 programme was modified as described in appendix A.6; predictions were carried out (run L3/3) with:

$$Pr_{eff,k} = Pr_{eff,z} = 5A_k^{\frac{1}{2}} + .004A_R^{\frac{1}{2}} + 0.1 \qquad (6.5\text{-}1)$$

where A_k is the local non-dimensional turbulence kinetic energy, k/U^2,

A_R is the local turbulence Reynolds number, $\rho k/\mu z$,

and the numerical factors were chosen, after a single preliminary run, to give reasonable agreement with the experimental observations; the remaining constants in the k-z model were kept as in run L3/1.

The resulting turbulence-intensity profiles are shown in figure 6.8. The modification effects a considerable improvement in the curves for low stream turbulence, rounding off the lower corners so that the predicted $\frac{u_r}{U}$ layer becomes much wider than the U-layer, in accordance with the observations. However the profiles for high stream turbulence are virtually unchanged, so that this modified version of the model still underpredicts the effect of a change in $(\frac{u_r}{U})_{IE}$ on the turbulence-intensity within the mixing layer. In addition, the predicted growth rates, and hence the θ-x distributions, are practically unaltered, and remain too low.

6.6 The effect of varying C_μ and C_D.

The remaining factors which are likely to be helpful in bringing theory and experiment into line are C_μ and C_D, which have been unchanged throughout all the computations so far presented.

Two short computer runs, L3/4 and L3/5, were made, with $U_E/U_I = 0.6$. In the first of these, C_μ was set at 1.1; in the second, C_D was given the value 0.09. The full sets of constants were:

TABLE 6.4 Shape factors for $x = 15cm$ in k-z predictions, Runs L3/4 and L3/5

U_E/U_I	Initial $\left(\frac{u_r}{U}\right)_{IE}$	L3/4			L3/5		
		$\frac{y_{nom}}{\theta}$	$\frac{y_{ms}}{\theta}$	$\frac{\eta}{\theta}$	$\frac{y_{nom}}{\theta}$	$\frac{y_{ms}}{\theta}$	$\frac{\eta}{\theta}$
0.6	.110	4.62	4.72	4.03	4.61	4.69	4.05
	.007	4.66	5.05	5.30	4.68	5.07	5.48

Predictions performed with programme LAYER-3

k-z constants :-

	C_μ	C_D	C_1	C_2	C_3	$Pr_{eff,k}$	$Pr_{eff,z}$
Run L3/4	1.1	0.10	3.0	.085	0.56	0.7	0.7
" L3/5	1.0	.09	3.0	.085	0.56	0.7	0.7

	C_μ	C_D	C_1	C_2	C_3	$Pr_{eff,k}$	$Pr_{eff,z}$
Run L3/4	1.1	0.1	3.0	.085	0.56	0.7	0.7
Run L3/5	1.0	0.09	3.0	.085	0.56	0.7	0.7

The results obtained are shown in figure 6.9. The effect of each change is to increase the predicted growth rate, and so generally to bring the θ-x curves nearer to the experimental ones. There are also changes, but comparatively minor ones, in the turbulence intensity profiles. The shape factors for these runs are given in Table 6.4.

6.7 Further changes in the coefficients.

Summarising the results of the k-z predictions up to this point, we see that:

a) The predicted spreading rates are generally on the low side, particularly for high stream turbulence cases.

b) The predicted values of the shape factors for the velocity and turbulence-intensity profiles are generally in good agreement with the experimental ones; the main discrepancy is in the values of η/θ for low stream turbulence levels at $U_E/U_I = 0.8$ where, probably, the experimental results are least reliable.

c) The predicted turbulence intensity layer is too narrow relative to the velocity layer, unless Pr_{eff}

is made to vary across the stream - high at the middle of the layer and low in the free streams.

The change which would help correct the spreading rates, and which can at present be made with the greatest confidence, is a decrease of C_D. The result of run L3/5 clearly suggests that .09 is a better value for this constant than 0.1. However, a change in C_D affects the predicted spreading rate for all values of $(u_r/U)_{IE}$, and therefore requires modification of the C_2-C_3 relation derived in section 4.8. From the results of a few additional asymptotic runs for $(u_r/U)_{IE} = 0$, and $C_D = .09$, it was possible to estimate the changes produced in figure 4.13, and so obtain a revised version of equation 4.8-2. It is:

$$C_3 = 8.4C_2 - .126 \qquad (6.7\text{-}1)$$

This suggested the following set of values for the next predictions run, L3/6:

C_μ	C_D	C_1	C_2	C_3
1.0	0.09	3.0	.085	0.59

In this run Pr_{eff} was varied in accordance with equation 6.5-1, to obtain the improvement mentioned in c) above.

TABLE 6.5 Shape factors for $x = 15$ cm in k-z predictions, Run L3/6

U_E/U_I	Initial $\left(\frac{u_r}{U}\right)_{IE}$	$\frac{y_{nom}}{\theta}$	$\frac{y_{ms}}{\theta}$	$\frac{\eta}{\theta}$
0.4	.110	4.62	4.85	4.06
	.007	4.65	4.98	5.59
0.6	.110	4.61	4.69	3.98
	.007	4.64	5.03	6.49
0.8	.110	4.64	4.69	3.48
	.007	4.60	5.01	7.91

Predictions performed with programme LAYER-3

k-z constants :-

C_μ	C_D	C_1	C_2	C_3
1.0	0.09	3.0	.085	0.59

$Pr_{eff,k}$ and $Pr_{eff,z}$ given by equation 6.5-1

Figures 6.10, 11 and 12 show the growth of θ against x predicted in this run, compared with the experimental results as in previous graphs, and the profile shape factors are listed in Table 6.5. The latest predictions are a small further improvement over the earlier ones. The spreading rates for low stream turbulence are now in good agreement, but for high stream turbulence the predicted gradients are still rather low. The velocity-profile shape factors follow earlier results with the k-z model, in exhibiting only a small change between high and low stream turbulence cases; this compares favorably with the larger change predicted with the mixing-length variants.

Fig. 6.13 is of interest in showing the wide range of variation of the effective Prandtl number which is produced by the tentative relation, equation 6.5-1, which has been used in these predictions.

7. CONCLUDING DISCUSSION

7.1 Introduction.

This final chapter attempts an unbiased assessment of the work reported in this thesis. The experimental work and the two turbulence models are discussed in turn, and the chapter concludes with some suggestions for further work in the same field.

A statement of the principal conclusions drawn from the present work follows this chapter.

7.2 The physical situation.

The experimental programme was designed to provide information against which the mixing-length hypothesis, and modifications of it, could be tested. For this purpose they have been found satisfactory. There are, however, two questions to which at present only partial answers exsit; they concern the effects of:

a) the departure from two-dimensionality of the flow, and

b) the finite angle between the two streams at entry to the working section.

Although it seems reasonably to suppose that both of these effects were small, it is desirable that confirmation should eventually be obtained.

For comparison with the k-z predictions, the experimental observations have the additional deficiency, that the total turbulence kinetic energy was not measured; this point has already been discussed in section 6.1. To make good this deficiency, detailed measurements of all three components of the fluctuating velocity field are required. A good deal of experimental work of this kind has been carried out, for example by Sunyach and Mathieu (reference 28), Wygnanski and Fiedler (reference 29) and Bradbury (reference 30). The observations in these cases have all, however, been confined to flows in which the free-stream turbulence levels were low, and so are not of direct assistance in the present investigation.

Another feature of the flows without the turbulence grids, whose significance became apparent in comparison with the k-z predictions, is the anomalous increase of measured turbulence intensity in the nominal free-stream regions. The cross-stream variation of Pr_{eff} introduced in section 6.5 implies one possible explanation for this phenomenon. Others are:

1. The observed effect, although appearing as an increase in the root-mean-square component of the hot-wire signal, is not all turbulence in the strict sense, but consists partly of more orderly fluctuations more properly classified as noise, and presumably associated with the intermittency of the

flow at the borders of the mixing layers. It remains to be determined whether or not such fluctuations play a significant part in the mixing process, but it seems unlikely that their effect is the same as that of ordinary turbulence. It may well be that fluctuations of this kind are present to different extents in different forms of apparatus, depending particularly on the presence or absence of containing walls around the stream.

b) The observations reflect a redistribution of turbulence kinetic energy between the three co-ordinate directions, $\overline{u^2}$ increasing at the expense of $\overline{v^2}$ and $\overline{w^2}$, the total kinetic energy decaying in the expected manner.

c) The readings indicate a genuine increase in turbulence kinetic energy, the result of generation within the fluid between the mixing layers. The time-mean velocity is nominally uniform and constant in this region, and it is generally supposed that turbulence generation cannot occur in such a flow. However, the conditions here are sufficiently complicated to raise doubts about the validity of that conclusion in this case.

Two other features of the observed flows merit mention here. Firstly, the frequency spectra for the free streams (described in section 5.8) show that the

turbulence structure was of a rather special kind, with a large proportion of its energy concentrated within a narrow frequency band. It will certainly be desirable to extend the experimental programme to cover free-stream turbulence of a more general kind; this should be possible with more complicated grid systems incorporating bars of various diameters.

Secondly, the experiments were carried out at effectively two levels of free-stream turbulence only - high and low. Results for other turbulence levels are needed to help discriminate between the analytical models. From the present results it is impossible to decide whether the relation between spreading rate $d\theta/dx$, and stream turbulence level is a linear one as predicted by the MU1 mixing-length model, or as predicted by the MU2 and k-z models, in which the effect of increasing $(u_r/U)_{IE}$ is initially negligible. The present experimental results suggest the former to be the case (see section 6.2), while Patel's results (reference 9) firmly support the latter.

7.3 The mixing-length model.

It has long been recognised that the Prandtl mixing-length hypothesis is so much simpler than the physical phenomenon it aims to represent that it cannot be expected to model more than a narrow range of turbulent

flows. The present investigation shows that in its basic form it is quite incapable of modelling the free-stream turbulence-effect, even in such a simple situation as the plane mixing layer in fluid flow at uniform density and pressure.

The modifications developed in this thesis are naturally able to improve on their parent, because of their increased complexity and because of the extra arbitrary and therefore freely disposable constants they contain. This is particularly true of the MU1 version containing two such constants in addition to the original one. Since these constants have been tailored to fit the particular conditions of the present experimental work, the good performance of the MU1 model should be regarded with some caution until it can be more widely tested.

It is possible that, when more extensive experimental results become available, a further modification of the model may be found desirable, for example, a combination of the MU1 and MU2 versions may give better predictions of the way in which the spreading rate, $d\theta/dx$, varies with $(u_r/U)_{IE}$ over the full range of the latter quantity.

The mixing-length model is a conceptually simple one, and its use requires relatively small amounts of computer time and capacity. It is likely to find many applications in engineering design. For such work, its main deficiency (which, on the other hand, might sometimes be an advantage in providing a desirable degree of freedom)

is its inability to predict x-wise variation of turbulence in the free streams. This requires the prescription of u_r/U along the edges of the mixing layer as part of the problem specification. It should also be remembered that the width of the turbulence layer cannot vary independently of the width of the velocity layer, as it can in the k-z model.

The present work has developed the character of the mixing-length model, and so broadened and extended its useful life. There does not now seem to be much possibility of further development.

7.4 The k-z model.

At first sight the performance of the k-z model is somewhat disappointing compared with that of the simpler ones, particularly the MU1 version. It must, however, be remembered that the latter have been more carefully tailored to fit the present experimental observations. In particular, because the observations were not sufficiently detailed, the initial conditions for the k-z predictions were not a good fit for each individual run, as was possible with the mixing-length calculations.

Two points are strongly in favour of the k-z model. First, that in its basic form (i.e. with constant values for C_D, C_1, C_2 and C_3, and with $C_\mu = 1$) it is likely that, when the best set of values for the constants has been found, it will give predictions to at least the

degree of accuracy acceptable in engineering design work, not only for flows of the kind at present under discussion, but for many other kinds also. Second, that it offers interesting possibilities for further development, by way of variation of the "constants", as has already been tried with Pr_{eff}. There is no reason, apart from lack of physical information, why others should not be dealt with in a similar way.

The two principal defects of the k-z model are:

a) its inability to differentiate between the components of the fluctuating motion in different directions, and

b) its use of a single value for frequency of the motion at each point in the field.

It remains to be seen how seriously these limit its usefulness, and whether or not they can be remedied if necessary. (For example, it might be possible to introduce a correlation factor to allow for variation in the relative magnitudes of u^2, v^2 and w^2, and/or to work in terms of more than one characteristic frequency.)

At present the greatest need, in the development of the k-z model, is for more comprehensive and detailed experimental results. on which to base firm recommendations for the values of the various coefficients in the k and z equations. The best set used so far, with all the coefficients treated as constants, is:-

C_μ	C_D	C_1	C_2	C_3	$Pr_{eff,k}$	$Pr_{eff,z}$
1.0	.09	3.0	.085	.59	0.7	0.7

The value assigned to C_μ is arbitrary, being associated with the hypothetical view of characteristic frequency z. When detailed experimental observations become available for flows with various preferred free-stream frequencies, C_μ may need to be changed. Alternatively, it might be satisfactory simply to multiply the "actual" free-stream frequency by a numerical factor, while retaining the value unity for C_μ.

From the results so far obtained with this model it appears that the value of .09 for C_D is still possibly too high. It is interesting to note that, using a somewhat difference analytical model, Rodi and Spalding (reference 22) found the same value for C_D to give the best overall fit for plane,zero-velocity-ratio mixing layers, plane jets, and radial (fan) jets, while for wall boundary layers the value 0.1 generally seems more appropriate. This suggests that C_D needs to be treated as a function of local flow properties, as Pr_{eff} was in section 6.5, but in this case decreasing with increase of A_k. It is likely that such a change could lead to improved accuracy, not only over the range of free-stream turbulence intensity, but also over the full range of velocity ratio.

The value of C_1 is the most doubtful of all those listed above; the term containing C_1 appears to have a negligible effect in the z equation and could probably be omitted altogether without significantly altering the accuracy of the predictions.

Note that the effective Prandtl numbers for k-transport and z-transport have, in this work, been held equal everywhere. It may be that some other practice will be seen to be desirable when more extensive experimental results are available.

7.5 Suggestions for future work.

The work done in the present investigation raises a number of questions about the development of free mixing layers between turbulent streams; the work outlined briefly below should provide many of the answers.

Experimental There is need to both widen the range of the measurements and to increase the number of quantities measured. The experimental programme should be extended to cover:

a) the whole range of stream velocity ratio, U_E/U_I,

b) other levels of free-stream turbulence,

c) streams with other preferred frequencies for the fluctuating motion, and with more complex turbulence structures,

d) flows with asymmetric turbulence distributions, i.e., high in one free stream and low in the other,

e) flows with different angles between the confluent streams,

and

f) flows enclosed on all four sides.

Additional quantities which should be measured are:

g) all three fluctuating velocity components, $\overline{u^2}$, $\overline{v^2}$ and $\overline{w^2}$,

h) turbulent shear stress, $\overline{\rho uv}$,

i) turbulence-energy frequency distributions at selected points in the flow,

j) direction of time-mean velocity.

This work could all be carried out on the existing apparatus with very little modification other than the installation of the additional instrumentation. It is also desirable that similar experiments be performed on larger apparatus, in which the widths of the free streams would be greater; this would allow the processes occurring in these regions to be examined in greater detail. This new apparatus could be designed to operate with air supply ducts of different width/height ratios, thus allowing the effects of departure from two-dimensionality to be more completely investigated.

Theoretical The main advances on the theoretical side are almost certainly to be made at the level of two-equation models of turbulence, such as the k-z model, or at higher levels. An indication of the lines of development most likely to lead to improved predictions with the k-z model has already been given in section 7.4. Apart from the general optimisation of the coefficients, each regarded as a constant, there is the possibility that

variation within the flow field may be desirable. Pr_{eff} has already been treated in this way, although only to a limited extent. C_D seems to be another quantity which should be made to vary as a function of local flow properties, but there is no reason why others should not be similarly dealt with. To a large extent the effort that it will be worth while devoting to such work will depend on the comprehensiveness and reliability of the experimental results available.

One refinement which it may be desirable to incorporate into the calculations independently of the choice of turbulence model, is an allowance for the effects of stream curvature at the outer edges of the mixing layer. These are almost certainly negligible when the stream velocity ratio is in the upper half of its range, but could well become significant as U_E/U_I approaches zero. It would probably be possible to introduce a satisfactory correction for this effect into the present boundary-layer calculations and avoid the necessity for a complete solution Navier-Stokes equation.

8. STATEMENT OF PRINCIPAL CONCLUSIONS

8.1a) Convincing experimental evidence has been obtained to show that the turbulence intensity of the free streams adjacent to a free mixing layer exerts a significant influence on its development.

8.1b) In particular, an increase in the external turbulence level causes an increase in the spreading rate of the layer, i.e., in the rate of mixing between the two streams. This effect is, proportinately, greater for velocity ratios close to unity than for lower ratios.

8.1c) Within the range of the experiments, an increase in the free-stream turbulence level also produces a roughly equal increase of turbulence level right through the stream.

8.1d) These effects are large enough to warrant the suggestion that observations of free turbulent shear flows which do not include measurement of the free-stream turbulence level must be regarded as incomplete.

8.2a) The Prandtl mixing length hypothesis is incapable of predicting the effect of free-stream turbulence, but a simple extension of Prandtl's model is able to predict the increases of both spreading rate and internal turbulence level. It is represented by the following equation for effective viscosity:

$$\mu_{eff} = \rho \ell^2 \left|\frac{\partial U}{\partial Y}\right| + A_1 \rho \ell U (B + \frac{U_E}{U_I})[(\frac{u_r}{U})_I (\frac{Y_E - Y}{Y_E - Y_I}) + (\frac{u_r}{U})_E (\frac{Y - Y_I}{Y_E - Y_I})]$$

Values proposed for the numerical constants are:

$$A_1 = 1.05 \quad , \quad B = 0.5$$

with the mixing length, ℓ, related to the momentum thickness by the equation:

$$\ell = 0.50\ \theta \quad .$$

8.2b) Another modification of the Prandtl hypothesis predicted the spreading rates rather less well, and the turbulence-intensity distributions much less well, than the first. In this second form the effective viscosity had a lower limit represented by the equation:

$$\mu_{eff} = A_2 \rho \ell U [(\frac{u_r}{U})_I (\frac{Y_E - Y}{Y_E - Y_I}) + (\frac{u_r}{U})_E (\frac{Y - Y_I}{Y_E - Y_I})]$$

The best value found for the constant A_2 was 2.0.

8.3a) The k-z model (a slightly modified form of Kolmogorov's proposal) can give moderately good predictions of the free-stream turbulence effect when constant values are assigned to the coefficients associated with the generation and dissipation terms in the differential equations for k and z (turbulence kinetic energy and characteristic frequency respectively). The best set of values found is:

$$C_D = .09 \ , \ C_1 = 3.0 \ , \ C_2 = .085 \ , \ C_3 = 0.59.$$

8.3b) Improvement in the k-z predictions can be achieved by treating at least some of the coefficients as functions of local flow properties, in particular, the local turbulence kinetic energy. Such further development of the model will require more detailed experimental information than is at present available.

REFERENCES

1. Prandtl, L. "Uber die ausgebildete Turbulenz". Z. angew. Math. u. Mech., 5, 136 (1925).

2. Kolmogorov, A.N. "Equations of turbulent motion of an incompressible fluid". Izv. Akad. Nauk SSR, VI, 1-2, 56, (1942). [Published in translation as Mech. Eng. Dept. Rept. ON/6. Imperial College, (1968): see appendix D of this thesis].

3. Patankar, S.V., and Spalding, D.B. "Heat and Mass Transfer in Boundary Layers". Morgan-Grampian, London (1967).

4. Spalding, D.B. "Heat and Mass Transfer in Boundary Layers. Part III. A newer version of the method". Mech. Eng. Dept. Rept. BL/TN/G/15, Imperial College, (1969).

5. Tollmien, W. "Berechnung turbulenter Ausbreitungsvorgange" Z. angew. Math. u. Mech., 6, 468 (1926).

6. Kuethe, A.M. "Investigations of the turbulent mixing regions formed by jets". J. App. Mech., 11, 3, A-87, (1935).

7. Görtler, H. "Berechnung von Ausgaben der freien Turbulenz auf Grund eines neuen Naherungsansatzes" Z. angew. Math. u. Mech., 22, 5, (1942).

8. Curtet, R, and Ricou, F. "Influence des conditions a l'entree de la chambre sur les characteristiques moyennes et de turbulence d'un jet de revolution en presence d'une vitesse ambiante dans une chambre cylindrique". 9th Congress de L'A.I.R.H., Dubrovnik, (1961).

9. Patel, R.P. "A study of two-dimensional symmetric and asymmetric turbulent shear flows". Ph.D. thesis, Dept. of Mech. Eng.,McGill Univ., (1970).

10. Sabin,C."An analytical and experimental study of the plane, incompressible, turbulent free shear layer with arbitrary velocity ratio and pressure gradient". Dept. of Mech. Eng. Rep. MD-9, Stanford Univ., (1963).

11. Woolman, B.G. "Decay of a velocity discontinuity". D.I.C. Thesis, Dept. of Mech. Eng., Imperial College,(1963).

12. Yakovlevskiy, O.V. "The problem of the thickness of the turbulent mixing zone on the boundary between two gas streams of different velocity and density". Izv. Akad. Nauk SSSR, 10, (1958) [Reported in Chap.1 of Reference 15].

13. Seban, R.A. and Back, L.H. "Velocity and temperature profiles in turbulent boundary layers with tangential injection". Trans. ASME, J.Heat Trans., 84, Series C, 1, 45, (1962).

14. Peerless, S.J. "An entrainment law derived from experimental results for the free turbulent shear layer." Mech. Eng. Dept. Rept. IC/HRJ/28, Imperial College, (1965).

15. Abramovich, G.N. "The Theory of turbulent jets". M.I.T. Press, (1963).

16. Halleen, R.M. "Literature review on subsonic free turbulent shear flow". Dept. of Mech. Eng. Rept. MD-11, Stanford Univ., (1964).

17. Sforza, P.M., Trentacoste, N.P., and Mons, R.F. "Turbulent mixing: a review, revaluation, and extension". Dept. of Aerospace Eng. and App. Mech., Poly. Inst. of Brooklyn Grad. Centre, (1967).

18. Liepmann, H.W., and Laufer, J. "Investigation of free turbulent mixing". N.A.C.A. Tech. Note 1257, (1947).

19. Baker, R.L.R. "The mixing of two parallel streams of dissimilar fluids". Ph.D. Thesis, Dept. of Chem. Eng., Illinois Inst. of Tech.,(1967).

20. Watt, W.E. "The velocity-temperature mixing-layer". Mech. Eng. Dept. Rept. UT Mech E TP 6705, Univ. of Toronto, (1967).

21. Lee, S.C. and Harsha, P.T. "The use of turbulent kinetic energy in free mixing studies". AIAA Journal, 8, (1970).

22. Rodi, W., and Spalding, D.B. "A two-parameter model of turbulence and its application to free jets". Mech. Eng. Dept. Rept. BL/TN/B/12, Imperial College, (1969).

23. Hinze, J.O. "Turbulence: an introduction to its mechanism and theory". McGraw-Hill, (1959).

24. Spalding, D.B. "The prediction of two-dimensional, steady, turbulent, elliptic flows". Mech. Eng. Dept. Rept. EF/TN/A/16, Imperial College, (1969).

25. Batchelor, G.K., and Townsend, A.A. "Decay of vorticity in istotropic turbulence". Proc. Roy. Soc. London, 190A, 534, (1947).

26. Goldstein, S. (ed.) "Modern developments in fluid dynamics, Vol.II" Oxford University Press, (1938)

27. Baines, W.D., and Peterson, E.G. "An investigation of flow through screens". Trans. ASME, 73, 467, (1951).

28. Sunyach, M., and Mathieu, J. "Zone de melange d'un jet plan". Int. J. Heat and Mass Trans., 12, 1679, (1969).

29. Wygnanski, I., and Fiedler, H.E. "The two-dimensional mixing region". J. Fl. Mech., 41, 2, (1970).

30. Bradbury, L.J.S. "The structure of a self-preserving turbulent plane jet". J. Fl. Mech., 23, 31, (1965).

31. Spalding, D.B. "The prediction of two-dimensional steady, turbulent, elliptic flows". Mech. Eng. Dept. Rep. EF/TN/A/16, Imperial College, (1969).

32. Spalding, D.B. Private note dated 30th March, 1970.

33. Bickley, W.G. "Formulae for numerical differentiation". Math. Gazette, 25, 19, (1941).

34. Collis, D.C., and Williams, M.J. "Two-dimensional convection from heated wires at low Reynolds numbers". J. Fl. Mech., 6, 357, (1959).

PRINCIPAL NOTATION

		Equation
A_1, A_2, B	Constants in effective-viscosity expressions	2.2-4, 2.2-5
A_k	Non-dimensional turbulence energy, k/U^2	6.5-1
A_r	Turbulence Reynolds number $\rho k/uz$	6.5-1
A,B,C,E,	Finite-difference coefficients	3.2-8, 3.3-5
a,c	Constants in Tollmien-Kuethe analysis	B.1-2, B.1-6
a,b,c,	Coefficients in principal differential equations	3.2-4
C_1, C_2, C_3	Coefficients in z equation	2.4-3
C_D	" " k "	2.4-2
C_μ	" " k-z shear law	2.4-1
D_1, D_2, D_3	" " Tollmien-Kuethe analysis	B.2-1
E_f	Specific turbulence energy at frequency f	5.8-1
F	Stream-function in Tollmien-Kuethe analysis	B.1-5
f	Frequency	5.8-1
k	Turbulence kinetic energy ($\equiv \frac{\overline{u^2}+\overline{v^2}+\overline{w^2}}{2}$)	2.4-2
ℓ	Prandtl mixing length	1.2-3
ℓ_s	Kolmogorov scale of turbulence	2.6-1
$\dot{m}''$	Entrainment rate into mixing layer	3.2-5, 3.2-6
M,M'	Non-dimensional entrainment parameters	3.3-3
N	Number of ω-intervals in finite-difference grid	
Pr_{eff}	Effective Prandtl number	2.4-2, 2.4-3
S_k, S_z	Source terms in principal differential equation	A.6-2, A.6-5

U	Time-mean velocity component in x direction	1.2-1
$\tilde{U}$	Velocity specified on velocity profile at grid line near edge of mixing layer	3.4-2
u_r	Root-mean square of fluctuating velocity	2.2-3
u,v,w	Fluctuating velocity components in x,y, z directions	
V	Time-mean velocity component in y direction	1.2-1
V	Non-dimensional shear parameter	3.3-3
x	Space co-ordinate in flow direction	Fig.1.1, 3.1
Y	Velocity profile shape factor for outer half-interval of grid	3.3-3
y,z	Space co-ordinates normal to flow direction	Fig.1.1, 3.1
y_I, y_E	Transverse position of grid boundaries	
y^*	Transverse distance measured from position of mean velocity	
y_{nom}, y_{ms}	Characteristic thicknesses of mixing layer	2.3-1, 2.3-2
z	Characteristic frequency of turbulent motion	2.4-3
$\alpha,\beta,\gamma,\delta$	Constants in Pr_{eff} expression	A.7-1
ε	Error in prediction of growth rate	6.2-1
η	Shape factor for relative turbulence intensity profile	4.7-1
θ	Momentum thickness of mixing layer	2.3-3
$\varkappa$	Constant in Pr_{eff} expression	A.7-1
λ	Mixing-length constant ($\equiv \frac{\ell}{\theta}$)	2.3-4
μ	Laminar viscosity coefficient	

μ_{eff}	Effective viscosity coefficient	1.2-2
μ_{turb}	Turbulent component of effective viscosity coefficient	
ρ	Fluid density	
τ	Shear Stress on xz plane	1.2-2
φ	Non-dimensional co-ordinate in Tollmien-Kuethe analysis	B.1-5
	Constant in Pr_{eff} expression	A.7-1
ψ	Stream function	3.2-1
ω	Non-dimensional stream function	3.2-2

Suffixes

E,I	Grid boundaries, and free streams
IE	Free-stream value (when the same in both I and E streams)
i	Grid-line index
2,NP2	"Slip" quantities at I and E boundaries

GRAPHS OF RESULTS

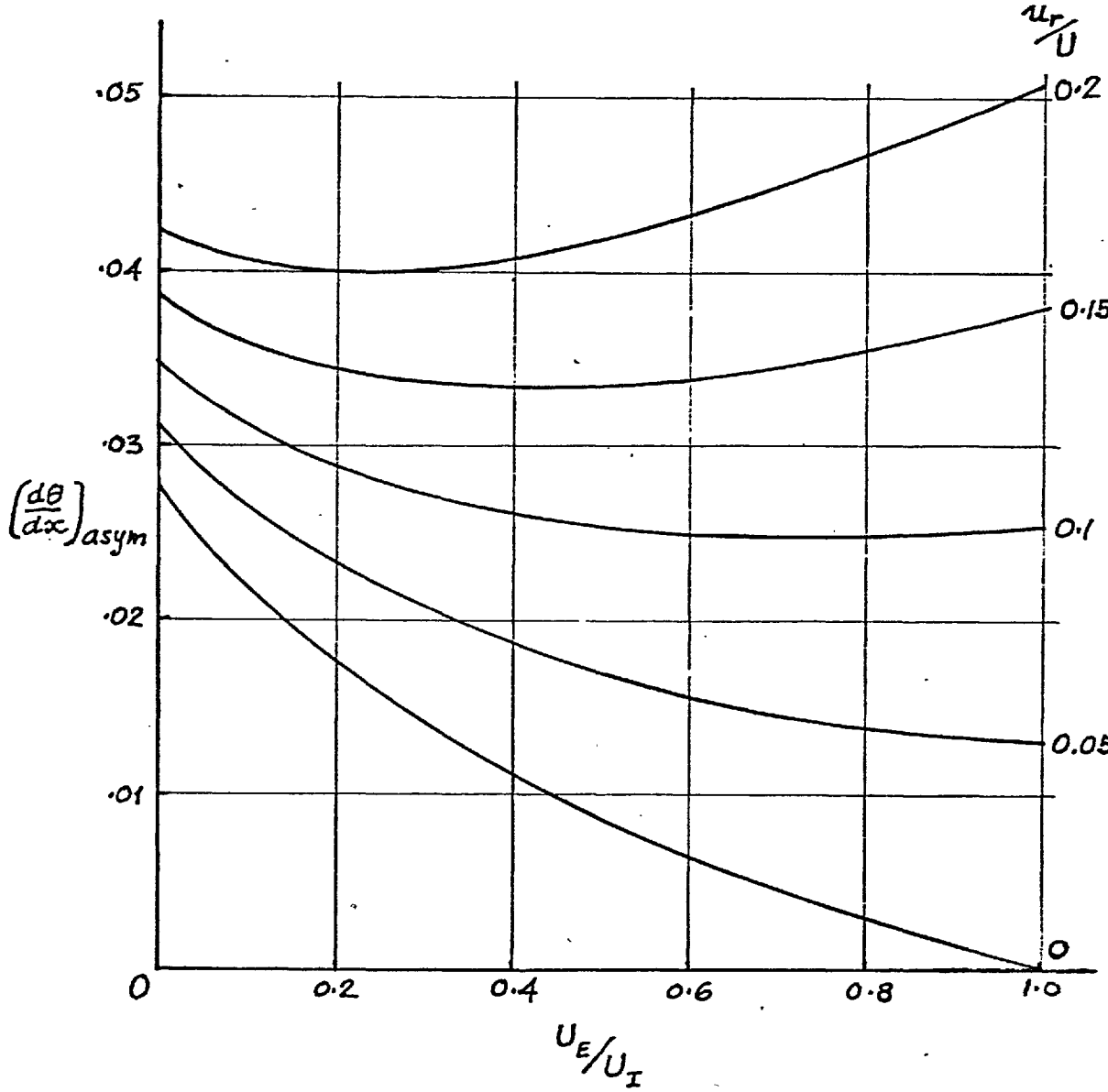
Figures 4.1 to 4.6: Modified mixing-length predictions
pp.152 to 157

Figures 4.8 and 4.10 to 4.13: k-z predictions
pp 158 to 162

Figures 5.7 to 5.21: Main experimental results
pp 163 to 177

Figures 5.22, 24 and 25: Auxiliary experimental results
pp 178 to 180

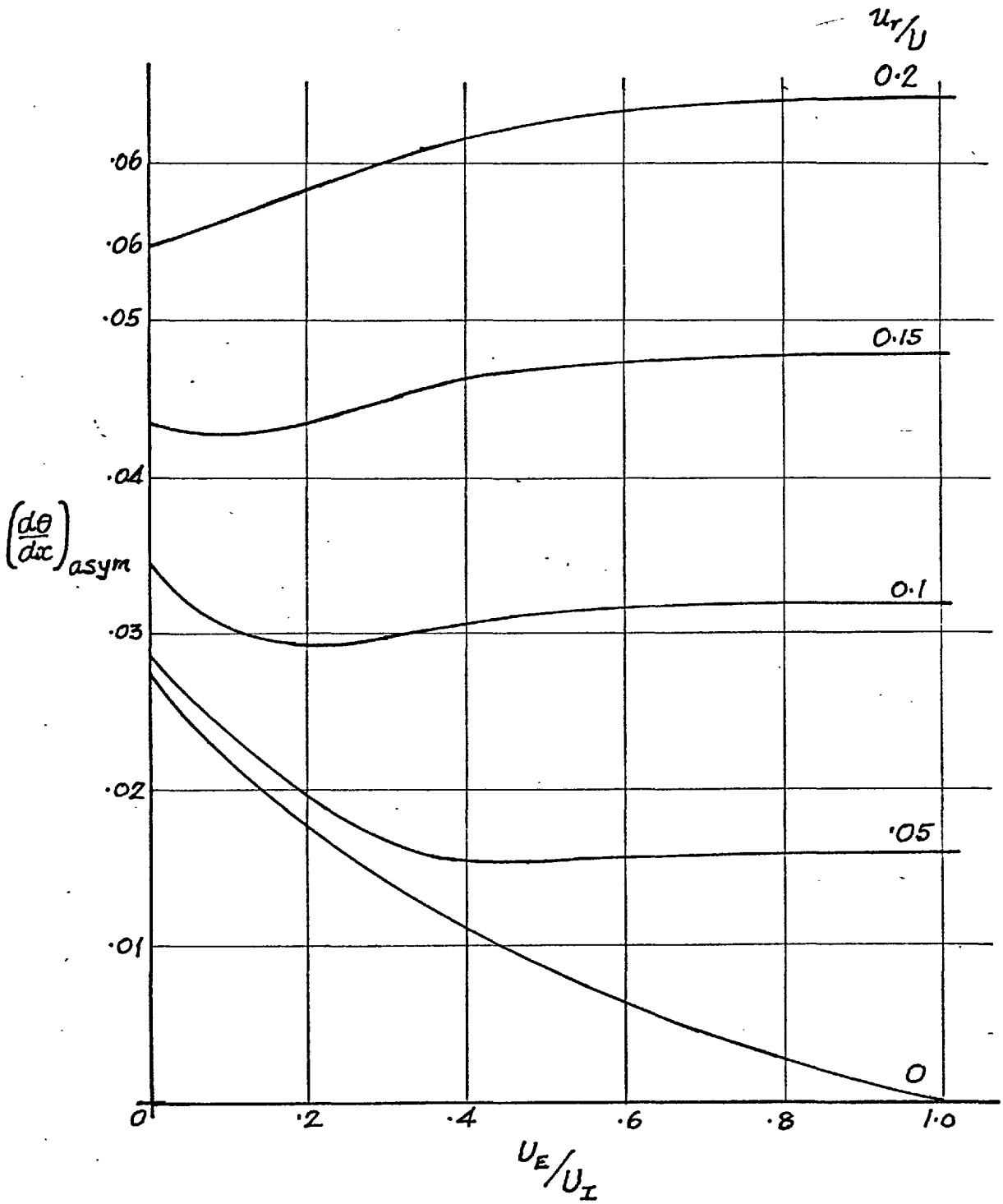
Figures 6.1 to 6.11 (except 6.2): Comparisons of predictions with experimental results
pp 181 to 190



Modified mixing-length predictions

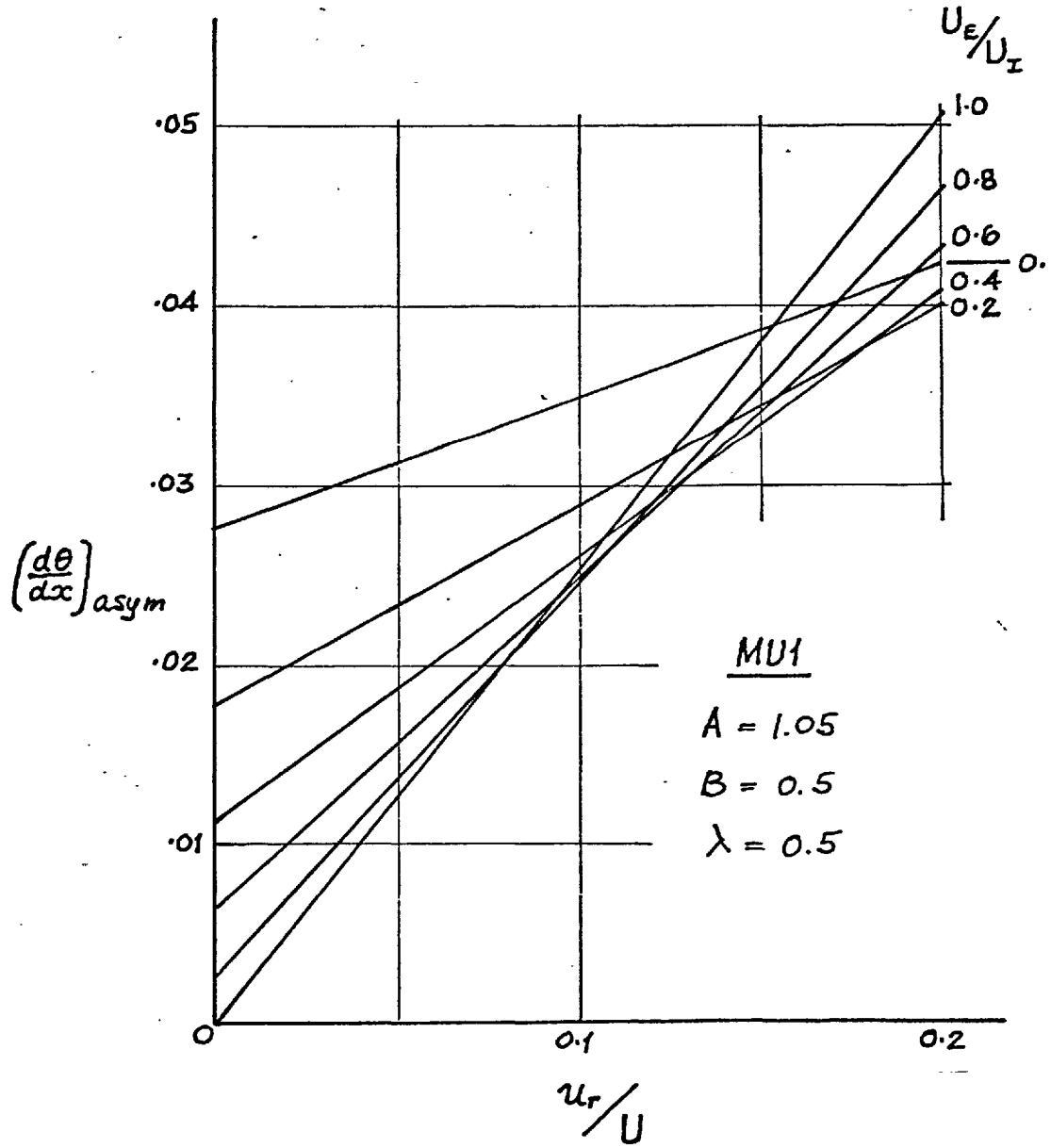
MU1 : $A_1 = 1.05$, $B = 0.5$, $\lambda = 0.5$

Figure 4.1



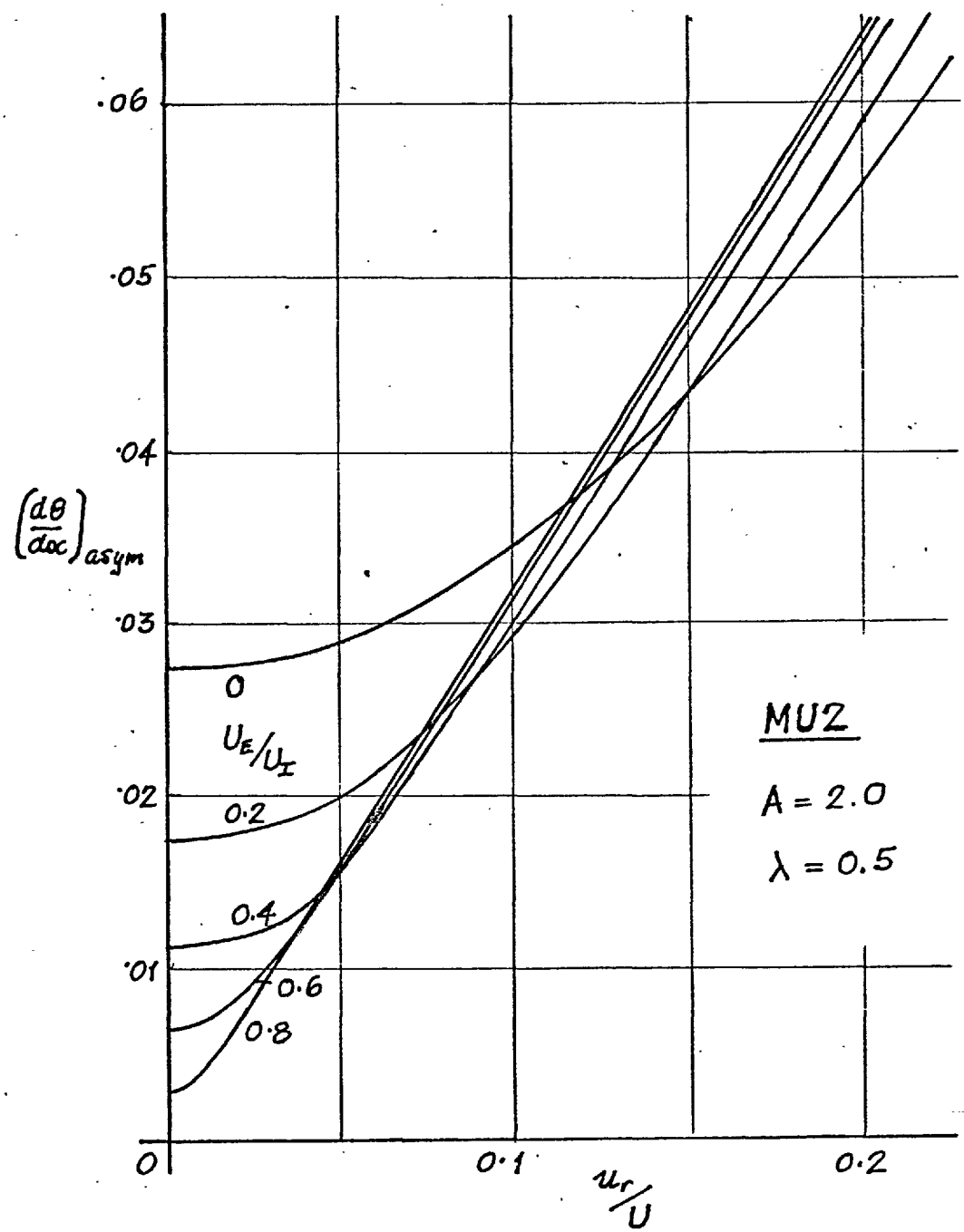
Modified mixing-length predictions
MU2 : $A_2 = 2.0$, $\lambda = 0.5$

Figure 4.2



Modified mixing-length predictions

Figure 4.3



Modified mixing-length predictions

Figure 4.4

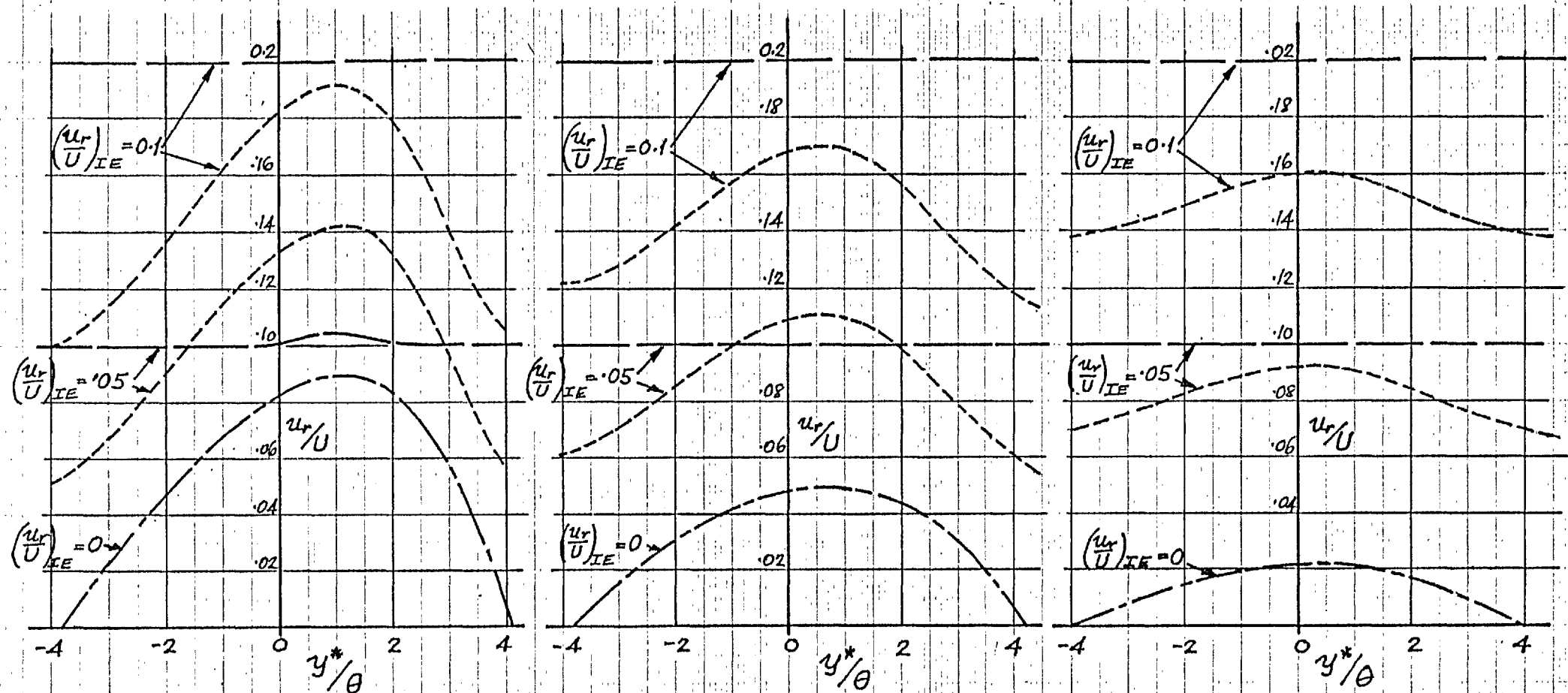


Figure 4.5

Modified mixing-length predictions : Relative turbulence intensity profiles

MU1 ——— MU2

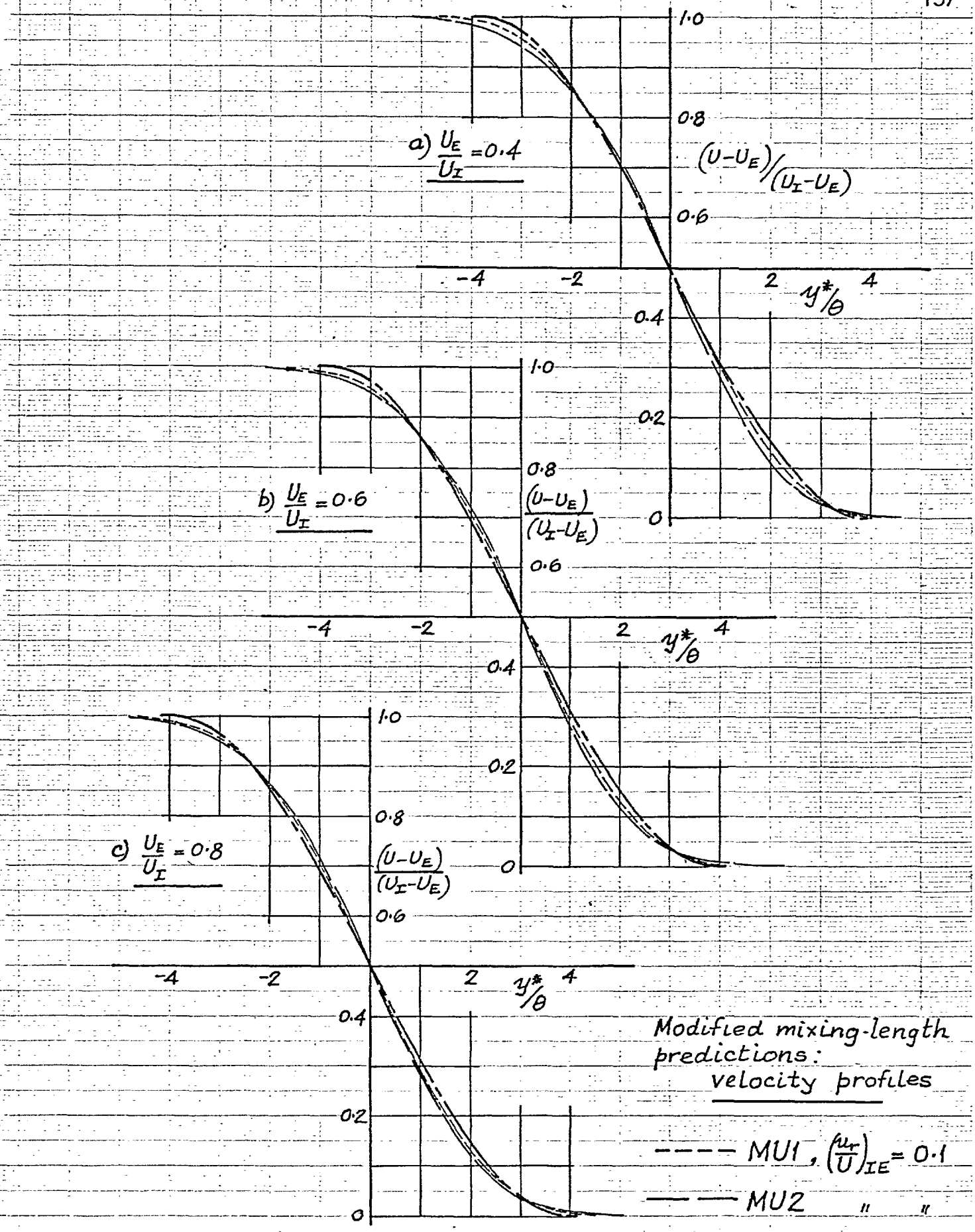
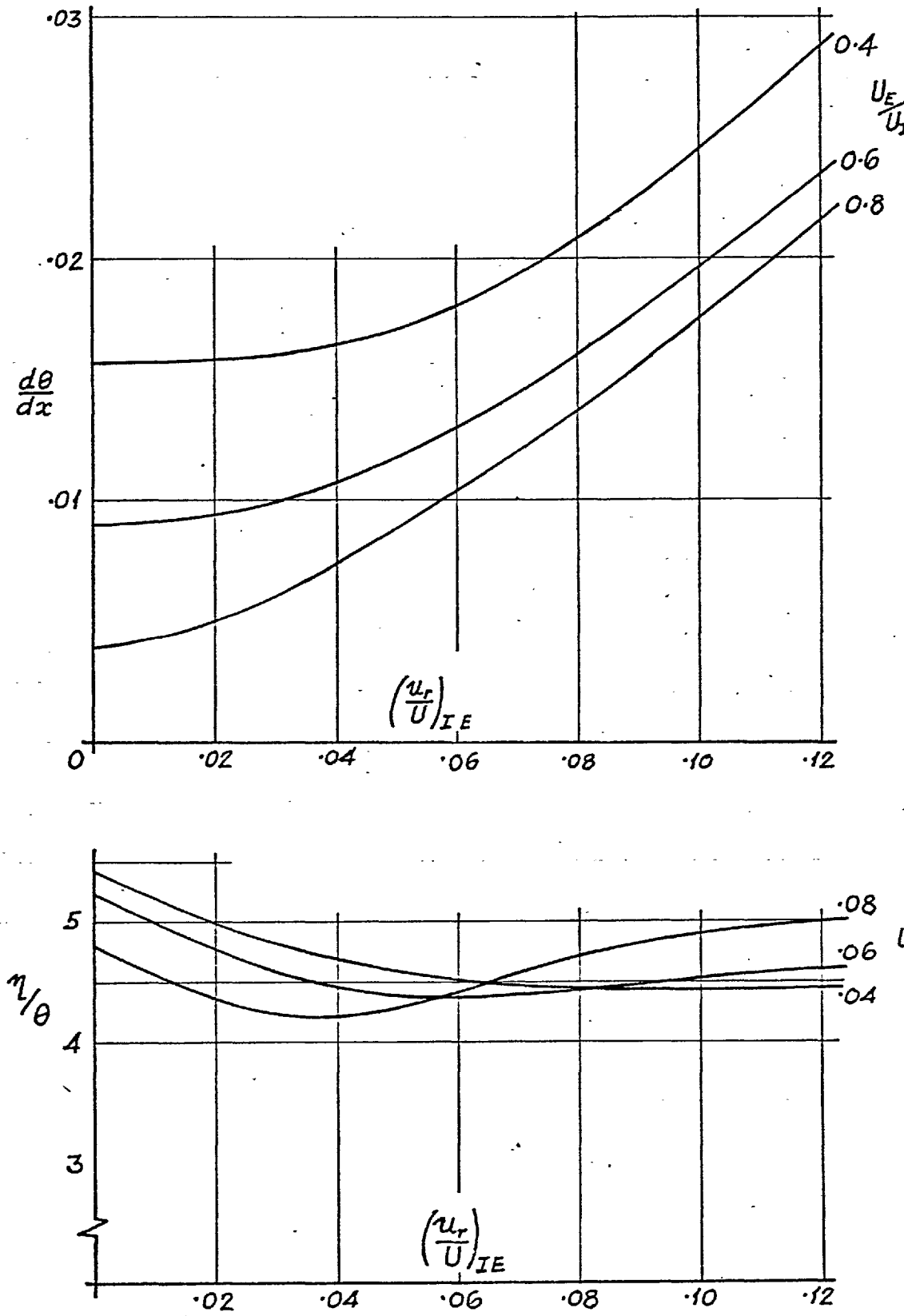

a) $\frac{U_E}{U_I} = 0.4$
b) $\frac{U_E}{U_I} = 0.6$
c) $\frac{U_E}{U_I} = 0.8$
$\frac{(U-U_E)}{(U_I-U_E)}$
y^*/θ
1.0
0.8
0.6
0.4
0.2
0
-4
-2
2
4
Modified mixing-length predictions:
velocity profiles
---- MU1, $\left(\frac{\mu_T}{U}\right)_{IE} = 0.1$
—— MU2 " "
———— " = 0.

Figure 4.6

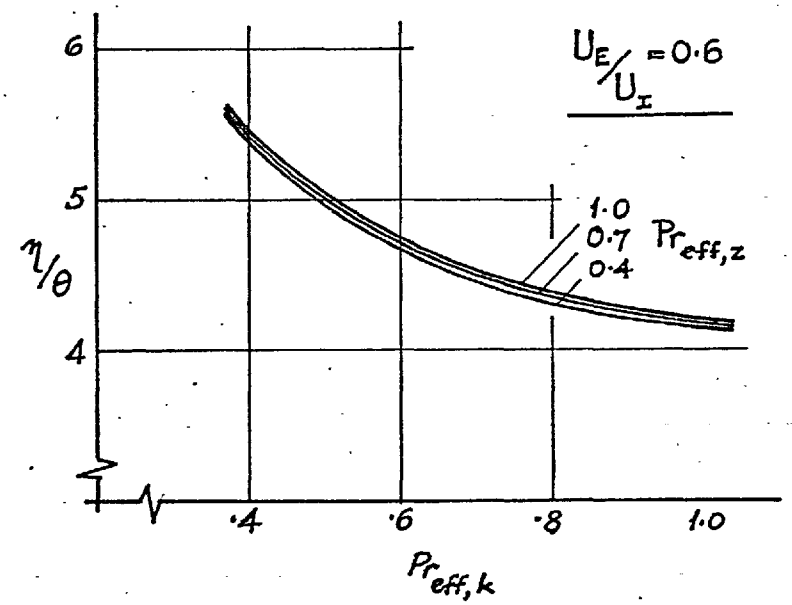


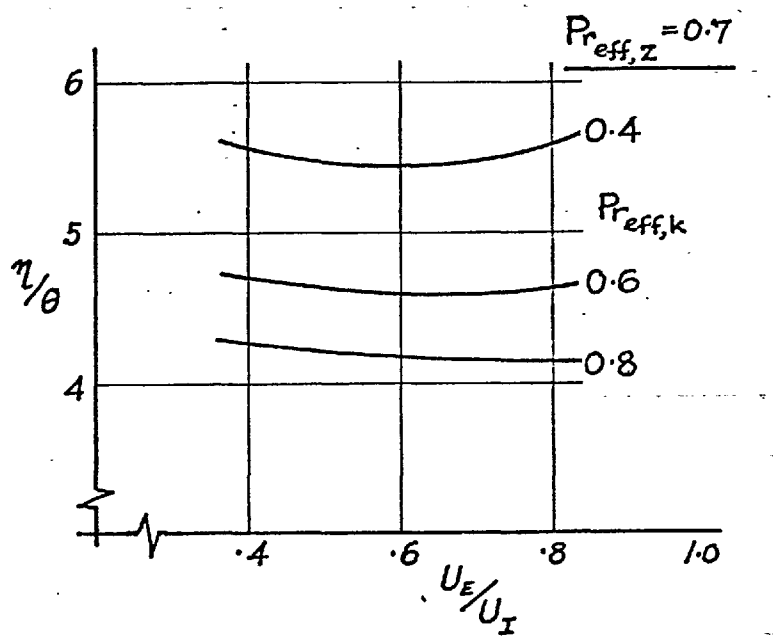
k-z predictions

$C_D = 0.1$, $C_1 = 3.0$, $C_2 = 0.1$, $C_3 = 0.56$

$Pr_{eff,k} = 0.7$, $Pr_{eff,z} = 0.7$

Figure 4.8



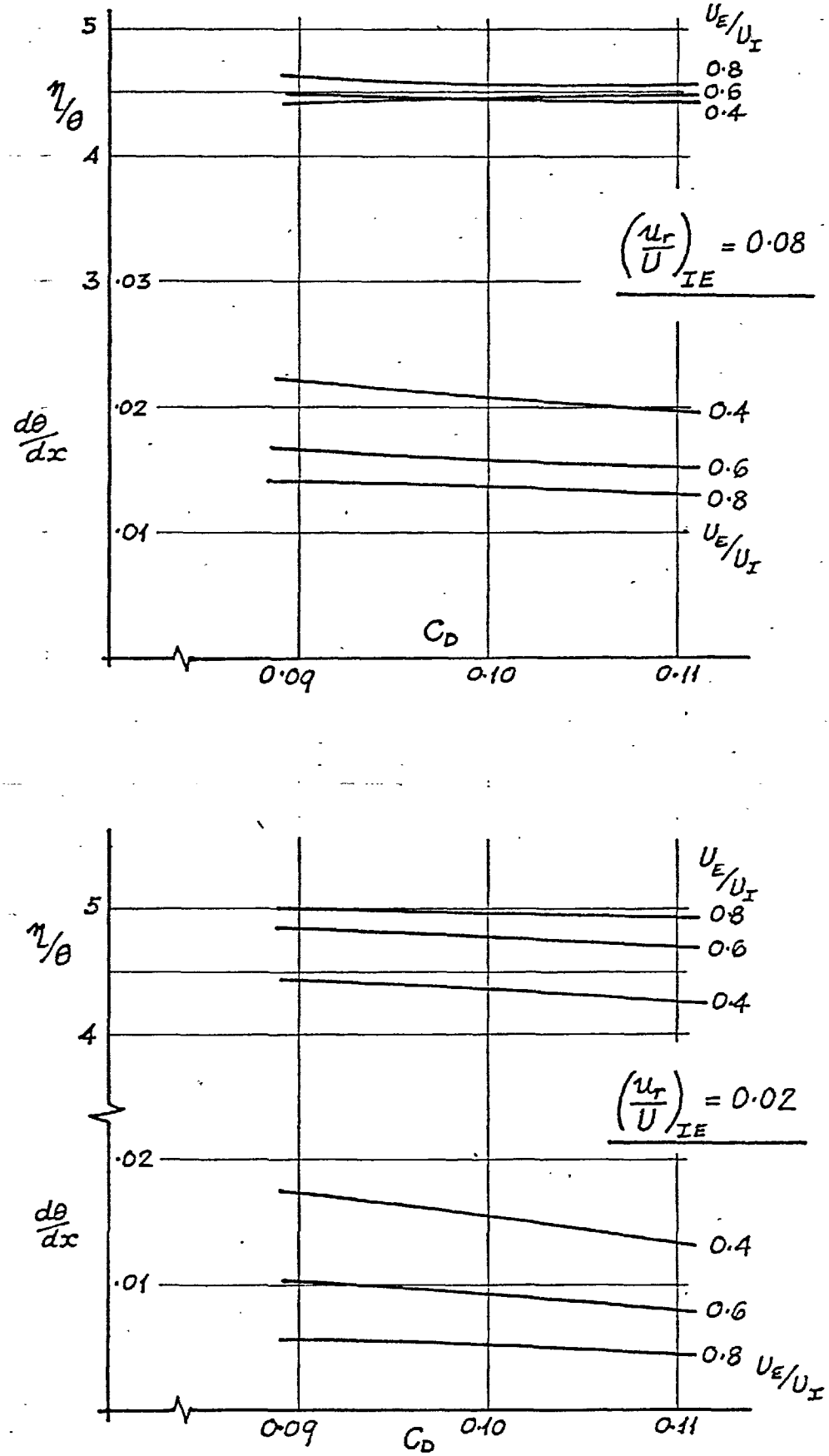


k-z predictions

$C_D = 0.1$, $C_1 = 3.0$, $C_2 = 0.1$, $C_3 = 0.56$

$\left(\frac{u_r}{U}\right)_{IE} = .06$, $\left(\frac{u_r}{U}\right)_{IE,initial} = 0.1$

Figure 4.10

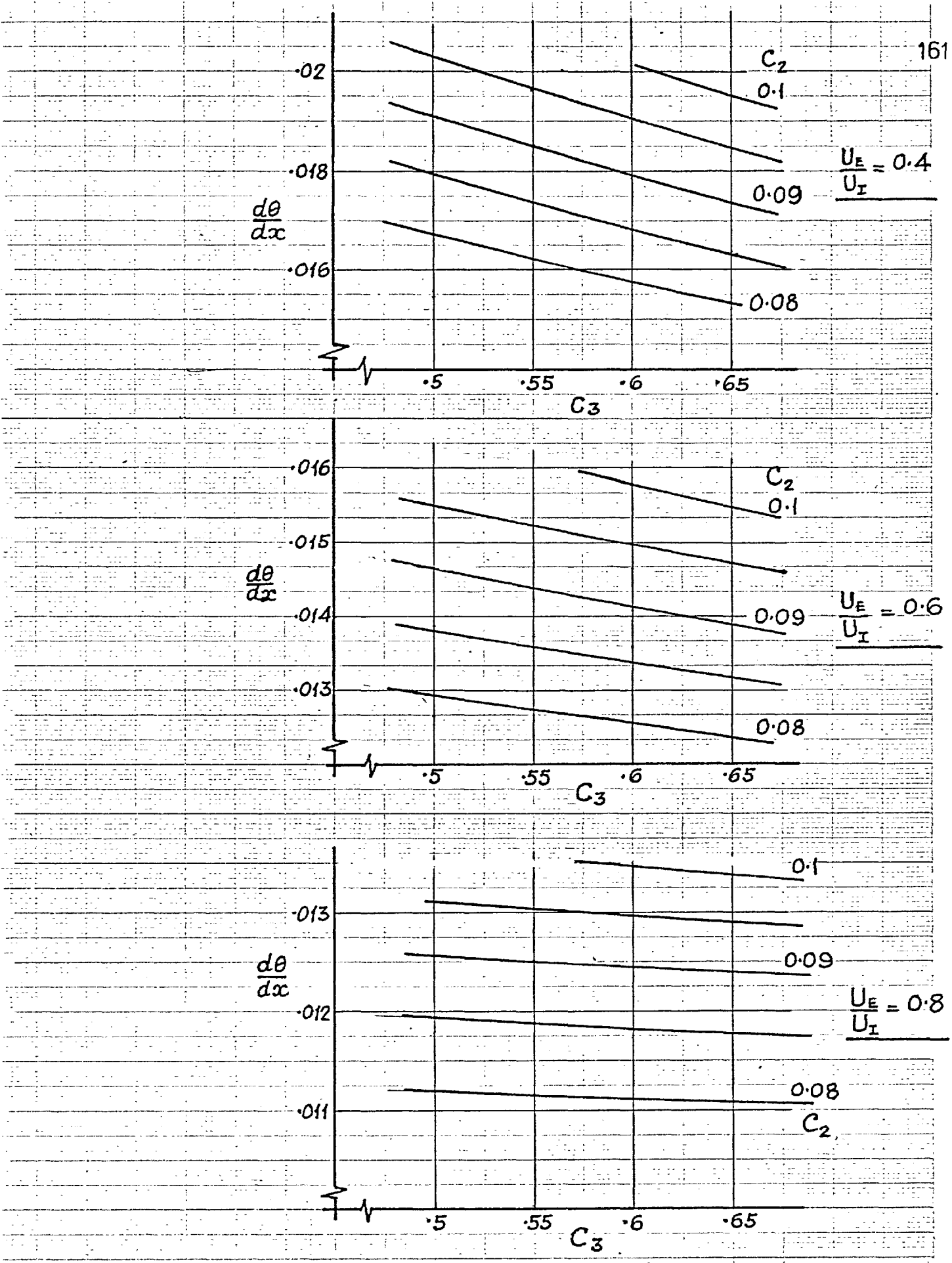


k-z predictions

$C_1 = 3.0$, $C_2 = 0.1$, $C_3 = 0.56$, $\left(\frac{u_r}{U}\right)_{IE,initial} = 0.2$

$Pr_{eff,k} = 0.7$, $Pr_{eff,z} = 0.7$

Figure 4.11

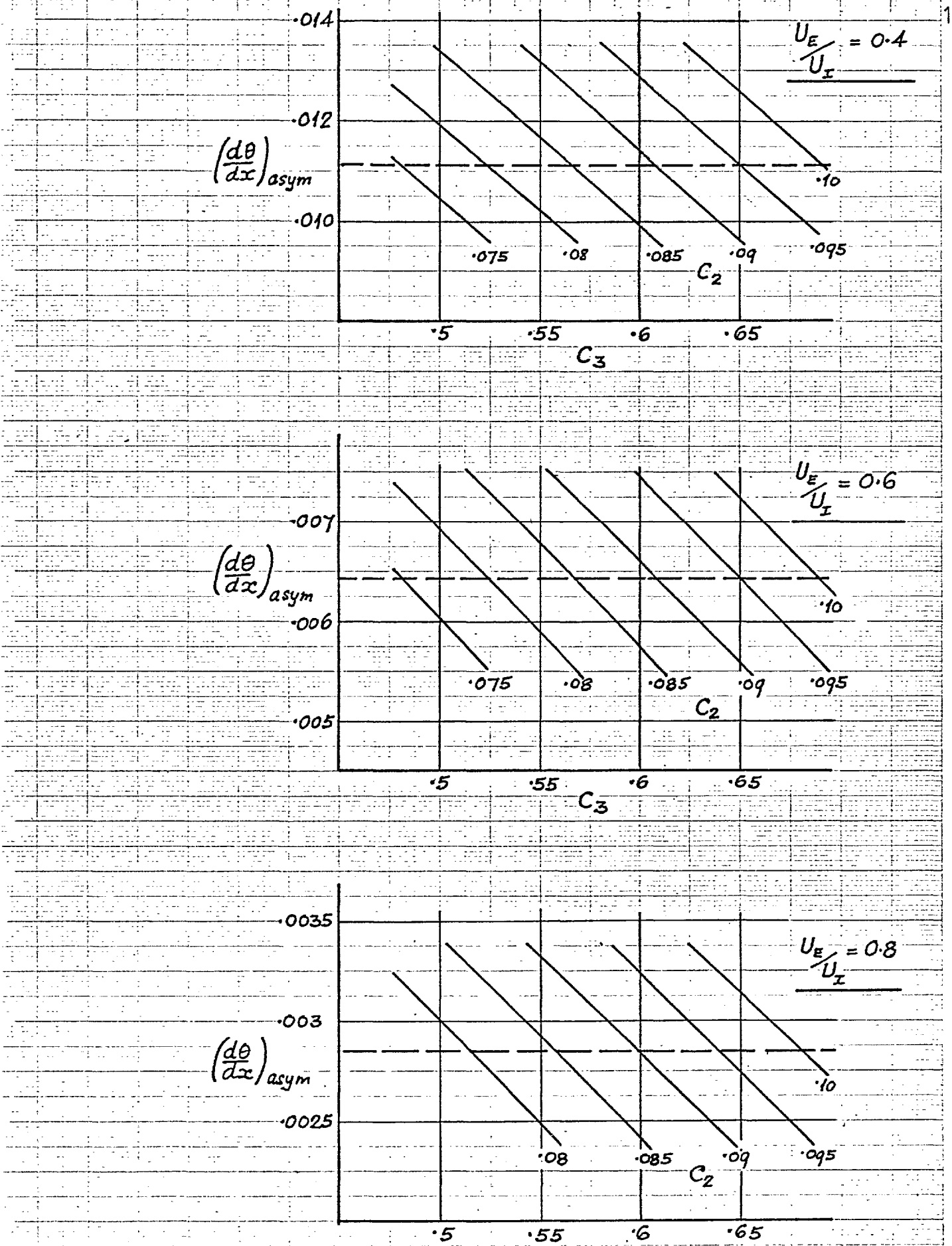


k-z predictions for $\left(\frac{u_r}{U}\right)_{IE} = 0.08$

$C_D = 0.1$, $C_1 = 3.0$, $\left(\frac{u_r}{U}\right)_{IE,initial} = 0.2$

$Pr_{eff,k} = 0.7$, $Pr_{eff,z} = 0.7$

Figure 4.12



k-z predictions for $\left(\frac{u_r}{U}\right)_{IE} = 0$

$C_D = 0.1$, $C_1 = 3.0$, $Pr_{eff,k} = 0.7$, $Pr_{eff,z} = 0.7$

——— Mixing-length solution

Figure 4.13

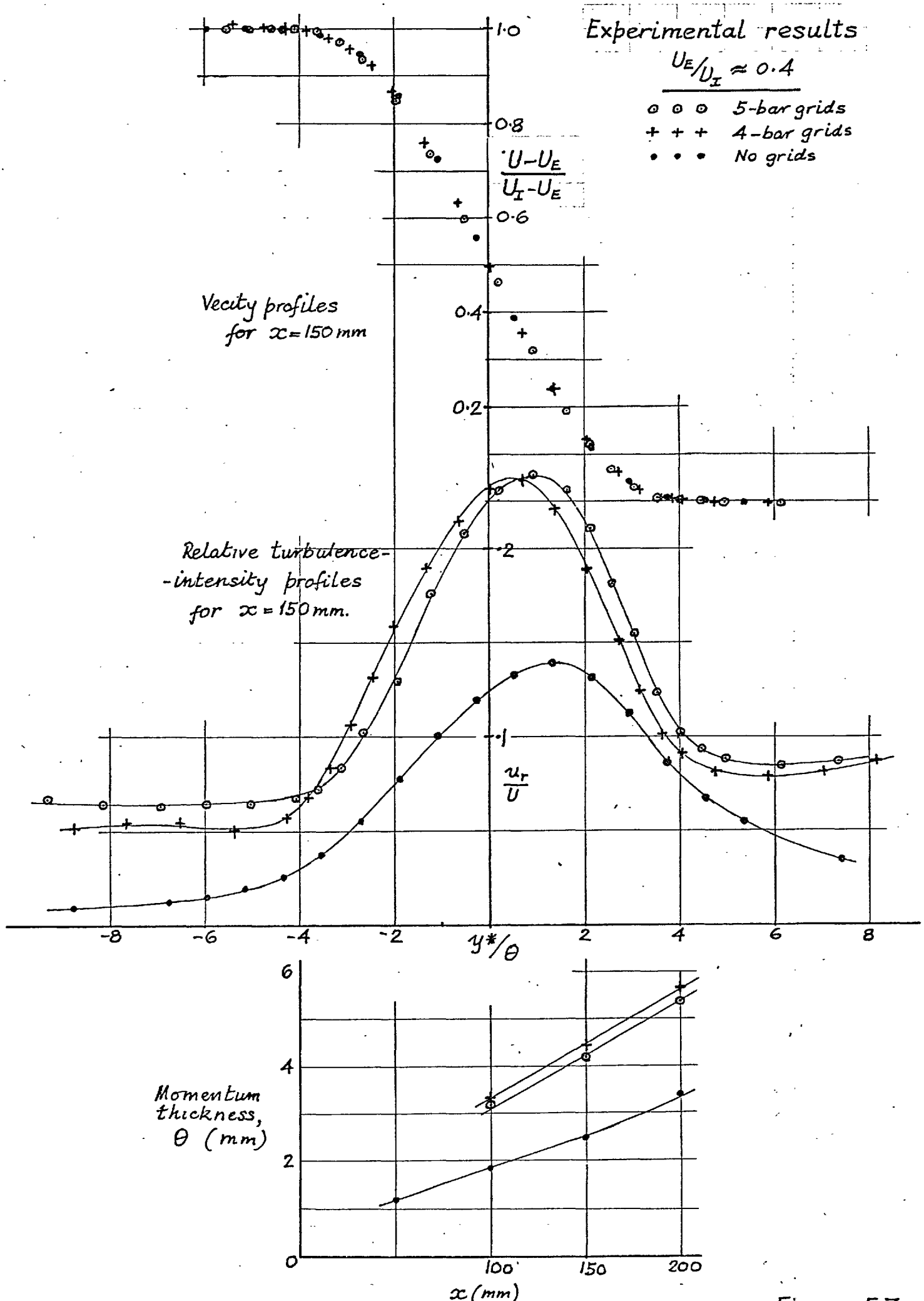

Experimental results
$U_E/U_I \approx 0.4$
5-bar grids
4-bar grids
No grids
$\frac{U-U_E}{U_I-U_E}$
Vecity profiles for $x = 150$ mm
Relative turbulence-intensity profiles for $x = 150$ mm.
$\frac{u_r}{U}$
y^*/θ
Momentum thickness, θ (mm)
x (mm)

Figure 5.7

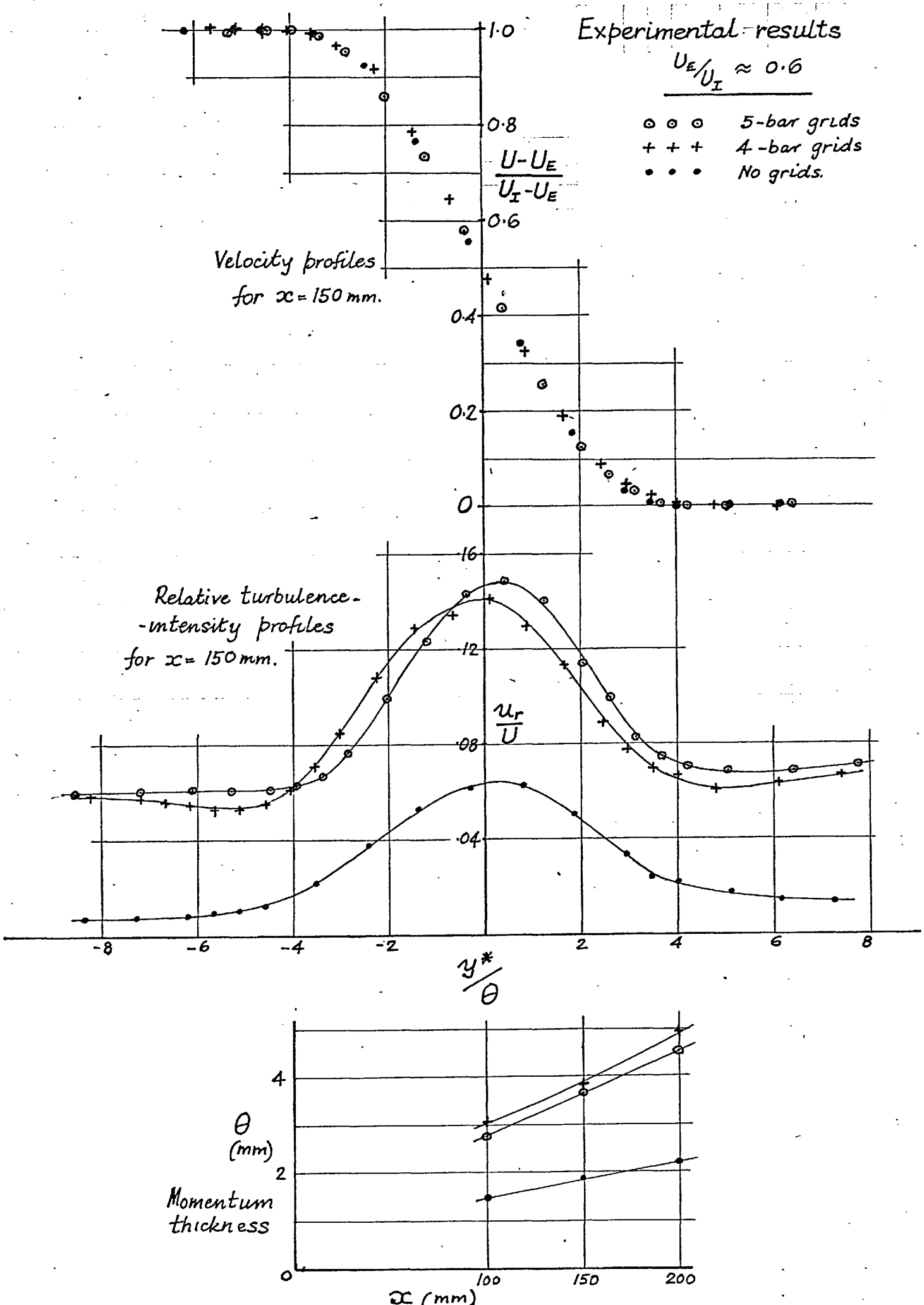

Experimental results
$U_E/U_I \approx 0.6$
5-bar grids
4-bar grids
No grids.
Velocity profiles for $x = 150$ mm.
$\frac{U-U_E}{U_I-U_E}$
1·0
0·8
0·6
0·4
0·2
0
Relative turbulence-intensity profiles for $x = 150$ mm.
$\frac{u_r}{U}$
·16
·12
·08
·04
-8
-6
-4
-2
2
4
6
8
$\frac{y^*}{\theta}$
Momentum thickness
θ (mm)
4
2
0
100
150
200
x (mm)

Figure 5.8

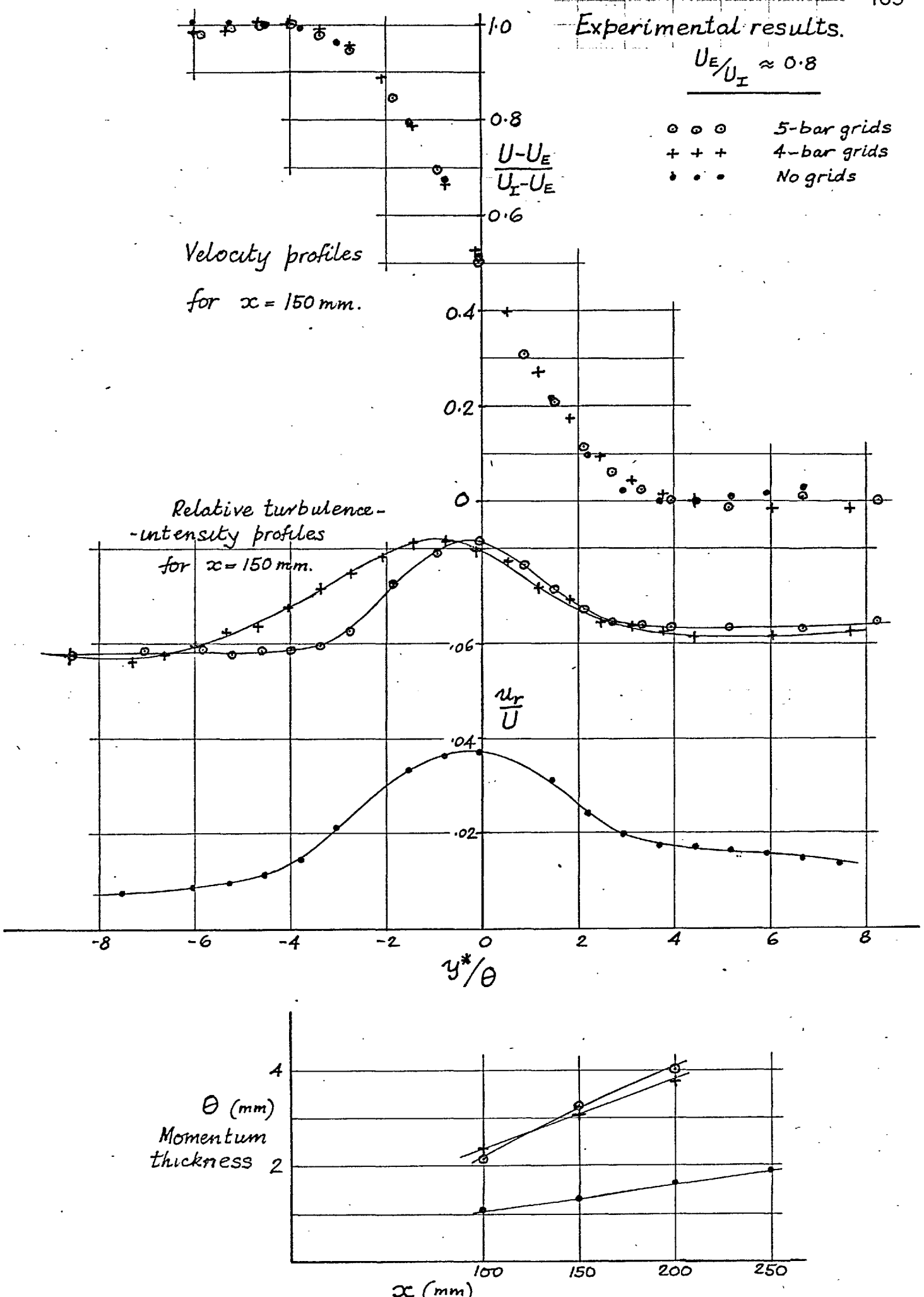
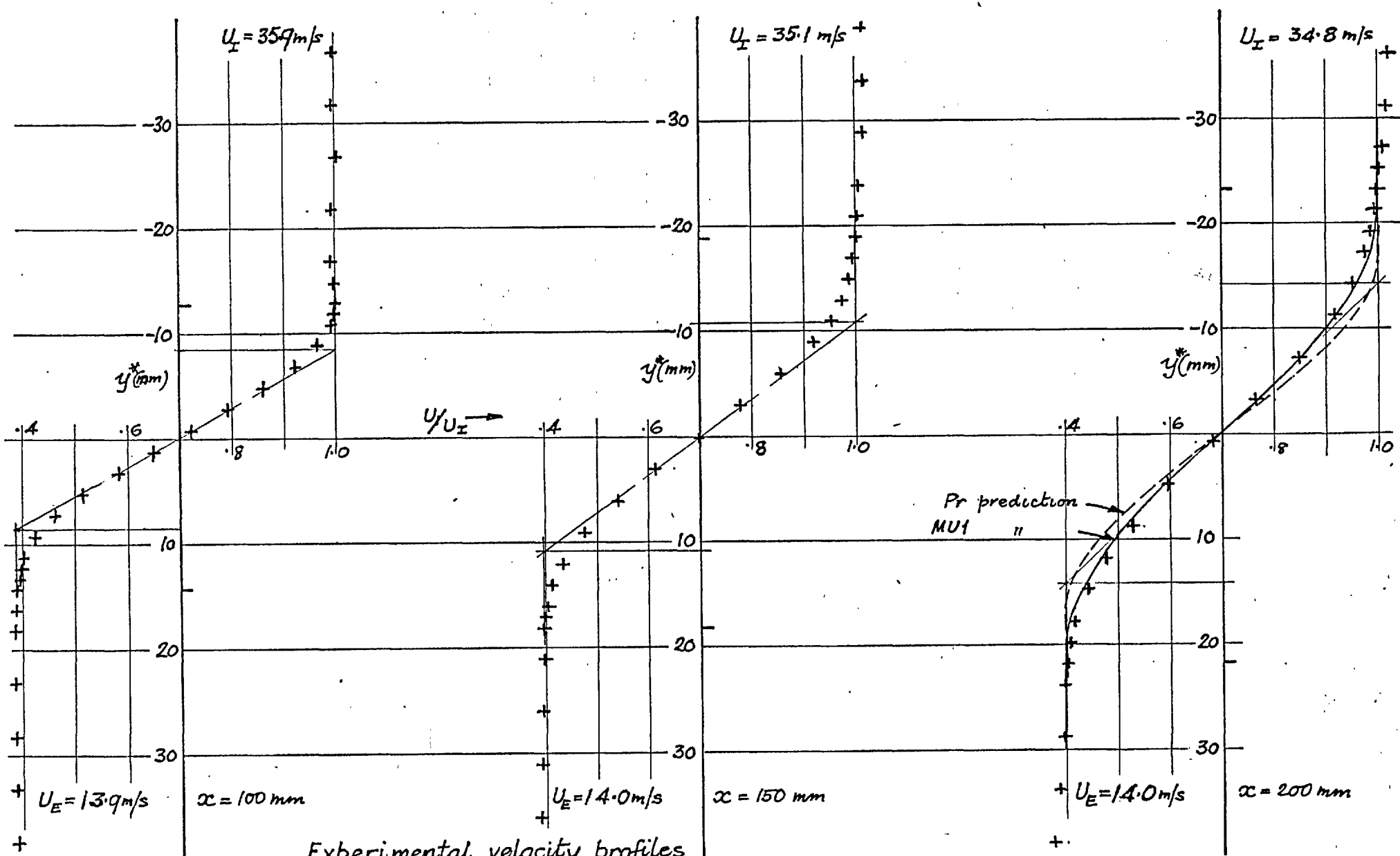

Experimental results.
$U_E/U_I \approx 0.8$
5-bar grids
4-bar grids
No grids
Velocity profiles
for $x = 150$ mm.
$\frac{U-U_E}{U_I-U_E}$
1.0
0.8
0.6
0.4
0.2
0
Relative turbulence-intensity profiles
for $x = 150$ mm.
$\frac{u_r}{U}$
.06
.04
.02
-8
-6
-4
-2
0
2
4
6
8
y^*/θ
θ (mm)
Momentum thickness
4
2
100
150
200
250
x (mm)

Figure 5.9



Experimental velocity profiles

RUN 5/57: 5-bar grids, $U_E/U_I \approx 0.4$

Figure 5.10

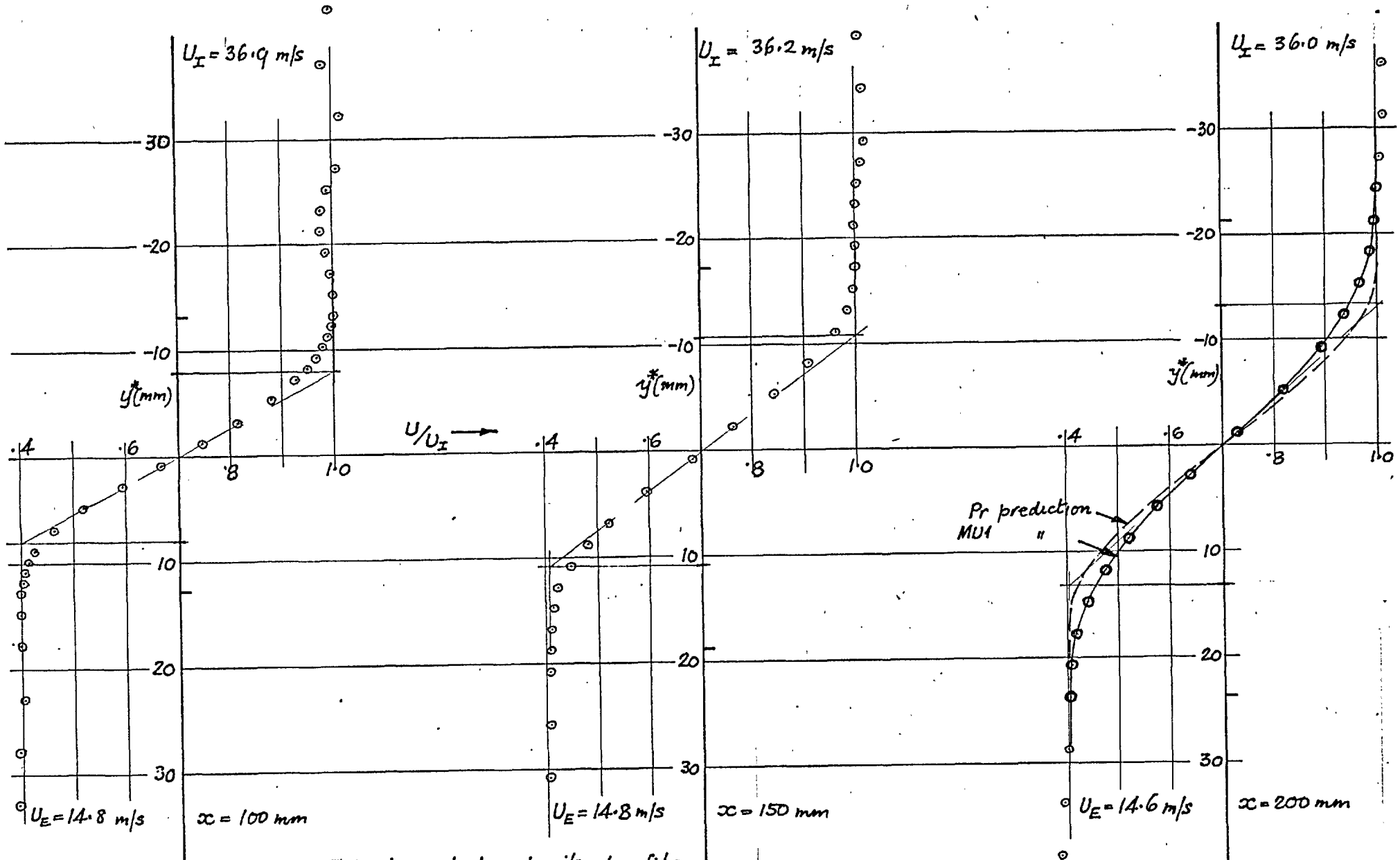


Figure 5.11

Experimental velocity profiles

RUN A/48 : 4-bar grids , $U_E/U_I \approx 0.4$

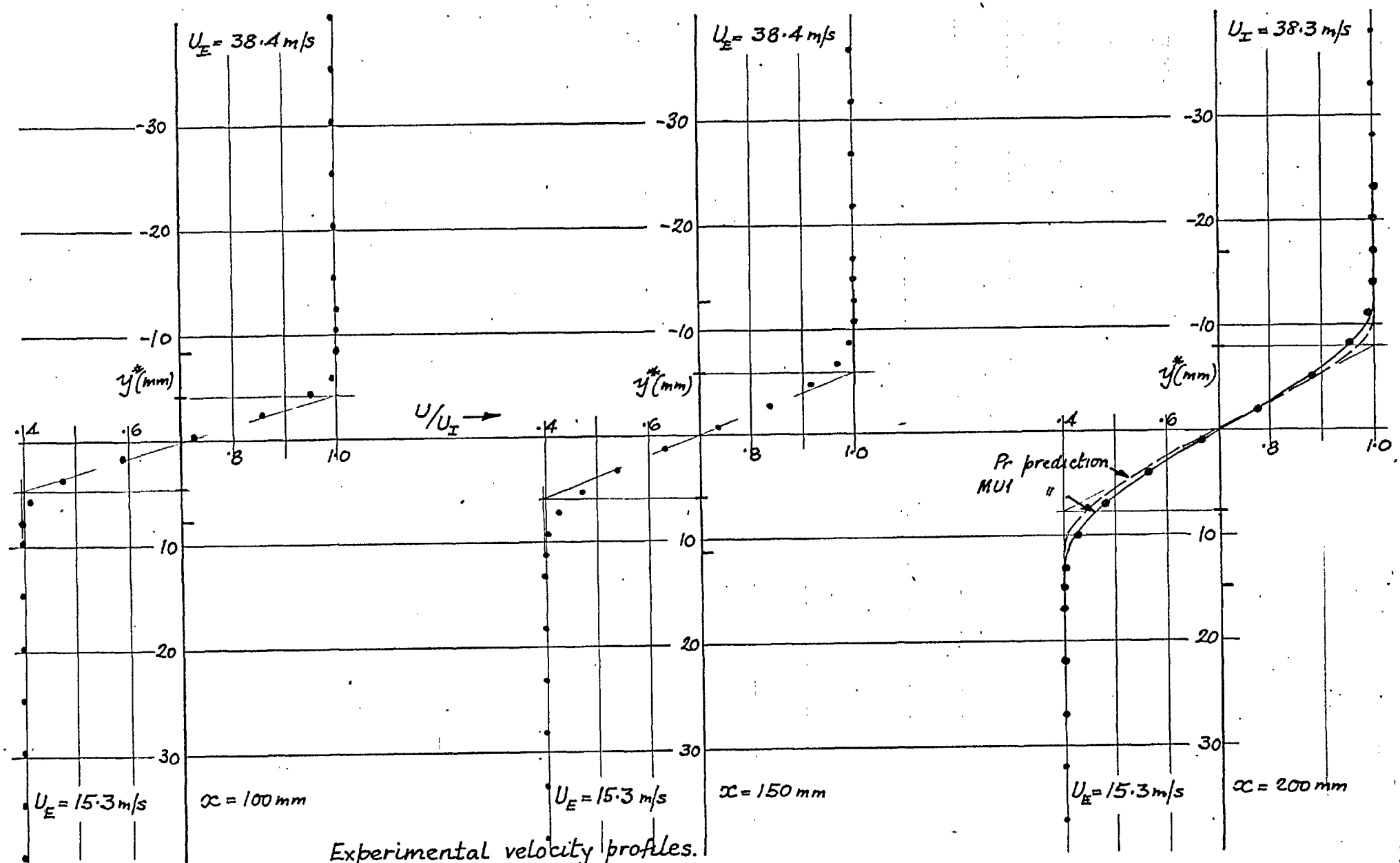


Figure 5.12

Experimental velocity profiles.

RUN 0/58 : No grids, $U_E/U_I \approx 0.4$

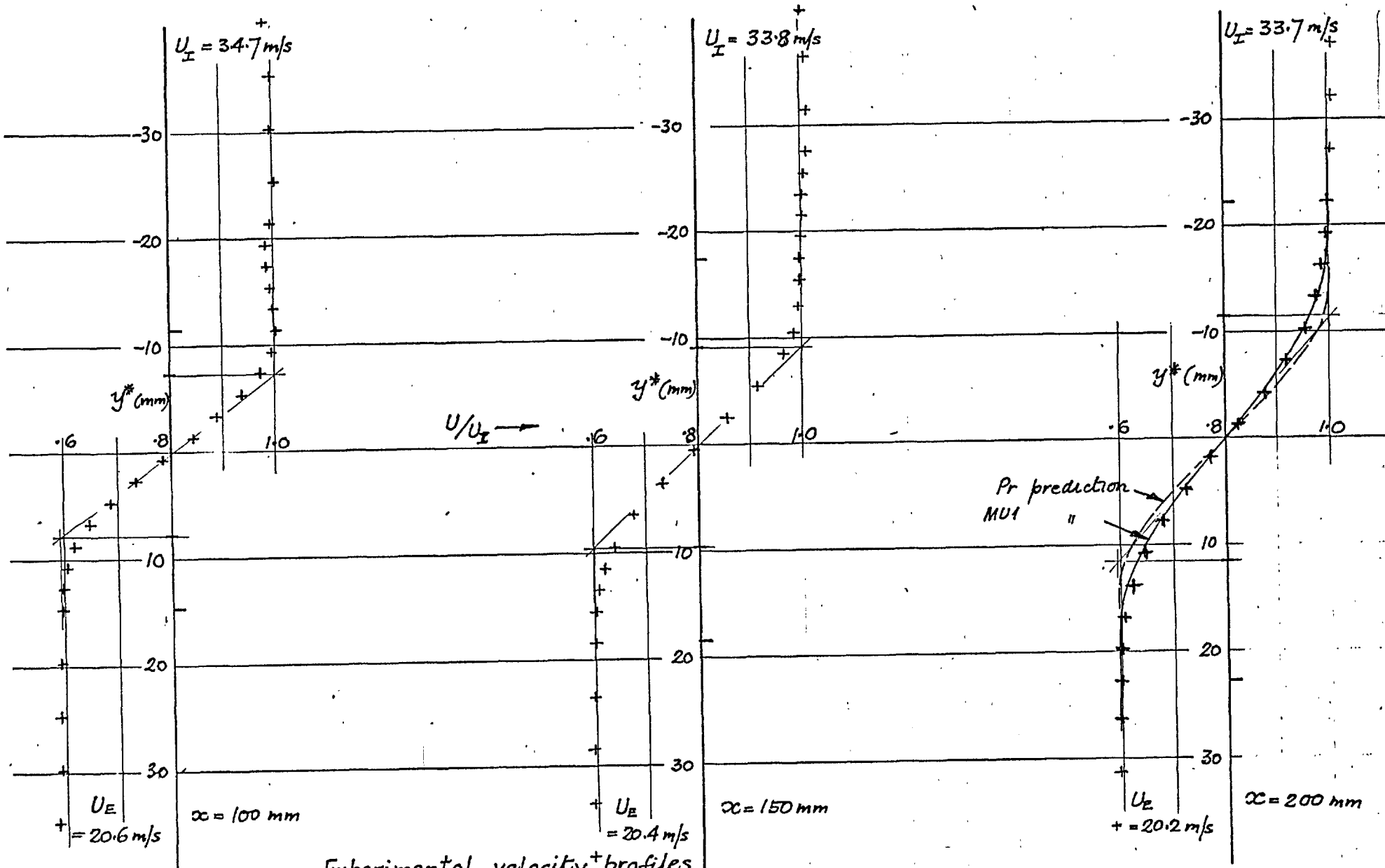


Figure 5.13

Experimental velocity profiles

RUN 5/54: 5-bar grids, $U_E/U_I \approx 0.6$

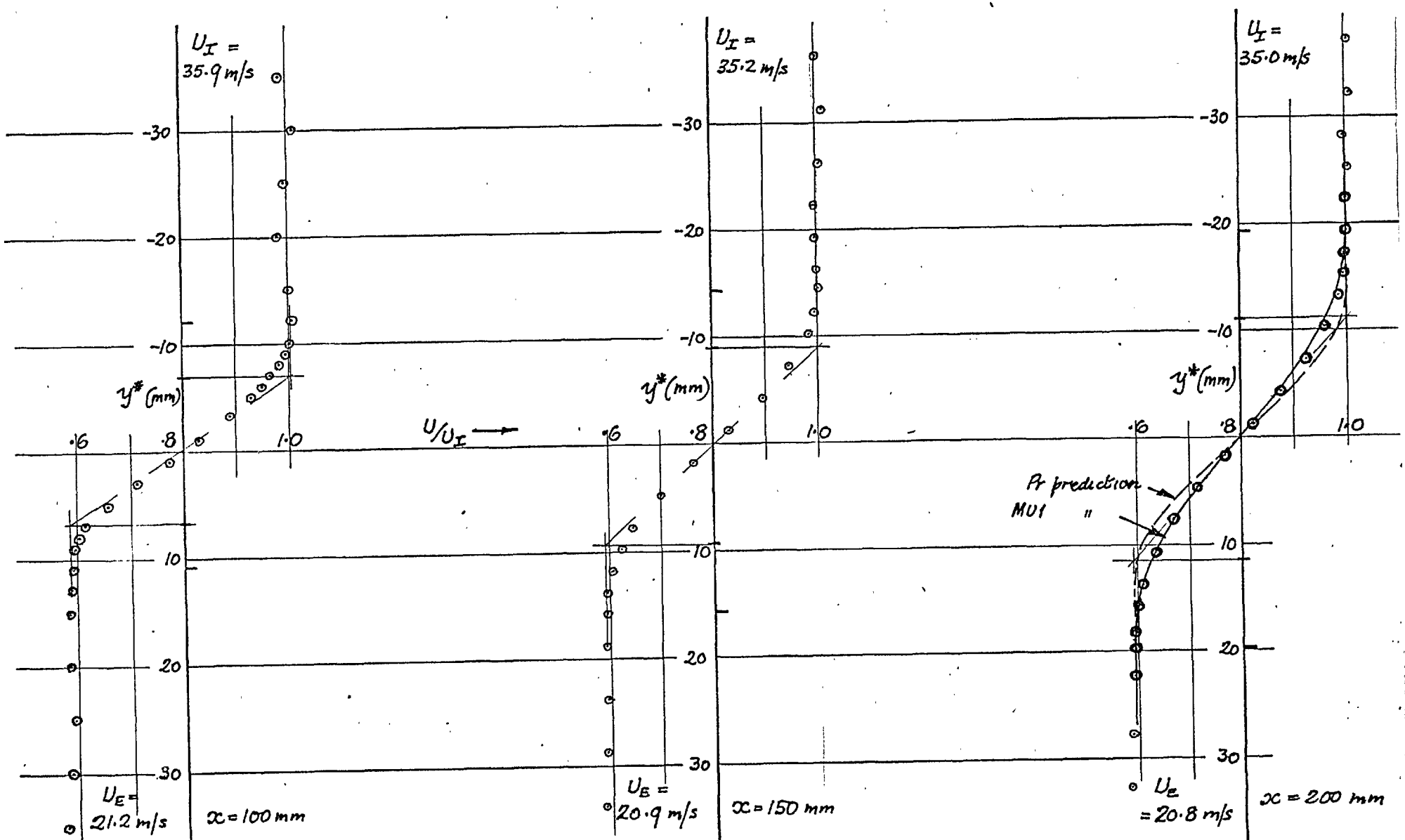
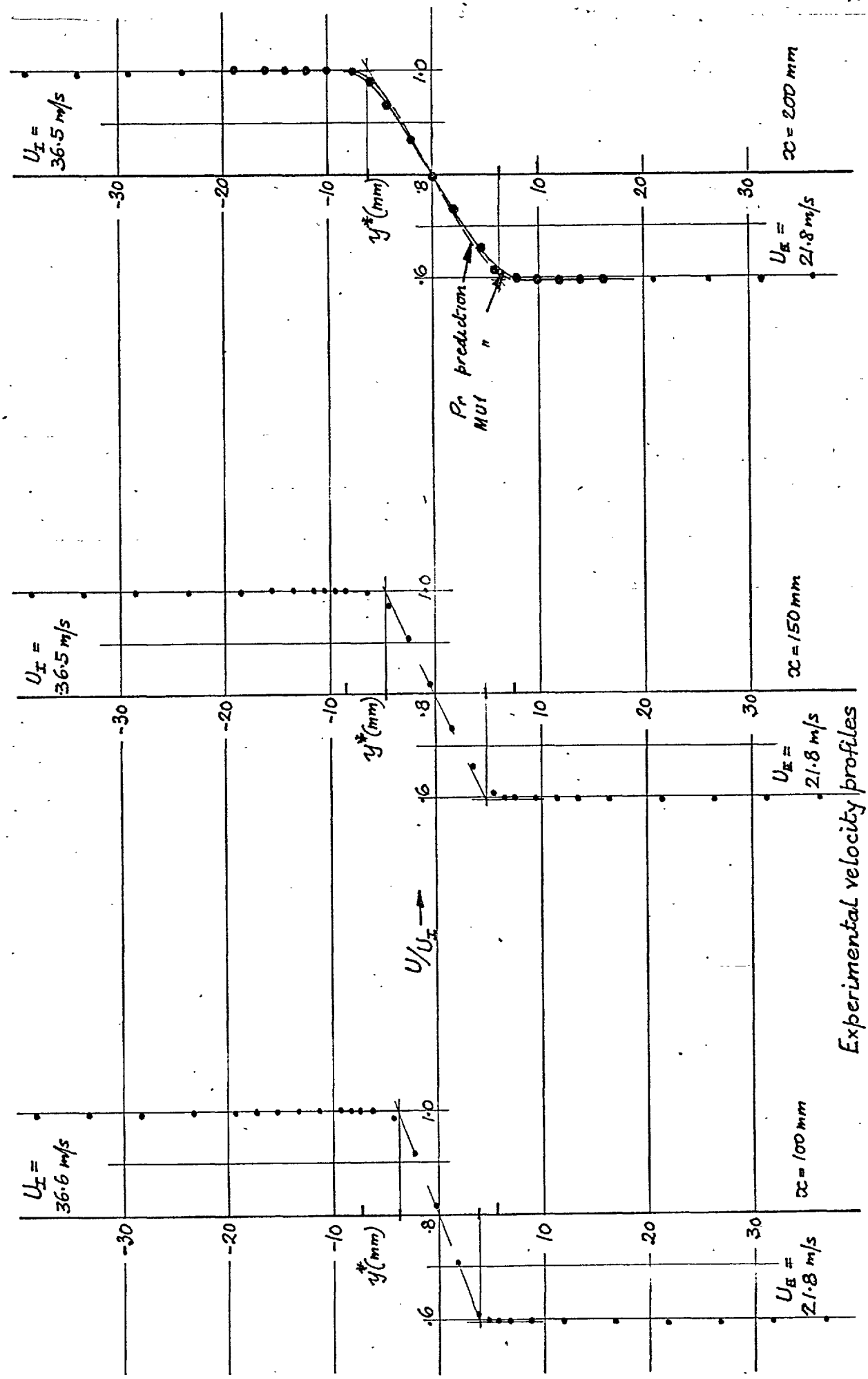


Figure 5.14

Experimental velocity profiles

RUN 4/49: 4-bar grids, $U_E/U_I \approx 0.6$



Experimental velocity profiles

RUN 0/59: No grads, $U_E/U_I \approx 0.6$

Figure 5.15

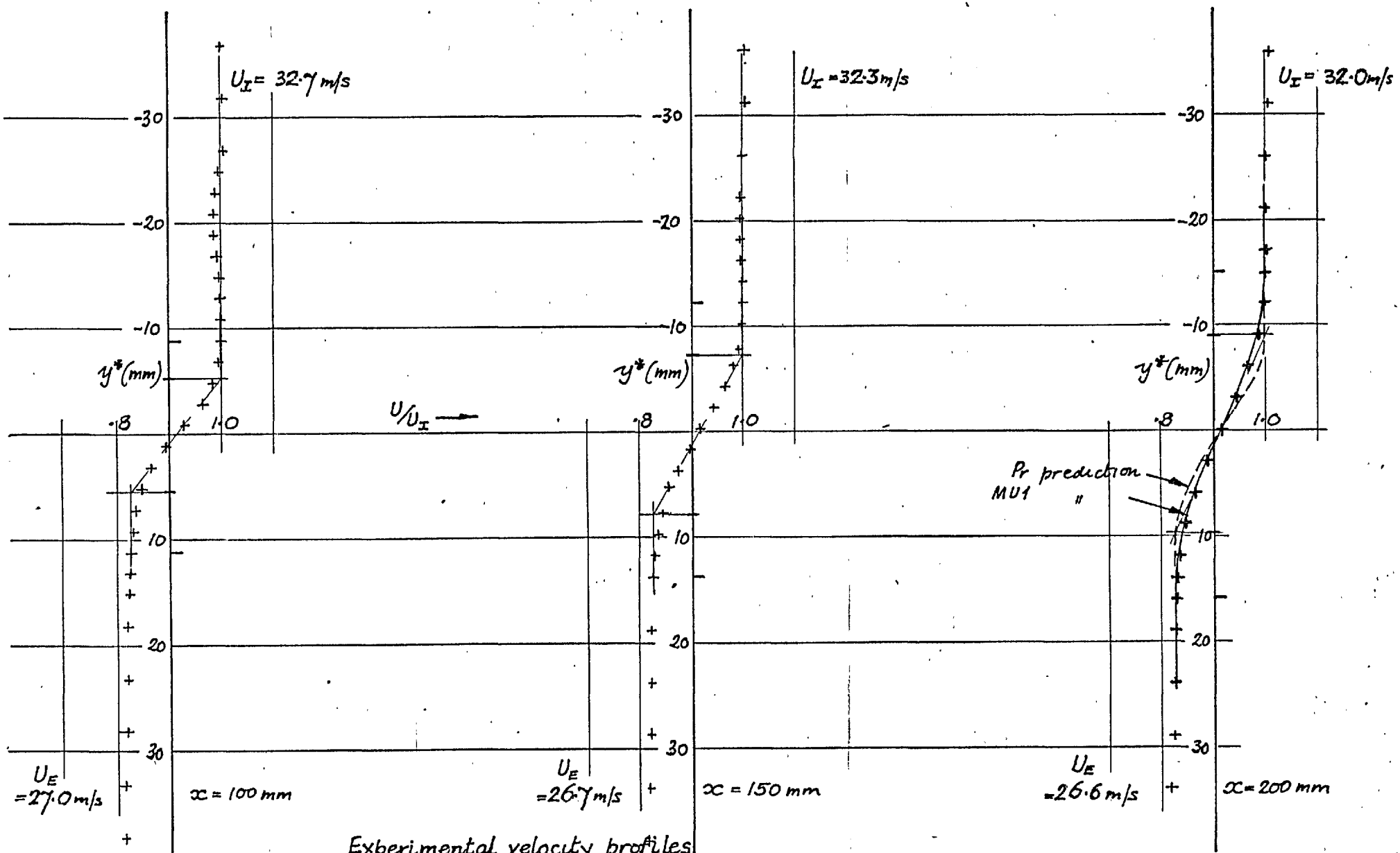


Figure 5.16

Experimental velocity profiles

RUN 5/53: 5-bar grids, $U_E/U_I \approx 0.8$

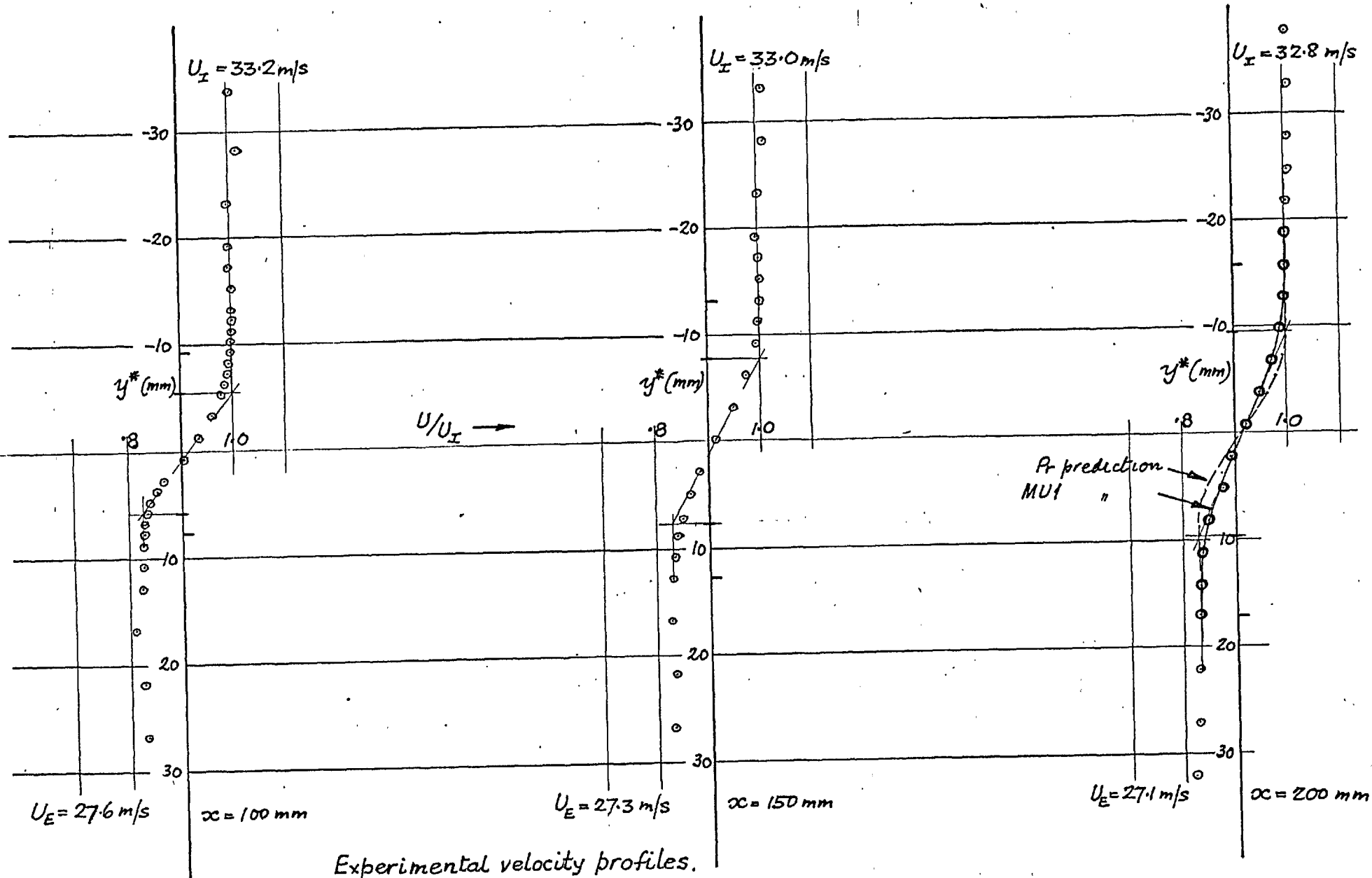


Figure 5.17

Experimental velocity profiles.

RUN 4/47: 4-bar grids, $U_E/U_I \approx 0·8$

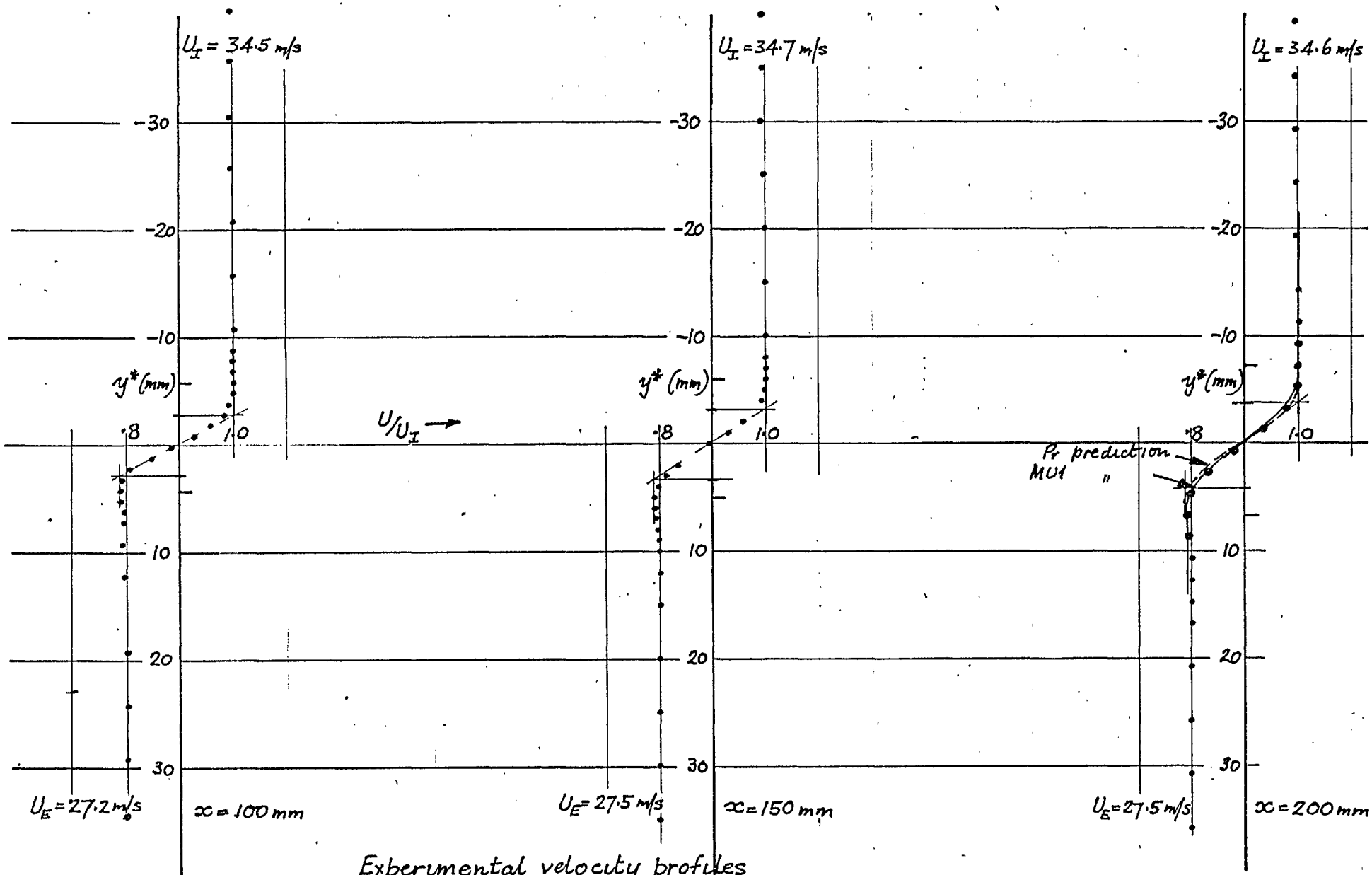


Figure 5.18

Experimental velocity profiles

RUN 0/60: No grids, $U_E/U_I \approx 0.8$

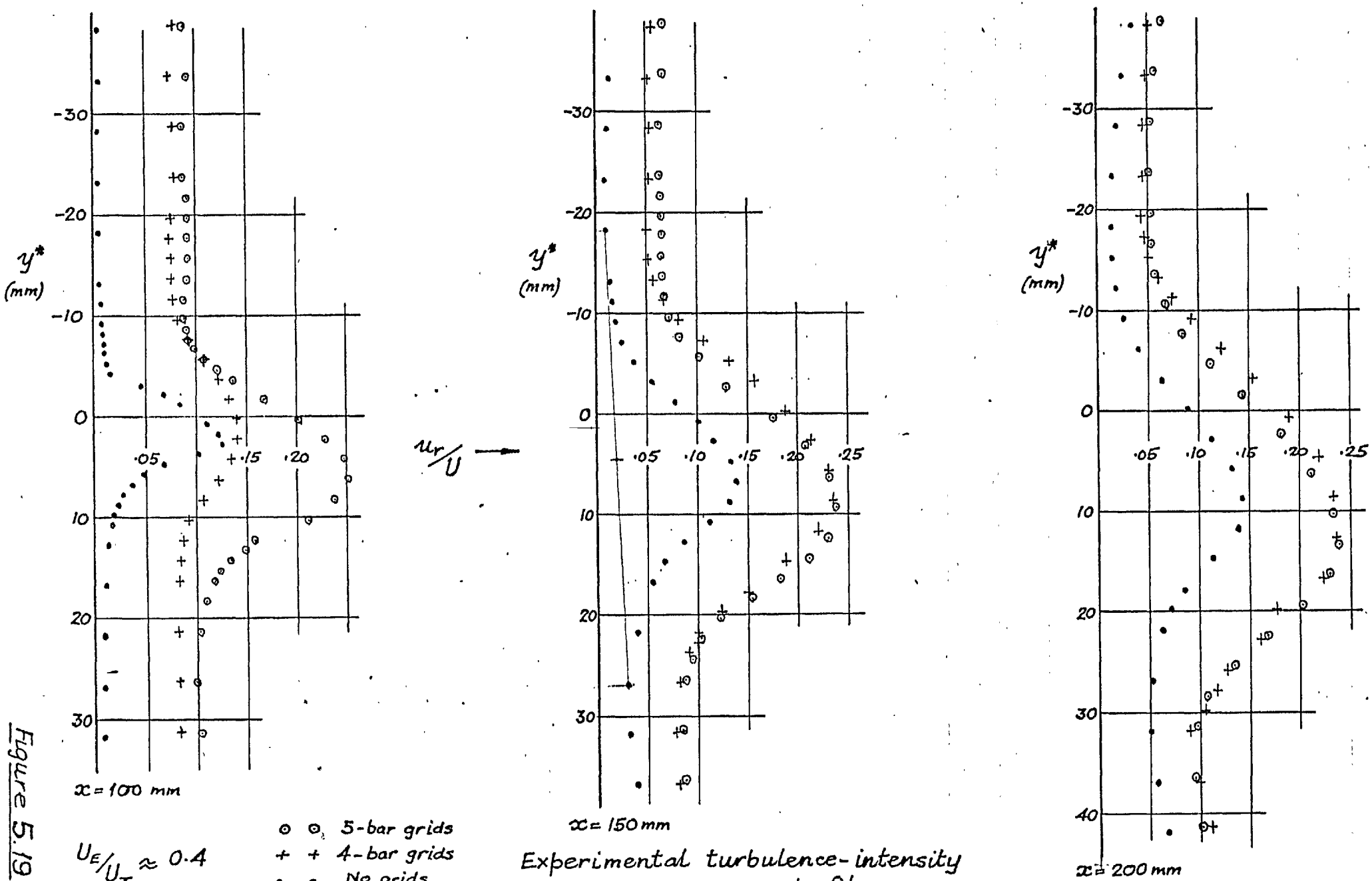
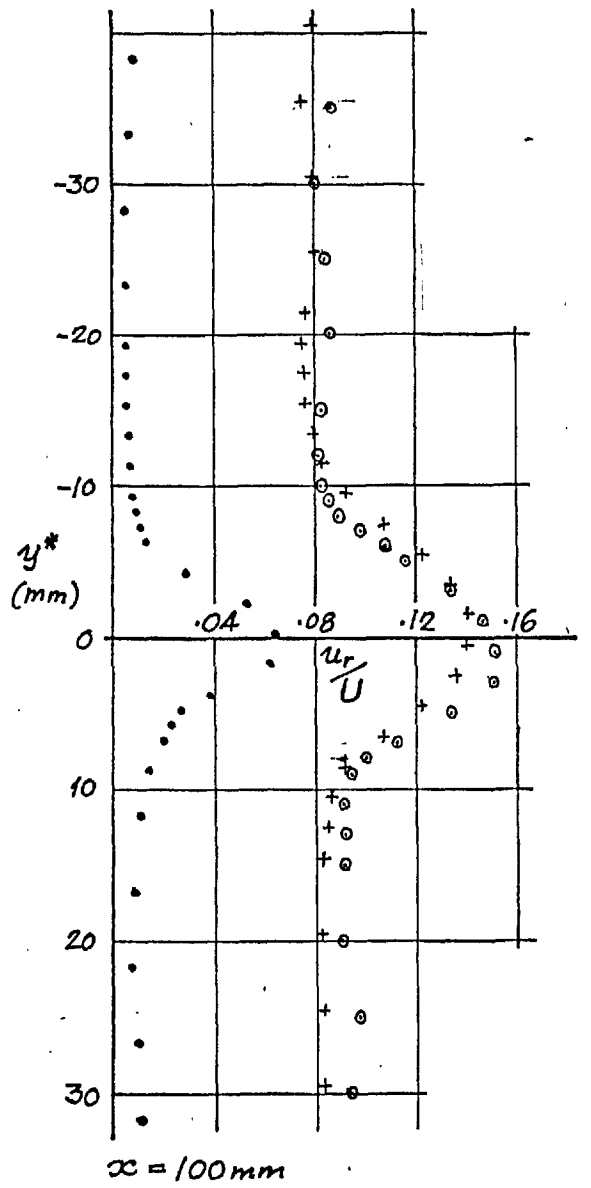
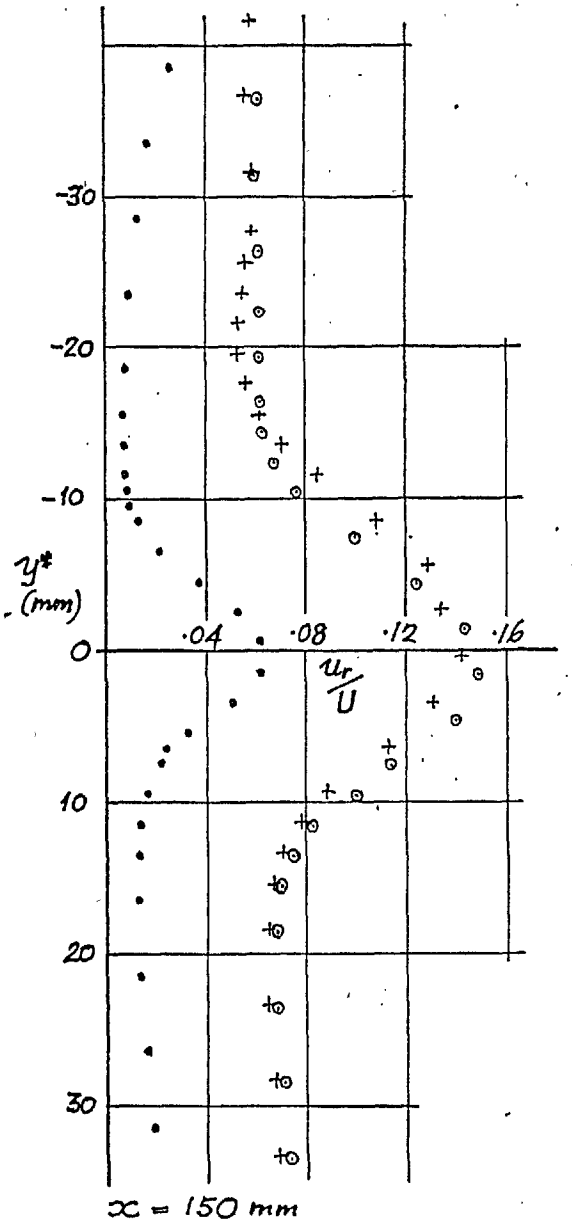
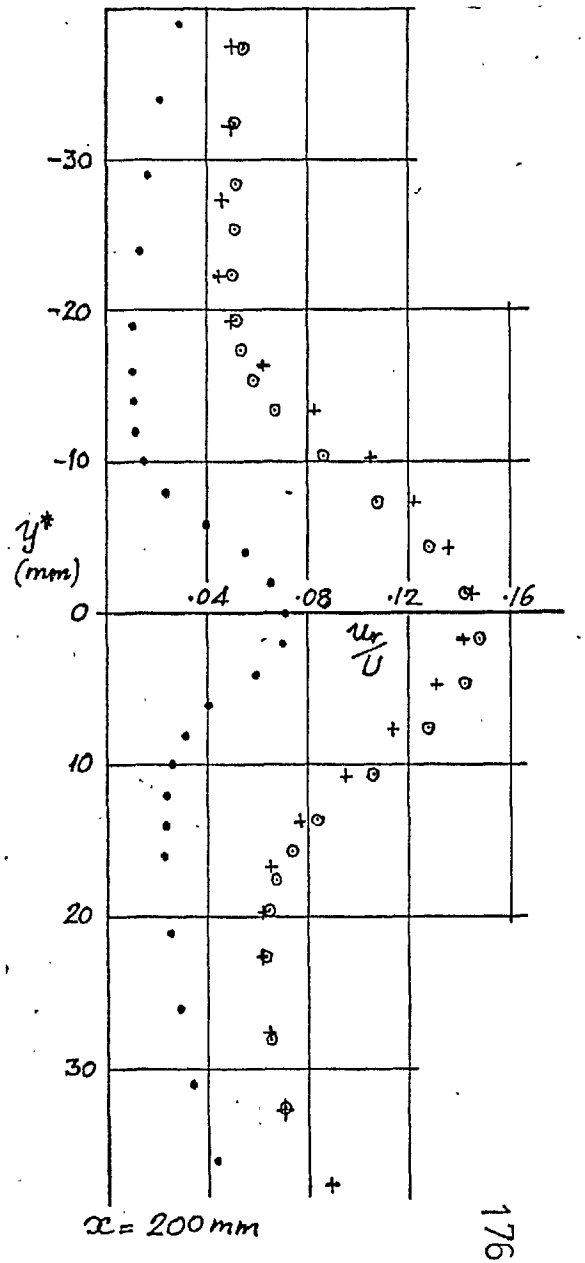


Figure 5.19

Experimental turbulence-intensity profiles







$\frac{U_E}{U_I} \approx 0.6$

o o 5-bar grids
+ + 4-bar grids
• • No grids

Figure 5.20 Experimental turbulence intensity profiles

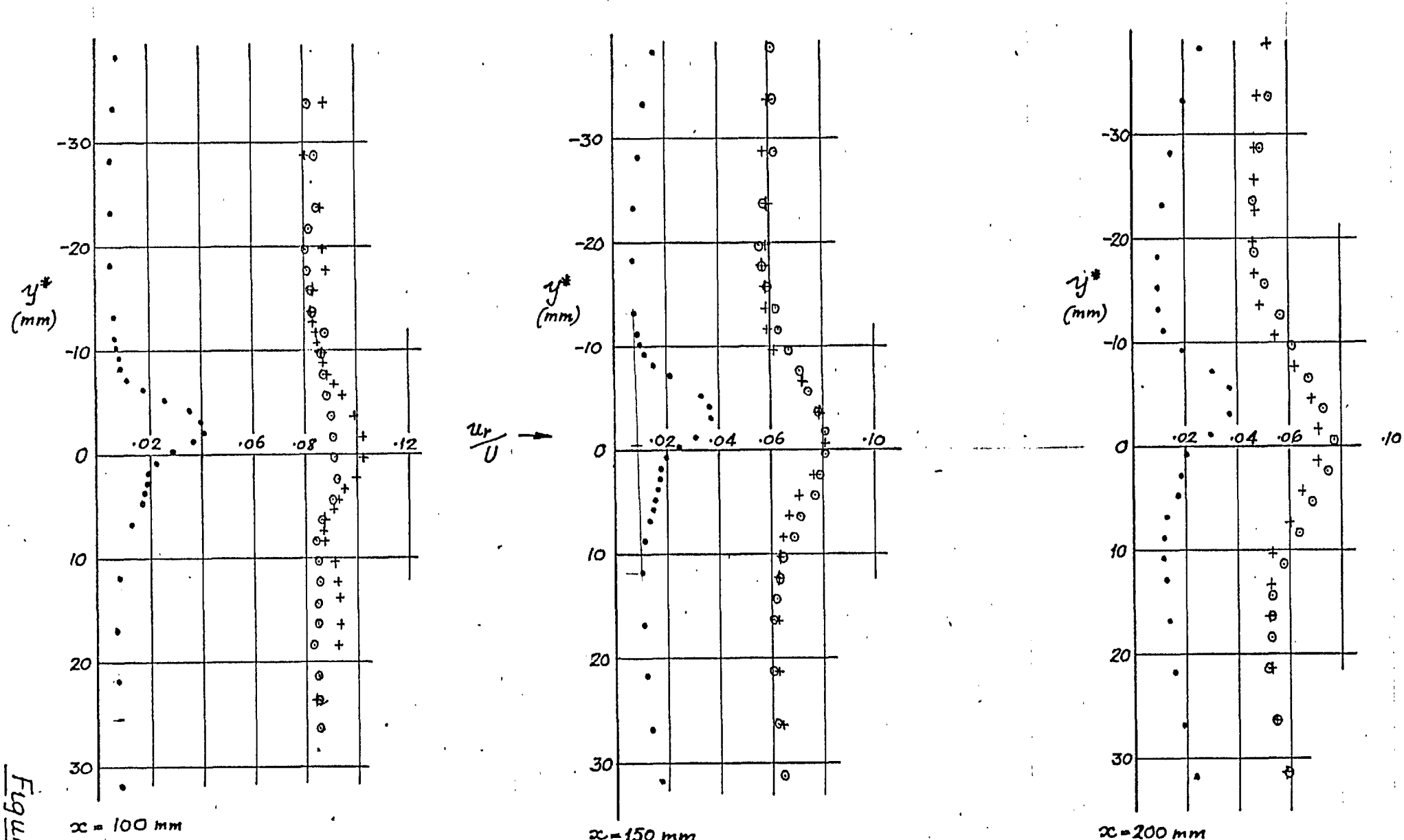


Figure 5.21

Experimental turbulence-intensity profiles

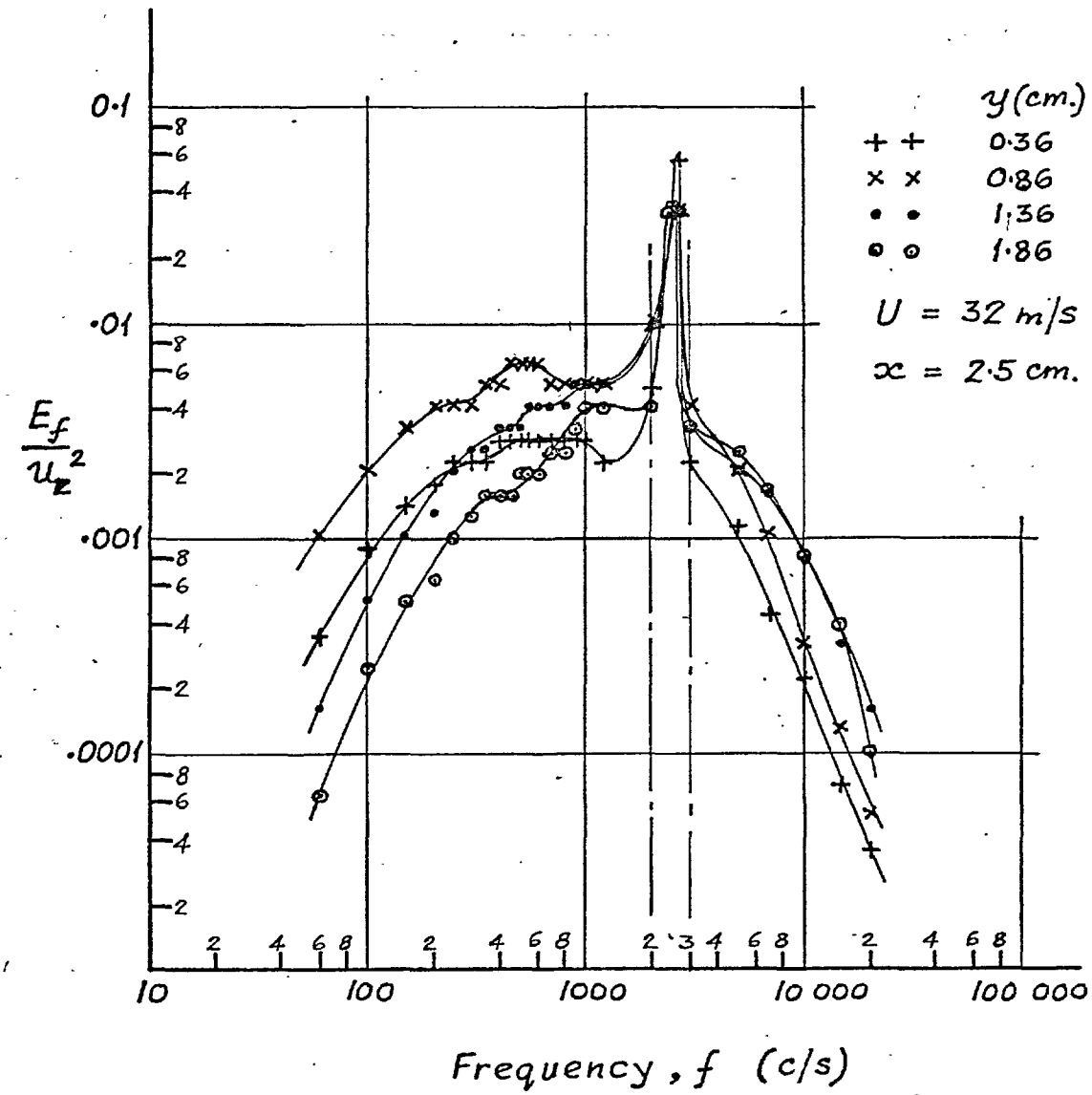

y(cm.)
+ + 0·36
× × 0·86
• • 1·36
o o 1·86
U = 32 m/s
x = 2·5 cm.
$\frac{E_f}{u_z^2}$
0·1
·01
·001
·0001
10
100
1000
10 000
100 000
Frequency, f (c/s)

Figure 5.22

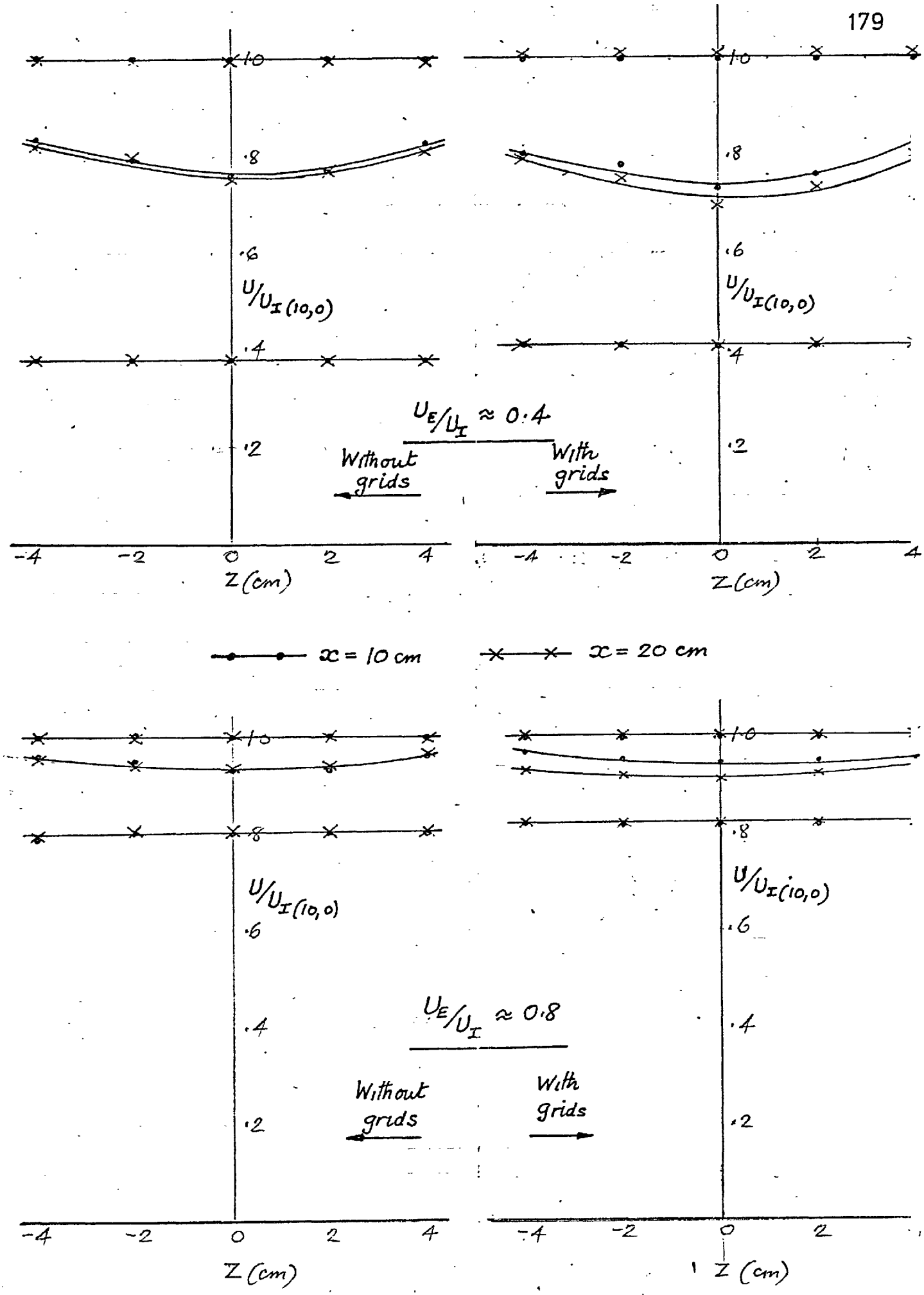

1·0
·8
·6
·4
·2
U/U_I(10,0)
$U_E/U_I \approx 0.4$
Without grids
With grids
-4
-2
0
2
4
Z (cm)
x = 10 cm
x = 20 cm
$U_E/U_I \approx 0.8$

Figure 5.24

5.9. Typical velocity profiles produced by various grid systems.
(at $x = 5$ cm)

——— 5-bar oscillating grid

——— $\frac{1}{16}$" Horizontal bars with adjustable spacing.

- - - - - - $\frac{3}{16}$" bars fixed at $\frac{1}{2}$" centres

——— $\frac{1}{8}$" " " " $\frac{3}{8}$" "

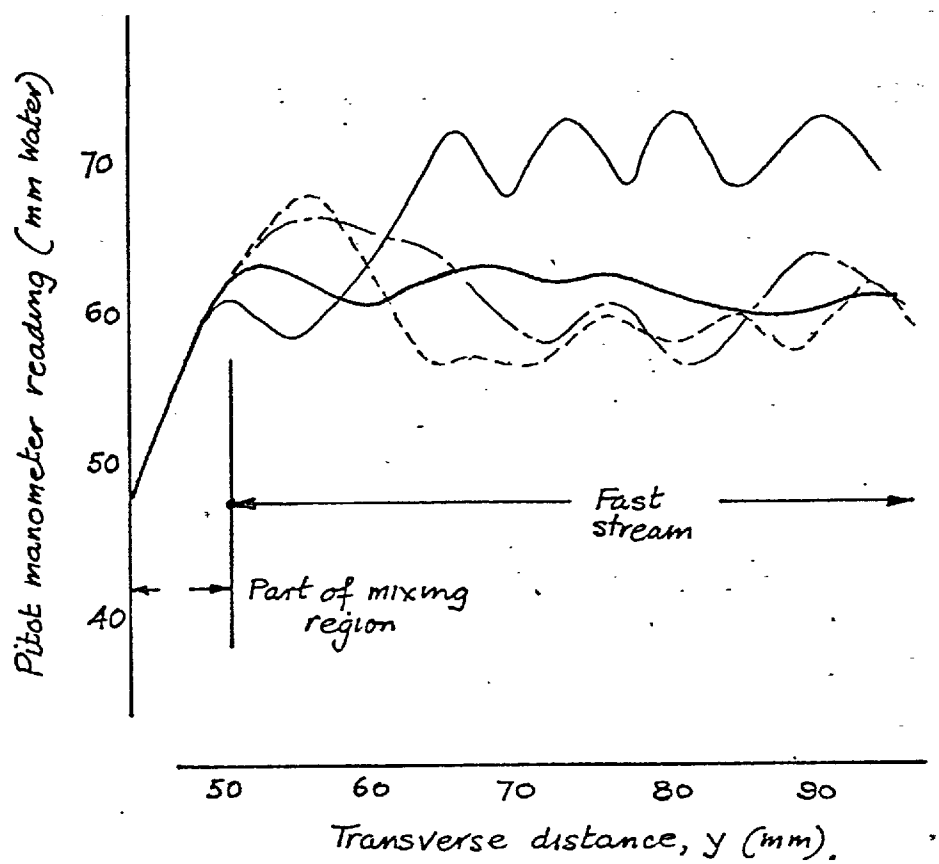


Figure 5.25

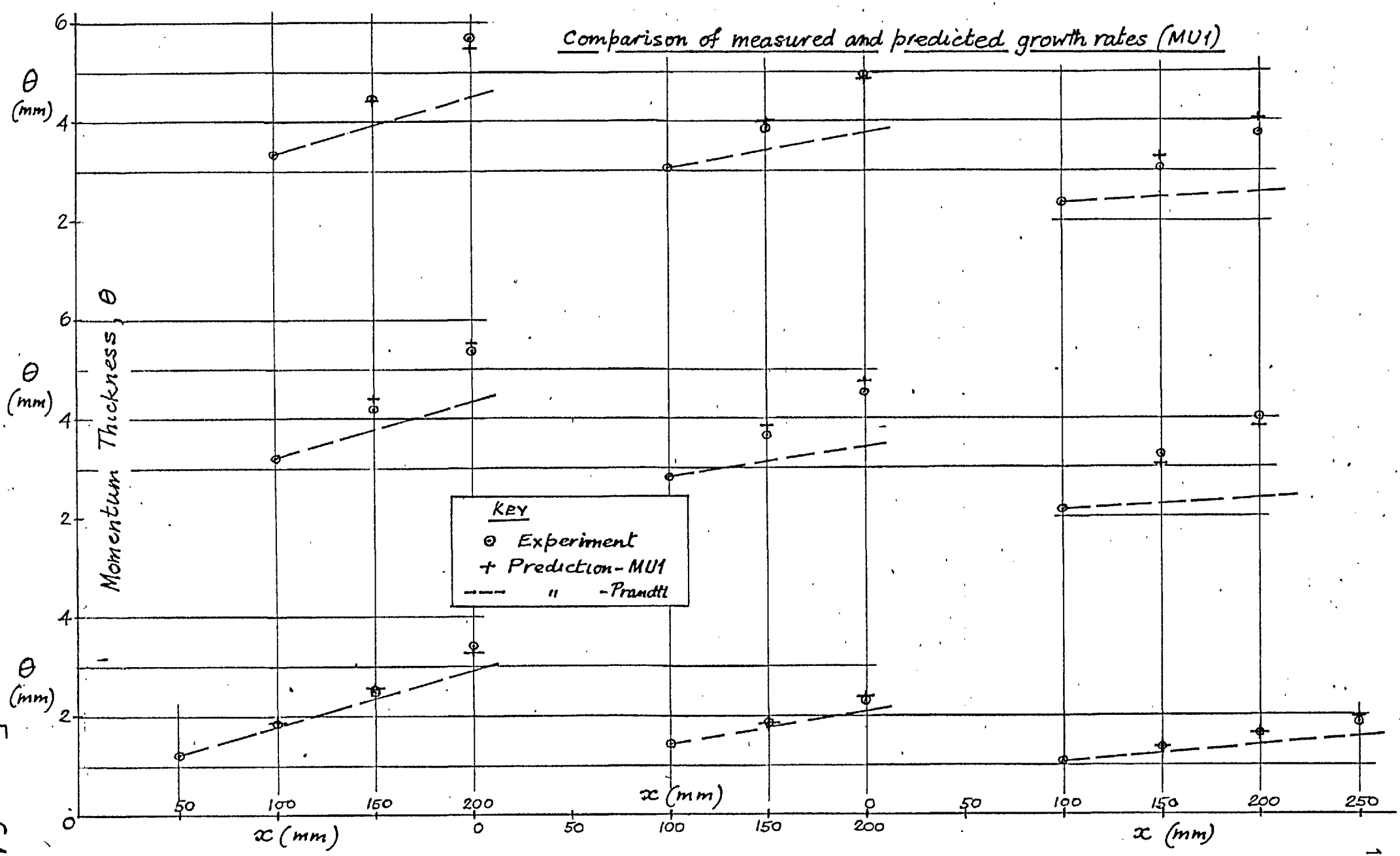

Comparison of measured and predicted growth rates (MU1)
Momentum Thickness, θ
θ (mm)
θ (mm)
θ (mm)
KEY
Experiment
Prediction - MU1
" - Prandtl
x (mm)
x (mm)
x (mm)

Figure 6.1

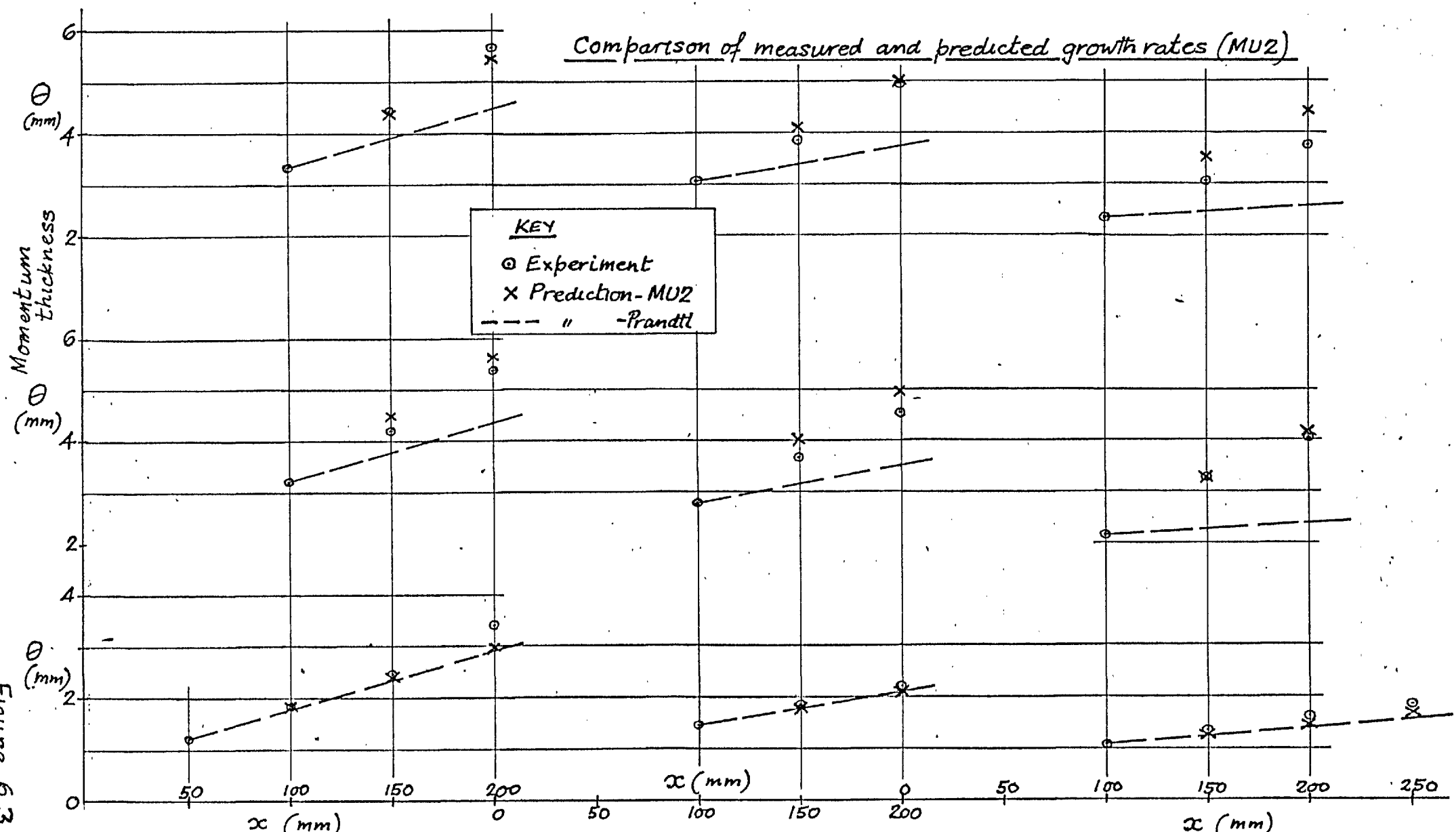
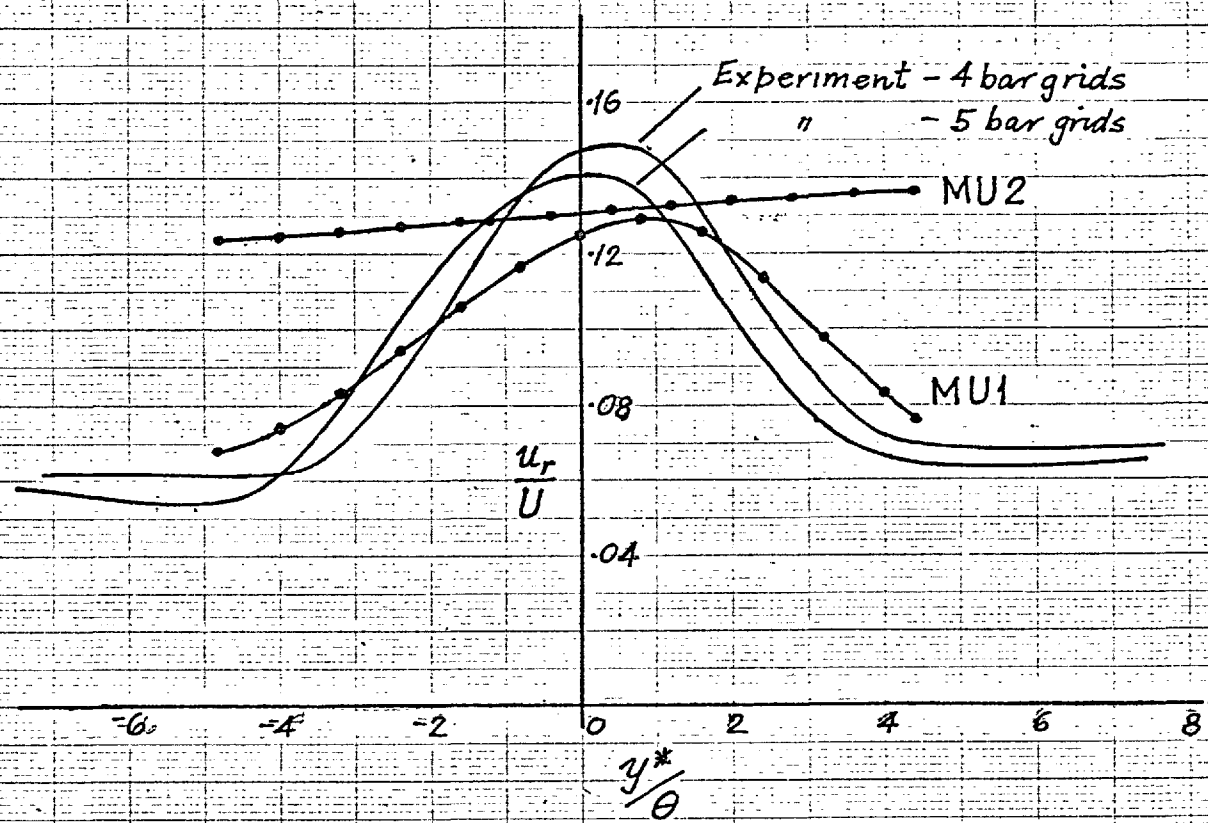

Comparison of measured and predicted growth rates (MU2)
KEY
Experiment
Prediction - MU2
" - Prandtl
Momentum thickness
θ (mm)
x (mm)
0
2
4
6
50
100
150
200
250

Figure 6.3



Comparison of relative turbulence intensity profiles from experiment and mixing-length predictions.

Figure 6.4

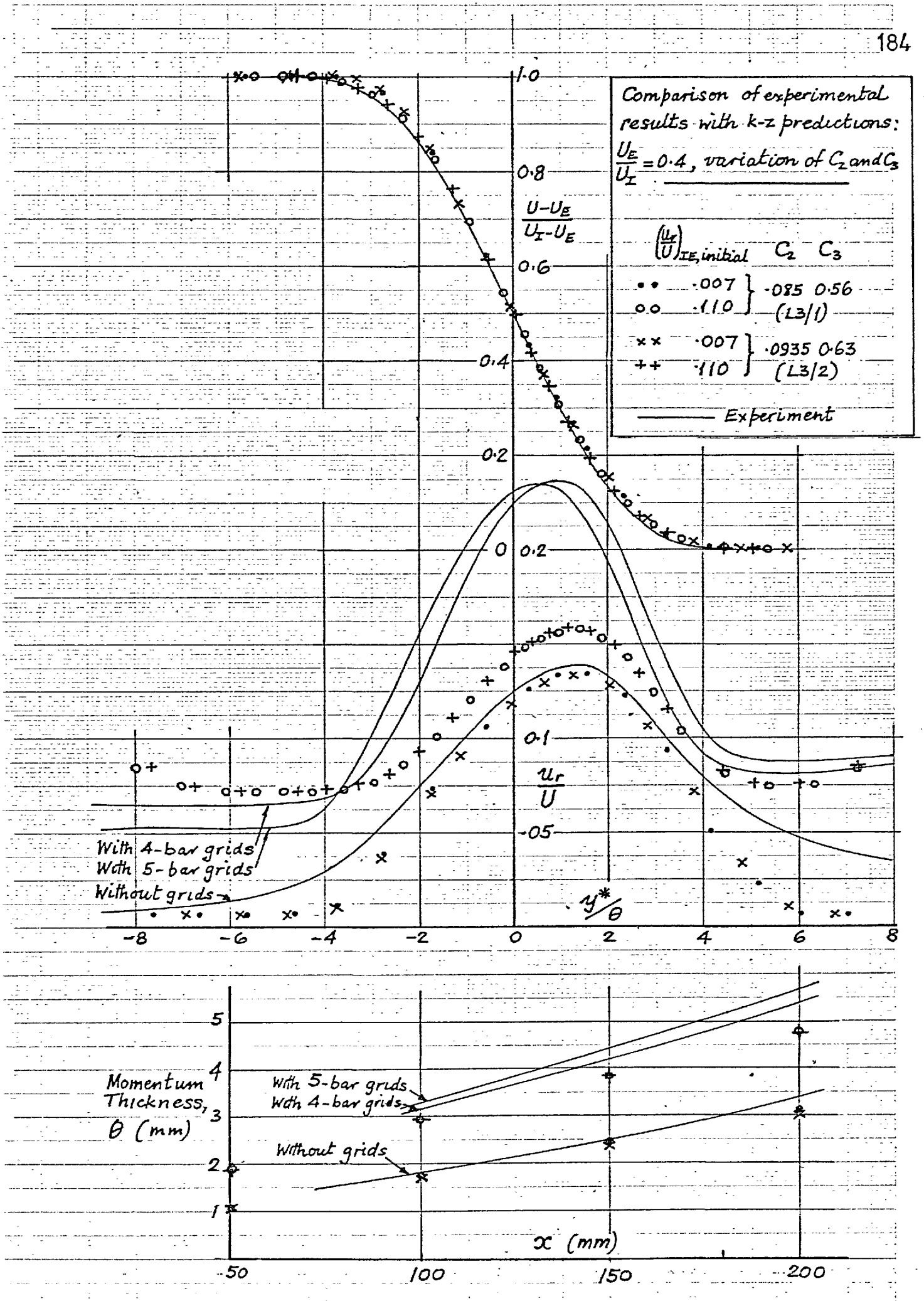

Comparison of experimental results with k-z predictions:
$\frac{U_E}{U_I} = 0.4$, variation of C_2 and C_3
$(\frac{u_r}{U})_{IE,initial}$ C_2 C_3
·007 ·085 0·56
·110 (L3/1)
·007 ·0935 0·63
·110 (L3/2)
Experiment
$\frac{U-U_E}{U_I-U_E}$
$\frac{u_r}{U}$
y^*/θ
With 4-bar grids
With 5-bar grids
Without grids
Momentum Thickness, θ (mm)
With 5-bar grids
With 4-bar grids
Without grids
x (mm)

Figure 6·5

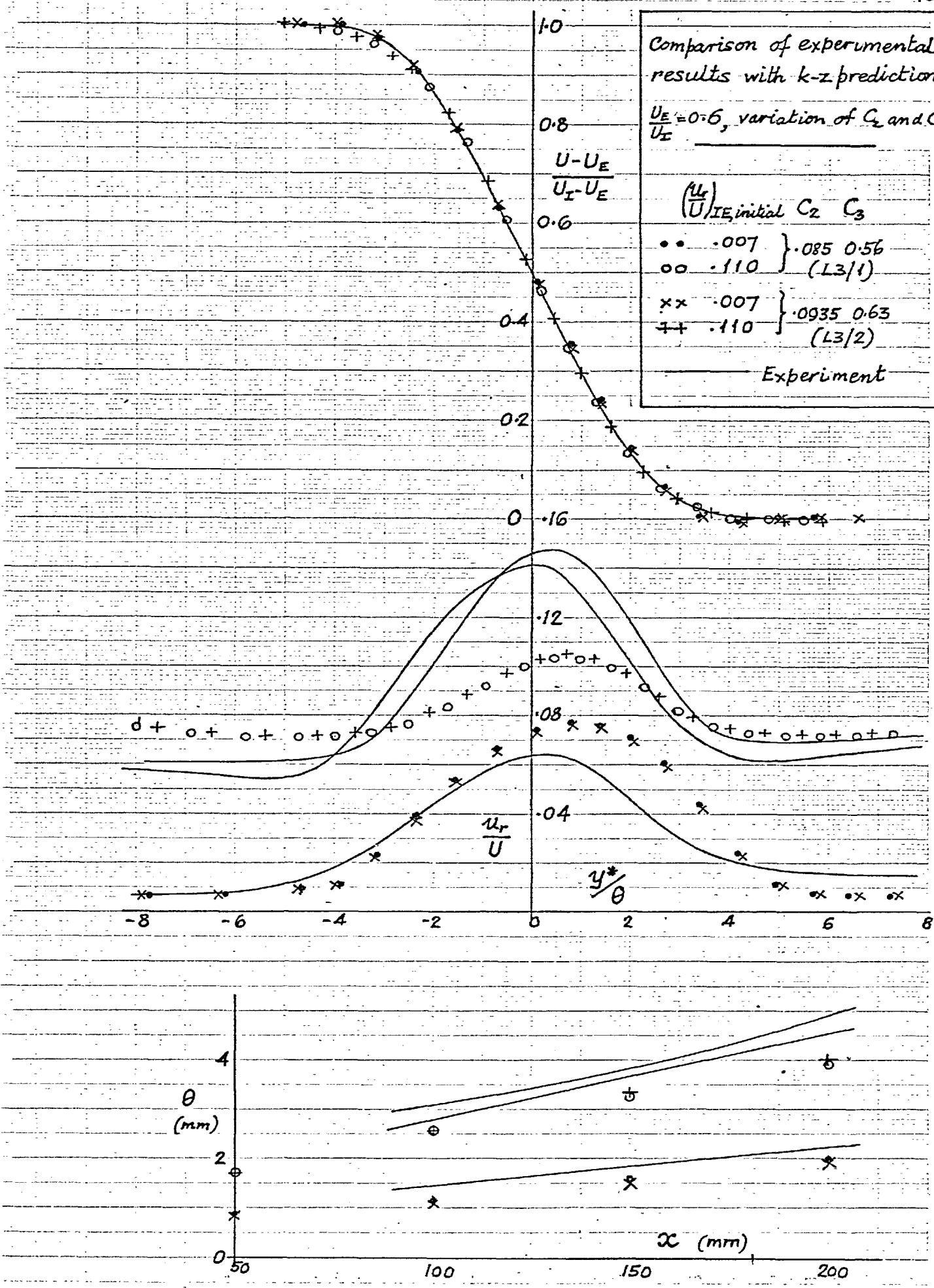
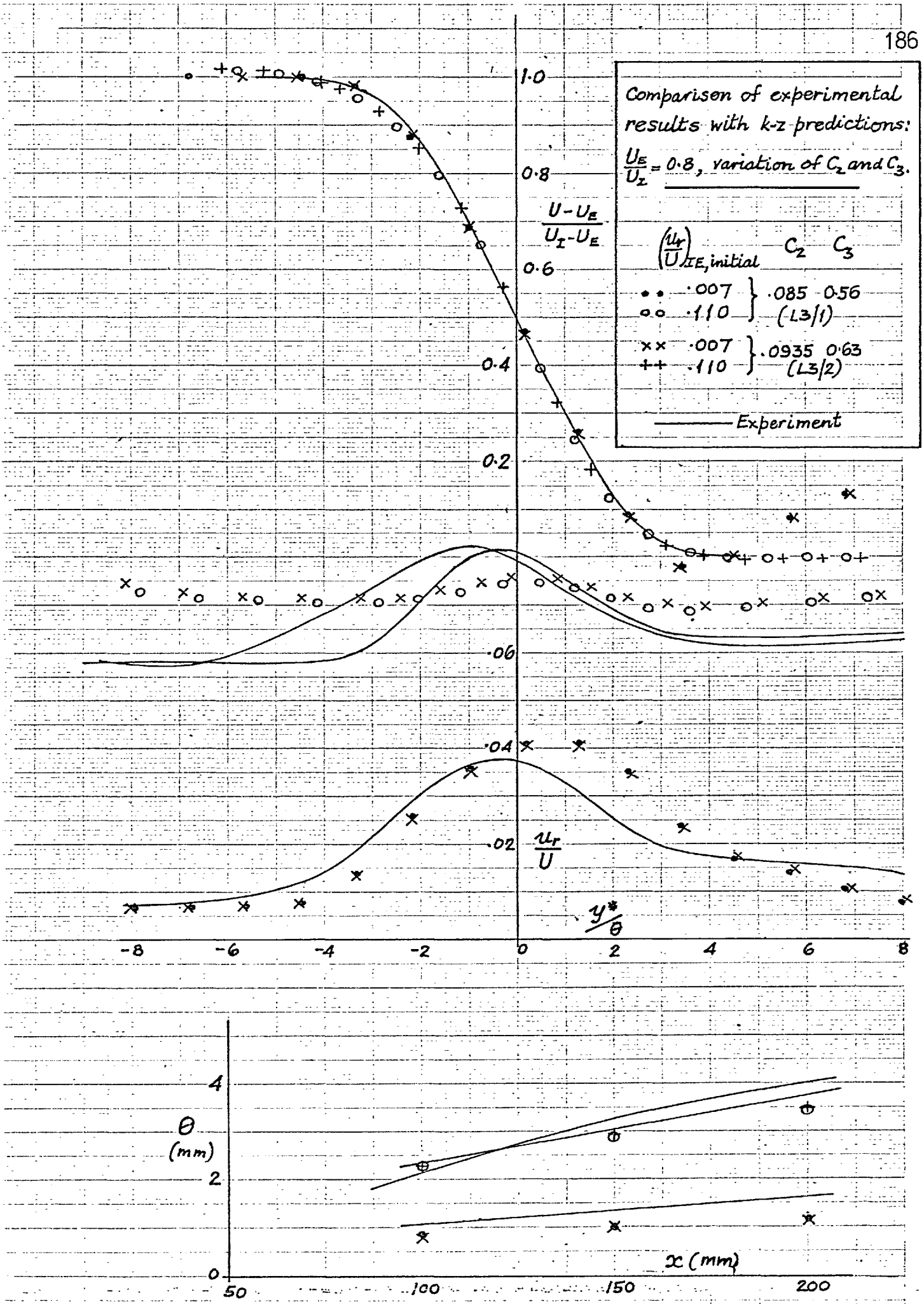
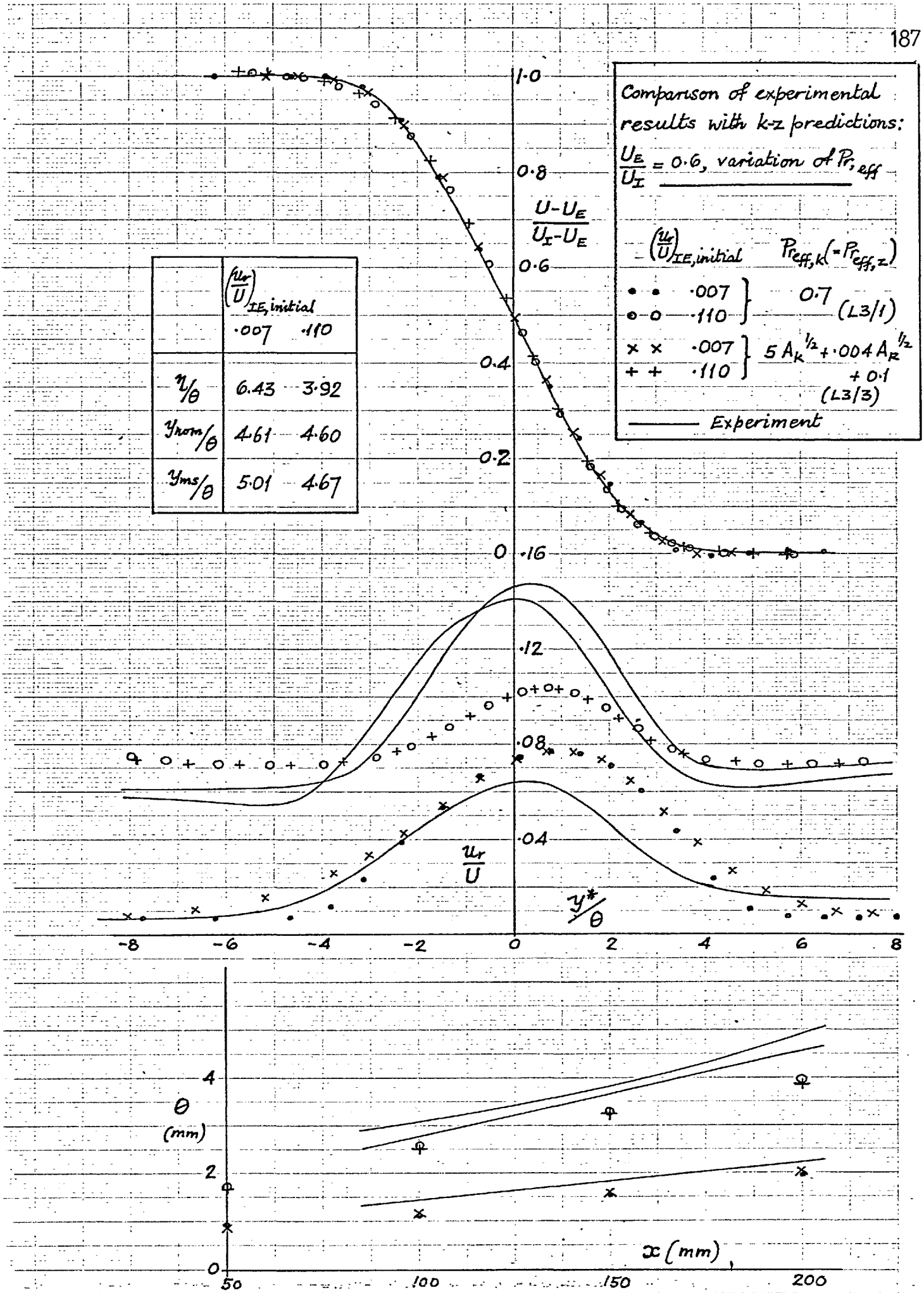

Comparison of experimental results with k-z predictions:
$\frac{U_E}{U_I}$ = 0·6, variation of C_2 and C_3
$\left(\frac{u_r}{U}\right)_{IE,initial}$ C_2 C_3
·007 ·085 0·56 (L3/1)
·110
·007 ·0935 0·63 (L3/2)
·110
Experiment
$\frac{U-U_E}{U_I-U_E}$
$\frac{u_r}{U}$
$\frac{y^*}{\theta}$
1·0
0·8
0·6
0·4
0·2
0
·16
·12
·08
·04
-8
-6
-4
-2
0
2
4
6
8
θ (mm)
4
2
0
50
100
150
200
x (mm)

Figure 6.6


Comparison of experimental results with k-z predictions:
$\frac{U_E}{U_I} = 0.8$, variation of C_2 and C_3.
$\left(\frac{u_r}{U}\right)_{IE,initial}$ C_2 C_3
·007 } .085 0.56 (L3/1)
·110 }
·007 } .0935 0.63 (L3/2)
·110 }
Experiment
$\frac{U-U_E}{U_I-U_E}$
$\frac{u_r}{U}$
$\frac{y^*}{\theta}$
1.0
0.8
0.6
0.4
0.2
·06
·04
·02
-8
-6
-4
-2
0
2
4
6
8

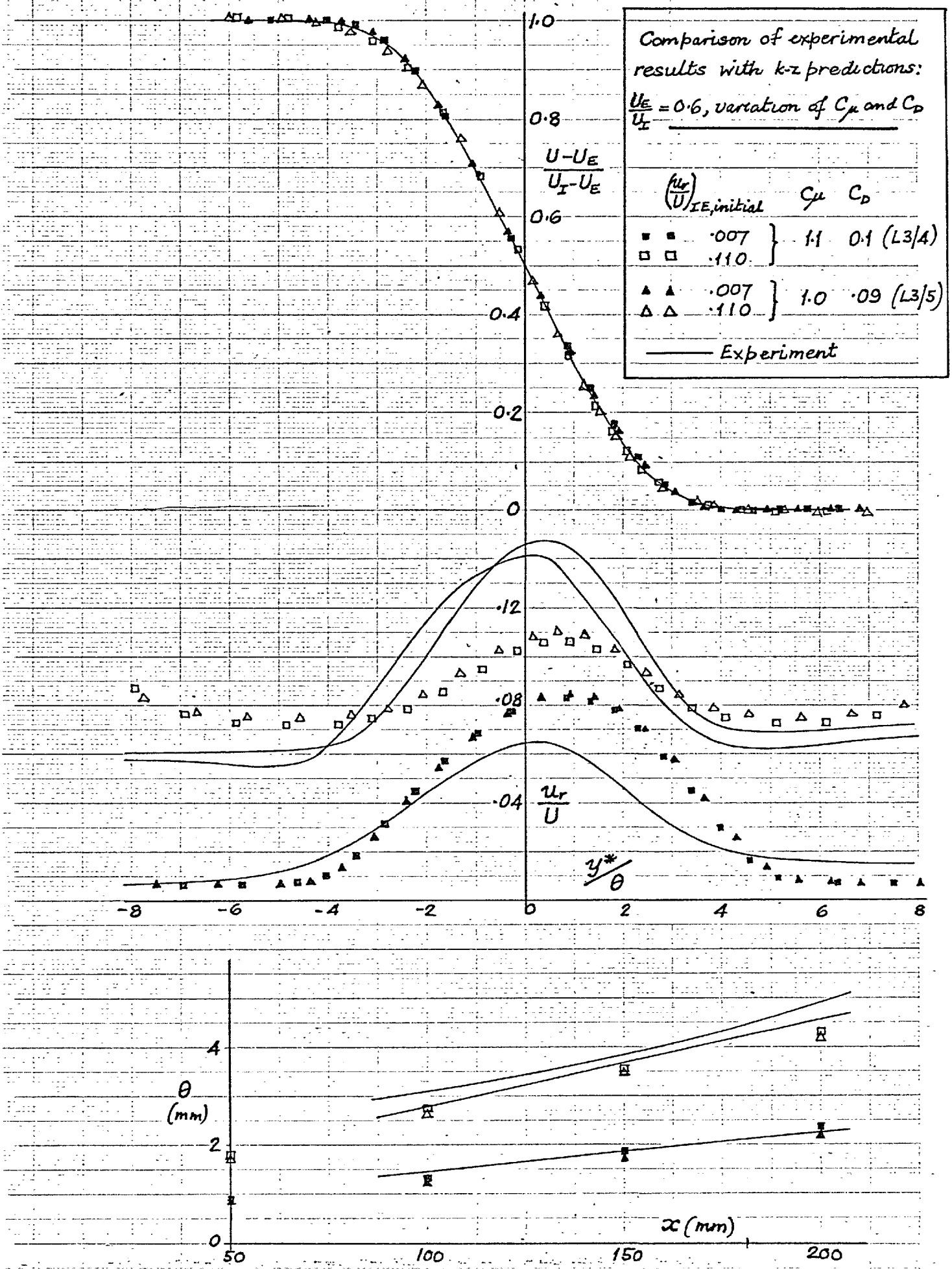
θ (mm)
4
2
0
50
100
150
200
x (mm)

Figure 6.7



	$\left(\frac{u_r}{U}\right)_{IE,initial}$ ·007	·110
η/θ	6.43	3.92
y_{rom}/θ	4.61	4.60
y_{rms}/θ	5.01	4.67

Figure 6.8


Comparison of experimental results with k-z predictions:
$\frac{U_E}{U_I} = 0.6$, variation of C_μ and C_D
$\left(\frac{u_r}{U}\right)_{IE,initial}$ C_μ C_D
·007 ·110 1·1 0·1 (L3/4)
·007 ·110 1·0 ·09 (L3/5)
Experiment
$\frac{U-U_E}{U_I-U_E}$
$\frac{u_r}{U}$
$\frac{y^*}{\theta}$
1·0
0·8
0·6
0·4
0·2
0
·12
·08
·04
-8
-6
-4
-2
0
2
4
6
8

θ (mm)
4
2
0
50
100
150
200
x (mm)

Figure 6.9

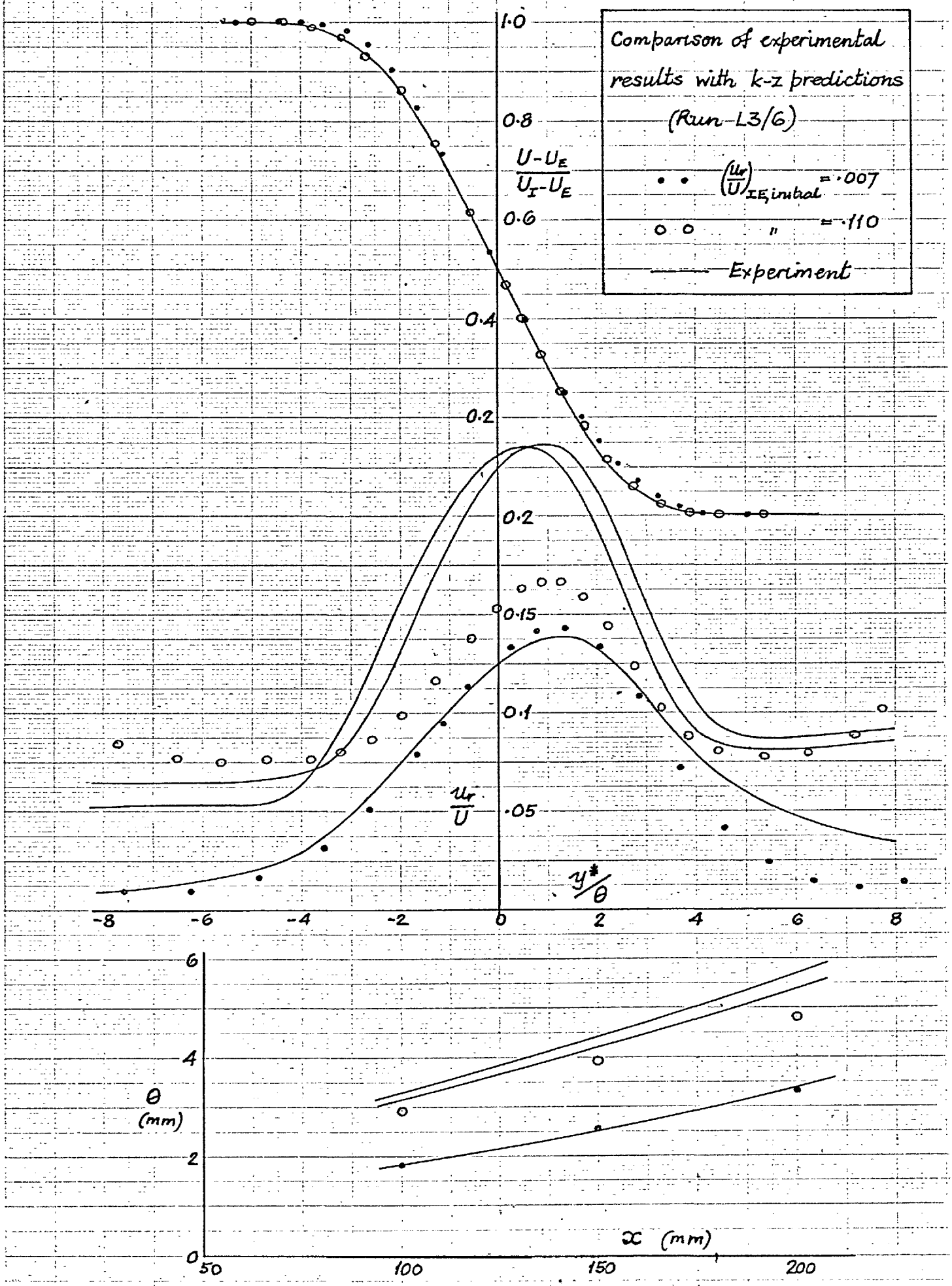
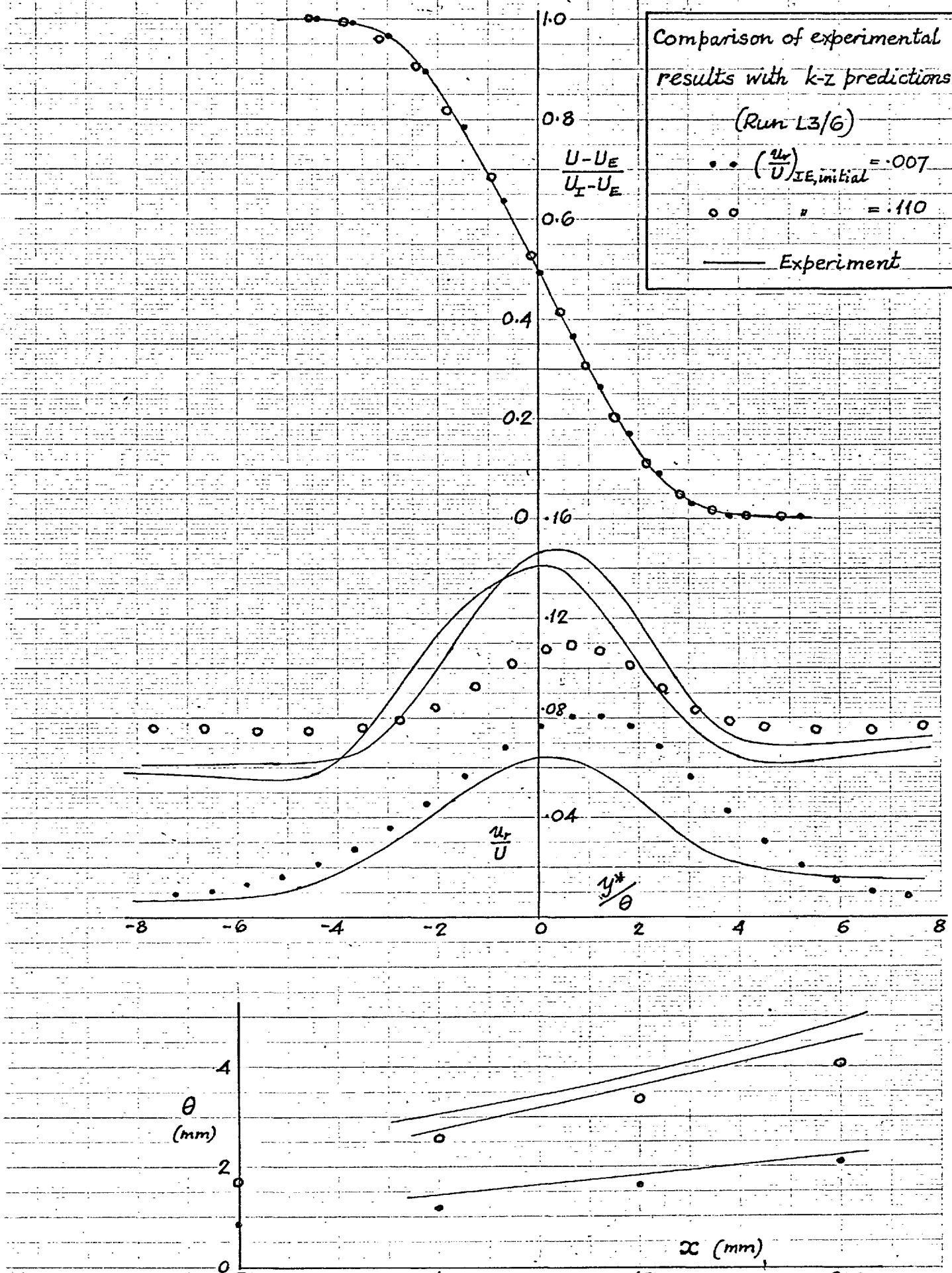
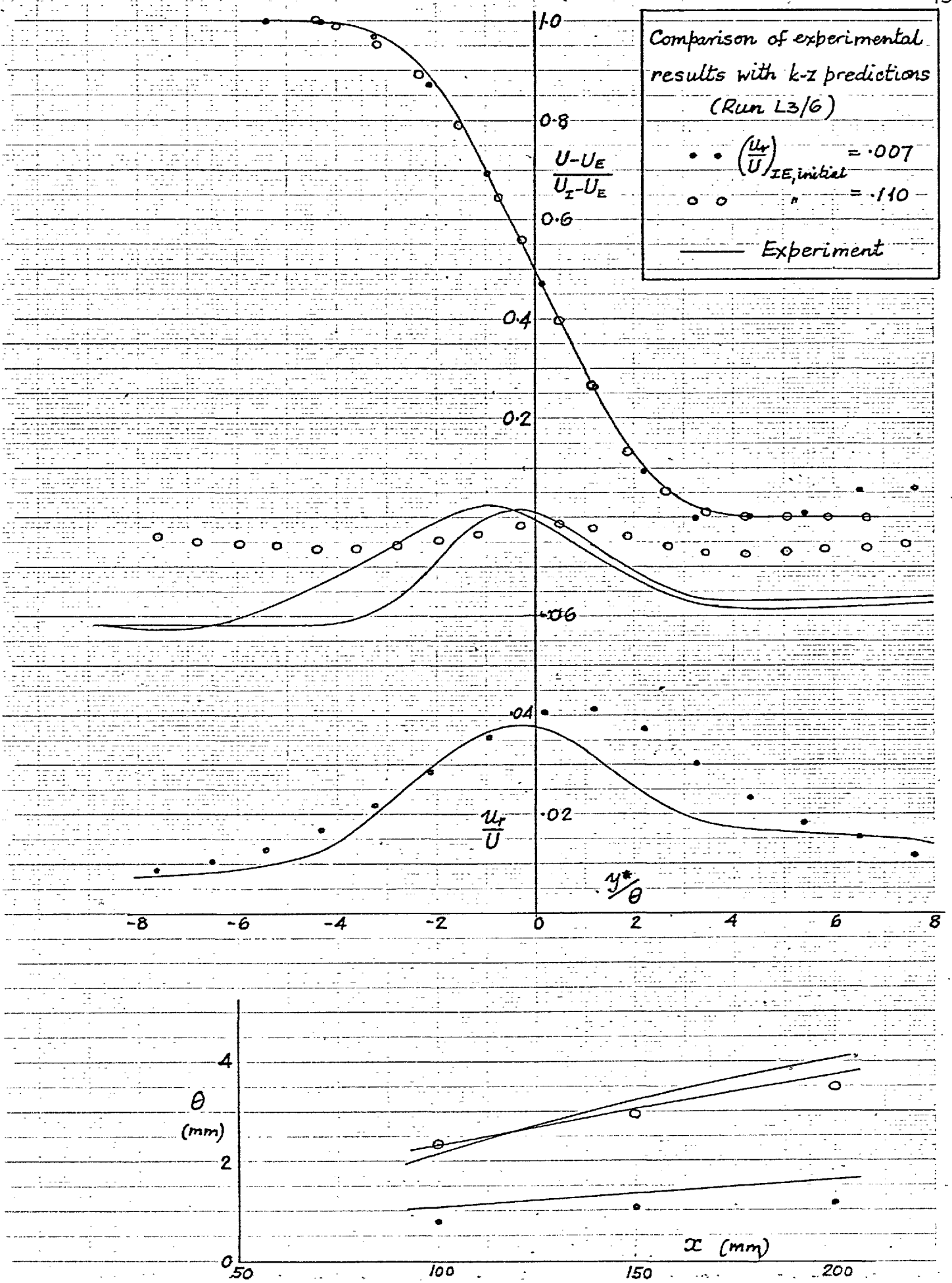

Comparison of experimental results with k-z predictions
(Run-L3/6)
$\left(\frac{u_r}{U}\right)_{IE,initial}$ = ·007
" = ·110
Experiment
$\frac{U-U_E}{U_I-U_E}$
1·0
0·8
0·6
0·4
0·2
0·2
0·15
0·1
·05
$\frac{u_r}{U}$
$\frac{y^*}{\theta}$
-8
-6
-4
-2
0
2
4
6
8
θ (mm)
6
4
2
0
50
100
150
200
x (mm)

Figure 6.10


Comparison of experimental results with k-ε predictions
(Run L3/6)
• • $(\frac{u_r}{U})_{IE,initial}$ = ·007
o o " = ·110
—— Experiment
1·0
0·8
0·6
0·4
0·2
0
$\frac{U-U_E}{U_I-U_E}$
·16
·12
·08
·04
$\frac{u_r}{U}$
$\frac{y^*}{\theta}$
-8
-6
-4
-2
0
2
4
6
8

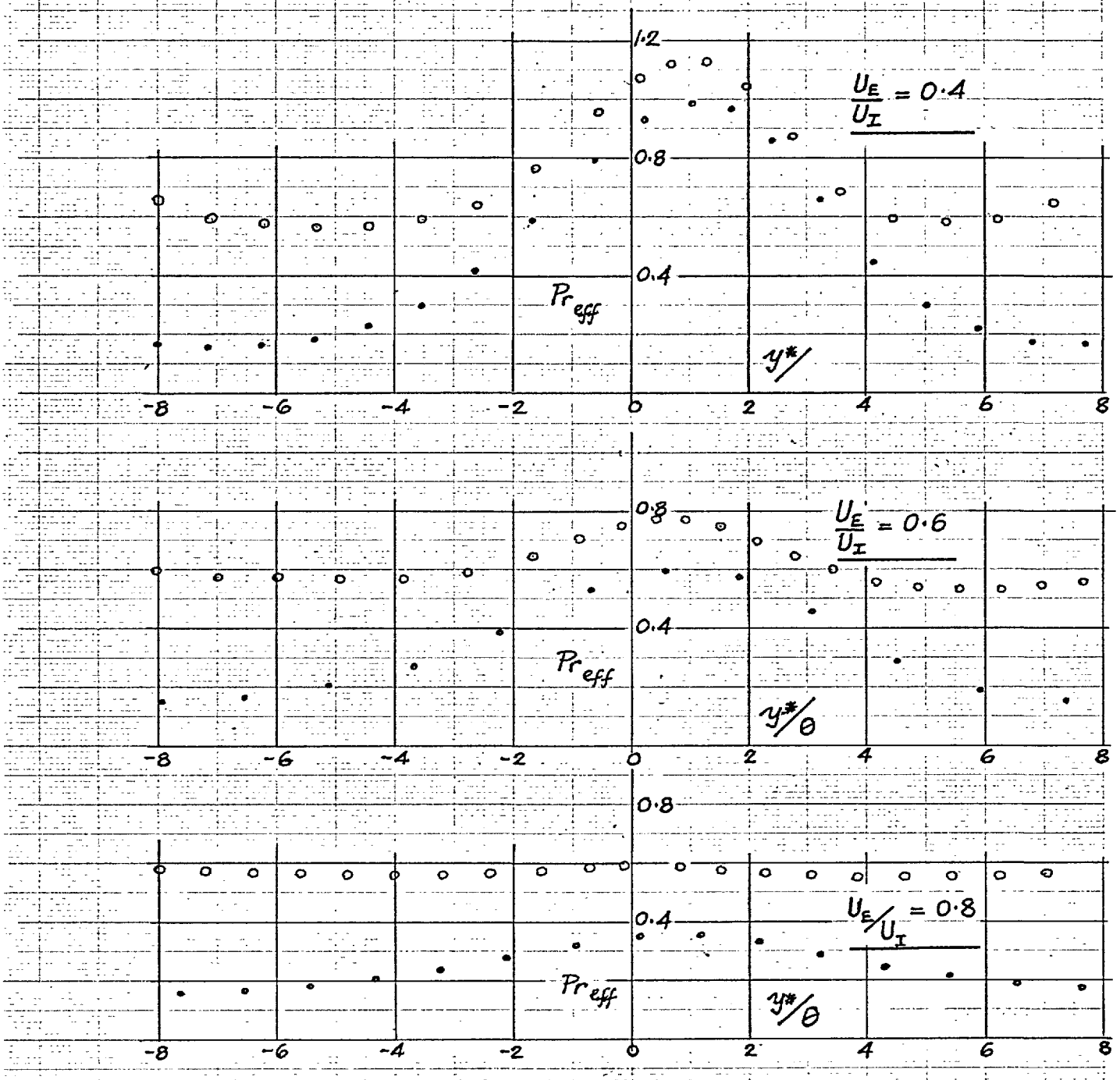
θ (mm)
4
2
0
50
100
150
200
x (mm)

Figure 6.11


Comparison of experimental results with k-z predictions (Run L3/6)
$\left(\frac{u_r}{U}\right)_{IE,initial}$ = ·007
" = ·110
Experiment
$\frac{U-U_E}{U_I-U_E}$
$\frac{u_r}{U}$
y^*/θ
1·0
0·8
0·6
0·4
0·2
·06
·04
·02
-8
-6
-4
-2
0
2
4
6
8

θ (mm)
4
2
0
50
100
150
200
x (mm)

Figure 6.12



Transverse distributions of Pr_{eff} in Run L3/6

$Pr_{eff} = 5 A_k^{1/2} + .004 A_R^{1/2} + 0.1$ (Eqn 6.5-1)

Figure 6.13

APPENDICES

APPENDIX A

SOME DETAILS OF THE FINITE-DIFFERENCE PREDICTION PROGRAMMES

A.1 The NEWMOD programme: general.

The NEWMOD programme was derived directly from the original Patankar-Spalding programme, which was subsequently published in reference 3. The main analytical modifications which were made have already been described in section 4.2. These were found to lead naturally to some structural changes - the original effective-viscosity subroutine (VEFF), and part of the subroutine COEFF were incorporated into the entrainment subroutine (ENTRN); in addition, subroutines and other subsections exclusively concerned with solid flow boundaries were deleted. Nevertheless, the programme retains a strong resemblance to its parent. A complete listing is given at the end of this appendix.

For plane mixing-layer predictions, the appropriate values of the main control parameters are as follows:

KIN = 2, KEX = 2, denote that both the I and E boundaries of the layer are bordered by free fluid streams.

KRAD = 0, for plane flow. (Note that in the programme, which is written for the general axi-symmetric case, the symbol R (representing the radial co-ordinate) appears frequently; for plane flow R is assigned the value unity throughout).

CSALFA = 1, indicates that the flow is perpendicular to the direction of R.

N = 20, this was the standard number of cross-stream grid intervals.

FRA = 0.1, this was the normal value of DX/Y(NP3), the ratio of forward step length to stream width.

Both N and FRA were chosen after an examination of the effects of varying the grid size, which is described in section A.10. The value of FRA used was deliberately conservative because of uncertainty occasioned by instability experienced in the early stages of development of the entrainment calculation.

The initial velocity profile was provided in the form of pairs of values of y and U; these were taken from the exact analytical solutions for zero free-stream turbulence produced by the KUESOL programme, (Appendix B.3).

A.2 NEWMOD: terminal procedure.

To ensure that computation ended when the asymptotic solution had been sufficiently closely approached, the value of $d^2\theta/dx^2$ was monitored at every tenth forward step. When the value was less than a specified size (usually 3×10^{-7}), the OUTPUT subroutine was called to print out the variables at that station. This was repeated three more times. The forward-marching prediction procedure was then halted and the final processing sequence described

below was executed. The adequacy of the monitoring was checked by examining the four sets of station print-outs produced. Practically all those variables which have constant values for the similarity solutions remained unchanged in the first three significant figures.

The final processing sequence comprised the following operations:

a) A check on the accuracy with which the force-momentum relation for the whole layer was satisfied, effected by calculating the error defined (for plane flow) by:

$$\dot{m}''U_I - \dot{m}''U_E - (\dot{m}''_I - \dot{m}''_E)I_m \qquad (A.2\text{-}1)$$

where $I_m = \Sigma(U_i + U_{i+1})(\omega_{i+1} - \omega_i)/2$; (A.2-2)

I_m thus represents the x-momentum flow rate within the layer, divided by the mass flow rate.

b) The calculation of the values of the velocity profile shape factors y_{nom}/θ and y_{ms}/θ; in this process an additional subroutine, CUBIC*, was used to interpolate between the value produced by the main prediction procedure, and to deduce the value of the transverse velocity gradient $\partial U/\partial y$.

---

*CUBIC, and the associated interpolation process, are described in section A.9.

c) The calculation of the dependent variables U, $(U - U_E)/(U_I - U_E)$, and $\theta . \partial U/\partial y$, for equal intervals of the transverse position co-ordinate y^*/θ, again using subroutine CUBIC.

d) Values of $\mu_{eff}/\rho\ell$ and $\mu_{eff}/\rho U\ell$ (the latter being the predicted relative turbulence intensity) were also calculated for equal intervals of y^*/θ; in this case linear interpolation was adequate because, in the basic finite-difference procedure, at each station μ_{eff} has a single value across each grid interval.

In interpreting the printed results from the programme it should be appreciated that these are all effectively in non-dimensional form. Since the faster free-stream velocity, U_I, is set at unity, the symbol U in the programme represents the local velocity ratio U/U_I. Similarly, the symbol RHO represents the ratio of local density to that of the free stream; it is, of course, unity everywhere for the present uniform-density predictions.

A.3 Calculation of the finite-difference coefficients and the entrainment rates.

The coefficients for the finite-difference equations for internal grid-lines (i.e. A, B, and C in equation 3.2-8) are calculated in subroutine COEFF. This has been modified in two ways from the standard form of reference 3.

First, material which is not used in computations of the present kind has been deleted; secondly, the preliminary sequence for calculating the small c's (as defined by equation 3.2-7) has been moved to subroutine ENTRN, so that the values for the 4th and Nth grid lines are directly available when required for the determination of the entrainment rates. Subroutine ENTRN also contains, for convenience, the sequence for effective viscosity (EMU), which was previously in a separate subroutine (VEFF).

The way in which the second half of ENTRN sets up and solves the two equations of the form 3.4-2, to obtain the values of the boundary entrainment rates $\dot{m}''_I$ and $\dot{m}''_E$ (AMI and AME) can easily be followed in the listing. The YDES device, which controls the length of the tails at each end of the velocity profile, is included in this sequence; its operation is described in section A.10.

The coefficients for the outer half-intervals of the grid are calculated separately in subroutine SLIP, in accordance with the definitions and analyses of section 3.3. Note that, for convenience in programming, the quantities Y, M, M', and V do not appear explicitly. Instead, quantities differing by a factor $(\rho U)_{2.5}$ $[=(\psi_E - \psi_I)\omega_3/2]$ are used at the I boundary, thus:

$$CYI \equiv Y \cdot (\rho U)_{2.5} = (\psi_E - \psi_I)/\delta x$$

$$CMI \equiv M \cdot (\rho U)_{2.5} = \dot{m}''_I \quad , \quad \text{etc;}$$

at the E boundary, the corresponding factor is $(\rho U)_{N+1.5}$ $[=(1-\omega_{N-1})(\psi_E - \psi_I)/2]$.

A.4 The NEWMOD-F programme.

This was basically identical with NEWMOD; the only differences concerned the initial and boundary conditions, the step length, and the arrangement for print-out, all of which were aimed at aligning the predictions and the experimental observations as closely as possible within the context of the mixing-length model.

The values of y and U for the experimental velocity profile for x = 10 cm were read in to define the starting point for the predictions, thus taking advantage of the ability of the finite-difference procedure to accept arbitrary initial conditions. In some cases where the number of experimental points was rather small, a few extra ones were obtained by visual interpolation on the profile. The value of N was within the range 13 to 18 for all NEWMOD-F predictions, and consequently possible inaccuracy arising from this cause could be expected to be small compared with probable experimental errors.

The boundary values of velocity, U_I and U_E, were kept constant throughout any one prediction, while the boundary values for $(\frac{u_r}{U})_I$ and $(\frac{u_r}{U})_E$ were calculated for each transverse grid line from a parabola fitting the observed values for the three traverse stations. These boundary conditions are displayed in Table 4.3.

The increment of x was the same for all forward steps, and a simple fraction of the distance between traverse stations. At these positions the final-processing

sequence described in section A.2 was brought into operation and full details of the predicted flow were printed out for comparison with the experimental results.

A listing of the MAIN section of NEWMOD-F follows at the end of this appendix; the remaining subroutines were identical with NEWMOD.

A.5 The LAYER programme: general notes.

The basic principles governing the operation of the GENMIX 4 programme of reference 4 as the same as those of its predicessor, reference 3. The development of the later programme has, however, included some changes of nomenclature, and a radical change of structure, and in particular a marked reduction in the number of subroutines. A comprehensive description and justification of the underlying analytical modifications is given in reference 4. For the flows at present under investigation, the most significant of these is in the method of calculating entrainment rate, which has already been described in the second half of section 3.4; little more needs to be said here about the basic GENMIX 4 programme.

For the present purpose, the LAYER programme can be regarded as GENMIX 4 shorn of those subroutines and smaller sections which relate exclusively to solid flow boundaries, and with its scope extended to encompass the new generation of turbulence models. The notes which follow concern the version eventually developed by the present author.

As usual, the MAIN section of the programme controls the application of the general procedure to the problem in hand, setting up the initial flow conditions, controlling the sequencing of the forward-marching integration process and adjusting the boundary conditions in the downstream direction, and arranging the final processing and printing out of the solution. Despite the greater complexity of the computation the operation of the programme is similar to the working of NEWMOD, and can be followed in the listing given at the end of this appendix.

The primary dependent variables other than ρ, U, r and y are represented by the two-dimensional array F(n, i). In the present calculations, n = 2 and n = 3 correspond to specific kinetic energy of turbulence, k, and frequency, z, respectively; n = 1 customarily represents the specific enthalpy, h, which was not required as a variable. The density was assigned a constant value for all grid lines at the commencement of each prediction run. To eliminate the unnecessary computation involved in the superfluous solution of the enthalpy equation, adjustments were made to the range of the DO loops in subroutine STRIDE concerned with the calculation of the coefficients and solution of the finite-difference equations. In all other respects this subroutine retained its standard form.

The computer sequences peculiar to the k-z turbulence model itself are contained in subroutine AUX, and are detailed in the following section.

Figure 4.7 shows the starting conditions used for the idealised k-z predictions. The initial width of the layer, $(y_E - y_I)_{in}$, was arbitrarily chosen, and the corresponding distance from the hypothetical origin of the layer, x_{in}, calculated from the expression:

$$x_{in} = \frac{(y_E - y_I)_{in}}{(.3 - \frac{U_E}{5U_I})[1 + 10(\frac{u_r}{U})_{IE}]} \qquad (A.5\text{-}1)$$

which approximates results from the mixing-length predictions. The velocity and relative turbulence intensity were assigned sinusoidal distributions; the maximum value for u_r/U was calculated from the expression:

$$(\frac{u_r}{U})_{max} = 0.2 - .199\ U_E/U_I \quad , \qquad (A.5\text{-}2)$$

which was derived from the experimental results. The initial boundary values of z were obtained from equation 2.5-4 (for the I boundary), and a simple linear distribution between them was assumed. In order to minimise the effect of possible differences between these initial profiles and the "correct" ones, the first fifty forward steps in the calculation procedure were considerably reduced in size to allow the differences to be eliminated rapidly.

The final processing of the finite-difference results was generally similar to that for NEWMOD, but although necessarily more comprehensive, was rather less elaborate. Subroutine CUBIC was called only to assist in the calculation of y_{ms}/θ.

For calculations with zero free-stream turbulence, only the final asymptotic (similarity) solution was printed out. For other cases, the initial value of u_r/U in the free streams was usually set at 0.2, and final-processing and printing arranged to occur at stations where the relative turbulence level diminished to 0.12, .08, .04 and .02 successively; the values of x at which these values of $(u_r/U)_{IE}$ occur were calculated in an early section of the programme (MAIN chapter 2), using equation 2.5-4.

The value of N was set at 19 (compared with 20 for the NEWMOD work) solely for convenience in tabulating the printed results.

A.6 LAYER: subroutine AUX.

The character of the turbulence model is largely defined by this subroutine, in which are calculated the values of effective viscosity, and the "source" terms appearing in the k and z equation.

Since the molecular component of shear stress is ignored in all calculations, the effective viscosity is equal to the turbulent component, and so its value can be calculated from equation 2.8-1. Almost invariably, C_μ was taken as unity, so that:

$$\mu_{eff} = \rho k/z \qquad \text{(A.6-1)}$$

(The effect of varying C_μ is described in Chapter 6).

The source terms (i.e. the last two in equation 2.7-1, and the last three in 2.7-2) are dealt with by the standard GENMIX 4 procedure. For the representative control volume depicted in figure 2.2, the appropriate integral for the k source terms is:

$$S_k = \int_{-}^{+} [\mu_{turb}(\frac{\partial U}{\partial y})^2 - C_D \rho k z] dy \qquad \text{(A.6-2)}$$

$$= \int_{-}^{+} \Phi_k dy, \text{ say, where } \Phi_k \text{ is the nett time rate of generation of k per unit volume.}$$

The expression for S_k can be restated , partly in finite-difference form, as:

$$S_k = S_{D,k} \cdot k_D \qquad \text{(A.6-3)}$$

$$\text{where } S_{D,k} = \tfrac{1}{2}(y_{i+1} - y_{i-1})_U \frac{d}{dk}(\Phi_k)_{U,i}$$

$$= \tfrac{1}{2}(y_{i+1} - y_{i-1})_U [\frac{\mu_{turb}}{k}(\frac{\partial U}{\partial y})^2 - C_D \rho z]_{U,i} \qquad \text{(A.6-4)}$$

In this way the source terms are expressed as a factor multiplying the unknown downstream value k_D, the factor itself containing only known, upstream quantities.

The corresponding expressions for the z source terms are:

$$S_z = \int_{-}^{+} [C_1 \frac{\mu_{turb}}{z} (\frac{\partial^2 U}{\partial y^2})^2 - \rho C_2 z^2 + \rho C_3 (\frac{\partial U}{\partial y})^2] dy \qquad (A.6\text{-}5)$$

$$= \tfrac{1}{2}(y_{i+1} - y_{i-1})(S_{U,z} + S_{D,z} \cdot z_D) \qquad (A.6\text{-}6)$$

where

$$S_{U,z} = [\frac{C_1 \mu_{turb}}{z} (\frac{\partial^2 U}{\partial y^2})^2 + C_3 \rho (\frac{\partial U}{\partial y})^2]_{U,i} \qquad (A.6\text{-}7)$$

and

$$S_{D,z} = \frac{d}{dz}(\Phi_z)_{U,i} = [-C_2 \rho z]_{U,i} \qquad (A.6\text{-}8)$$

The main DO loop in AUX performs these calculations (of $S_{D,k}$, $S_{U,z}$ and $S_{D,z}$) for all interior grid lines. The outer half intervals require slightly different treatment, in a separate sequence in the same subroutine.

A.7 Special features of LAYER-3.

Apart from the additions required by the exploratory extensions of the k-z model described in chapter 6, the LAYER-3 programme version was basically identical with LAYER; the differences which occur arise only from the different flow conditions being simulated.

The starting profiles for LAYER-3 are indicated by figure 4.14; they were intended to model conditions in a real flow a short distance downstream from the outlet plane of the air supply ducts. The calculation sequence which establishes these initial profiles is contained in Chapter

5 of the MAIN section of the programme. The listing of this is included at the end of this appendix. The velocity was assumed to vary sinusoidally except in the two uniform-velocity free-stream regions. In these, the relative turbulence intensity was set at .110 or .007 (to simulate flows with and without the turbulence grids in operation). The corresponding initial values of z for high-turbulence flows were calculated from the same value of Strouhal number, $\frac{zd}{U}$, as that derived from the frequency spectrum of the turbulence (described in section 5.8), allowing for the fact that these measurements were made .025 m downstream; for low-turbulence flows an arbitrary initial value of 100 was assigned to z.

In the non-uniform-velocity sections, the free-stream values of k and z were augmented by amounts based on the mixing-length expressions derived in section 2.6. For the outer mixing layers these expressions were used directly in conjunction with the assumed sinusoidal velocity distribution. In the central wake region the same treatment without further modification would have resulted in improbable distributions for k and z; to make them more realistic the central troughs in these profiles were bridged by a straight line joining the peaks, as indicated in figure 4.14. As with the LAYER predictions, the initial step size (for the first 100 steps, in this case) was made very small, to reduce the effect, of the arbitrariness of the starting conditions, on the results predicted downstream.

The main control parameters KIN, KEX, KRAD etc. retain the same values as before. The free boundaries of the computation grid represent the outer edges of the outer mixing layers, of course. Small arbitrary initial values were assigned to k and z at these boundaries, and they were varied with x in the way prescribed in section 2.5. The limits of the central velocity layer were located at each grid station by a search sequence (in MAIN, Chapter 8) which, moving outward from the middle found where the difference between the velocities for two successive grid points were less than a prescribed amount (ULIMNI and ULIMNE for the high- and low-speed boundaries; the standard values for these were .002 times the respective free stream velocities). In a few instances (for large x and low U_E/U_I) this sequence failed to produce a satisfactory result because of the merging of the inner and outer layers. For such cases a reserve sequence was introduced to locate the position of lowest transverse velocity gradient, $\frac{\partial U}{\partial y}$. The grid-lines located in this way were identified by the subscripts NI and NE in the programme. The value of momentum thickness, θ, was calculated between these limits, instead of across the whole grid, as before. These calculations, and the calculations of y_{nom} and y_{ms}, were based on simple linear interpolation between the points on the predicted velocity profiles (see MAIN, chapter 10).

To allow for the difference between the widths of the velocity mixing layer and the turbulence kinetic energy layer, the limits of the latter were separately located (in MAIN, chapter 10). They were taken to be the points in the I and E "free-stream" zones, at which the values of k were least. These points are identified by subscripts NIF and NEF respectively, and shape factor ξ was computed between them. The shape factor for the relative turbulence intensity profile, η, was determined in a very similar way, but owing to minor irregularities in the k and z profiles, the minimum values of these quantities did not always occur at the same grid point. Subscripts NIT and NET indicate the limits of the u_r/U layer.

To permit transverse variation of the effective Prandtl numbers for k and z, the appropriate parts of subroutine AUX were changed to correspond to the algebraic expressions:

$$Pr_{eff,k} = \alpha A_k^{\,n} + \beta A_r^{\,m} + \varkappa \qquad \text{(A.7-1)}$$

$$Pr_{eff,z} = \gamma A_k^{\,p} + \delta A_r^{\,q} + \chi \qquad \text{(A.7-2)}$$

where $$A_k = k/U^2 \qquad \text{(A.7-3)}$$

$$A_r = k/z \qquad \text{(A.7-4)}$$

and $\varkappa$ and χ are constants.

A_r is thus closely related to the local turbulence Reynolds number, A_R ($\equiv \rho k/\mu z$); A_k and A_R are two of the quantities which Spalding (reference 24) has tentatively suggested as arguments of the "constants" in the k-z and k-w turbulence models.

As with the NEWMOD-F predictions, print-out was arranged at x-intervals of .05 m, to coincide with the experimental traverse stations, and the numbers involved in the computations represented the absolute magnitudes of the respective physical quantities in S.I. units.

A.8 The relationship between the k-z and k-w models.

The k-z and k-w models are very similar methods of describing turbulent motion. The symbol w represents the square of the characteristic frequency of the fluctuating motion, i.e., $w \equiv z^2$. The same differential equation for k is used in both models (equation 2.4-2; the equation for w is (in plane flow):

$$U\frac{\partial w}{\partial x} + V\frac{\partial w}{\partial y} = \frac{1}{\rho}\frac{\partial}{\partial y}\left(\frac{\mu_{turb}}{Pr_{eff,w}}\frac{\partial w}{\partial y}\right) + C_1'\frac{\mu_{turb}}{\rho}\left(\frac{\partial^2 U}{\partial y^2}\right)^2 - C_2' w^{3/2} + C_3' w^{\frac{1}{2}}\left(\frac{\partial U}{\partial y}\right)^2 \qquad \text{(A.8-1)}$$

with $$\mu_{turb} = C_\mu \rho k w^{-\frac{1}{2}} \qquad \text{(A.8-2)}$$

That a significant difference between the two models exists can be shown by substituting in A.8-1 for w and dw

in terms of z and dz; after division by 2z the right hand side of the resulting equation is:

$$\frac{\partial}{\partial y}\left(\frac{\mu_{turb}}{Pr_{eff,w}}\cdot\frac{\partial z}{\partial y}\right)+\frac{\mu_{turb}}{Pr_{eff,w}z}\left(\frac{\partial z}{\partial y}\right)^2+\frac{C_1'}{2}\frac{\mu_{turb}}{\rho z}\left(\frac{\partial^2 U}{\partial y^2}\right)^2$$

$$-\frac{C_2'}{2}z^2+\frac{C_3'}{2}\left(\frac{\partial U}{\partial y}\right)^2 \qquad \text{(A.8-3)}$$

Comparison of this expression with the right-hand side of equation 2.4-3, shows that:

$$C_1 = C_1'/2,\ C_2 = C_2'/2,\ C_3 = C_3'/2\ , \qquad \text{(A.8-4)}$$

and also that the second term is omitted altogether. It is argued (Spalding, reference 29) that as a result of this latter difference, the C's are more likely to be nearly constant than the C' 's, and the k-z model consequently more satisfactory than the k-w one.

A.9 Subroutine CUBIC.

This short subroutine is used frequently in the final processing of results from the main finite-difference programmes, especially NEWMOD and NEWMOD-F. It evaluates the coefficients required to fit a cubic expression to any set of four points transferred to it. It is used for three purposes:-

a) to calculate values of y for which $(U-U_E)/(U_I-U_E)$ has specified values, in the calculation of y_{nom} and y_{ms},

b) to calculate values of U corresponding to specified y's, in obtaining the equally-spaced output, and

c) to determine transverse gradients, $\partial U/\partial y$, in the calculation of y_{ms}.

In applications of kind b), the finite-difference output, consisting of linear U-ω segments, is replaced by a series of cubic U-y segments, and in the process, an adjustment, ϵ, is made to the values of U so that the mass flow rate corresponding to the cubic curve is the same as that for the section of the finite-difference profile that it replaces. However this precaution was found to be largely unnecessary, as with N = 20 the values of ϵ were too small to be significant for normal purposes (usually less than 1×10^{-3}).

A.10 Effects of varying grid mesh size and entrainment parameters.

Some of the early work with the finite-difference programmes was necessarily occupied in establishing suitable values for the various computational parameters involved. The most important of these were:-

a) The number of cross-tream grid intervals, N.

b) The size of the forward step between one transverse grid line and the next.

c) The constants used in the sequence controlling the rate of lateral expansion of the grid.

The following notes apply mainly to the NEWMOD programme, but very similar results hold for LAYER also.

Since a linear U-ω relation in each interval is an essential feature of the method, finite-difference solutions obtained with few cross-stream intervals are likely to be less accurate than those produced with larger values of N. The effect of varying N depends on the details of the grid-control system, i.e. the effects of a) and c) are interlinked. In NEWMOD, an arbitrary velocity difference, UDIF, was used to determine $\widetilde{U}_4$ (appearing in equation 3.4-2) thus:

$$\widetilde{U}_4 = U_1 - \text{VDESI}\ (U_1 - U_{N+3}) \qquad \text{(A.10-1)}$$

where VDESI is a factor whose value is increased at each step by an amount:

$$\Delta(\text{VDESI}) = (U_1 - U_3 + \text{UDIF}) \qquad \text{(A.10-2)}$$

[In LAYER, this two-tier system was replaced by a simpler one which achieved the required result in a single stage].

Figures A.1, A.2, and A.3 show some of the results of two sets of asymptotic flow predictions with various values of N, U_E/U_I, and $(u_r/U)_{IE}$. In one set UDIF was held constant, while in the other it was varied in accordance with the formula:

$$\text{UDIF} = 1.3(1-U_E/U_I)/N^2 \qquad \text{(A.10-3)}$$

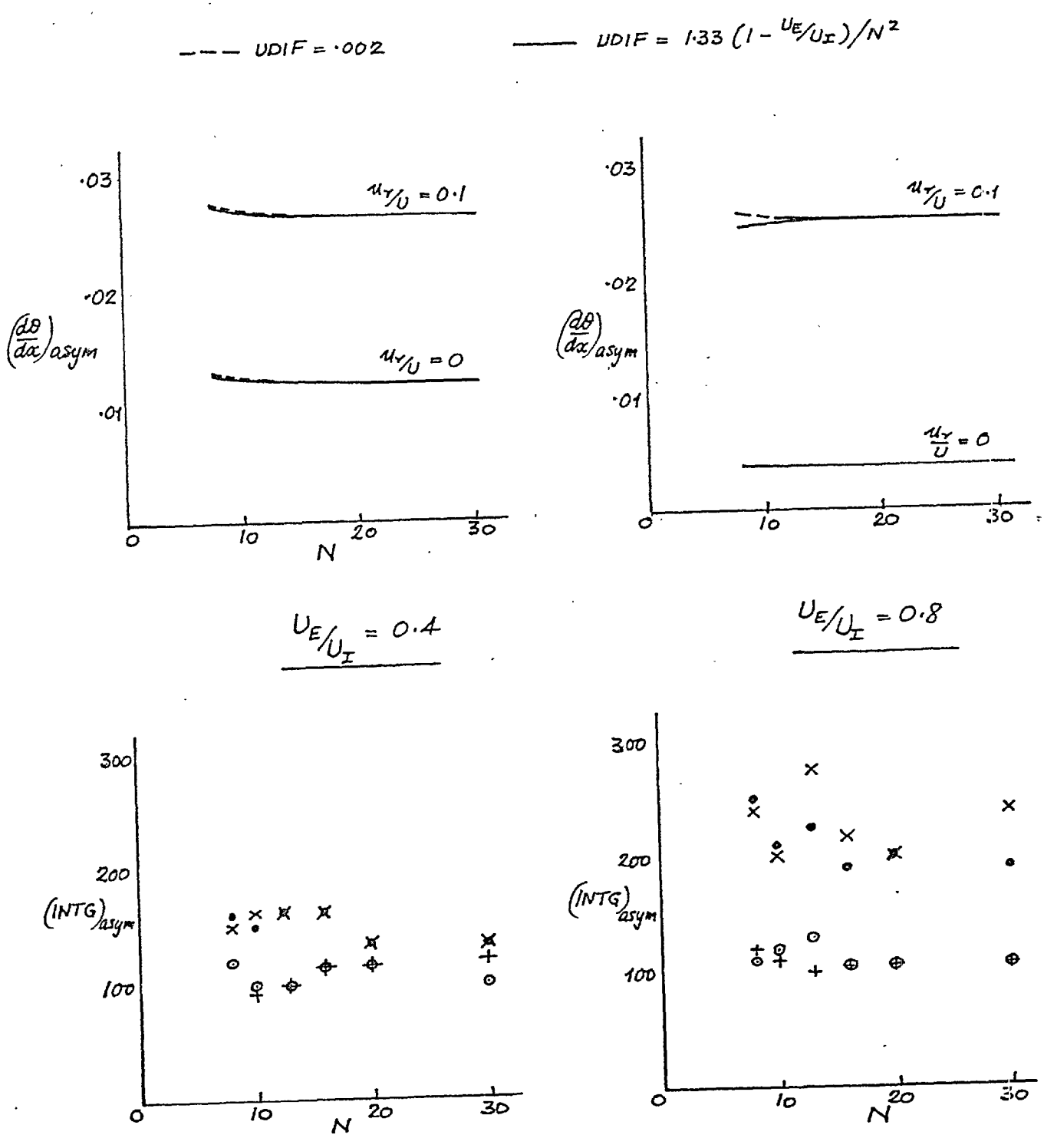
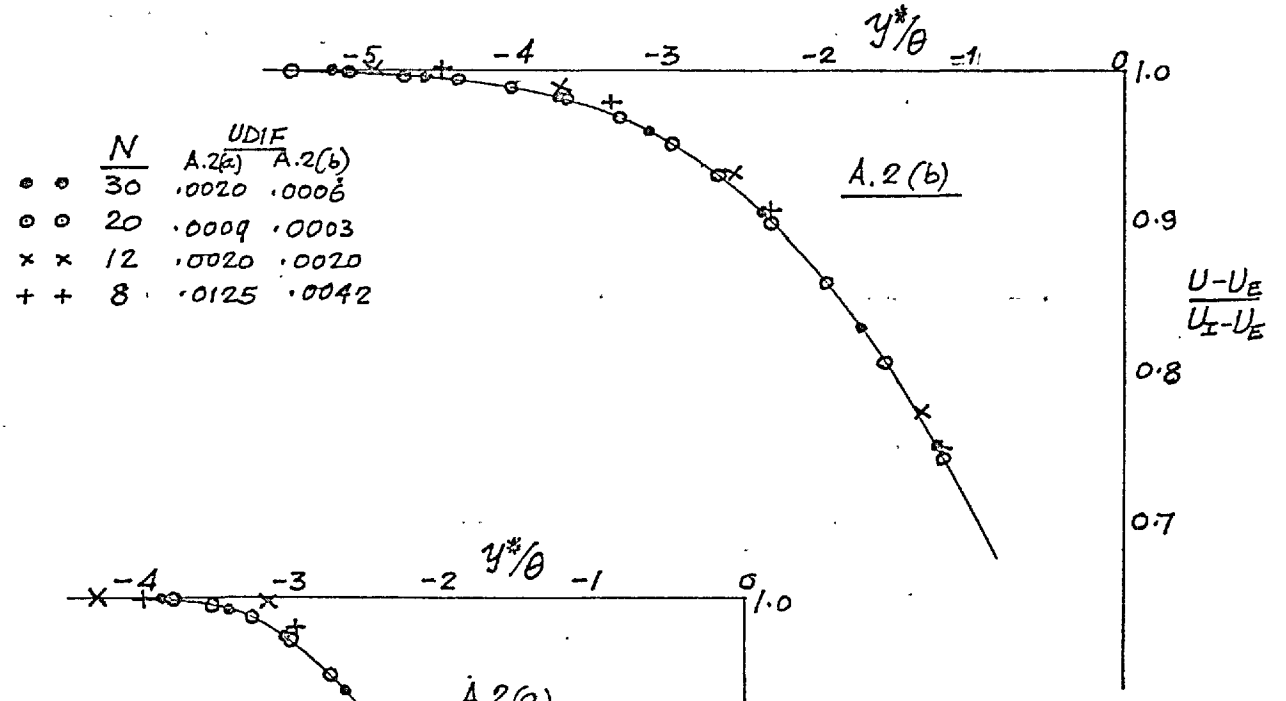

UDIF = ·002
UDIF = 1·33 (1 − UE/UI)/N²
·03
·02
·01
(dθ/dx)asym
ur/U = 0·1
ur/U = 0
0
10
20
30
N
UE/UI = 0·4
UE/UI = 0·8
300
200
100
(INTG)asym
UDIF = ·002 , { ur/U = 0 × × ; ur/U = 0·1 + +
UDIF = 1·33 (1−UE/UI)/N² { ur/U = 0 • • ; ur/U = 0·1 ⊙ ⊙

Figure A.1.



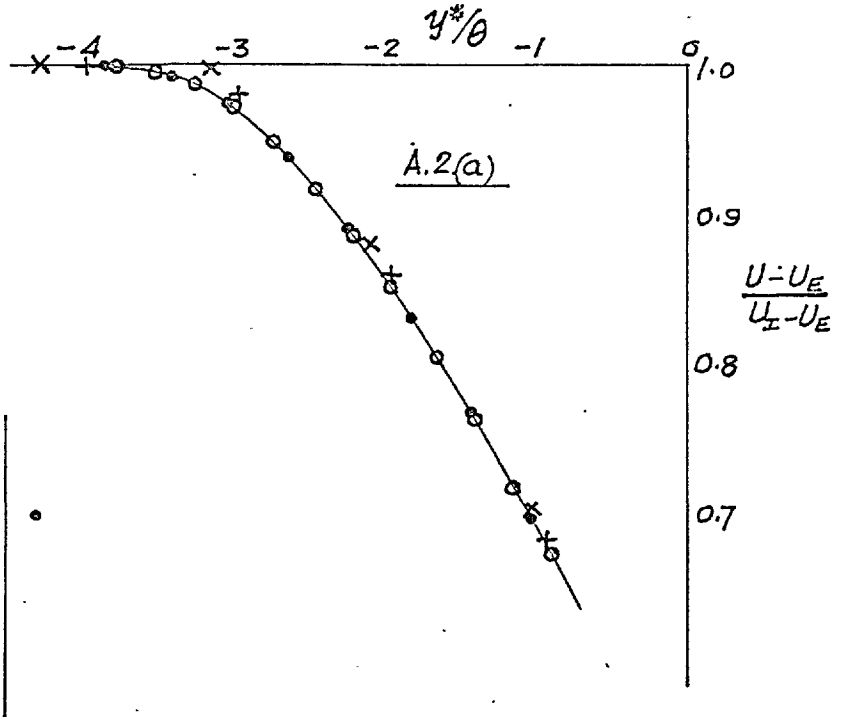


Figure A.2

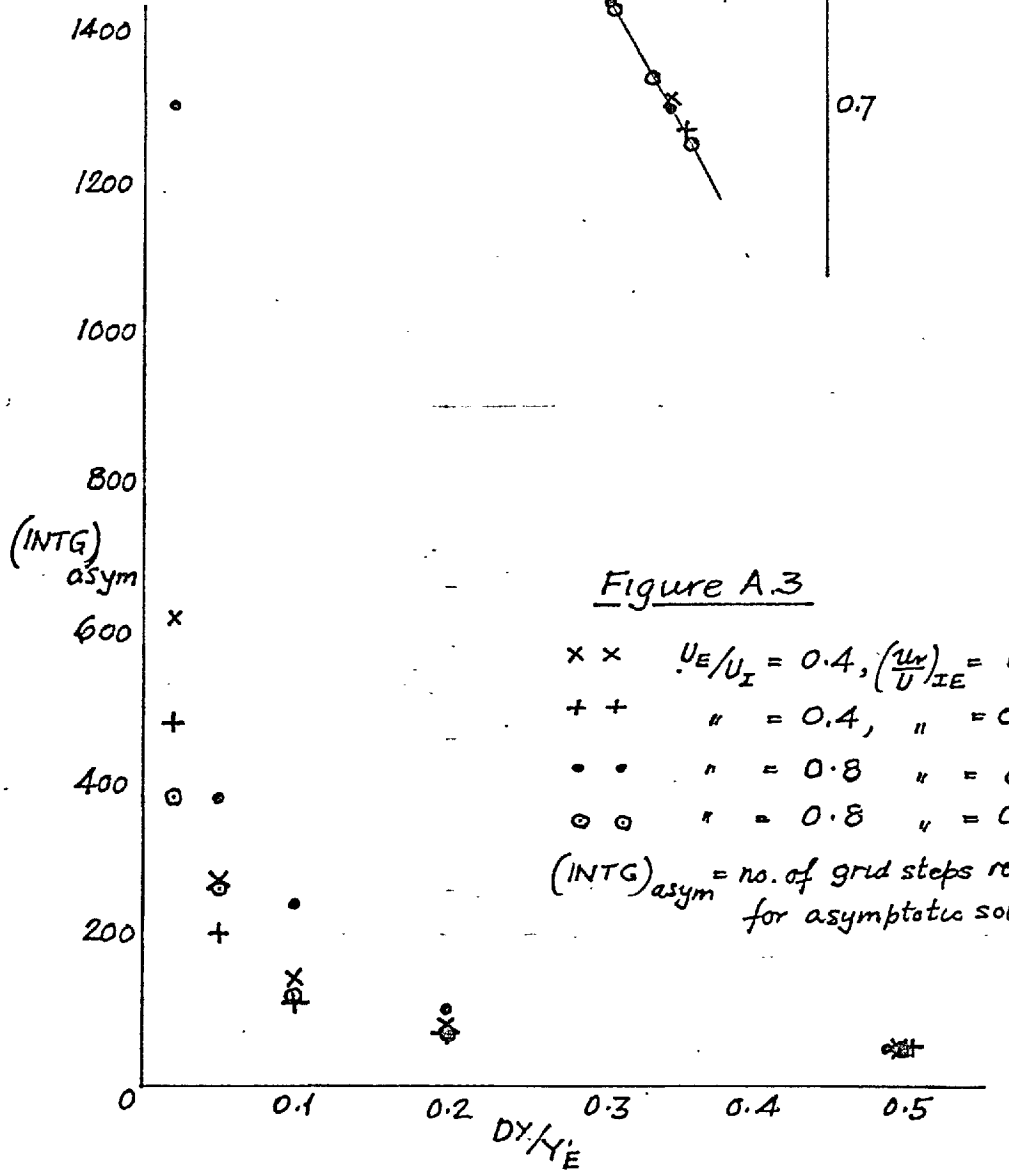


Figure A.3

× × $U_E/U_I = 0.4, \left(\frac{u_r}{U}\right)_{IE} = 0$

+ + " = 0.4, " = 0.1

• • " = 0.8 " = 0

⊙ ⊙ " = 0.8 " = 0.1

$(INTG)_{asym}$ = no. of grid steps required for asymptotic solution.

The upper graphs in figure A.1, and the part-velocity profiles in A.2 indicate that for low values of N it is necessary to choose the parameters in the entrainment control sequence with considerable care, but also that when N is 20 or more the solution is much less sensitive.

The lower graphs in figure A.1 show that $(INTG)_{asym}$, the number of forward steps required to reach the asymptotic solution (defined by $d^2\theta/dx^2 < 3 \times 10^{-7}$) is also affected by changes in N and UDIF, although not in a very clear manner. The most important influence on $(INTG)_{asym}$ is the size of the forward step, as seen in figure A.3.

Apart from affecting the number of steps required, variation of DX has very little effect on the solution. DX may be varied by a factor of 100 without altering the resultant value of $(d\theta/dx)_{asym}$ by more than 0.1%. This allows the size of forward steps to be decided on other grounds, for example in NEWMOD-F, by the desire for grid-lines to coincide with measuring stations.

LISTING OF NEWMOD PROGRAMME

```
$IBFTC MAIN
      COMMON/GEN/PEI,AMI,AME,DPDX,XU,XD,XP,XL,DX,INTG,CSALFA
     1/V/U(43),F(2,43),R(43),RHO(43),OM(43),Y(43)
     1/F/FTI,FTE,ATURB,K,VDESI,VDESE,M,L
     1/T/VDR(43),THETA,DTDX,D2TDX2,FRA
     1/C/SC(43),AU(43),BU(43),CU(43),A(2,43),B(2,43),C(2,43)
     1/I/N,NP1,NP2,NP3,NEQ,NPH,KEX,KIN,KASE,KRAD
     1/R/EFFVIS(43),VEFRAT(43),ETOT,BTURB,IMU
      COMMON/L/AK,ALMG,AL
      DIMENSION YI(43),UI(43),YR(43),YOTH(43)
      DIMENSION VDRN(3),YN(3),RTI(4)
C     MODIFIED P25 PROGRAMME
C1  READ IN DATA AND ESTABLISH INITIAL VELOCITY PROFILE
C   IMU=1 DENOTES MU1 EFFECTIVE VISCOSITY FORMULATION
C   IMU=2 DENOTES MU2 EFFECTIVE VISCOSITY FORMULATION
      IMU=1
      N=20
      VDRN(1)=.9
      VDRN(2)=.5
      VDRN(3)=.1
      NP1=N+1
      NP2=N+2
      NP3=N+3
      DELYT=0.4
      ALMG=0.50
      ATURB=1.05
      BTURB=0.5
    8 READ(5,10)(YI(I),UI(I),I=3,NP1)
      READ(5,12)VRAT,(RTI(J),J=1,4)
      FRA=0.1
      DO 32 J=1,4
      RTNTI=RTI(J)
      RTNTE=RTI(J)
   16 INTG=0
      AMI=.050
      AME=-.030
      K=0
      L=0
      XU=5.
      DTDX=0.
      DPDX=0.
      D2LMT=3.0E-07
      VDESI=.015
      VDESE=.010
C  INITIAL VELOCITY PROFILE
      Y(1)=0.
      Y(NP3)=1.0
      U(1)=1.
      U(NP3)=U(1)*VRAT
      DO 9 I=3,NP1
      Y(I)=YI(I)
    9 U(I)=UI(I)
      WRITE(6,50)
```

```
      WRITE(6,51)VRAT,RTNTI,RTNTE
      GO TO (53,54),IMU
   53 WRITE(6,55)ATURB,BTURB,ALMG
      GO TO 56
   54 WRITE(6,57)ATURB,ALMG
   56 CONTINUE
      WRITE(6,52)N,FRA,VDESI,VDESE
      FTI=RTNTI**2/2.
      FTE=(VRAT*RTNTE)**2/2.
      CALL BEGIN
      GO TO 25
   15 CALL READY
   25 CONTINUE
      INTG=INTG+1
C2  CALCULATE FORWARD STEP SIZE
      DX=FRA*Y(NP3)
      DXLIM=0.2+.001*FLOAT(INTG)
      IF(DX.GT.DXLIM)DX=DXLIM
      XD=XU+DX
      K=K+1
C3  CALCULATE MOMENTUM THICKNESS AND DIFFERENTIALS
      THETA=0.
      DO 17 I=1,NP3
   17 VDR(I)=(U(I)-U(NP3))/(U(1)-U(NP3))
      DO 18 I=2,NP1
      Z=.5*(VDR(I)+VDR(I+1))
   18 THETA=THETA+(Y(I+1)-Y(I))*(Z-Z*Z)
      DTDX=(THETA-THETP)/(XU-XP)
      D2TDX2=(DTDX-DTDXP)/(XU-XP)
      CALL ENTRN
      IF(K.LT.10)GO TO 26
      IF(ABS(D2TDX2).GT.D2LMT.OR.XU.LT.20.)GO TO 27
      CALL OUTPUT
C4  CHECK CONDITIONS FOR TERMINATION
      L=L+1
      IF(L.GT.1)GO TO 22
      IF(INTG.GT.300)GO TO 19
   27 K=0
      IF(XD.GT.50..AND.ABS(D2TDX2).GT.1.0E-04)GO TO 29
C5  ADJUST ASYMPTOTICITY CRITERION
      IF(XD.GT.50..AND.L.LT.2)D2LMT=6.0E-07
      IF(XD.GT.80..AND.L.LT.2)D2LMT=1.0E-06
      IF(XD.GT.90..AND.L.LT.2)D2LMT=5.0E-06
      IF(XD.GT.250.)GO TO 20
   26 CALL COEFF
      CALL SOLVE(AU,BU,CU,U,NP3)
C  SETTING UP VELOCITIES AT A SYMMETRY LINE
      IF(KIN.NE.3) GO TO 71
      U(1)=U(2)
      IF(KRAD.EQ.0)U(1)=.75*U(2)+.25*U(3)
   71 IF(KEX.EQ.3)U(NP3)=.75*U(NP2)+.25*U(NP1)
   30 XP=XU
      XU=XD
      THETP=THETA
      DTDXP=DTDX
      PEI=PEI+DX*(R(1)*AMI-R(NP3)*AME)
      GO TO 15
   22 WRITE(6,99)EFFVIS(1),Y(2),U(2),EFFVIS(NP3),Y(NP2),U(NP2)
```

```
C6  CHECK OVERALL MOMENTUM BALANCE
C   FORMULATION FOR PLANE UNIFORM-DENSITY FLOW
      DMOM=0.
      DO 24 I=2,NP1
   24 DMOM=DMOM+(U(I+1)+U(I))*(OM(I+1)-OM(I))/2.
      ERRMOM=AMI-AME*U(NP3)-DMOM*(AMI-AME)
      ERRMOM=ERRMOM/(DMOM*(AMI-AME))
      WRITE(6,114)DMOM,ERRMOM
      WRITE(6,115)VDESI,VDESE
C7  CALCULATE ALTERNATIVE REPRESENTATIVE TRANSVERSE DIMENSIONS AND
C                                                          GRADIENTS
      DO 28 L=1,3
      DO 33 I=3,N
      IF(VDR(I).GT.VDRN(L))GO TO 33
      CALL CUBIC(U,Y,I,AC,BC,CC,DC,DINT)
      DELM=U(I)*Y(I)-U(I-1)*Y(I-1)-DINT
      EPS=(PEI*(OM(I)-OM(I-1))-DELM)/(U(I)-U(I-1))
      UN=VDRN(L)*(U(1)-U(NP3))+U(NP3)
      YN(L)=Y(I)+BC*(UN-U(I))+CC*(UN**2-U(I)**2)+DC*(UN**3-U(I)**3)-EPS
      IF(L.NE.2)GO TO 28
      YMS=(U(NP3)-U(2))*(BC+2.*CC*UN+3.*DC*UN**2)
      YMSOTH=YMS/THETA
      GO TO 28
   33 CONTINUE
   28 CONTINUE
      YNOM=YN(3)-YN(1)
      YNOTH=YNOM/THETA
      YMOTH=YN(2)/THETA
      YSTRI=(YN(2)-YN(1))/THETA
      YSTRE=(YN(3)-YN(2))/THETA
      DYMDX=YMOTH*DTDX
      DYMSDX=YMS*DTDX/THETA
      DYNDX=YNOM*DTDX/THETA
      DYSIDX=YSTRI*DTDX
      DYSEDX=YSTRE*DTDX
      WRITE(6,117)
      WRITE(6,118)YMSOTH,YNOTH,YSTRI,YSTRE,YMOTH
      WRITE(6,119)DTDX,DYMSDX,DYNDX,DYSIDX,DYSEDX,DYMDX
C   ADJUSTMENT OF BOUNDARY VALUES
      Y(2)=Y(1)
      Y(NP2)=Y(NP3)
      U(2)=U(1)
      U(NP2)=U(NP3)
C8  CALCULATE EQUALLY-SPACED VALUES
      WRITE(6,120)
      DO 34 I=1,22
      YRTEQ=DELYT*FLOAT(I-11)
      YEQ=YRTEQ*THETA+YN(2)
      YREQ=YEQ/Y(NP3)
      IF(YEQ.LT.Y(2))GO TO 34
      IF(YEQ.GT.Y(NP2))GO TO 34
      L=4
   35 IF(Y(L).GT.YEQ)GO TO 36
      L=L+1
      GO TO 35
   36 IF(L.GT.NP1)L=NP1
      IF(YEQ.GT.Y(3))GO TO 37
      DC=((U(3)-U(2))/Y(3)**2-(U(4)-U(2))/Y(4)**2)/(Y(3)-Y(4))
      CC=(U(3)-U(2))/Y(3)**2-DC*Y(3)
      UEQ=U(2)+CC*YEQ**2+DC*YEQ**3
```

```
      DUDY=-2.*CC*YEQ-3.*DC*YEQ**2
      GO TO 38
   37 IF(YEQ.LT.Y(NP1))GO TO 39
      DY1SQ=(Y(NP2)-Y(NP1))**2
      DY2SQ=(Y(NP2)-Y(N))**2
      DC=((U(NP1)-U(NP2))/DY1SQ-(U(N)-U(NP2))/DY2SQ)/(Y(N)-Y(NP1))
      CC=(U(NP1)-U(NP2))/(Y(NP2)-Y(NP1))**2-DC*(Y(NP2)-Y(NP1))
      DYEQ=Y(NP2)-YEQ
      UEQ=U(NP2)+CC*DYEQ**2+DC*DYEQ**3
      DUDY=2.*CC*DYEQ+3.*DC*DYEQ**2
      GO TO 38
   39 CALL CUBIC(Y,U,L,AC,BC,CC,DC,DINT)
      EPS=(DINT-PEI*(OM(L)-OM(L-1)))/(Y(L)-Y(L-1))
      UEQ=U(L)+BC*(YEQ-Y(L))+CC*(YEQ**2-Y(L)**2)+DC*(YEQ**3-Y(L)**3)-EP
      DUDY=-BC-2.*CC*YEQ-3.*DC*YEQ**2
   38 VDREQ=(UEQ-U(NP3))/(U(1)-U(NP3))
      THDUDY=100.*THETA*DUDY
      L=2
   41 IF(Y(L).GT.YEQ)GO TO 40
      L=L+1
      GO TO 41
   40 EFVEQ=EFFVIS(L)-(EFFVIS(L)-EFFVIS(L-1))*(Y(L)-YEQ)/(Y(L)-Y(L-1))
      RTNT=EFVEQ/(UEQ*10.)
      WRITE(6,121)YREQ,YRTEQ,UEQ,VDREQ,THDUDY,EFVEQ,RTNT
   34 CONTINUE
   32 CONTINUE
   31 STOP
   29 WRITE(6,100)
      CALL OUTPUT
      GO TO 32
   19 WRITE(6,101)
      CALL OUTPUT
      GO TO 32
   20 WRITE(6,102)
      CALL OUTPUT
      GO TO 32
   10 FORMAT(14F5.2)
   12 FORMAT(5F5.2)
   50 FORMAT(1H1,48HPLANE,ISOTHERMAL,ISOBARIC,HOMOGENEOUS,TURBULENT ,
     1    12HMIXING LAYER//5X,31HMODIFIED PRANDTL MIXING-LENGTH ,
     2    54HTURBULENCE MODEL,WITH EFFECTIVE VISCOSITY AUGMENTED TO/
     3    40X,34HACCOUNT FOR FREE-STREAM TURBULENCE//)
   51 FORMAT(1X,15HVELOCITY RATIO=,F4.2,5X,21HREL TURB INTENSITIES,,
     1    9HI-STREAM,,F5.3,2X,9HE-STREAM,,F5.3//)
   52 FORMAT(5X,2HN=,I2,5X,6HDX/YE=,F5.3,5X,6HVDESI=,F6.4,5X,6HVDESE=,
     1    F6.4//)
   55 FORMAT(5X,6HATURB=,F5.3,5X,6HBTURB=,F5.3,5X,5HALMG=,F5.3//)
   57 FORMAT(5X,6HATURB=,F5.3,5X,5HALMG=,F5.3//)
   99 FORMAT(5X,6HEM20L=,1PE9.2,3X,3HY2=,E9.2,3X,3HU2=,E10.3,10X,
     1    7HENP10L=,E9.2,3X,5HYNP2=,E9.2,3X,5HUNP2=,E10.3//)
  100 FORMAT(10X,22HD2TDX2 EXCEEDS 1.0E-04)
  101 FORMAT(10X,18HINTG EXCEEDS LIMIT)
  102 FORMAT(10X,15HX EXCEEDS LIMIT)
  114 FORMAT(5X,22HSIGMA U(MEAN)*DEL(OM)=,F6.4,5X,9HMOMENTUM ,
     1    19HCONSERVATION ERROR=,1PE9.2//)
  115 FORMAT(5X,21HFINAL VALUES-  VDESI=,F6.4,3X,6HVDESE=,F7.4//)
  117 FORMAT(1H0,14HDIMENSION DELY,7X,5HTHETA,12X,3HYMS,13X,4HYNOM,11X,
     1    5HYSTRI,11X,5HYSTRE,11X,5HYMOTH//)
  118 FORMAT(5X,10HDELY/THETA,12X,5(10X,F6.3)//)
```

```
  119 FORMAT(5X,10HD(DELY)/DX,1P6E16.3//)
  120 FORMAT(1H0,9X,4HYREQ,3X,10HYSTR/THETA,5X,1HU,8X,3HVDR,5X,
     1    7HTH*DUDY,4X,5HEFVEQ,4X,4HRTNT/50X,4HX100,6X,4HX100)
  121 FORMAT(5X,F10.3,F10.2,2F10.3,3F10.2,F10.4)
      END

      SUBROUTINE BEGIN
      COMMON/GEN/PEI,AMI,AME,DPDX,XU,XD,XP,XL,DX,INTG,CSALFA
     1/F/FTI,FTE,ATURB,K,VDESI,VDESE,M,L
     1/I/N,NP1,NP2,NP3,NEQ,NPH,KEX,KIN,KASE,KRAD
     1/T/VDR(43),THETA,DTDX,D2TDX2,FRA
     1/V/U(43),F(2,43),R(43),RHO(43),OM(43),Y(43)
      COMMON/L/AK,ALMG,AL
      DIMENSION OMT10(43)
C     KEX,KIN=1,2,3 FOR WALL,FREE BOUNDARY, OR LINE OF SYMMETRY
      KEX=2
      KIN=2
C     NEQ=NUMBER OF DIFF. EQNS. SOLVED
      NEQ=1
C     KRAD=0 INDICATES PLANE FLOW
      KRAD=0.
      KASE=2
      DO 5 I=1,NP3
      R(I)=1.0
    5 RHO(I)=1.0
      CSALFA=1.
C  CALCULATION OF SLIP VELOCITIES AND DISTANCES
      U11=U(1)*U(1)
      U13=U(1)*U(3)
      U33=U(3)*U(3)
      SQ=84.*U11-12.*U13+9.*U33
      U(2)=(16.*U11-4.*U13+U33)/(2.*(U(1)+U(3))+SQRT(SQ))
      Y(2)=Y(3)*(U(2)+U(3)-2.*U(1))*.5/(U(2)+U(3)+U(1))
      U11=U(NP1)*U(NP1)
      U13=U(NP1)*U(NP3)
      U33=U(NP3)*U(NP3)
      SQ=84.*U33-12.*U13+9.*U11
      U(NP2)=(16.*U33-4.*U13+U11)/(2.*(U(NP1)+U(NP3))+SQRT(SQ))
      Y(NP2)=Y(NP3)-(Y(NP3)-Y(NP1))*(U(NP2)+U(NP1)-2.*U(NP3))*.5/
     1(U(NP2)+U(NP1)+U(NP3))
C  CALCULATION OF OMEGA VALUES
      OM(1)=0.
      OM(2)=0.
      DO 49 I=3,NP2
   49 OM(I)=OM(I-1)+.5*(RHO(I)*U(I)*R(I)+RHO(I-1)*U(I-1)*R(I-1))*
     1(Y(I)-Y(I-1))
      PEI=OM(NP2)
       DO 59 I=3,NP1
   59 OM(I)=OM(I)/PEI
      OM(NP2)=1.
      OM(NP3)=1.
      DO 60 I=3,NP1
   60 OMT10(I)=10.*OM(I)
      WRITE(6,52)
```

```
      WRITE(6,53)Y(1),(Y(I),I=3,NP1),Y(NP3)
      WRITE(6,54)U(1),(U(I),I=3,NP1),U(NP3)
      WRITE(6,55)OM(1),(OMTIC(I),I=3,NP1),OM(NP3)
      WRITE(6,56)Y(2),U(2),R(1),Y(NP2),U(NP2)
   52 FORMAT(5X,17HSTARTING PROFILES)
   53 FORMAT( 5X,1HY,1X,21F5.2)
   54 FORMAT( 5X,1HU,1X,21F5.2)
   55 FORMAT(2X,4H100M,1X,21F5.2)
   56 FORMAT(10X,3HY2=,F6.3,2X,3HU2=,F6.3,24X,3HR1=,F4.1,24X,5HYNP2=,
     1    F6.3,2X,5HUNP2=,F6.3,///)
      RETURN
      END

      SUBROUTINE COEFF
      COMMON/GEN/PEI,AMI,AME,DPDX,XU,XD,XP,XL,DX,INTG,CSALFA
     1/C/SC(43),AU(43),BU(43),CU(43),A(2,43),B(2,43),C(2,43)
     1/I/N,NP1,NP2,NP3,NEQ,NPH,KEX,KIN,KASE,KRAD
     1/V/U(43),F(2,43),R(43),RHO(43),OM(43),Y(43)
      COMMON/L/AK,ALMG,AL
      DIMENSION G1(43),G2(43),G3(43),D(2,43),S1(43),S2(43),S3(43)
C  THE CONVECTION TERM
      SA=R(1)*AMI/PEI
      SB=(R(NP3)*AME-R(1)*AMI)/PEI
      DO 71 I=3,NP1
      OMD=OM(I+1)-OM(I-1)
      P2=.25/DX
      P3=P2/OMD
      P1=(OM(I+1)-OM(I))*P3
      P3=(OM(I)-OM(I-1))*P3
      P2=3.*P2
      Q=SA/OMD
      R2=-SB*.25
      R3=R2/OMD
      R1=-(OM(I+1)+3.*OM(I))*R3
      R3=(OM(I-1)+3.*OM(I))*R3
      G1(I)=P1+Q+R1
      G2(I)=P2+R2
      G3(I)=P3-Q+R3
      CU(I)=-P1*U(I+1)-P2*U(I)-P3*U(I-1)
C  THE DIFFUSION TERM
      AU(I)=2./OMD
      BU(I)=SC(I-1)*AU(I)/(OM(I)-OM(I-1))
      AU(I)=SC(I)*AU(I)/(OM(I+1)-OM(I))
   71 CONTINUE
C  COEFFICIENTS IN THE FINAL FORM
      DO 91 I=3,NP1
      RL=1./(G2(I)+AU(I)+BU(I)-S2(I))
      AU(I)=(AU(I)-G1(I))*RL
      BU(I)=(BU(I)-G3(I))*RL
   91 CU(I)=-CU(I)*RL
      CALL SLIP
      RETURN
      END
```

```
      SUBROUTINE CUBIC(Y,W,L,A,B,C,D,DINT)
      DIMENSION Y(4),W(4),DY(3),DY2(3),DY3(3),DW(3)
    9 DO 10 J=1,3
      K=L+J-2
      DY(J)=Y(K)-Y(K-1)
      DY2(J)=Y(K)**2-Y(K-1)**2
      DY3(J)=Y(K)**3-Y(K-1)**3
   10 DW(J)=W(K)-W(K-1)
      EWY1=DW(1)*DY(2)-DW(2)*DY(1)
      EWY2=DW(2)*DY(3)-DW(3)*DY(2)
      EY21=DY2(1)*DY(2)-DY2(2)*DY(1)
      EY22=DY2(2)*DY(3)-DY2(3)*DY(2)
      EY31=DY3(1)*DY(2)-DY3(2)*DY(1)
      EY32=DY3(2)*DY(3)-DY3(3)*DY(2)
      D=(EWY1*EY22-EWY2*EY21)/(EY31*EY22-EY32*EY21)
      C=(EWY1*EY32-EWY2*EY31)/(EY32*EY21-EY31*EY22)
      B=(DW(2)-C*DY2(2)-D*DY3(2))/DY(2)
      A=W(L)-B*Y(L)-C*Y(L)**2-D*Y(L)**3
      DINT=A*DY(2)+B*DY2(2)/2.+C*DY3(2)/3.+D*(Y(L)**4-Y(L-1)**4)/4.
      RETURN
      END
```

```
      SUBROUTINE ENTRN
      COMMON/GEN/PEI,AMI,AME,DPDX,XU,XD,XP,XL,DX,INTG,CSALFA
     1/C/SC(43),AU(43),BU(43),CU(43),A(2,43),B(2,43),C(2,43)
     1/F/FTI,FTE,ATURB,K,VDESI,VDESE,M,L
     1/T/VDR(43),THETA,DTDX,D2TDX2,FRA
     1/I/N,NP1,NP2,NP3,NEQ,NPH,KEX,KIN,KASE,KRAD
     1/L1/YL,UMAX,UMIN,FR,YIP,YEM
     1/V/U(43),F(2,43),R(43),RHO(43),OM(43),Y(43)
     1/R/EFFVIS(43),VEFRAT(43),ETOT,BTURB,IMU
      COMMON/L/AK,ALMG,AL
C  CALCULATION OF ENTRAINMENT RATES BY SIMULTANEOUS SOLUTION OF
C  FORCE-MOMENTUM EQUATIONS NEAR BOUNDARIES
C  MIXING-LENGTH HYPOTHESIS MODIFIED TO ALLOW FOR FREE-STREAM TURBULENCE
      AL=ALMG*THETA
      AUR=ATURB*SQRT(2.*FTI)
      FTRAT=SQRT(FTE/FTI)*U(1)/U(NP3)
      DO 98 I=2,NP1
      RH=.5*(RHO(I)+RHO(I+1))
      UMRAT=(U(I)+U(I+1))/(2.*U(1))
      YRAT=(Y(I)+Y(I+1))/(2.*Y(NP3))
      DUDY=ABS((U(I)-U(I+1))/(Y(I)-Y(I+1)))
      TBRAT=1.+YRAT*(FTRAT-1.)
      EXTURB=AUR*TBRAT*UMRAT*(BTURB+U(NP3)/U(1))
      EMU=RH*AL*(AL*DUDY+EXTURB)
      VEFRAT(I)=EXTURB/(AL*DUDY)
      EFFVIS(I)=(EMU+EMUP)/(2.*AL)
      EMUP=EMU
      IF(I.EQ.2)EFFVIS(1)=EMU/AL
      IF(I.EQ.NP1)EFFVIS(NP3)=EMU/AL
```

```
C   CALCULATION OF SMALL C 'S
      R2RUI=R(I)*R(I)*RHO(I)*U(I)
      DTOIP1=R(I+1)*R(I+1)*RHO(I+1)*U(I+1)
   98 SC(I)=(R2RUI+DTOIP1)*.5*EMU/(PEI*PEI)
      VDFACI=1.0
      VDFACE=0.6
      UDIF=1.33*(1.-U(NP3)/U(1))/(FLOAT(N))**2
      VDESI=VDESI+VDFACI*(U(3)-U(1)+UDIF)
      IF(VDESI.GT..06)VDESI=.06
      IF(VDESI.LT.-.06)VDESI=-.06
      VDESE=VDESE+VDFACE*(U(NP3)-U(NP1)+UDIF)
      IF(VDESE.GT..03)VDESE=.03
      IF(VDESE.LT.-.10)VDESE=-.10
      UBI=U(1)-VDESI*(U(1)-U(NP3))
      UBE=U(NP3)+VDESE*(U(1)-U(NP3))
      A4=SC(4)*(U(5)-U(4))/(OM(5)-OM(4))
      B4=SC(3)*(U(4)-U(3))/(OM(4)-OM(3))
      C4=(UBI-U(4))/DX
      D4=DPDX/(RHO(4)*U(4))
      A4=PEI*(OM(5)-OM(3))*(A4-B4-C4-D4)/(U(5)-U(3))
      AN=SC(N-1)*(U(N)-U(N-1))/(OM(N)-OM(N-1))
      BN=SC(N)*(U(N+1)-U(N))/(OM(N+1)-OM(N))
      CN=(UBE-U(N))/DX
      DN=DPDX/(RHO(N)*U(N))
      AN=PEI*(OM(N+1)-OM(N-1))*(AN-BN-CN-DN)/(U(N+1)-U(N-1))
      AMI=(OM(N)*A4-OM(4)*AN)/(R(1)*(OM(N)-OM(4)))
      AMI=(AMI+AMIP)/2.
      AMIP=AMI
      IF(AMI.LT.0.0)AMI=0.0
      AMIM=.10+SQRT(FTI)/2.
      IF(AMI.GT.AMIM)AMI=AMIM
      AME=((1.-OM(4))*AN-(1.-OM(N))*A4)/(R(N+3)*(OM(N)-OM(4)))
      AME=(AME+AMEP)/2.
      AMEP=AME
      IF(AME.GT.0.0)AME=0.0
      AMEM=-.04-SQRT(FTI)/6.
      IF(AME.LT.AMEM)AME=AMEM
      IF(L.LT.5)GO TO 4
      IF(K.LT.9)GO TO 4
      WRITE(6,6)PEI,SC(3),SC(4),B4,C4,A4
      WRITE(6,7)SC(N-1),SC(N),BN,CN,AN
    4 CONTINUE
    5 RETURN
    6 FORMAT(3X,4HPEI=,F6.3,3X,8HSC(3)   =,1PE10.3,3X,6HSC(4)=,E10.3,3X,
     1    3HB4=,E10.3,3X,3HC4=,E10.3,3X,3HA4=,E10.3)
    7 FORMAT(16X,8HSC(N-1)=,1PE10.3,3X,6HSC(N)=,E10.3,3X,3HBN=,E10.3,3X
     1      3HCN=,E10.3,3X,3HAN=,E10.3)
      END
```

```
      SUBROUTINE OUTPUT
      COMMON/GEN/PEI,AMI,AME,DPDX,XU,XD,XP,XL,DX,INTG,CSALFA
     1/C/SC(43),AU(43),BU(43),CU(43),A(2,43),B(2,43),C(2,43)
     1/I/N,NP1,NP2,NP3,NEQ,NPH,KEX,KIN,KASE,KRAD
     1/L1/YL,UMAX,UMIN,FR,YIP,YEM
     1/F/FTI,FTE,ATURB,K,VDESI,VDESE,M,L
     1/R/EFFVIS(43),VEFRAT(43),ETOT,STURB,IMU
     1/T/VDR(43),THETA,DTDX,D2TDX2,FRA
     1/V/U(43),F(2,43),R(43),RHO(43),OM(43),Y(43)
      DIMENSION YR10(43),UT10(43),VDR10(43),TDR10(43),T10(43),YOTH(43)
      COMMON/L/AK,ALMG,AL
      DO 16 I=1,NP3
      YR10(I)=10.*Y(I)/Y(NP3)
      VDR10(I)=10.*VDR(I)
      YOTH(I)=Y(I)/THETA
   16 UT10(I)=10.*U(I)
      WRITE(6,49)INTG,XU
      WRITE(6,50)(Y(I),I=3,NP1),Y(NP3)
      WRITE(6,51)(YR10(I),I=3,NP1)
      WRITE(6,61)(YOTH(I),I=3,NP1),YOTH(NP3)
      WRITE(6,52)(VDR10(I),I=3,NP1)
      WRITE(6,53)UT10(1),(UT10(I),I=3,NP1),UT10(NP3)
      IF(NEQ.EQ.1)GO TO 20
      DO 17 I=3,NP3
   17 TDR10(I)=10.*(F(1,I)-F(1,1))/(F(1,NP3)-F(1,1))
      WRITE(6,55)(TDR10(I),I=3,NP1),TDR10(NP3)
      IF(F(1,NP3).LT.1.)GO TO 18
      WRITE(6,56)(F(1,I),I=3,NP1),F(1,NP3)
      GO TO 20
   18 DO 19 I=3,NP3
   19 T10(I)=10.*F(1,I)
      WRITE(6,57)(T10(I),I=3,NP1),T10(NP3)
   20 EFFVIS(2)=RHO(1)*ATURB*SQRT(2.*FTI)
      EFFVIS(NP2)=RHO(NP3)*ATURB*SQRT(2.*FTE)
   21 DO 12 I=2,NP2
   12 EFFVIS(I)=100.*EFFVIS(I)
      WRITE(6,59)(EFFVIS(I),I=2,NP2)
   22 WRITE(6,60)(VEFRAT(I),I=2,NP1)
      WRITE(6,58)VDESI,VDESE
      WRITE(6,54)AMI,AME,AL,THETA,DTDX,D2TDX2
      RETURN
   49 FORMAT(1H0,2X,11HSTEP NUMBER,I4,5X,2HX=,F6.2//)
   50 FORMAT(9X,10H    Y  0.00,20F5.2)
   51 FORMAT(9X,10H10YR  0.00,20F5.2)
   52 FORMAT(8X,11H10VDR 10.00,20F5.2)
   53 FORMAT(10X,4H10U ,21F5.2//)
   54 FORMAT(1H0,8X,4HAMI=,1PE10.3,2X,4HAME=,E10.3,3X,3HAL=,0PF6.4,3X,
     1    6HTHETA=,1PE9.2,2X,5HDTDX=,E10.3,2X,7HD2TDX2=,E9.2,///)
   55 FORMAT(8X,11H10TDR  0.00,20F5.2)
```

```
   56 FORMAT(12X,7HT   1.00,20F5.2//)
   57 FORMAT(10X,9H10T 10.00,20F5.2//)
   58 FORMAT(3X,33HPROFILE CONTROL CONSTANTS--VDESI=,F6.3,3X,6HVDESE=,
     1    F6.3//)
   59 FORMAT(3X,10H100XEFFVIS,1X,21F5.2)
   60 FORMAT(7X,6HVEFRAT,4X,20F5.2//)
   61 FORMAT(6X,13HY/THETA   0.00,20F5.2//)
      END
```

```
      SUBROUTINE READY
      COMMON/GEN/PEI,AMI,AME,DPDX,XU,XD,XP,XL,DX,INTG,CSALFA
     1/F/FTI,FTE,ATURB,K,VDESI,VDESE,M,L
     1/I/N,NP1,NP2,NP3,NEQ,NPH,KEX,KIN,KASE,KRAD
     1/V/U(43),F(2,43),R(43),RHO(43),OM(43),Y(43)
C  Y NEAR THE I BOUNDARY
      Y(2)=OM(3)/(RHO(2)*U(2)+RHO(3)*U(3))
      Y(3)=Y(2)+OM(3)*2./(RHO(2)*U(2)+3.*RHO(3)*U(3))
C  Y'S FOR INTERMEDIATE GRID POINTS
      DO 50 I=4,NP1
   50 Y(I)=Y(I-1)+2.*(OM(I)-OM(I-1))/(RHO(I-1)*U(I-1)+RHO(I)*U(I))
C  Y NEAR THE E BOUNDARY
      Y(NP2)=Y(NP1)+2.*(1.-OM(NP1))/(3.*RHO(NP1)*U(NP1)+RHO(NP2)*U(NP2)
      Y(NP3)=Y(NP2)+(1.-OM(NP1))/(RHO(NP1)*U(NP1)+RHO(NP2)*U(NP2))
   51 DO 54 I=2,NP3
   54 Y(I)=PEI*Y(I)/R(1)
   56 Y(2)=2.*Y(2)-Y(3)
      Y(NP2)=2.*Y(NP2)-Y(NP1)
      RETURN
      END
```

```
      SUBROUTINE SLIP
      COMMON/GEN/PEI,AMI,AME,DPDX,XU,XD,XP,XL,DX,INTG,CSALFA
     1/C/SC(43),AU(43),BU(43),CU(43),A(2,43),B(2,43),C(2,43)
     1/F/FTI,FTE,ATURB,K,VDESI,VDESE,M,L
     1/I/N,NP1,NP2,NP3,NEQ,NPH,KEX,KIN,KASE,KRAD
     1/V/U(43),F(2,43),R(43),RHO(43),OM(43),Y(43)
      COMMON/L/AK,ALMG,AL
C     FORMULATION FOR COEFFICIENTS IN PLANE FLOW WITH ZERO PRESSURE GRADT
      CVI=2.*SC(2)*PEI/OM(3)
      CMI=AMI
      CMDI=(AME-AMI)*OM(3)/4.
      CYI=.5*OM(3)*PEI/DX
      CEI=CVI+CMI-CMDI+1.5*CYI
      AU(2)=(CVI-CMI-CMDI-.5*CYI)/CEI
      BU(2)=2.*CMI/CEI
      CU(2)=.5*CYI*(3.*U(2)+U(3))/CEI
      CVE=2.*SC(NP1)*PEI/(1.-OM(NP1))
      CME=-AME
      CMDE=(AME-AMI)*(1.-OM(NP1))/4.
      CYE=.5*(1.-OM(NP1))*PEI/DX
      CEE=CVE+CME-CMDE+1.5*CYE
      AU(NP2)=2.*CME/CEE
      BU(NP2)=(CVE-CME-CMDE-.5*CYE)/CEE
      CU(NP2)=.5*CYE*(U(NP1)+3.*U(NP2))/CEE
      RETURN
      END
```

```
      SUBROUTINE SOLVE(A,B,C,F,NP3)
C     THIS SOLVES EQUATIONS OF THE FORM
C     F(I)=A(I)*F(I+1)+B(I)*F(I-1)+C(I)
C     FOR I=2,NP2
      DIMENSION A(NP3),B(NP3),C(NP3),F(NP3)
      NP2=NP3-1
      B(2)=B(2)*F(1)+C(2)
      DO 48 I=3,NP2
      T=1./(1.-B(I)*A(I-1))
      A(I)=A(I)*T
   48 B(I)=(B(I)*B(I-1)+C(I))*T
      DO 50 I=2,NP2
      J=NP2-I+2
   50 F(J)=A(J)*F(J+1)+B(J)
      RETURN
      END
```

LISTING OF NEWMOD-F PROGRAMME (MAIN SECTION ONLY)

```
      COMMON/GEN/PEI,AMI,AME,DPDX,XU,XD,XP,XL,DX,INTG,CSALFA
     1/V/U(43),F(2,43),R(43),RHO(43),OM(43),Y(43)
     1/F/FTI,FTE,ATURB,K,VDESI,VDESE,M,L
     1/T/VDR(43),THETA,DTDX,D2TDX2,FRA
     1/C/SC(43),AU(43),BU(43),CU(43),A(2,43),B(2,43),C(2,43)
     1/I/N,NP1,NP2,NP3,NEQ,NPH,KEX,KIN,KASE,KRAD
     1/R/EFFVIS(43),VEFRAT(43),ETOT,BTURB,IMU
      COMMON/L/AK,ALMG,AL
      DIMENSION YI(43),UI(43),YR(43),YOTH(43)
      DIMENSION XSTAT(5),TINTI(5),TINTE(5),VDRN(3),YN(3)
C     MODIFIED P25 PROGRAMME
      DELYT=0.4
      VDRN(1)=.9
      VDRN(2)=.5
      VDRN(3)=.1
      NSTEP=40
    8 READ(5,9)NRUN,NSTAT,N,(XSTAT(L),TINTI(L),TINTE(L),L=1,NSTAT)
      DPDX=0.
      NP1=N+1
      NP2=N+2
      NP3=N+3
      READ(5,10)YI(1),UI(1),(YI(I),UI(I),I=3,NP1),YI(NP3),UI(NP3)
      READ(5,11)INDEX,ALMG,ATURB,VDESI,VDESE
      ALMG=.50
      DO 32 IMU=1,2
C     IMU=1 DENOTES MU1 EFFECTIVE VISCOSITY EXPRESSION
C     IMU=2 DENOTES MU2 EFFECTIVE VISCOSITY EXPRESSION
      ATURB=1.05
      IF(IMU.EQ.2)ATURB=2.0
      BTURB=0.5
      INTG=0
      K=20
      NSTPST=0
      L=1
      DO 7 I=1,NP3
      Y(I)=YI(I)
    7 U(I)=UI(I)
      LIMINT=(NSTAT-1)*NSTEP+1
      XU=XSTAT(1)
      VRAT=U(NP3)/U(1)
      WRITE(6,50)
      WRITE(6,51)NRUN,VRAT,TINTI(1),TINTE(1)
      IF(IMU.EQ.1)WRITE(6,122)N,NSTEP,ATURB,BTURB,ALMG
      IF(IMU.EQ.2)WRITE(6,52)N,NSTEP,ATURB,ALMG
      CALL BEGIN
   12 DX=(XSTAT(L+1)-XSTAT(L))/FLOAT(NSTEP)
      IF(L.GT.(NSTAT-2))GO TO 14
      TG1=(TINTI(L)-TINTI(L+1))/(XSTAT(L)-XSTAT(L+1))
      TG2=(TINTI(L+1)-TINTI(L+2))/(XSTAT(L+1)-XSTAT(L+2))
      A1=(TG1-TG2)/(XSTAT(L)-XSTAT(L+2))
      B1=TG1-A1*(XSTAT(L)+XSTAT(L+1))
      C1=TINTI(L)-A1*XSTAT(L)**2-B1*XSTAT(L)
      TG1=(TINTE(L)-TINTE(L+1))/(XSTAT(L)-XSTAT(L+1))
      TG2=(TINTE(L+1)-TINTE(L+2))/(XSTAT(L+1)-XSTAT(L+2))
```

```
      AE=(TG1-TG2)/(XSTAT(L)-XSTAT(L+2))
      BE=TG1-AE*(XSTAT(L)+XSTAT(L+1))
      CE=TINTE(L)-AE*XSTAT(L)**2-BE*XSTAT(L)
      IF(INTG.EQ.0)GO TO 16
   14 NSTPST=NSTPST+NSTEP
      L=L+1
   15 CALL READY
      K=K+1
      INTG=INTG+1
   16 RLTII=AI*XU**2+BI*XU+CI
      RLTIE=AE*XU**2+BE*XU+CE
      FTI=RLTII**2/2.
      FTE=(RLTIE*U(NP3)/U(1))**2/2.
      XD=XU+DX
      THETA=0.
      DO 17 I=1,NP3
   17 VDR(I)=(U(I)-U(NP3))/(U(1)-U(NP3))
      DO 18 I=2,NP1
      Z=.5*(VDR(I)+VDR(I+1))
   18 THETA=THETA+(Y(I+1)-Y(I))*(Z-Z*Z)
      DTDX=(THETA-THETP)/(XU-XP)
      D2TDX2=(DTDX-DTDXP)/(XU-XP)
      CALL ENTRN
      IF(K.LT.20)GO TO 26
      CALL OUTPUT
      K=0
   26 IF(INTG.EQ.NSTPST)GO TO 22
   27 CALL COEFF
      CALL SOLVE(AU,BU,CU,U,NP3)
C  SETTING UP VELOCITIES AT A SYMMETRY LINE
      IF(KIN.NE.3) GO TO 71
      U(1)=U(2)
      IF(KRAD.EQ.0)U(1)=.75*U(2)+.25*U(3)
   71 IF(KEX.EQ.3)U(NP3)=.75*U(NP2)+.25*U(NP1)
   30 XP=XU
      XU=XD
      IF(XU.GT.XSTAT(NSTAT))GO TO 31
      THETP=THETA
      DTDXP=DTDX
      PEI=PEI+DX*(R(1)*AMI-R(NP3)*AME)
      IF(INTG.GT.LIMINT)GO TO 31
      IF(INTG.EQ.0)GO TO 14
      IF(INTG.EQ.NSTPST)GO TO 12
      GO TO 15
   22 LSTAT=L
      WRITE(6,100)LSTAT,XU,THETA
C    FORMULATION FOR UNIFORM DENSITY
C    CALCULATION OF REPRESENTATIVE TRANSVERSE DIMENSIONS
      DO 28 L=1,3
      DO 33 I=3,N
      IF(VDR(I).GT.VDRN(L))GO TO 33
      CALL CUBIC(U,Y,I,AC,BC,CC,DC,DINT)
      DELM=U(I)*Y(I)-U(I-1)*Y(I-1)-DINT
      EPS=(PEI*(OM(I)-OM(I-1))-DELM)/(U(I)-U(I-1))
      UN=VDRN(L)*(U(1)-U(NP3))+U(NP3)
      YN(L)=Y(I)+BC*(UN-U(I))+CC*(UN**2-U(I)**2)+DC*(UN**3-U(I)**3)-EPS
      IF(L.NE.2)GO TO 28
      YMS=(U(NP3)-U(2))*(BC+2.*CC*UN+3.*DC*UN**2)
      YMSOTH=YMS/THETA
```

```
      GO TO 28
   33 CONTINUE
   28 CONTINUE
C    ADJUSTMENT OF BOUNDARY VALUES
      Y2C=Y(2)
      YNP2C=Y(NP2)
      U2C=U(2)
      UNP2C=U(NP2)
      Y(2)=Y(1)
      Y(NP2)=Y(NP3)
      U(2)=U(1)
      U(NP2)=U(NP3)
      ETA=0.
      RTIP=EFFVIS(2)/U(1)
      RTIM=0.
      DO 200 I=3,NP2
      RTI=EFFVIS(I)/U(I)
      IF(RTI.GT.RTIM)RTIM=RTI
      ETA=ETA+(RTI+RTIP)*(Y(I)-Y(I-1))
      RTIP=RTI
  200 CONTINUE
      ETA=ETA-Y(NP3)*(RLTII+RLTIE)
      ETOT=ETA/(RTIM*2.-RLTII-RLTIE)/THETA
      YNOM=YN(3)-YN(1)
      YNOTH=YNOM/THETA
      YMOTH=YN(2)/THETA
      YSTRI=(YN(2)-YN(1))/THETA
      WRITE(6,117)
      WRITE(6,118)YMSOTH,YNOTH,YSTRI,ETOT,YMOTH
C CALCULATION OF EQUALLY-SPACED VALUES
      WRITE(6,120)
      M=INT(Y(NP3)/(2.*DELYT*THETA))*2+4
      DO 34 I=1,M
      YRTEQ=DELYT*FLOAT(I-M/2)
      YSTAR=YRTEQ*THETA
      YEQ=YSTAR+YN(2)
      YREQ=YEQ/Y(NP3)
      IF(YEQ.LT.Y(2))GO TO 34
      IF(YEQ.GT.Y(NP2))GO TO 34
      L=4
   35 IF(Y(L).GT.YEQ)GO TO 36
      L=L+1
      GO TO 35
   36 IF(L.GT.NP1)L=NP1
      IF(YEQ.GT.Y(3))GO TO 37
      DC=((U(3)-U(2))/Y(3)**2-(U(4)-U(2))/Y(4)**2)/(Y(3)-Y(4))
      CC=(U(3)-U(2))/Y(3)**2-DC*Y(3)
      UEQ=U(2)+CC*YEQ**2+DC*YEQ**3
      DUDY=-2.*CC*YEQ-3.*DC*YEQ**2
      GO TO 38
   37 IF(YEQ.LT.Y(NP1))GO TO 39
      DY1SQ=(Y(NP2)-Y(NP1))**2
      DY2SQ=(Y(NP2)-Y(N))**2
      DC=((U(NP1)-U(NP2))/DY1SQ-(U(N)-U(NP2))/DY2SQ)/(Y(N)-Y(NP1))
      CC=(U(NP1)-U(NP2))/(Y(NP2)-Y(NP1))**2-DC*(Y(NP2)-Y(NP1))
      DYEQ=Y(NP2)-YEQ
      UEQ=U(NP2)+CC*DYEQ**2+DC*DYEQ**3
      DUDY=2.*CC*DYEQ+3.*DC*DYEQ**2
      GO TO 38
```

```
 39 CALL CUBIC(Y,U,L,AC,BC,CC,DC,DINT)
    EPS=(DINT-PEI*(OM(L)-OM(L-1)))/(Y(L)-Y(L-1))
    UEQ=U(L)+BC*(YEQ-Y(L))+CC*(YEQ**2-Y(L)**2)+DC*(YEQ**3-Y(L)**3)-EP
    DUDY=-BC-2.*CC*YEQ-3.*DC*YEQ**2
 38 VDREQ=(UEQ-U(NP3))/(U(1)-U(NP3))
    THDUDY=100.*THETA*DUDY
    L=2
 41 IF(Y(L).GT.YEQ)GO TO 40
    L=L+1
    GO TO 41
 40 EFVEQ=EFFVIS(L)-(EFFVIS(L)-EFFVIS(L-1))*(Y(L)-YEQ)/(Y(L)-Y(L-1))
    RTNT=EFVEQ/(UEQ*10.)
    WRITE(6,121)YREQ,YSTAR,YRTEQ,UEQ,VDREQ,THDUDY,EFVEQ,RTNT
 34 CONTINUE
    Y(2)=Y2C
    Y(NP2)=YNP2C
    U(2)=U2C
    U(NP2)=UNP2C
    L=LSTAT
    IF(L.EQ.NSTAT)GO TO 32
    GO TO 27
 32 CONTINUE
    GO TO (8,31),INDEX
 31 STOP
  9 FORMAT(I5,I2,I3/15F5.2)
 10 FORMAT(16F5.2)
 11 FORMAT(I5,4F5.2)
 50 FORMAT(1H1,48HPLANE,ISOTHERMAL,ISOBARIC,HOMOGENEOUS,TURBULENT ,
   1    12HMIXING LAYER//5X,31HMODIFIED PRANDTL MIXING-LENGTH ,
   2    54HTURBULENCE MODEL,WITH EFFECTIVE VISCOSITY AUGMENTED TO/
   3    40X,34HACCOUNT FOR FREE-STREAM TURBULENCE//)
 51 FORMAT(5X,36HFINITE-DIFFERENCE PREDICTION FOR RUN,I3/5X,
   1   15HVELOCITY RATIO=,F4.2,5X,8HTINT(I)=,F5.3,3X,8HTINT(E)=,F5.3/
 52 FORMAT(5X,2HN=,I2,5X,6HNSTEP=,I2,5X,6HATURB=,F5.3,5X,
   1    5HALMG=,F5.3//)
 57 FORMAT(5X,4F10.3)
100 FORMAT(1H0,7HSTATION,I2,5X,2HX=,F5.2,2HCM,5X,6HTHETA=,F5.3,2HCM/
117 FORMAT(1H0,14HDIMENSION DELY,7X,5HTHETA,12X,3HYMS,13X,4HYNOM,11X,
   1    5HYSTRI,11X,4HETOT,12X,5HYMOTH//)
118 FORMAT(5X,10HDELY/THETA,12X,5(10X,F6.3)//)
120 FORMAT(1H0,9X,4HYREQ,5X,5HYSTAR,3X,10HYSTR/THETA,5X,1HU,8X,3HVDR,
   1    5X,7HTH*DUDY,4X,5HEFVEQ,4X,4HRTNT/60X,4HX100,6X,4HX100,5X,
   2    3HX10)
121 FORMAT(5X,F10.3,2F10.2,2F10.3,4F10.2)
122 FORMAT(5X,2HN=,I2,5X,6HNSTEP=,I2,5X,6HATURB=,F5.3,5X,6HBTURB=,
   1    F5.3,5X,5HALMG=,F5.3//)
    END
```

LISTING OF LAYER PROGRAMME

```
C************************  G E N K L 3  ( DECK 1 )  ************************
C   2/4/70  CHANGE TO KOLMOGOROV (K-Z) MODEL
C                                                    S.I.UNITS
C  000000000000000000000000000000000000000000000  PRELIMINARIES
C  ************  ****  COMMON  BLOCKS SECTION  ************
      DIMENSION RTIR(5),XUPRT(5)
      DIMENSION YR(43),SPYR(43)
      DIMENSION A(5,5),B(5),AB(5),AC(5),AD(5),SPDES(5)
      DIMENSION YSTAR(43),YSTOT(43),RTI(43)
      COMMON/BPLOT/YPLOT(8,43),XPLOT(43)
      COMMON/GENRAL/ AJE(5),AJI(5),CSALFA,DPDX(43),DX,EMU(43),F(5,43),
     1  FS(5,43),H,IFIN,INDE(5),INDI(5),ISTEP,ITEST,IUTRAP,KEX,KIN,KRAD,
     2  N,NEQ,NPH,NP1,NP2,NP3,CM(43),PEI,PR(5),PREF(5,43),PSIE,PSII,
     3  R(43),RHO(43),RVE,RVI,RU(43),SD(5,43),SU(5,43),TAUE,TAUI,U(43),
     4  XD,XU,Y(43),YE,YI
      COMMON/GK3/ALMG,CD,CRIT,C1,C2,C3,IPRINT,PRESS,RTCD,CM
      COMMON/PRMOD/ALF,BET,GAM,DEL,EXPN,EXPM,EXPP,EXPQ,AKAP,ACHI
C  ---------------------------------------------------------------------
      IRUN=1
C---------------------------------------------------------------------
C  1111111111111111111111111111111111111111  PARAMETERS
      UC=.05
      UC=.02
      DO 121 ICD=1,2
      CD=(11.-FLOAT(ICD))/100.
      DO 120 IRTI=1,4
      RTNT=FLOAT(IRTI)*.01
      IPRTIN=1
      ALF=0.
      BET=0.
      GAM=0.
      DEL=0.
      AKAP=0.7
      ACHI=0.7
      EXPN=.5
      EXPM=.5
      EXPP=.5
      EXPQ=.5
      C1=3.
      C2=.1
      C2=.085
      C3=.56
      FRA=.1
      F2LIMI=.01
      F2LIME=.01
      ULIMI=.002
      ULIME=.001
      IOUT=0
      KTH=0
      DXLIM=.01
      IPRINT=0
      IPRINT=1
      IUTRAP=1
      ITEST=0
```

```
C  ------------------------------------------------------------------
C  2222222222222222222222222222222222222222  GRID AND GEOMETRY
      NSTA=10
      NSTA=50
      NSTA=200
      NSTTH=10
      N=19
            NP1=N+1
            NP2=N+2
            NP3=N+3
      NP3D2=NP3/2
            ISTEP=0
            IFIN=0
      ANSTA=NSTA
      ANSTTH=NSTTH
      LASTEP=800
      LASTEP=1200
      LASTEP=2200
      UA=1.
      UB=1.
      F2INI=(RTNT*UA)**2*1.5+1.E-20
      F2INE=(RTNT*UC)**2*1.5+1.E-20
      F2FAC=1.
      XURAT=4.
      XUIN=1./(.3-.2*UC)/(1.+10.*RTNT)
      XUL=0.
      XUP=0.
      THETL=0.
      THETP=0.
      XULAST=1.E9
C     R(1) ADJUSTMENT MADE JUST BEFORE CALL STRIDE(1)
            CSALFA=1.
      KRAD=0
      KIN=2
      KEX=2
      IF(RTNT.EQ.0.)GO TO 42
C   CALCULATE VALUES OF X FOR WHICH PROFILE PRINT-OUT IS REQUIRED
C   KSTAT=NUMBER OF STATIONS AT WHICH PROFILE PRINT-OUT IS REQUIRED
C   RTIR=FREE-STREAM RELATIVE TURBULENCE INTENSITY DIVIDED BY INITIAL VA
      KSTAT=4
      RTIR(1)=0.6
      RTIR(2)=0.4
      RTIR(3)=0.2
      RTIR(4)=.1
      XEXP=2.*C2/CD
      DO 25 K=1,KSTAT
   25 XUPRT(K)=XUIN/RTIR(K)**XEXP
      K=1
C  ------------------------------------------------------------------
C  3333333333333333333333333333333333333333 DEPENDENT VARIABLE SELECTION
C      U(I)=VELOCITY
C      F(1,I)=STAGNATION ENTHALPY
C   ENTHALPY EQUATION NOT SOLVED
C      F(2,I)=KINETIC ENERGY OF TURBULENCE
C      F(3,I)=Z=FREQUENCY
C      FS(1,I)=TEMPERATURE
C      FS(3,I)=DIMENSIONLESS LENGTH
   42 CONTINUE
      NEQ=4
            NPH=NEQ-1
```

```
C  ------------------------------------------------------------
C  4444444444444444444444444444444444444444  MATERIAL CONSTANTS
C                                                  S.I. UNITS
      WMOL=29.
      VIS=0.
      GASCON=8300./WMOL
      CM=1.
      FRA=FRA/CM
      RTCD=SQRT(CD)
      CDDC2=CD/C2
      CRIT=4.
C  ------------------------------------------------------------
C  5555555555555555555555555555555555555555555  INITIAL CONDITIONS
      PRESS=1.E5
      TA=300.
      TB=TA
      TC=TA
      RHA=PRESS/(TA*GASCON)
      R(1)=1.
      YNP3=1.
      Y(N)=YNP3
      PI=3.1416
            OM(1)=0.
      OM(2)=0.
      UM=(UA+UC)/2.
      YR(2)=0.
      YR(NP2)=1.0
      DYR=1./FLOAT(N)
      SPYR(2)=0.
      SPYR(NP2)=0.
      UROP=(UA-UC)/(UA+UC)/PI
      FLOB=UM*RHA*YNP3
      PSII=0.
      PEI=FLOB
      PSIE=PSII+PEI
      DO 50 I=2,N
      YR(I+1)=FLOAT(I-1)*DYR
      SPYR(I+1)=SIN(PI*YR(I+1))
   50 OM(I+1)=OM(I)+DYR+UROP*(SPYR(I+1)-SPYR(I))
      OM(NP2)=1.
      OM(NP3)=1.
      NM=N/4
      RTIM=0.2-.199*UC
      XU=XUIN
      U(1)=UA
      F(1,1)=CP*TA+.5*UA*UA
      F(2,1)=F2INI
      F(3,1)=UA/(C2*XU)
      FS(1,1)=TA
      RHO(1)=RHA
      U(NP3)=UC
      F(1,NP3)=CP*TC+.5*UC*UC
      F(2,NP3)=F2INE
      F(3,NP3)=UC/(C2*XU)+1.E-10
      FS(1,NP3)=TA
      RHO(NP3)=RHA
      DO 55 I=2,NP2
      RHO(I)=RHA
      IF(I.GT.NM.AND.I.LT.(N-NM+3))GO TO 56
      DELU=(UA-UC)*SQRT(1.-SPYR(I)**2)
      U(I)=UM+DELU/2.
      IF(I.GT.(N/2))U(I)=U(I)-DELU
      GO TO 57
```

```
   56 U(I)=UM+(UA-UC)*COS(PI*YR(I))/2.
   57 RTI(I)=RTIM*(1.-COS(2.*PI*YR(I)))/2.+RTNT
      F(2,I)=(RTI(I)*U(I))**2*1.5
      F(2,I)=F(2,I)*F2FAC
      F(3,I)=F(3,1)+OM(I)*(F(3,NP3)-F(3,1))+1.E-10
      F(1,I)=CP*TB+.5*U(I)**2+F(2,I)
      FS(1,I)=TA
   55 CONTINUE
      RTI(1)=RTNT
      RTI(NP3)=RTNT
      F2DIF=(RTIM*(UA-UC))**2
      UDIF=U(1)-U(NP3)
C  ********************  START OF MAIN LOOP  ********************
C  6666666666666666666666666666666666666666  THERMODYNAMIC PROPERTIES
   60 CONTINUE
      IF(ISTEP.GT.0)ITEST=0
C  ----------------------------------------  TEST 1
      IF(ITEST.EQ.0) GO TO 1001
      TEST=1001.
      WRITE(6,107) TEST,R(1), D X, XU
      WRITE(6,101) (U(I),I=1,NP3)
      WRITE(6,101) (F(1,I),I=1,NP3)
      WRITE(6,101) (F(2,I),I=1,NP3)
      WRITE(6,101) (F(3,I),I=1,NP3)
 1001 CONTINUE
      IF(KIN.EQ.3) U(1)=U(2)-.25*(U(2)-U(3))*FLOAT(1-KRAD)
      U1SQ=U(1)**2
      F2MIN=1.E-20
      F2MAX=U1SQ*2.
      F3CON=(U(1)-U(NP3))/(Y(N)*RTCD)
      F3MIN=F3CON*.01
      F3MAX=F3CON*100.
      DO 61 I=1,NP3
      IF(F(2,I).GT.F2MAX) F(2,I)=F2MAX
      IF(F(2,I).LT.F2MIN) F(2,I)=F2MIN
      IF(F(3,I).GT.F3MAX) F(3,I)=F3MAX
      IF(F(3,I).LT.F3MIN) F(3,I)=F3MIN
   61 CONTINUE
C  ----------------------------------------  TEST 2
      IF(ITEST.EQ.0) GO TO 1002
      TEST=1002.
      WRITE(6,100)
     1             TEST,U1SQ,F2MIN,F2MAX,F3MIN,F3MAX
      WRITE(6,101) (FS(1,I),I=1,NP3)
      WRITE(6,101) (RHO(I),I=1,NP3)
 1002 CONTINUE
C-------------------------------------------------  ADJUST R(1)
      R(1)=1.
      IF(KASE.LT.20) R(1)=XU
      IF(KASE.LT.15) R(1)=0.
      IF(KASE.LT.15.AND.KIN.EQ.2) R(1)=SQRT(ABS(2.*PSII/RHO(1)*U(1)))
C  STRIDE 1 STRIDE 1 STRIDE 1 STRIDE 1 STRIDE 1 STRIDE 1
            CALL STRIDE(1)
      IF(IPRTIN.EQ.1)GO TO 102
   59 IPRTIN=0
```

```
C  ------------------------------------------------------------------
C  7777777777777777777777777777777777777  FORWARD STEP
      DX=FRA*Y(NP3D2)
      IF(ISTEP.LT.50)DX=.1*DX
   70           IF(DX.GT.XULAST - XU) DX = XULAST - XU
                IF(DX.GT.0.) GO TO 72
      WRITE(6,700)
700   FORMAT(10X,22HDX IS ZERO OR NEGATIVE)
                IFIN = 1
                GO TO 102
   72       XD=XU+DX
C  ------------------------------------------------------------------
C   88888888888888888888888888888888888888888888888888888888888888888
C   8A8A8A8A8A8A8A8A8A8A8A8A8A8A8A   ADJUST LONGITUDINAL CONDITIONS
C  FREE BOUNDARIES AT BOTH I AND E
      F(2,1)=F2IN1/(XD/XUIN)**CDDC2
      F(2,NP3)=F(2,1)*F2INE/F2IN1
      F(3,1)=U(1)/(C2*XD)
      F(3,NP3)=U(NP3)/(C2*XD)+1.E-10
80    IF(ISTEP.NE.IAX) GO TO 84
      KIN=3
      RMI=0.
      IF(KASE.GE.10.AND.KASE.LT.15) R(1)=0.
      PSII=0.
C  ------------------------------------  PRESSURE GRADIENT
   84 IF(ISTEP.GT.0)GO TO 85
      DP=0.
      DO 86 I=1,NP3
   86 DPDX(I)=0.
   85 PRESS=PRESS+DP
C   8888888888888888888888888888   CALCULATE THETA,DTDX,ETC
      UTH=0.
      AMOM=0.
      DO 88 I=2,NP1
      OMDIF=OM(I+1)-OM(I)
      UM=(U(I)+U(I+1))/2.
      RHM=(RHO(I)+RHO(I+1))/2.
      UTH=UTH+OMDIF*(UM-RU(NP3)/RHM)
   88 AMOM=AMOM+(U(I+1)+U(I))*OMDIF
      AMOM=.5*AMOM*PEI+U(1)*PSII
      THETA=(PEI*(U(1)-UTH)-RU(NP3)*U(1)*Y(NP3))
      THETA=THETA/((RU(1)-RU(NP3))*(U(1)-U(NP3)))
      DTDX1=(THETA-THETL)/(XU-XUL)
      XUL=XU
      THETL=THETA
      IF(FLOAT(ISTEP/NSTTH).NE.FLOAT(ISTEP)/ANSTTH)GO TO 2000
      DTDX10=(THETA-THETP)/(XU-XUP)
      D2TDX2=(DTDX10-DTDXP)/(XU-XUP)
      XUP=XU
      THETP=THETA
      DTDXP=DTDX10
 2000 CONTINUE
C  ------------------------------------  TEST 3
      IF(ITEST.EQ.0) GO TO 1003
      TEST=1003.
      WRITE(6,100) TEST,UBAR,DYNHED,REX,DA,DP,PRESS,RMI,KIN,KEX,
     1             ISTEP,IEND
      WRITE(6,101) (Y(I),I=1,NP3)
      WRITE(6,101) (R(I),I=1,NP3)
      WRITE(6,101) (RU(I),I=1,NP3)
 1003 CONTINUE
```

```
C  ------------------------------------------------------------------
C  99999999999999999999999999999999  TRANSPORT AND SOURCE PROPERTIES
   90        DO 92 I=1,NP3
92    EMU(I)=VIS*FS(1,I)
C  ---------------------------------------  TEST 4
      IF(ITEST.EQ.0) GO TO 1004
      TEST=1004.
      WRITE(6,100) TEST,DX,DP,XU
      WRITE(6,101) (EMU(I),I=1,NP3)
 1004 CONTINUE
C  CALL TURBULENT CONTRIBUTION
C//////////////  TEMPORARILY CANCEL PRINTOUT FROM AUX  ///////
      IPRINT=0
      CALL AUX
      IF(ITEST.EQ.1) WRITE(6,101) (EMU(I),I=1,NP3),XU
C  ------------------------  ENTRAINMENT CONTROL
      IF(KIN.NE.2) GO TO 94
      RMI=R(4)*RHO(4)*F(2,4)/F(3,4)/Y(4)
      RATU=ABS((U(1)-U(4))/UDIF)
      RMI=RMI*(RATU/ULIMI)**1.5
   94 IF(KEX.NE.2) GO TO 96
      RME=-R(N)*RHO(N)*F(2,N)/F(3,N)/(Y(NP3)-Y(N))
      RATU=ABS((U(NP3)-U(N))/UDIF)
      RME=RME*(RATU/ULIME)**1.5
   96 CONTINUE
C  ------------------------------  LIMIT DX
      GRO=RMI-RME
      IF(GRO*DX.GT.PEI*DXLIM) DX=DXLIM*PEI/GRO
      XD=XU+DX
   95        CALL STRIDE(2)
C  ------------------------------------------------------------------
C  10 10 10 10 10 10 10 10 10 10 10 10 10 10 10 10 10 10  OUTPUT
            IF(ISTEP.GT.0) GO TO 106
C  ---------------------------------------------------  HEADINGS
      WRITE(6,2100)UC,RTNT,FRA,N,IRUN
      WRITE(6,109)CD,C1,C2,C3,ALF,BET,GAM,DEL
 2100 FORMAT(1H1,7H UE/UI=,F4.2,3X,6HRTNT0=,F6.4,60X,4HFRA=,F5.3,3X,
     1    2HN=,I3,3X,5HIRUN=,I2)
  109 FORMAT(1H0,5H  CD=,F5.3,3X,3HC1=,F5.3,3X,3HC2=,F5.3,3X,3HC3=,F5.3,
     1    3X,6HPREF2=,F5.2,1H+,F4.1,5HX AAK,3X,6HPREF3=,F5.2,1H+,F4.2,
     2    5HX AAZ/)
  100 FORMAT(1H ,1P8E 11.3, 4I6)
  107 FORMAT(1H1,1P8E 11.3, 4I6)
  106       CONTINUE
C  ---------------------------------------  TEST 5.
      IF(ITEST.EQ.0) GO TO 1005
      TEST=1005.
      WRITE(6,100) TEST,RMI,RME,U(1),U(NP3),XU
 1005 CONTINUE
C  ------------------------------------  STATION VARIABLES  ----------
C  ------------------------------------  TESTS FOR PRINT-OUT  ---------
      IF(RTNT.EQ.0.)GO TO 1020
      IF(XU.GT.XUPRT(K))GO TO 102
 1020 CONTINUE
      IF(ISTEP.EQ.LASTEP.OR.ISTEP.EQ.(LASTEP-NSTA))GO TO 102
      IF(ISTEP.EQ.IAX) GO TO 102
      IF(ITEST.EQ.1) GO TO 102
      IF(IFIN.EQ.1) GO TO 102
      IPRINT=0
```

```
      GO TO 105
  102 IPRINT=1
      IF(ISTEP.GT.0)GO TO 1021
      YHU=Y(NP3)
      WRITE(6,2099)XUIN
 2099 FORMAT(5X,29HINITIAL PROFILES FOR ALL RUNS//5X,5HXUIN=,1PE10.3//
     1    10X,5HOMEGA)
      WRITE(6,101) (OM(I),I=1,NP3)
  101       FORMAT(1H ,5X,1P11E11.3)
      GO TO 1006
C  ---------------------------  CALCULATION OF YHALF VALUES ETC  ----
 1021 HUDIF=.5*ABS(U(NP3)-U(1))
      UMN=.5*(U(1)+U(NP3))
      IF(HUDIF.NE.0.) GO TO 1080
      YHU=.5*Y(NP3)
      GO TO 1090
 1080      DO 1082 I=2,NP2
      DIF=ABS(U(I)-U(1))
      IF(DIF.LT.HUDIF) GO TO 1082
      CALL CUBIC(U,Y,I,A,B,C,D)
      YHU=A+B*UMN+C*UMN**2+D*UMN**3
      CALL CUBIC(Y,U,I,AA,BB,CC,DD)
      UGRAD=BB+2.*CC*YHU+3.*DD*YHU**2
      YMS=(U(NP3)-U(1))/UGRAD
      YMSOT=YMS/THETA
      GO TO 1090
 1082 CONTINUE
 1090 TENTH=.1*ABS(U(NP3)-U(1))
      DO 1091 I=2,NP2
      DIF=ABS(U(I)-U(1))
      IF(DIF.LT.TENTH) GO TO 1091
      T=ABS(U(I)-U(I-1))
      IF(T.NE.0.) T=(DIF-TENTH)/T
      YPT1=Y(I)-T*(Y(I)-Y(I-1))
      GO TO 1092
 1091 CONTINUE
 1092 DO 1093 I=2,NP2
      IDASH=N+4-I
      DIF=ABS(U(IDASH)-U(NP3))
      IF(DIF.LT.TENTH) GO TO 1093
      T=ABS(U(IDASH+1)-U(IDASH))
      IF(T.NE.0.) T=(DIF-TENTH)/T
      YPT9=Y(IDASH)+T*(Y(IDASH+1)-Y(IDASH))
      GO TO 1094
 1093 CONTINUE
 1094 YNM=YPT9-YPT1
      YNMOT=YNM/THETA
      DYNMDX=YNMOT*DTDX10
      YNP2D=Y(NP2)/YNM
 1083 CONTINUE
      YSIOT=(YHU-YPT1)/THETA
      YSEOT=(YPT9-YHU)/THETA
      DO 2009 I=1,NP3
 2009 RTI(I)=SQRT(2.*F(2,I)/3.)/(U(I)+1.E-20)
      DO 2010 I=1,NP3
      YSTAR(I)=Y(I)-YHU
 2010 YSTOT(I)=YSTAR(I)/THETA
 1081 CONTINUE
      ZETA=0.
```

```
      ETA=0.
      DO 2018 I=2,NP1
      ZETA=ZETA+(F(2,I)+F(2,I+1))*(Y(I+1)-Y(I))
      ETA=ETA+(RTI(I)+RTI(I+1))*(Y(I+1)-Y(I))
      IF(I.LT.4.OR.I.GT.N)GO TO 2018
      IF(F(2,I+1).GT.F(2,I))IFM=I+1
      IF(RTI(I+1).GT.RTI(I))ITM=I+1
 2018 CONTINUE
      ZETA=ZETA-(F(2,1)+F(2,NP3))*Y(NP3)
      ETA=ETA-(RTI(1)+RTI(NP3))*Y(NP3)
      ZETOT=ZETA/(F(2,IFM)*2.-F(2,1)-F(2,NP3))/THETA
      ETOT=ETA/(RTI(ITM)*2.-RTI(1)-RTI(NP3))/THETA
10850 WRITE(6,1087)XU,RMI,RME,AMOM,YMSOT,YSIOT,YSEOT,YNMOT,ISTEP
 1087 FORMAT(5X,2HXU,9X,3HRMI,8X,3HRME,7X,4HAMOM,7X,5HYMSOT,6X,5HYSIOT,
     1    6X,5HYSEOT,6X,5HYNMOT,30X,5HISTEP/1H ,1P8E11.3,28X,I4/)
      WRITE(6,2001)THETA,DTDX1,DTDX10,D2TDX2,YNM,DYNMDX
      WRITE(6,2015)ZETA,IFM,ZETOT,ETA,ITM,ETOT,YHU,YMSOT
 2001 FORMAT(5X,6HTHETA=,1PE10.3,3X,6HDTDXI=,E10.3,3X,7HDTDX10=,E10.3,
     1    3X,7HD2TDX2=,E10.3,3X,4HYNM=,E10.3,3X,7HDYNMDX=,E10.3/)
 2015 FORMAT(5X,5HZETA=,1PE10.3,2X,4HIFM=,I2,2X,6HZETOT=,E10.3,
     1    5X,4HETA=,E10.3,2X,4HITM=,I2,2X,5HETOT=,E10.3,5X,4HYHU=,E10.3,
     2    2X,6HYMSOT=,E10.3/)
      IPRINT=0
      IF(ISTEP.EQ.0)GO TO 1006
      IF(ISTEP.EQ.LASTEP.OR.ISTEP.EQ.(LASTEP-NSTA))GO TO 1006
C  ------------------------------  PROFILE VARIABLES  --------------
C  ----------------------------------------  TEST 6
      IF(ITEST.EQ.0) GO TO 1006
      TEST=1006.
      WRITE(6,100) TEST
 1006 CONTINUE
      DO 1070 I=1,NP3
 1070 XPLOT(I)=Y(I)/YHU
      WRITE(6,1076)
1076  FORMAT(10X,22HDIMENSIONLESS DISTANCE)
      WRITE(6,101) R(1),(XPLOT(I),I=2,NP2),Y(NP3)
      WRITE(6,1077)
1077  FORMAT(10X,22HDIMENSIONLESS VELOCITY)
      DO 1072 I=1,NP3
 1072 YPLOT(1,I)=(U(I)-U(NP3))/UDIF
      WRITE(6,101) U(1),(YPLOT(1,I),I=2,NP2),U(NP3)
10782 WRITE(6,1062)
1062  FORMAT(10X,14HF(2,I)/UDIF**2)
      UDIFSQ=UDIF**2
      DO 1073 I=1,NP3
 1073 YPLOT(3,I)=F(2,I)/UDIFSQ
      WRITE(6,101) (YPLOT(3,I),I=1,NP3)
      IF(ISTEP.EQ.0)THETA=Y(NP3)/10.
      F3REF=UDIF/THETA
      WRITE(6,10631)
10631 FORMAT(10X,12HF(3,I)/F3REF)
      DO 1074 I=1,NP3
 1074 YPLOT(4,I)=F(3,I)/F3REF
      WRITE(6,101) (YPLOT(4,I),I=1,NP3)
      WRITE(6,2012)
      WRITE(6,101)(RTI(I),I=1,NP3)
      IF(ISTEP.EQ.0.AND.IPRTIN.EQ.1)GO TO 59
10651 WRITE(6,1079)
 1079 FORMAT(10X,20HDIMENSIONLESS LENGTH)
```

```
      DO 1075 I=1,NP3
      YPLOT(6,I)=YPLOT(6,I)*Y(NP3)/THETA
 1075 YPLOT(5,I)=SQRT(F(2,I))/F(3,I)/Y(NP3)
      WRITE(6,101) F(3,1),(YPLOT(5,I),I=2,NP2),F(3,NP3)
C  YPLOT(6,I), (7,I), (8,I) ASSIGNED IN AUX EXCEPT AS FOLLOWS ...
C   EDGE VALUES OF YPLOT(6)(=ALMG)ARBITRARILY SET AT ZERO
      CON=RHO(1)*(U(1)-U(NP3)+1.E-30)*Y(NP3)
      YPLOT(6,1)=0.
      YPLOT(7,1)=RHO(1)*F(2,1)/(F(3,1)*CON)
      YPLOT(8,1)=0.
      YPLOT(6,NP3)=0.
      YPLOT(7,NP3)=RHO(NP3)*F(2,NP3)/(F(3,NP3)*CON)
      YPLOT(8,NP3)=0.
      WRITE(6,10601) (YPLOT(6,I),I=1,NP3)
10601 FORMAT(10X,4HALMG/(6X,1P11E11.3))
      WRITE(6,10602) (YPLOT(7,I),I=1,NP3)
10602 FORMAT(10X,5HEMUTD/(6X,1P11E11.3))
      WRITE(6,10603) (YPLOT(8,I),I=1,NP3)
10603 FORMAT(10X,4HTAUD/(6X,1P11E11.3))
      PREF(2,1)=PREF(2,2)
      PREF(2,NP3)=PREF(2,NP2)
      PREF(3,1)=PREF(3,2)
      PREF(3,NP3)=PREF(3,NP2)
      WRITE(6,2013)
      WRITE(6,101)(PREF(2,I),I=1,NP3)
 2016 CONTINUE
      WRITE(6,2014)
      WRITE(6,101)(PREF(3,I),I=1,NP3)
 2017 CONTINUE
 2013 FORMAT(10X,5HPREF2)
 2014 FORMAT(10X,5HPREF3)
      WRITE(6,2011)
      WRITE(6,101)(YSTOT(I),I=1,NP3)
      WRITE(6,2002)
 2002 FORMAT(1X//)
 2011 FORMAT(10X,11HYSTAR/THETA)
 2012 FORMAT(10X,18HREL TURB INTENSITY)
      IF(RTNT.EQ.0.)GO TO 105
      IF(K.GE.KSTAT)GO TO 110
      K=K+1
  105 CONTINUE
      IF(ISTEP.EQ.LASTEP-1) IPRINT=1
C  ------------------------------------------------------------------
C  11 11 11 11 11 11 11 11 11 11 11 11 11 11 11 11 11   TERMINATION
            IF(IFIN.EQ.1) GO TO 110
      IF(ISTEP.LT.LASTEP.AND.XU.LT.XULAST) GO TO 112
      GO TO 110
  112 CONTINUE
C  ------------------------------------------------------------------
C  STRIDE 3 STRIDE 3 STRIDE 3 STRIDE 3 STRIDE 3
            CALL STRIDE(3)
            GO TO 60
  110       CONTINUE
C  ------------------------------------------------------------------
C  12 12 12 12 12 12 12 12 12 12 12 12 12 12 12 12   OUTPUT SUMMARY
      IRUN=IRUN+1
  120 CONTINUE
      STOP
      END
```

```
      SUBROUTINE AUX
      COMMON/GENRL/NEQ,NPH,N,NP1,NP2,NP3,   KIN,KEX,KRAD,CSALFA,
     1   ISTEP,ITEST,IFIN,IUTRAP,IPRINT,   OM(100),R(100),Y(100),
     2   U(100),RHO(100),RU(100),EMU(100),   F(3,100),SD(3,100),
     3   SU(3,100),PREF(3,100),PR(3),   RME,RMI,PSIE,PSII,PEI,
     4   YE,YI,PRESS,DPDX(100),XU,XD,DX
      COMMON/GK3KZ/CD,C1,C2,C3,CP,CM,RTCD,CRIT, NI,NE,IMU,URAT,UI,RHOIE
     1   ALF,BET,GAM,DEL,EXPN,EXPM,EXPP,EXPQ,AKAP,ACHI,
     2   XPLOT(100),YPLOT(8,100)
C    EXTRA SOURCE TERM ADDED 21/10/70
C    TO ACCOUNT FOR TURBULENCE GENERATED BY LATERAL PRESSURE WAVES
    7 FORMAT(3X,I3,1P11E11.3)
      F2MC=.1
      F2M1=.2
      F2M2=.2
      DO 20 I=3,NP1
C  EFFECTIVE VISCOSITY
      EMUT=RHO(I)*F(2,I)/F(3,I)
      EMUT=EMUT*CM
      EMU(I)=EMUT
C  VELOCITY-GRADIENT FUNCTIONS
      DUDYM=(U(I)-U(I-1))/(Y(I)-Y(I-1))
      DUDYP=(U(I+1)-U(I))/(Y(I+1)-Y(I))
      DUDY=.5*(DUDYM+DUDYP)
      IF(ITEST.EQ.1)WRITE(6,7)I,EMUT,DUDYM,DUDYP,DUDY
      D2UDY2=2.*(DUDYP-DUDYM)/(Y(I+1)-Y(I-1))
   26 DUDYSQ=DUDY**2
      PREF(2,I)=AKAP
      PREF(3,I)=ACHI
      IF(ALF.EQ.0..AND.BET.EQ.0.)GO TO 29
      AAK=F(2,I)/U(I)**2
      AAR=F(2,I)/F(3,I)
      PREF(2,I)=ALF*AAK**EXPN+BET*AAR**EXPM+AKAP
   29 IF(GAM.EQ.0..AND.DEL.EQ.0.)GO TO 30
      PREF(3,I)=GAM*AAK**EXPP+DEL*AAR**EXPQ+ACHI
   30 CONTINUE
      IF(ITEST.EQ.1)WRITE(6,7)I,AAK,PREF(2,I),AAZ,PREF(3,I)
C    SOURCES
C    SOURCE=SU(J,I)+F(J,I)*SD(J,I)
      RDY=R(I)*.5*(Y(I+1)-Y(I-1))
      SU(2,I)=0.
      SD(2,I)=RDY*(EMUT*DUDYSQ/F(2,I)-CD*RHO(I)*F(3,I))
      SU(3,I)=RDY*(C1*EMUT*D2UDY2**2/F(3,I)+C3*RHO(I)*DUDYSQ)
      SD(3,I)=-RDY*C2*RHO(I)*F(3,I)
      IF(ITEST.EQ.1)WRITE(6,7)I,RDY,SD(2,I),SU(3,I),SD(3,I)
      IF(IPRINT.NE.2)GO TO 20
      CON=RHOIE*UI*(1.-URAT)*(Y(NE)-Y(NI))
      IF(ABS(DUDY).LT.1.E-30)GO TO 27
      ALMG=SQRT(ABS(EMUT/(RHO(I)*DUDY)))/(Y(NE)-Y(NI))
      GO TO 28
   27 ALMG=1.E30
   28 CONTINUE
      EMUTD=EMUT/CON
      TAUD=EMUT*DUDY/RHO(I)/U(1)**2
C---------------------  FOR PLOT ROUTINE
```

```
      YPLOT(6,I)=ALMG
      YPLOT(7,I)=EMUTD
      YPLOT(8,I)=-TAUD
  101 FORMAT(1H ,2X,1P11E11.3)
20    CONTINUE
      NM3=N-3
      DO 23 I=3,7
   23 SU(2,I)=SU(2,8)
      DO 22 I=NM3,NP1
   22 SU(2,I)=SU(2,N-4)
      DELSU=(SU(2,NE+1)-SU(2,NI-1))/(Y(NE+1)-Y(NI-1))
      DO 21 I=NI,NE
   21 SU(2,I)=SU(2,NI-1)+DELSU*(Y(I)-Y(NI-1))
C  ----------------------------------------EDGE REGIONS
C  ----------------------------------------
      DO 40 KIE=1,2
      KI=1
      LI=2
      MI=3
      YB=YI
      IF(KIE.EQ.1)GO TO 41
      KI=N+3
      LI=N+2
      MI=N+1
      YB=YE
   41 F2=.75*F(2,LI)+.25*F(2,MI)
      F3=.75*F(3,LI)+.25*F(3,MI)
      DUDY=(U(MI)-U(LI))/(Y(MI)-Y(LI))/2.
      DUDYSQ=DUDY**2
      D2UDY2=DUDY/YB
      UM=.75*U(LI)+.25*U(MI)
      AAK=F2/UM**2
      AAR=F2/F3
      PREF(2,LI)=ALF*AAK**EXPN+BET*AAR**EXPM+AKAP
      PREF(3,LI)=GAM*AAK**EXPP+DEL*AAR**EXPQ+ACHI
      RDY=YB*(R(KI)+(R(LI)+R(MI))/2.)/2.
      SU(2,LI)=SU(2,MI)
      EMUT=RHO(KI)*F2/F3
      EMUT=EMUT*CM
      EMU(LI)=EMUT
      SD(2,LI)=RDY*(EMUT*DUDYSQ/F2-CD*RHO(KI)*F3)
      SU(3,LI)=RDY*(C1*EMUT*D2UDY2**2/F3+C3*RHO(KI)*DUDYSQ)
      SD(3,LI)=-RDY*C2*RHO(KI)*F3
      IF(IPRINT.NE.2)GO TO 40
      YPLOT(6,LI)=SQRT(ABS(EMUT/(RHO(LI)*DUDY)))/(Y(NE)-Y(NI))
      YPLOT(7,LI)=EMUT/CON
      YPLOT(8,LI)=-EMUT*DUDY/RHO(LI)/UB**2
   40 CONTINUE
  230 IF(IPRINT.EQ.1) WRITE(6,100) SD(2,2),SU(2,2),SD(2,NP2),SU(2,NP2),
     1                SD(3,2),SU(3,2),SD(3,NP2),SU(3,NP2)
  100 FORMAT(1H ,4X,7HSD(2,2),4X,7HSU(2,2),4X,9HSD(2,NP2),2X,
     1       9HSU(2,NP2),2X,7HSD(3,2),4X,7HSU(3,2),4X,9HSD(3,NP2),2X,
     2       9HSU(3,NP2)                                    /(1H ,2X,1P11E11.3))
C  ----------------------------VISCOSITIES FOR INTERVALS
      DO 3 I=2, NP1
      EMU(I)=.5*(EMU(I)+EMU(I+1))
3     EM U(I)=EMU(I)/(Y(I+1)-Y(I))
      RETURN
      END
```

```
      SUBROUTINE STRIDE(ISW)
C  STRIDE SUBROUTINE FOR GENMIX4 VERSION OF PATANKAR-SPALDING PROGRAM
C***********  D.B.SPALDING, IMPERIAL COLLEGE, AUGUST 1969  ***********
      DIMENSION A(5,43),AU(43),B(5,43),BU(43),C(5,43),CU(43),FDIFE(5),
     1  FDIFI(5),GE(5),GI(5),TTPF(5)
      COMMON/GENRAL/ AJE(5),AJI(5),CSALFA,DPDX(43),DX,EMU(43),F(5,43),
     1  FS(5,43),H,IFIN,INDE(5),INDI(5),ISTEP,ITEST,IUTRAP,KEX,KIN,KRAD
     2  N,NEQ,NPH,NP1,NP2,NP3,OM(43),PEI,PR(5),PREF(5,43),PSIE,PSII,
     3  R(43),RHO(43),RME,RMI,RU(43),SD(5,43),SU(5,43),TAUE,TAUI,U(43),
     4  XD,XU,Y(43),YE,YI
C
      GO TO (1000,2000,3000), ISW
C
C************************************  S T R I D E 1  ***************
 1000 IF(ISTEP.GT.0) GO TO 1100
      OM(1)=0.
      OM(2)=0.
      OM(NP2)=1.
      OM(NP3)=1.
      OMI=.5*OM(3)
      OME=.5*(1.-OM(NP1))
      BPE=1.
      BPI=1.
      Y(1)=0.
      IF(KRAD.EQ.1) GO TO 1100
      DO 1001 I=1,NP3
 1001 R(I)=1.
      R25=1.
      RN15=1.
      IF(ITEST.EQ.0) GO TO 9018
      WRITE(6,9010) (R(I),I=1,NP3),R25,RN15
 9010 FORMAT(1H ,1P11E11.3)
 9018 CONTINUE
C----------------------------  CALCULATION OF RHO*U 'S  ---------------
 1100 DO 1101 I=1,NP3
 1101 RU(I)=RHO(I)*U(I)
      RU3=RU(3)
      RUN1=RU(NP1)
      DO 1102 I=2,NP1
      RU(I)=.5*(RU(I)+RU(I+1))
      IF(RU(I).GT.0.)GO TO 1102
      IF(ITEST.EQ.0)WRITE(6,1200)
 1200 FORMAT(3X,25HAN RU IS ZERO OR NEGATIVE)
      ITEST=1
      IFIN=1
1102  CONTINUE
      IF(ITEST.EQ.0) GO TO 9019
      WRITE(6,9010) (RU(I),I=1,NP3),RUN1,RU3,PEI
 9019 CONTINUE
C----------------------------  CALCULATION OF Y 'S AND R 'S  ----------
C  ------------------------------------  Y'S FOR PLANE GEOMETRY
      YI=PEI*OMI/(BPI*RU(2))
      Y(3)=YI+PEI*OM(3)/(RU(2)+RU3)
      Y(2)=2.*YI-Y(3)
      DO 1103 I=4,NP1
 1103 Y(I)=Y(I-1)+PEI*(OM(I)-OM(I-1))/RU(I-1)
      YN15=Y(NP1)+PEI*(1.-OM(NP1))/(RU(NP1)+RUN1)
      YE=PEI*OME/(BPE*RU(NP1))
      Y(NP3)=YN15+YE
```

```
      Y(NP2)=2.*YN15-Y(NP1)
      IF(KRAD.EQ.0) RETURN
C  ----------------------  Y'S AND R'S FOR AXISYMMETRICAL GEOMETRY
      IF(CSALFA.EQ.0.) GO TO 1110
C  ---------------------------------------  CSALFA NE ZERO
      COSD2=.5*CSALFA
      IF(R(1).NE.0.) GO TO 1105
C----------------------------------------  R(1)=0.
      DO 1106 I=2,NP3
      Y(I)=SQRT(ABS(Y(I)/COSD2))
 1106 R(I)=Y(I)*CSALFA
      YI=SQRT(ABS(YI/COSD2))
      YN15=SQRT(ABS(YN15/COSD2))
      GO TO 1107
C  ---------------------------------------  R(1) NE 0.
 1105 R1D2=.5*R(1)
      R1D2SQ=R1D2*R1D2
      DO 1104 I=2,NP3
      Y(I)=Y(I)/(R1D2+SQRT(ABS(R1D2SQ+COSD2*Y(I))))
 1104 R(I)=R(1)+Y(I)*CSALFA
      YI=YI/(R1D2+SQRT(ABS(R1D2SQ+COSD2*YI)))
      YN15=YN15/(R1D2+SQRT(ABS(R1D2SQ+COSD2*YN15)))
 1107 R25=R(1)+YI*CSALFA
      RN15=R(1)+YN15*CSALFA
      YE=Y(NP3)-YN15
      RETURN
C  ---------------------------------------  CSALFA EQ ZERO
 1110 DO 1111 I=2,NP3
      Y(I)=Y(I)/R(1)
 1111 R(I)=R(1)
      YI=YI/R(1)
      YN15=YN15/R(1)
      R25=R(1)
      RN15=R(1)
      YE=Y(NP3)-YN15
      RETURN
C************************************  S T R I D E 2  ***************
C  ------------------------------  PRELIMINARIES FOR COEFFICIENTS
 2000 PX=PEI/DX
           G=RMI-RME
           PD8=.125*PX
      PD4=.25*PX
           PG=PX+G
           PGD8=.125*PG
      PGD4=PGD8+PGD8
           RMID2=.5*RMI
           GD4=.25*G
           BOMP=OM(3)-OM(2)
      PGOMP=PGD4*BOMP
      P4OMP=PD4*BOMP
C  ---------------------------------------  GRID POINT 2
C----------------------------------------  TAUI, BPI, T1
      IF(KIN.NE.1) GO TO 2001
      GO TO 2002
 2001 T1=0.
      IF(KRAD.EQ.0) BPI=.33333+.66667*RU(1)/RU(2)
      IF(KRAD.EQ.1) BPI=(R(1)*(5.*RU(1)+RU(2))+3.*R25*
     1                    (RU(1)+RU(2)))/6./(R(1)+R25)/RU(2)
C  ---------------------  BOUNDARY COEFFICIENTS FOR VELOCITY
```

```
 2002         HLP=RMID2-GD4*(OM(2)+OM(3))
              AHLP=ABS(HLP)
       THLP=HLP+HLP
              TP=EM U(2)
       TTP=TP+AHLP+ABS(TP-AHLP)
       AD=TTP-THLP-T1-PGOMP
       BD=2.*(T1+RMI)
       CD=P4OMP*(3.*U(2)+U(3))-DPDX(2)*(R(1)+R25)*YI
       DU=AD+BD+PX*BOMP
       AU(2)=AD/DU
       BU(2)=BD/DU
       CU(2)=CD/DU
C  ------------------------------  BOUNDARY COEFFICIENTS FOR F'S
       IF(NEQ.EQ.1) GO TO 2304
       DO 2300 J=2,NPH
       TPF2=TP/PREF(J,2)
       TTPF(J)=TPF2+AHLP+ABS(TPF2-AHLP)
       IF(KIN.NE.1) GO TO 2301
              IF(INDI(J).EQ.2) GO TO 2303
       AJI(J)=GI(J)*(F(J,1)-.5*(F(J,2)+F(J,3))-FDIFI(J))
       GO TO 2302
 2301  T1F=0.
       FDIFI(J)=0.
C  ---------------------------------------  COEFFICIENTS
 2302  ADF=TTPF(J)-THLP-T1F-PGOMP+.5*SD(J,2)
       BDF=2.*(T1F+RMI)
       DF=ADF+BDF+PX*BOMP-2.*SD(J,2)
       T=-T1F*FDIFI(J)
       GO TO 2305
 2303  ADF=TTPF(J)-THLP-PGOMP+.5*SD(J,2)
       BDF=0.
       DF=ADF+PX*BOMP-2.*SD(J,2)+RMI*2.
       T=RMI*F(J,1)+AJI(J)*R(1)
 2305  TT=3.*F(J,2)+F(J,3)
       CDF=P4OMP*TT+2.*(T+SU(J,2))
       A(J,2)=ADF/DF
       B(J,2)=BDF/DF
 2300  C(J,2)=CDF/DF
C  ---------------------------------------  GRID POINT NP2
C----------------------------------------  TAUE, BPE, TNP3
 2304  IF(KEX.NE.1) GO TO 2003
       GO TO 2310
 2003  TNP3=0.
       IF(KRAD.EQ.0) BPE=.33333+.66667*RU(NP3)/RU(NP1)
       IF(KRAD.EQ.1) BPE=(R(NP3)*(5.*RU(NP3)+RU(NP1))+3.*RN15*
      1              (RU(NP3)+RU(NP1)))/6./(R(NP3)+ RN15)/RU(NP1)
C  --------------------  BOUNDARY COEFFICIENTS FOR VELOCITY
 2310  BOMM=OM(NP2)-OM(NP1)
       HLM=RMID2-GD4*(OM(NP1)+OM(NP2))
       AHLM=ABS(HLM)
       THLM=HLM+HLM
       TM=EM U(NP1)
       TTM=TM+AHLM+ABS(TM-AHLM)
       PGOMM=PGD4*BOMM
       P4OMM=PD4*BOMM
       AD=2.*(TNP3-RME)
       BD=TTM+THLM-TNP3-PGOMM
       CD=P4OMM*(3.*U(NP2)+U(NP1))-DPDX(NP2)*(RN15+R(NP3))*YE
       DU=AD+BD+PX*BOMM
```

```
      AU(NP2)=AD/DU
      BU(NP2)=BD/DU
      CU(NP2)=CD/DU
      IF(NEQ.EQ.1) RETURN
C     ----------------------  BOUNDARY COEFFICIENTS FOR F'S
      DO 2320 J=2,NPH
      TMF=TM/PREF(J,NP1)
      TTMF=TMF+AHLM+ABS(TMF-AHLM)
      IF(KEX.NE.1) GO TO 2311
      IF(INDE(J).EQ.2) GO TO 2313
      AJE(J)=GE(J)*(.5*(F(J,NP2)+F(J,NP1))+FDIFE(J)-F(J,NP3))
      GO TO 2312
 2311 TNP3F=0.
      FDIFE(J)=0.
C     ---------------------------------------  COEFFICIENTS
 2312 ADF=2.*(TNP3F-RME)
      BDF=TTMF+THLM-TNP3F-PGOMM+.5*SD(J,NP2)
      DF=ADF+BDF+PX*BOMM-2.*SD(J,NP2)
      T=-TNP3F*FDIFE(J)
      GO TO 2315
 2313 ADF=0.
      BDF=TTMF+THLM-PGOMM+.5*SD(J,NP2)
      DF=BDF+PX*BOMM-2.*SD(J,NP2)-RME*2.
      T=-RME*F(J,NP3)-AJE(J)*R(NP3)
 2315 TT=3.*F(J,NP2)+F(J,NP1)
      CDF=P4OMM*TT+2.*(T+SU(J,NP2))
      A(J,NP2)=ADF/DF
      B(J,NP2)=BDF/DF
 2320 C(J,NP2)=CDF/DF
      RETURN
C*************************************  S T R I D E 3  ***************
 3000 DO 3005 I=3,NP1
           BOMM=BOMP
           BOMP=OM(I+1)-OM(I)
           BOM=BOMM+BOMP
           BOMT3=BOM*3.
           PGOMM=PGOMP
      PGOMP=PGD4*BOMP
      PBOM=PX*BOM
      THLM=THLP
           HLP=RMID2-GD4*(OM(I+1)+OM(I))
      THLP=HLP+HLP
           AHLP=ABS(HLP)
      TTM=TTP
           TP=EM U(I)
      TTP=TP+AHLP+ABS(TP-AHLP)
      AD=TTP-THLP-PGOMP
      BD=TTM+THLM-PGOMM
      CD=PD4*(BOMT3*U(I)+BOMP* U(I+1)+BOMM*U(I-1))-
     1      DPDX(I)*R(I)*(Y(I+1)-Y(I-1))
           DU=AD+BD+PBOM
           AU(I)=AD/DU
           BU(I)=BD/DU
           CU(I)=CD/DU
C     ---------------------------------------  START OF J LOOP
           IF(NEQ.EQ.1) GO TO 3005
      DO 3004 J=2,NPH
 3002 TTMF=TTPF(J)
 3003 TPF=EM U(I)/PREF(J,I)
```

```
      TTPF(J)=TPF+AHLP+ABS(TPF-AHLP)
      AD=TTPF(J)-THLP-PGOMP
      BD=TTMF+THLM-PGOMM
      CD=PD4*(BOMT3*F(J,I)+BOMP*F(J,I+1)+BOMM*F(J,I-1))
      CD=CD+2.*SU(J,I)
      DF=AD+BD+PBOM-2.*SD(J,I)
            A(J,I)=AD/DF
            B(J,I)=BD/DF
 3004       C(J,I)=CD/DF
 3005 CONTINUE
      IF(ITEST.EQ.0) GO TO 9013
      WRITE(6,9001) (AU(I),I=2,NP2)
      WRITE(6,9002) (BU(I),I=2,NP2)
      WRITE(6,9003) (CU(I),I=2,NP2)
 9001 FORMAT(7H AU(I) ,1P11E11.3)
 9002 FORMAT(7H BU(I) ,1P11E11.3)
 9003 FORMAT(7H CU(I) ,1P11E11.3)
      IF(NEQ.EQ.1) GO TO 9013
      DO 9000 J=2,NPH
      WRITE(6,9004) (A(J,I),I=2,NP2)
      WRITE(6,9005) (B(J,I),I=2,NP2)
 9000 WRITE(6,9006) (C(J,I),I=2,NP2)
 9004 FORMAT(8H A(J,I) ,1P11E11.3)
 9005 FORMAT(8H B(J,I) ,1P11E11.3)
 9006 FORMAT(8H C(J,I) ,1P11E11.3)
 9013 CONTINUE
C-----------------------------                    -----------------
      IF(KIN.EQ.2.AND.RU(1).NE.0.) U(1)=U(1)-DPDX(1)*DX/RU(1)
      IF(KEX.EQ.2.AND.RU(NP3).NE.0.) U(NP3)=U(NP3)-DPDX(NP3)*DX/RU(NP3)
C-----------------------------   SOLVE FOR DOWNSTREAM U 'S  -------------
 3047  BU(2)=BU(2)*U(1)+CU(2)
      DO 3048 I=3,NP2
      T=1./(1.-BU(I)*AU(I-1))
      AU(I)=AU(I)*T
 3048 BU(I)=(BU(I)*BU(I-1)+CU(I))*T
      DO 3050 IDASH=2,NP2
      I=N+4-IDASH
      U(I)=AU(I)*U(I+1)+BU(I)
C  TEST FOR NEGATIVE VELOCITY
C      IUTRAP=0 NO ACTION,  =1 SET U'S TO ZERO,  =2 PRINT AND STOP
      IF(IUTRAP.EQ.0) GO TO 3050
      IF(I.EQ.2.OR.I.EQ.NP2.OR.U(I).GE.0.) GO TO 3050
      IF(IUTRAP.EQ.1) GO TO 3051
      IFIN=1
      ITEST=1
      WRITE(6,3120)
 3120  FORMAT(10X,33HAT LEAST ONE VELOCITY IS NEGATIVE)
      RETURN
 3051 U(I)=1.E-30
 3050 CONTINUE
      IF(KIN.EQ.3)U(1)=.5*(U(2)+U(3))
      IF(KEX.EQ.3)U(NP3)=.5*(U(NP1)+U(NP2))
   72 IF(NEQ.EQ.1) GO TO 3060
      DO 3320 J=2,NPH
C-----------------------------   SOLVE FOR DOWNSTREAM F 'S  -------------
      B(J,2)=B(J,2)*F(J,1)+C(J,2)
      DO 3148 I=3,NP2
      T=1./(1.-B(J,I)*A(J,I-1))
      A(J,I)=A(J,I)*T
```

```
 3148 B(J,I)=(B(J,I)*B(J,I-1)+C(J,I))*T
      DO 3150 IDASH=2,NP2
      I=N+4-IDASH
 3150 F(J,I)=A(J,I)*F(J,I+1)+B(J,I)
C--------------------------  ADJUST F(J,1) AND F(J,NP3)  ------------
      GO TO (3210,3220,3230),KIN
 3210 IF(INDI(J).EQ.2) F(J,1)=FDIFI(J)+.5*(F(J,2)+F(J,3))+AJI(J)/GI(J)
      GO TO 3220
3230  F(J,1)=.5*(F(J,2)+F(J,3))
 3220 GO TO (3310,3320,3330),KEX
 3310 IF(INDE(J).EQ.2) F(J,NP3)=FDIFE(J)+.5*(F(J,NP2)+
     1                                F(J,NP1))-AJE(J)/GE(J)
      GO TO 3320
3330  F(J,NP3)=.5*(F(J,NP1)+F(J,NP2))
 3320 CONTINUE
3060  XU=XD
      PSII=PSII-RMI*DX
      PSIE=PSIE-RME*DX
      PEI=PSIE-PSII
      ISTEP=ISTEP+1
      RETURN
      END
```

LISTING OF LAYER-3 PROGRAMME (MAIN SECTION ONLY)

```
C************************  G E N K L 3  ************************

C   2/4/70  CHANGE TO KOLMOGOROV (K-Z) MODEL
C                                                    S.I.UNITS
C  000000000000000000000C0000000000000000000000000  PRELIMINARIES
C  ************  ****  COMMON  BLOCKS SECTION  ************
      DIMENSION IP1(4),IP2(4),RTI(100),YSTAR(100),YSTOT(100),XUPRT(10)
      COMMON/GENRL/NEQ,NPH,N,NP1,NP2,NP3,    KIN,KEX,KRAD,CSALFA,
     1    ISTEP,ITEST,IFIN,IUTRAP,IPRINT,    OM(100),R(100),Y(100),
     2    U(100),RHO(100),RU(100),EMU(100),    F(3,100),SD(3,100),
     3    SU(3,100),PREF(3,100),PR(3),    RME,RMI,PSIE,PSII,PEI,
     4    YE,YI,PRESS,DPDX(100),XU,XD,DX
      COMMON/GK3KZ/CD,C1,C2,C3,CP,CM,RTCD,CRIT,  NI,NE,IMU,URAT,UI,RHOIE
     1    ALF,BET,GAM,DEL,EXPN,EXPM,EXPP,EXPQ,AKAP,ACHI,
     2    XPLOT(100),YPLOT(8,100)
C   PREDICTION OF DEVELOPMENT OF THREE PLANE PARALLEL MIXING LAYERS
C   FORMED WHEN TWO FLUID STREAMS ISSUE INTO STATIONARY ATMOSPHERE
C   UNIFORM FLUID TEMPERATURE AND PRESSURE
C   URAT=RATIO OF STREAM VELOCITIES,UI/UE
C  ------------------------------------------------------------------
C  111111111111111111111111111111111111111111  PARAMETERS
      DATA NEQ,KIN,KEX,KRAD,CSALFA/4,2,2,0,1.0/,
     1    ITEST,IPRINT,IUTRAP,IFIN/0,0,0,0/,
     2    R(1),XUL,XUP,THETL,THETP,NSTTH/1.,0.,0.,0.,0.,10/,
     3    DXLIM,ULIMI,DX,FRA/.01,.005,2.E-06,.05/,
     4    NSTA,IRUN,KSTAT,LASTEP/50,1,4,1200/,
     5    YC,YTE,F3FAC,XUIN,CRIT,ELFAC/.10,.05,.35,.02,4.,2./,
     6    OM(1),OM(2),OM(NP3),EXPN,EXPM,EXPP,EXPQ/0.,0.,1.,.5,.5,.5,.5,/
      DO 121 IURAT=40,80,20
      URAT=FLOAT(IURAT)/100.
      DO 120 IRTI=7,110,103
      RTNT=FLOAT(IRTI)/1000.
      CM=1.0
      CD=.09
      C1=3.
      C2=.085
      C3=0.59
      UI=35.
      UA=.01*UI
      UC=UA
      WTE=FLOAT(IP2(3)-IP1(2))*YC/FLOAT(N)
      F2INI=(RTNT*UI)**2*1.5
      IF(RTNT.GT..02)F3FAC=1./70.
      XUINI=F3FAC/C2-.025
      F3INI=UI/(XUINI*C2)
      F3INE=F3INI*URAT
      F2A=(UA*.01)**2*1.5
      F3A=UA/(C2*XUIN)
      F2C=(UC*.01)**2*1.5
      F3C=UC/(C2*XUIN)
      URTE=URAT*0.9
      DO 5 K=1,KSTAT
    5 XUPRT(K)=XUINI+.05*FLOAT(K)
```

```
C  ------------------------------------------------------------------
C  222222222222222222222222222222222222222  GRID AND GEOMETRY
           NP1=N+1
           NP2=N+2
           NP3=N+3
      NP3D2=NP3/2
      ND2=N/2
      ULIME=ULIMI
      ULI=UI/100.
      ULE=ULI*URAT
      ANSTA=NSTA
      ANSTTH=NSTTH
      XULAST=XUINI+0.25
C  ------------------------------------------------------------------
C  333333333333333333333333333333333333 DEPENDENT VARIABLE SELECTION
C       U(I)=VELOCITY
C     F(1,I)=STAGNATION ENTHALPY
C   ENTHALPY EQUATION NOT SOLVED
C    IN STRIDE(3),COEFFICIENTS NOT CALCULATED WHEN J=1
C      F(2,I)=KINETIC ENERGY OF TURBULENCE
C      F(3,I)=Z=FREQUENCY
           NPH=NEQ-1
C  ------------------------------------------------------------------
C  444444444444444444444444444444444444444  MATERIAL CONSTANTS
C                                                S.I. UNITS
      ALF=5.0
      BET=0.1
      GAM=5.0
      DEL=0.1
      AKAP=0.1
      ACHI=0.1
C    PRESS=1.0E05
C    TIE=300.
      RHOIE=1.17
      VIS=0.
      PR(1)=0.
      PR(2)=0.
      PR(3)=0.
      RTCD=SQRT(CD)
      CDDC2=CD/C2
C  ------------------------------------------------------------------
C  555555555555555555555555555555555555555  INITIAL CONDITIONS
           ISTEP=0
      XU=XUINI
      XD1F=XUINI-XUIN
      DATA N,(IP1(KP),IP2(KP),KP=1,4)/96,2,12,46,50,50,54,88,98/
      IOLI=IP2(1)
      IOLE=IP1(4)
      NI=IP1(2)
      NE=IP2(3)
      NEM1=NE-1
      NIF=NI
      NEF=NE
      IMU=IP1(3)
      WYR=1./FLOAT(IP2(3)-IP1(2))
      DO 500 I=3,NP1
      IF(I.GT.IP1(2))GO TO 501
      U(I)=UI
      F(3,I)=F3INI
      GO TO 502
```

```
  501 IF(I.GE.IP2(3))GO TO 503
      U(I)=UI*(1.+(URAT-1.)*FLOAT(I-IP1(2))*WYR)
      F(3,I)=F3INI*U(I)/UI
      GO TO 502
  503 U(I)=UI*URAT
      F(3,I)=F3INE
  502 F(2,I)=(U(I)*RTNT)**2*1.5
  500 CONTINUE
      WRITE(6,4999)NI,NE,IOLI,IOLE,IMU
      WRITE(6,4998)(U(I),I=NI,NE),(F(2,I),I=NI,NE),(F(3,I),I=NI,NE)
 4999 FORMAT(5X,10I5)
 4998 FORMAT(5X,1P10E11.3/6X,1P10E11.3/7X,1P10E11.3)
      DO 510 KP=1,4
      GO TO (511,512,513,514),KP
  511 UR1=UA/UI
      UR2=1.
      FFAC=1.
      GO TO 515
  512 UR1=1.
      UR2=URTE
      FFAC=(1.+URAT-2.*URTE)/(1.-URTE)/2.
      GO TO 515
  513 UR1=URTE
      UR2=URAT
      FFAC=2.*(1.-URTE)/(1.+URAT-2.*URTE)
      GO TO 515
  514 UR1=URAT
      UR2=UC/UI
      FFAC=1.
  515 UM=UI*(UR1+UR2)/2.
      UF=(UR2-UR1)*UI/2.
      DYRDPI=FLOAT(IP2(KP)-IP1(KP))/3.1416
      DUDYF=FLOAT(N)*UF/DYRDPI/YC
      YRM=FLOAT(IP1(KP)+IP2(KP))/2.
      IL1=IP1(KP)
      IL2=IP2(KP)
      EL=.07*FLOAT(IP2(KP)-IP1(KP))*YC/FLOAT(N)
      IF(KP.EQ.2.OR.KP.EQ.3)EL=.07*WTE/ELFAC
      DO 516 I=IL1,IL2
      PHI=(FLOAT(I)-YRM)/DYRDPI
      U(I)=UM+SIN(PHI)*UF
      F3ML=DUDYF*COS(PHI)/RTCD*FFAC
      F2ML=(F3ML*EL)**2*RTCD
      F(2,I)=F(2,I)+F2ML
  516 F(3,I)=F(3,I)+ABS(F3ML)
  510 CONTINUE
      WRITE(6,4998)(U(I),I=NI,NE),(F(2,I),I=NI,NE),(F(3,I),I=NI,NE)
      IMUP1=IMU+1
      IMUM1=IMU-1
      DF2DY=(F(2,IMU+2)-F(2,IMU-2))/4.
      DF3DY=(F(3,IMU+2)-F(3,IMU-2))/4.
      DO 517 I=IMUM1,IMUP1
      F(2,I)=F(2,IMU-2)+DF2DY*FLOAT(I+2-IMU)
  517 F(3,I)=F(3,IMU-2)+DF3DY*FLOAT(I+2-IMU)
      WRITE(6,4998)(U(I),I=NI,NE),(F(2,I),I=NI,NE),(F(3,I),I=NI,NE)
      DO 530 I=3,NP2
      OM(I)=OM(I-1)+(U(I-1)+U(I))/2.
      IF(I.EQ.NP3D2)OMTE=OM(I)
      IF(I.EQ.NP2)OMC=OM(I)
  530 CONTINUE
```

```
      DO 531 I=3,NP2
  531 OM(I)=OM(I)/OMC
      FLOI=RHOIE*OMTE*YTE/FLOAT(ND2)
      FLOE=RHOIE*(OMC-OMTE)*(YC-YTE)/FLOAT(ND2)
      FLOTOT=FLOI+FLOE
      PSII=0.
      PEI=FLOTOT
      PSIE=PSII+PEI
      U(1)=UA
      F(2,1)=F2A
      F(2,2)=F2A
      F(3,1)=F3A
      F(3,2)=F3A
      U(NP3)=UC
      F(2,NP2)=F2C
      F(2,NP3)=F2C
      F(3,NP2)=F3C
      F(3,NP3)=F3C
      DO 540 I=1,NP3
  540 RHO(I)=RHOIE
      F2DIF=F2INI*(1.+URAT**2)
      F2MAXI=UI**2
      F2MAXE=(UI*URAT)**2
      F2MINI=F2MAXI*1.E-20
      F2MINE=F2MAXE*1.E-20
      F3CON=UI*(1.-URAT)/(YC*RTCD)
      F3MIN=F3CON*.01
      F3MAX=F3CON*100.
      F3MAXI=F3MAX
      F3MAXE=F3MAX
      F3MINI=F3MIN
      F3MINE=F3MIN
C  6666666666666666666666666666666666666666  START OF MAIN LOOP
   60 CONTINUE
C   LIMITATION OF EXCESSIVE F2 AND F3 VALUES
C   ---------------------------------------  TEST 1
      IF(ITEST.EQ.0) GO TO 1001
      WRITE(6,1)ISTEP
    1 FORMAT(1H1,6HISTEP=,I5)
      TEST=1001.
      WRITE(6,100)TEST,R(1),DX,XU
      WRITE(6,101) (U(I),I=1,NP3)
      WRITE(6,101) (F(2,I),I=1,NP3)
      WRITE(6,101) (F(3,I),I=1,NP3)
 1001 CONTINUE
      F2MXI=F2INI*(XUINI/XU)**CDDC2*10.
      F2MNI=F2MXI/100.
      F2MXE=F2MXI*URAT**2
      F2MNE=F2MXE/100.
      F3MXI=UI/(XU*C2)*10.
      F3MNI=F3MXI/100.
      F3MXE=F3MXI
      F3MNE=F3MXE/100.
      DO 61 I=3,NP1
      F2MAX=UI**2/10.
      F2LIM=5.
      F3LIM=5.
```

```
      F2ULM=(F(2,I-1)+F(2,I+1))*F2LIM
      F2LLM=F2ULM/F2LIM**2
      F3ULM=(F(3,I-1)+F(3,I+1))*F3LIM
      F3LLM=F3ULM/F3LIM**2
      IF(F(2,I).GT.F2ULM)F(2,I)=F2ULM
      IF(F(2,I).GT.F2MAX)F(2,I)=F2MAX
      IF(F(2,I).LT.F2LLM)F(2,I)=F2LLM
      IF(F(3,I).GT.F3ULM)F(3,I)=F3ULM
      IF(F(3,I).GT.F3MAX)F(3,I)=F3MAX
      IF(F(3,I).LT.F3LLM)F(3,I)=F3LLM
   61 CONTINUE
       IF(ISTEP.GT.0)GO TO 4997
      WRITE(6,4998)(U(I),I=NI,NE),(F(2,I),I=NI,NE),(F(3,I),I=NI,NE)
 4997 CONTINUE
C  ------------------------------------------  TEST 2
      IF(ITEST.EQ.0) GO TO 1002
      TEST=1002.
      WRITE(6,100)TEST,F2MAXE,F3CON,F2MXI,F3MXI
      WRITE(6,101) (RHO(I),I=1,NP3)
 1002 CONTINUE
C-------------------------------------------------  ADJUST R(1)
C  STRIDE 1 STRIDE 1 STRIDE 1 STRIDE 1 STRIDE 1 STRIDE 1
            CALL STRIDE(1)
C  ------------------------------------------------------------------------
C  77777777777777777777777777777777777  FORWARD STEP
      IF(ISTEP.LT.100)GO TO 72
      DX=FRA*(Y(NE)-Y(NI))
   72       XD=XU+DX
C  ------------------------------------------------------------------------
C  88888888888888888888888888888888  ADJUST LONGITUDINAL CONDITIONS
C   BOTH EDGES OF FLOW-FIELD ARE FREE BOUNDARIES
      F(2,1)=F2A*(XUIN/(XD-XDIF))**CDDC2
      F(2,NP3)=F(2,1)*F2C/F2A
      F(3,1)=UA/(C2*(XD-XDIF))
      F(3,NP3)=F(3,1)*UC/UA
   84 IF(ISTEP.GT.0)GO TO 85
      DO 86 I=1,NP3
   86 DPDX(I)=0.
   85 CONTINUE
      UDIF=U(NI)-U(NE)
      IF(ISTEP.LT.20)GO TO 2000
      ULIMNI=UI/FLOAT(ISTEP+100)
      IF(ULIMNI.LT.(UI/500.))ULIMNI=UI/500.
      ULIMNE=ULIMNI*URAT
      NEP=NE
C   LOCATE BOUNDARIES OF VELOCITY MIXING LAYERS
      DO 81 I=1,NP3D2
      INI=IMU-I
      IF((U(INI)-U(INI+1)).GT.ULIMNI)GO TO 81
      NI=INI
      GO TO 82
   81 CONTINUE
   82 DO 831 I=1,NP3D2
      INE=IMU+I
      IF((U(INE)-U(INE+1)).GT.ULIMNE)GO TO 831
      NE=INE+1
      GO TO 832
  831 CONTINUE
```

```
  832 IF(NE.LT.(NEP+4))GO TO 83
      DUDYM=-10000.
      DO 833 I=NEP,N
      DUDY=(U(I)-U(I-1))/(Y(I)-Y(I-1))
      IF(DUDY.LE.DUDYM)GO TO 834
      DUDYM=DUDY
      GO TO 833
  834 NE=I-1
      GO TO 83
  833 CONTINUE
   83 CONTINUE
      ILO2=IOLI/2
      DO 835 I=ILO2,NI
      IF((U(I+1)-U(I)).GT.ULI)GO TO 835
      IOLI=I+1
      GO TO 836
  835 CONTINUE
  836 ILO2=(NP3-IOLE)/2
      DO 837 I=ILO2,NP3D2
      NOL=NP2-I
      IF((U(NOL-1)-U(NOL)).GT.ULE)GO TO 837
      IOLE=NOL-1
      GO TO 838
  837 CONTINUE
  838 IF(IOLE.LT.NE)IOLE=NE

C    CALCULATE MOMENTUM THICKNESS
      UTH=0.
      AMOM=0.
      NEM1=NE-1
      DO 88 I=NI,NEM1
      OMDIF=OM(I+1)-OM(I)
      UM=(U(I)+U(I+1))/2.
   88 UTH=UTH+OMDIF*UM
      UEI=U(NE)*U(NI)*(Y(NE)-Y(NI))*RHOIE/PEI
      DOMUN=(OM(NE)-OM(NI))*(U(NE)+U(NI))
      THETA=PEI*(DOMUN-UTH-UEI)/RHOIE/(U(NI)-U(NE))**2
      DO 89 I=2,NP1
      OMDIF=OM(I+1)-OM(I)
   89 AMOM=AMOM+(U(I+1)+U(I))*OMDIF
      AMOM=.5*AMOM*PEI+U(1)*PSII
      DTDXI=(THETA-THETL)/(XU-XUL)
      XUL=XU
      THETL=THETA
      IF(FLOAT(ISTEP/NSTTH).NE.FLOAT(ISTEP)/ANSTTH)GO TO 2000
      DTDX10=(THETA-THETP)/(XU-XUP)
      D2TDX2=(DTDX10-DTDXP)/(XU-XUP)
      WRITE(6,2099)ISTEP,NI,NE,IMU,XU,THETA,DTDX1,DTDX10,D2TDX2,
     I    Y(NI),Y(NE)
 2099 FORMAT(3X,4I4,1P8E12.3)
      XUP=XU
      THETP=THETA
      DTDXP=DTDX10
 2000 CONTINUE
C  ---------------------------------------  TEST 3
      IF(ITEST.EQ.0) GO TO 1003
      TEST=1003.
      WRITE(6,101) (Y(I),I=1,NP3)
      WRITE(6,101) (RU(I),I=1,NP3)
 1003 CONTINUE
C  ------------------------------------------------------------
```

```
C  99999999999999999999999999999999  TRANSPORT AND SOURCE PROPERTIES
C  ------------------------------  VARIABLE TRANSPORT PROPERTIES
C   LAMINAR VISCOSITY SEQUENCE DELETED
C   CALCULATE TURBULENT CONTRIBITION
C   IPRNT=2 ENSURES CALCULATION OF ALMG,EMUTD,AND TAUD IN AUX
      IF(XU.GT.XUPRT(K))IPRINT=2
      CALL AUX
      IF(ITEST.EQ.1) WRITE(6,101) (EMU(I),I=1,NP3),XU
C  ------------------------  ENTRAINMENT CONTROL
      RMI=R(4)*RHO(4)*F(2,4)/F(3,4)/Y(4)
      RATU=ABS((U(1)-U(4))/UDIF)
      RMI=RMI*(RATU/ULIMI)**1.5
      RME=-R(N)*RHO(N)*F(2,N)/F(3,N)/(Y(NP3)-Y(N))
      RATU=ABS((U(NP3)-U(N))/UDIF)
      RME=RME*(RATU/ULIME)**1.5
C  ------------------------------  LIMIT DX
      GRO=RMI-RME
      IF(GRO*DX.GT.PEI*DXLIM) DX=DXLIM*PEI/GRO
      XD=XU+DX
C  STRIDE 2 STRIDE 2 STRIDE 2 STRIDE 2 STRIDE 2.......
   95       CALL STRIDE(2)
C  ------------------------------------------------------------------
C  10 10 10 10 10 10 10 10 10 10 10 10 10 10 10 10 10 10  OUTPUT
           IF(ISTEP.GT.0) GO TO 106
C  ------------------------------------------------  HEADINGS
      WRITE(6,109)IRUN,CD,C1,C2,C3,ALF,EXPN,BET,EXPM,AKAP,GAM,EXPP,DEL
     2   EXPQ,ACHI
      WRITE(6,2100)UI,URAT,RTNT,N,FRA
  109 FORMAT(1H1,2X,3HRUN,I2,5X,3HCD=,F5.3,3X,3HC1=,F5.3,3X,3HC2=,F5.3
     1   3X,3HC3=,F5.3//3X,6HPR(K)=,F5.2,7H*A(K)**,F4.2,1H+,F5.2,
     2   7H*A(R)**,F4.2,1H+,F4.2,3X,6HPR(Z)=,F5.2,7H*A(K)**,F4.2,1H+,
     3   F5.2,7H*A(R)**,F4.2,1H+,F4.2//)
 2100 FORMAT(5X,3HUI=,F4.1,3X,6HUE/UI=,F4.2,3X,6HRTNTO=,F5.3,10X,
     1   2HN=,I3,3X,4HFRA=,F5.3/)
  100 FORMAT(1H ,1P8E 11.3, 416)
  107 FORMAT(1H1,1P8E 11.3, 416)
      WRITE(6,101) (OM(I),I=1,NP3)
  101      FORMAT(1H ,5X,1P11E11.3)
  106       CONTINUE
C  ------------------------------------  TEST 5.
      IF(ITEST.EQ.0) GO TO 1005
      TEST=1005.
      WRITE(6,100) TEST,RMI,RME,U(1),U(NP3),XU
 1005 CONTINUE
C  ----------------------------------  STATION VARIABLES  ---------
C  ----------------------------------  TESTS FOR PRINT-OUT  --------
      IF(ISTEP.EQ.0)GO TO 102
      IF(XU.GT.XUPRT(K))GO TO 102
      IF(ITEST.EQ.1) GO TO 102
      IF(IFIN.EQ.1) GO TO 102
      GO TO 105
  102 IPRINT=1
      IF(ISTEP.NE.0)GO TO 1021
      YNM=Y(NP3)
      YHU=Y(IMU)
      THETA=(Y(NE)-Y(NI))/8.
      GO TO 1081
```

```
C   CALCULATE REPRESENTATIVE TRANSVERSE DIMENSIONS YNOM,YMS
 1021 HUDIF=UDIF/2.
 1080 DO 1082 I=NI,NE
      DIF=ABS(U(I)-U(NI))
      IF(DIF.LT.HUDIF) GO TO 1082
      T=ABS(U(I)-U(I-1))
      IF(T.NE.0.) T=(DIF-HUDIF)/T
      YHU=Y(I)-T*(Y(I)-Y(I-1))
      YMS=(Y(I-1)-Y(I))*(U(NI)-U(NE))/(U(I-1)-U(I))
      IF((YHU-Y(I-1)).LT..25*(Y(I)-Y(I-1)))YMS=(Y(I)-Y(I-2))*
     1   (U(NI)-U(NE))/(U(I-2)-U(I))
      IF((Y(I)-YHU).LT..25*(Y(I)-Y(I-1)))YMS=(Y(I+1)-Y(I-1))*
     1   (U(NI)-U(NE))/(U(I-1)-U(I+1))
      YMSOT=YMS/THETA
      IMU=I
      GO TO 1090
 1082 CONTINUE
 1090 TENTH=.1*ABS(U(NI)-U(NE))
      DO 1091 I=NI,NE
      DIF=ABS(U(I)-U(NI))
      IF(DIF.LT.TENTH) GO TO 1091
      T=ABS(U(I)-U(I-1))
      IF(T.NE.0.) T=(DIF-TENTH)/T
      YPT1=Y(I)-T*(Y(I)-Y(I-1))
      GO TO 1092
 1091 CONTINUE
 1092 DO 1093 I=1,NE
      IDASH=NE+2-I
      DIF=ABS(U(IDASH)-U(NE))
      IF(DIF.LT.TENTH) GO TO 1093
      T=ABS(U(IDASH+1)-U(IDASH))
      IF(T.NE.0.) T=(DIF-TENTH)/T
      YPT9=Y(IDASH)+T*(Y(IDASH+1)-Y(IDASH))
      GO TO 1094
 1093 CONTINUE
 1094 YNM=YPT9-YPT1
      YNMOT=YNM/THETA
      DYNMDX=YNMOT*DTDX10
      YNP2D=Y(NP2)/YNM
      YS1OT=(YHU-YPT1)/THETA
      YSEOT=(YPT9-YHU)/THETA
 1081 CONTINUE
      DO 2009 I=1,NP3
 2009 RTI(I)=SQRT(2.*F(2,I)/3.)/(U(I)+1.E-20)
      DO 2010 I=1,NP3
      YSTAR(I)=Y(I)-YHU
 2010 YSTOT(I)=YSTAR(I)/THETA

C   LOCATE BOUNDARIES OF K AND TURB. INT. LAYERS
      F2MX=F(2,IMU)
      F2MNI=F(2,NI)
      F2MNE=F(2,NE)
      RTIMX=RTI(IMU)
      RTMNI=RTI(NI)
      RTMNE=RTI(NE)
      IFM=IMU
      NIF=NI
      NEF=NE
      ITM=IMU
      NIT=NI
      NET=NE
      NIP2=NI+2
      NEM3=NE-3
```

```
      DO 2050 I=IOLI,IOLE
      IF(I.GT.NEM3)GO TO 2052
      IF(I.GT.NIP2)GO TO 2051
      IF(F(2,I).GT.F2MNI)GO TO 2053
      NIF=I
      F2MNI=F(2,I)
      GO TO 2050
 2053 IF(RTI(I).GT.RTMNI)GO TO 2050
      NIT=I
      RTMNI=RTI(I)
      GO TO 2050
 2051 IF(F(2,I).LE.F2MX)GO TO 2054
      IFM=I
      F2MX=F(2,I)
      GO TO 2050
 2054 IF(RTI(I).LE.RTIMX)GO TO 2050
      ITM=I
      RTIMX=RTI(I)
      GO TO 2050
 2052 IF(F(2,I).GE.F2MNE)GO TO 2055
      NEF=I
      F2MNE=F(2,I)
 2055 IF(RTI(I).GE.RTMNE)GO TO 2050
      NET=I
      RTMNE=RTI(I)
 2050 CONTINUE
      ZETA=0.
      ETA=0.
      NEFM1=NEF-1
      NETM1=NET-1
      DO 2056 I=NIF,NEFM1
 2056 ZETA=ZETA+(F(2,I)+F(2,I+1))*(Y(I+1)-Y(I))
      ZETA=ZETA-(F(2,NEF)+F(2,NIF))*(Y(NEF)-Y(NIF))
      ZETOT=ZETA/(F2MX*2.-F(2,NEF)-F(2,NIF))/THETA
      DO 2057 I=NIT,NETM1
 2057 ETA=ETA+(RTI(I)+RTI(I+1))*(Y(I+1)-Y(I))
      ETA=ETA-(RTI(NET)+RTI(NIT))*(Y(NET)-Y(NIT))
      ETOT=ETA/(RTIMX*2.-RTI(NET)-RTI(NIT))/THETA
10850 WRITE(6,1087)XU,RMI,RME,AMOM,YMSOT,YSIOT,YSEOT,YNMOT,
     1    ISTEP,NI,NE,IMU
 1087 FORMAT(5X,2HXU,9X,3HRMI,8X,3HRME,7X,4HAMOM,7X,5HYMSOT,
     1    6X,5HYSIOT,6X,5HYSEOT,6X,5HYNMOT,8X,5HISTEP,4X,2HNI,3X,2HNE,
     2    3X,3HIMU/1H ,1P8E11.3,4X,2I6,I5,I6)
      WRITE(6,2001)THETA,DTDX1,DTDX10,D2TDX2,YNM,DYNMDX
 2001 FORMAT(5X,6HTHETA=,1PE10.3,3X,6HDTDX1=,E10.3,3X,7HDTDX10=,E10.3,
     1    3X,7HD2TDX2=,E10.3,3X,4HYNM=,E10.3,3X,7HDYNMDX=,E10.3/)
      WRITE(6,1096)NIF,IFM,NEF,ZETA,ZETOT,NIT,ITM,NET,ETA,ETOT,IOLI,IO
 1096 FORMAT(3X,11HNIF,IFM,NEF,3I4,2X,5HZETA=,F7.5,2X,6HZETOT=,F5.2,
     1    4X,11HNIT,ITM,NET,3I4,3X,4HETA=,F7.5,2X,5HETOT=,F5.2,4X,
     2    9HIOLI,IOLE,2I3//)
      IPRINT=0
C  ------------------------------------  TEST 6
      IF(ITEST.EQ.0) GO TO 1006
      TEST=1006.
      WRITE(6,100) TEST
 1006 CONTINUE
C  ------------------------------  PROFILE VARIABLES  ----------
      DO 1070 I=1,NP3
      YPLOT(2,I)=U(I)/UI
```

```
 1070 XPLOT(I)=Y(I)/YNM
      WRITE(6,1076)
1076  FORMAT(10X,22HDIMENSIONLESS DISTANCE)
      WRITE(6,101) R(1),(XPLOT(I),I=2,NP2),Y(NP3)
      WRITE(6,1077)
1077  FORMAT(10X,22HDIMENSIONLESS VELOCITY)
      WRITE(6,101)(YPLOT(2,I),I=1,NP3)
      WRITE(6,2013)
 2013 FORMAT(10X,6HF(2,I))
      WRITE(6,101)(F(2,I),I=1,NP3)
      WRITE(6,2014)
 2014 FORMAT(10X,6HF(3,I))
      WRITE(6,101)(F(3,I),I=1,NP3)
      WRITE(6,2012)
      WRITE(6,101)(RTI(I),I=1,NP3)
      IF(ISTEP.EQ.0)GO TO 105
      WRITE(6,1078)
 1078 FORMAT(10X,25HVELOCITY DIFFERENCE RATIO)
      DO 1072 I=1,NP3
 1072 YPLOT(1,I)=(U(I)-U(NE))/UDIF
      WRITE(6,101) U(1),(YPLOT(1,I),I=2,NP2),U(NP3)
      IF(IPRINT.EQ.0)GO TO 2020
10782 WRITE(6,1062)
1062  FORMAT(10X,14HF(2,I)/UDIF**2)
      UDIFSQ=UDIF**2
      DO 1073 I=1,NP3
 1073 YPLOT(3,I)=F(2,I)/UDIFSQ
      WRITE(6,101) (YPLOT(3,I),I=1,NP3)
      F3REF=UDIF/THETA
      WRITE(6,10631)
10631 FORMAT(10X,12HF(3,I)/F3REF)
      DO 1074 I=1,NP3
 1074 YPLOT(4,I)=F(3,I)/F3REF
      WRITE(6,101) (YPLOT(4,I),I=1,NP3)
10651 WRITE(6,1079)
 1079 FORMAT(10X,20HDIMENSIONLESS LENGTH)
      DO 1075 I=1,NP3
      YPLOT(6,I)=YPLOT(6,I)*(Y(NE)-Y(NI))/THETA
 1075 YPLOT(5,I)=SQRT(F(2,I))/F(3,I)/(Y(NE)-Y(NI))
      WRITE(6,101) F(3,1),(YPLOT(5,I),I=2,NP2),F(3,NP3)
C  YPLOT(6,I), (7,I), (8,I) ASSIGNED IN AUX EXCEPT AS FOLLOWS ...
C   EDGE VALUES OF YPLOT(6)(=ALMG)ARBITRARILY SET AT ZERO
      CON=RHOIE*UI*(1.-URAT)*(Y(NE)-Y(NI))
      YPLOT(6,1)=0.
      YPLOT(7,1)=RHO(1)*F(2,1)/(F(3,1)*CON)
      YPLOT(8,1)=0.
      YPLOT(6,NP3)=0.
      YPLOT(7,NP3)=RHO(NP3)*F(2,NP3)/(F(3,NP3)*CON)
      YPLOT(8,NP3)=0.
      WRITE(6,10601) (YPLOT(6,I),I=1,NP3)
10601 FORMAT(10X,4HALMG/(6X,1P11E11.3))
      WRITE(6,10602) (YPLOT(7,I),I=1,NP3)
10602 FORMAT(10X,5HEMUTD/(6X,1P11E11.3))
      WRITE(6,10603) (YPLOT(8,I),I=1,NP3)
10603 FORMAT(10X,4HTAUD/(6X,1P11E11.3))
 2015 CONTINUE
 2020 CONTINUE
      IF(ALF.EQ.0..AND.BET.EQ.0.)GO TO 2021
      PREF(2,1)=0.0
```

```
      PREF(2,NP3)=0.0
      WRITE(6,2016)
      WRITE(6,101)(PREF(2,I),I=1,NP3)
 2021 IF(GAM.EQ.0..AND.DEL.EQ.0.)GO TO 2022
      PREF(3,1)=0.0
      PREF(3,NP3)=0.0
      WRITE(6,2017)
      WRITE(6,101)(PREF(3,I),I=1,NP3)
 2022 CONTINUE
 2016 FORMAT(10X,5HPREF2)
 2017 FORMAT(10X,5HPREF3)
      WRITE(6,2011)
      WRITE(6,101)(YSTOT(I),I=1,NP3)
      WRITE(6,2002)
 2002 FORMAT(1X//)
 2011 FORMAT(10X,11HYSTAR/THETA)
 2012 FORMAT(10X,18HREL TURB INTENSITY)
      IF(K.GE.KSTAT)GO TO 110
      K=K+1
  105 CONTINUE
C     ------------------------------------------------------------------
C     11 11 11 11 11 11 11 11 11 11 11 11 11 11 11 11 11    TERMINATION
      IF(IFIN.EQ.1)GO TO 110
      IF(ISTEP.LT.LASTEP.AND.XU.LT.XULAST) GO TO 112
      GO TO 110
112   CONTINUE
C     ------------------------------------------------------------------
C     STRIDE 3 STRIDE 3 STRIDE 3 STRIDE 3 STRIDE 3
            CALL STRIDE(3)
      IF(ISTEP.EQ.LASTEP.OR.XU.GT.XULAST)IFIN=1
            GO TO 60
  110       CONTINUE
C     ------------------------------------------------------------------
      IRUN=IRUN+1
  120 CONTINUE
  121 CONTINUE
      STOP
      END
```

APPENDIX B

THE TOLLMIEN-KUETHE SOLUTIONS

B.1.

A convenient starting point for the analysis presented by Tollmien (reference 5) and extended by Kuethe (reference 6) is the boundary-layer momentum equation in the form:

$$U\frac{\partial U}{\partial x} + V\frac{\partial U}{\partial y} = \frac{1}{\rho}\cdot\frac{\partial}{\partial y}\left(\rho \ell^2 \frac{\partial U}{\partial y}\frac{\partial U}{\partial y}\right) \qquad \text{(B.1-1)}$$

This equation results from the combination of equations 1.2-1 and 1.2-3. In it ℓ represents the Prandtl mixing length. Tollmien took:

$$\ell = cx \quad , \qquad \text{(B.1-2)}$$

thereby implying that the boundary layer grows linearly from a line source of turbulence at x = 0. For the case with ρ constant, equation B.1-1 then reduces to:

$$U\frac{\partial U}{\partial x} + V\frac{\partial U}{\partial y} = 2c^2x^2\frac{\partial U}{\partial y}\cdot\frac{\partial^2 U}{\partial y^2} \quad , \qquad \text{(B.1-3)}$$

subject to the boundary conditions that $\frac{\partial U}{\partial y}$ is zero at both edges of the layer (the I and E boundaries), and that velocity U has known values at these edges. The usual stream function, ψ, is introduced, defined by:

$$U \equiv \frac{\partial \psi}{\partial y} \quad , \quad V \equiv -\frac{\partial \psi}{\partial x} \qquad \text{(B.1-4)}$$

The transformation:

$$\psi \equiv (2c^2)^{1/3} U_I \cdot F \quad , \quad \varphi = \frac{y}{(2c^2)^{1/3} x} \qquad \text{(B.1-5)}$$

leads to the following expressions, in which $a \equiv (2c^2)^{-1/3}$:-

$$\left.\begin{aligned} U &\equiv \frac{\partial \psi}{\partial y} = U_I \cdot \frac{dF}{d\varphi} \\ \frac{\partial U}{\partial y} &\equiv \frac{\partial^2 \psi}{\partial y^2} = \frac{U_I\, a}{x} \cdot \frac{d^2F}{d\varphi^2} \\ \frac{\partial^2 U}{\partial y^2} &\equiv \frac{\partial^3 \psi}{\partial y^3} = \frac{U_I\, a^2}{x^2} \cdot \frac{d^3F}{d\varphi^3} \\ -V &\equiv \frac{\partial \psi}{\partial x} = \frac{U_I}{a}\left(F - \varphi \cdot \frac{dF}{d\varphi}\right) \\ \frac{\partial U}{\partial x} &= \frac{\partial^2 \varphi}{\partial x \partial y} = -\frac{U_I\, ya}{x^2} \cdot \frac{d^2F}{d\varphi^2} \end{aligned}\right\} \qquad \text{(B.1-6)}$$

Substitution of these expressions into equation (B.1-3), leads to the simple result:

$$F + \frac{d^3F}{d\varphi^3} = 0 \quad , \qquad \text{(B.1-7)}$$

provided that $\frac{d^2F}{d\varphi^2}$ is not zero; this condition holds throughout the zone of interest, since $\frac{\partial U}{\partial y}$ is finite everywhere except at the I and E boundaries. The boundary conditions take the form:

$$\left.\begin{aligned} &\text{at } \varphi = \varphi_I \quad , \quad \frac{dF}{d\varphi} = 1 \quad , \quad \frac{d^2F}{d\varphi^2} = 0 \\ &\text{at } \varphi = \varphi_E \quad , \quad \frac{dF}{d\varphi} = 0 \quad , \quad \frac{d^2F}{d\varphi^2} = 0 \end{aligned}\right\} \qquad \text{(B.1-8)}$$

The condition $(\frac{dF}{d\varphi})_E = 0$ indicates that Tollmien's solution applies to the case $U_E = 0$. However, on examining the solution to equation B.1-7, which Tollmien obtained as:

$$F = C_1 e^{-\varphi} + C_2 e^{\varphi/2} \cos(\frac{\sqrt{3}}{2}\varphi) + C_3 e^{\varphi/2} \sin(\frac{\sqrt{3}}{2}\varphi), \quad \text{(B.1-9)}$$

one sees that a fifth condition is required in order to determine the three constants, C_1, C_2 and C_3, and φ_I, φ_E, the values of φ defining the boundaries of the solution. For the fifth condition, Tollmien took:

$$F_I = \varphi_I \quad , \quad \text{(B.1-10)}$$

which corresponds to $V_I = 0$, i.e., to zero transverse velocity at the I boundary. Kuethe subsequently used an alternative condition, and showed that the U-velocity profiles resulting from the solution are not affected by the choice, which is basically concerned with the alignment of the x-axis with the I and E boundaries of the layer.

Kuethe's other modifications of Tollmien's work were:-

a) replacement of the third boundary condition by: $(\frac{dF}{d\varphi})_E = U_E/U_I$, thereby extending the solution to layers with non-zero overall velocity ratio; and

b) the mathermatical device of taking $(\varphi - \varphi_I)$ as the independent variable, to simplify the numerical work.

The numerical details of Tollmien's solution are readily available in reference 15 (displayed in Tables 2.1

and 2.2 of that work); some of the values given appear to be wrong, however, specifically those near the E boundary. In reference [6] the information is given mainly in the form of rather inadequate graphs. In view of these difficulties, it was decided to recalculate the solutions.

B.2.

Kuethe's form of the solution to equation (B.1-7) may be written as:

$$F = D_1 e^{-\varphi'} + D_2 e^{\varphi'/2} \cos\frac{\sqrt{3}}{2}\varphi' + D_3 e^{\varphi'/2} \sin\frac{\sqrt{3}}{2}\varphi' \quad \text{(B.2-1)}$$

where $\varphi' = \varphi - \varphi_I$, and D_1, D_2, and D_3 are constants. It follows that:

$$\frac{dF}{d\varphi'} = -D_1 e^{-\varphi'} + \frac{e}{2}^{\varphi'/2} \cos\frac{\sqrt{3}}{2}\varphi'(D_2+\sqrt{3}D_3) + \frac{e}{2}^{\varphi'/2} \sin\frac{\sqrt{3}}{2}\varphi'(D_3-\sqrt{3}C_2) \quad \text{(B.2-2)}$$

and

$$\frac{d^2F}{d\varphi'^2} = D_1 e^{-\varphi'} + \frac{e}{2}^{\varphi'/2} \cos\frac{\sqrt{3}}{2}\varphi'(\sqrt{3}D_3-D_2) - \frac{e}{2}^{\varphi'/2} \sin\frac{\sqrt{3}}{2}\varphi'(D_3+\sqrt{3}D_2) \quad \text{(B.2-3)}$$

Substitution in these equations, as appropriate, of the five boundary conditions leads to:

$$1 = -D_1 + \tfrac{1}{2}(D_2 + \sqrt{3}D_3) \quad \text{(B.2-4)}$$

$$0 = D_1 + \tfrac{1}{2}(\sqrt{3}D_3 - D_2) \qquad \text{(B.2-5)}$$

$$\frac{U_E}{U_I} = -D_1 e^{-\varphi'_E} + \frac{e}{2}^{\varphi'_E/2}\cos\frac{\sqrt{3}}{2}\varphi'_E(D_2+\sqrt{3}D_3) + \frac{e}{2}^{\varphi'_E/2}\sin\frac{\sqrt{3}}{2}\varphi'_E(D_3-\sqrt{3}D_2) \qquad \text{(B.2-6)}$$

$$0 = D_1 e^{-\varphi'_E} + \frac{e}{2}^{\varphi'_E/2}\cos\frac{\sqrt{3}}{2}\varphi'_E(\sqrt{3}D_3-D_2) - \frac{e}{2}^{\varphi'_E/2}\sin\frac{\sqrt{3}}{2}\varphi'_E(D_3+\sqrt{3}D_2) \qquad \text{(B.2-7)}$$

$$\varphi_I = D_1 + D_2 \qquad \text{(B.2-8)}$$

The first pair of equations, together with the last, quickly yield:

$$D_1 = \frac{\varphi_I - 1}{3} \quad , \quad D_2 = \frac{2\varphi_I + 1}{3} \quad , \quad D_3 = \frac{1}{\sqrt{3}} \qquad \text{(B.2-9)}$$

B.3.

The KUESOL computer programme was written to solve equations B.2-6, 7 and 9, to carry out a numerical differentiation check on the results, and then to derive the values of quantities which enable a comprehensive comparison to be made between the Tollmien-Kuethe solutions and those obtained with the Patankar-Spalding method. The programme was run on the PUFFT facility of the IBM 7090 (subsequently 7094) digital computer at Imperial College.

A listing of the programme is given at the end of this Appendix. The solution consists essentially of a double iteration procedure which is performed by the

sequence of statements between comment cards C2 and C4. The variable ER represents the error resulting from the substitution into equation B.2-6 of an incorrect value for φ_E'; GRDER represents the gradient of the error ER as φ_I changes:-

$$ER \equiv -D_1 e^{-\varphi_E'} + \frac{e}{2}^{\varphi_E'/2} \cos\frac{\sqrt{3}}{2}\varphi_E'(D_2+3D_3) + \frac{e}{2}^{\varphi_E'/2} \sin\frac{\sqrt{3}}{2}\varphi_E'(D_3-3D_2) - U_E/U_I$$

$$GRDER \equiv \frac{\partial ER}{\partial \varphi_I} = -e^{-\varphi_E'}\frac{dD_1}{d\varphi_I} - D_1 e^{-\varphi_E'} + \text{other terms}$$

$$= -e^{-\varphi_E'}\left(\frac{1}{3} - \frac{\varphi_1 - 1}{3}\right) + \text{" "}$$

$$= -e^{-\varphi_E'}\varphi_I/3 + \text{" "}$$

The other terms are found to be much smaller than the first, and are neglected. The action of the first iteration loop is thus to adjust φ_I until ER is less than 1×10^{-6}, while φ_E remains unchanged.

In a similar way the second iteration loop adjusts the value of φ_E' in order to reduce ERV, the error in equation B.2-7. In this case, however, after each adjustment of φ_E' (and the corresponding change of φ_E), the calculation sequence returns to the beginning of the <u>first</u> loop, in order to ensure that ER remains within its prescribe limit. The quantity GRDERV therefore has to take account of the action of both loops, and so:

TABLE B.1

Comparison of results of present solution (S.J.P) with those quoted by Kuethe (Reference 4) (A.M.K.)

Velocity Ratio U_E/U_I	ϕ_I		$-\phi_E$		$-D_1$		D_2	
	SJP	AMK	SJP	AMK	SJP	AMK	SJP	AMK
0	·9814	·981	2·035	2·040	·00620	·0062	·9876	·987
0·2	·9436	·940	1·621	1·625	·01881	·020	·9624	·960
0·4	·8855	·885	1·305	1·305	·03816	·038	·9234	·924
0·6	·7975	·797	1·024	1·024	·06752	·067	·8650	·866
0·8	·6514	·647	0·7360	·733	·1162	·117	·7676	·766
0·9	·5242	·522	·5569	·558	·1586	·159	·6828	·682

All velocity ratios: $D_3 = 0.5774$

$$GRDERV = \frac{\partial ERV}{\partial \varphi'_E} + \frac{\partial ERV}{\partial \varphi_I} \times \frac{\partial ER/\partial \varphi'_E}{\partial ER/\partial \varphi_I}$$

By again ignoring small terms containing $e^{\varphi'_E/2}$, the following approximate expression, for GRDERV is obtained:

$$GRDERV = -2D_1 e^{-\varphi'_E}$$

The whole iteration procedure is found to converge very rapidly, especially as quite accurate values for φ_I and φ_E, obtainable from the published work of Tollmien and Kuethe, are available as the starting point.

In Table B.1, opposite, the results of the present solution are compared with those of Kuethe.

B.4.

The solution of the basic equation having been completed, the calculation of various derived quantities - mainly cross-stream integrals - for comparison with the finite-difference solutions, follows. These are defined below:-

$$ENTRAT \equiv \left(\frac{d^3F}{d\varphi^3}\right)_I / \left(\frac{d^3F}{d\varphi^3}\right)_E = \frac{F_I}{F_E} \qquad (B.4\text{-}1)$$

The significance of this quantity as the ratio of the rates of entrainment through the I and E boundaries is shown in:

$$\text{ETA} \equiv \int_I^E \frac{U}{U_I} d\left(\frac{y}{y_E - y_I}\right) = \int_I^E \frac{dF}{d\varphi} d\left(\frac{\varphi}{\varphi_E - \varphi_I}\right) = \frac{F_E - F_I}{(\varphi_E - \varphi_I)}$$

(B.4-2)

$$\text{ZETA} \equiv \int_I^E \frac{U - U_E}{U_I - U_E} d\left(\frac{y}{y_E - y_I}\right) = \frac{1}{\left(1 - \frac{U_E}{U_I}\right)} \left[\frac{F_E - F_I}{\varphi_E - \varphi_I} - \frac{U_E}{U_I}\right]$$

(B.4-3)

$$\text{THETA} \equiv \int_I^E \left(\frac{U - U_E}{U_I - U_E}\right)\left(1 - \frac{U - U_E}{U_I - U_E}\right) d\left(\frac{y}{y_E - y_I}\right)$$

$$= \frac{1}{\left(1 - \frac{U_E}{U_I}\right)^2} \cdot \frac{\left(1 + \frac{U_E}{U_I}\right)(F_E - F_I)}{(\varphi_E - \varphi_I)} - \frac{U_E}{U_I} \frac{1}{(\varphi_E - \varphi_I)} \int_I^E \left(\frac{dF}{d\varphi}\right)^2 d\varphi$$

(B.4-5)

FINTI and FINTE are intermediate quantities used in determining the value of THETA, thus:

$$\int_I^E \left(\frac{dF}{d\varphi}\right)^2 d\varphi = \text{FINTE} - \text{FINTI} \qquad \text{(B.4-6)}$$

The manner of calculating FINTE and FINTI is clearly shown in the programme listing.

B.5.

The next section of the programme (C.5) is a straightforward sequence for calculating the co-ordinates $\left(\frac{dF}{d}, \varphi\right)$ of points on the velocity profile, and the corresponding

values of F, for twenty equal intervals of φ. Values of F are also calculated for three extra points outside each boundary. These are for use in section C6, where an independent check on the solution is performed, using Bickley's seven-point formula (from Ref. 33) for calculating $\frac{d^3F}{d\varphi^3}$ as D3FDPH for all the points on the profile.

The results from these two sections are printed out in tabular form. The last column shows the difference between the values of $\frac{d^3F}{d\varphi^3}$ calculated from the exact solution and by the Bickley formula. They provide a sufficient check on the solution, being all in the orders -5, -6, or -7, and equal in magnitude to the terms neglected in the Bickley formulation.

B.6.

Section C7 is a simple iteration loop which determines the three values of φ' for which VDR = 0.1, 0.5, and 0.9; $(\text{VDR} \equiv \frac{U - U_E}{U_I - U_E})$. This leads, in the following section, to the calculation of the various cross-stream dimension ratios, whose definitions are repeated here for convenience:

$$\text{YMSOT} \equiv \varphi_{ms}/\theta \equiv \frac{1}{\theta \times [\frac{d(\text{VDR})}{dy}]_{0.5}}$$

$$\text{YNOTH} \equiv \varphi_n/\theta \equiv (\varphi_{0.1} - \varphi_{0.9})/\theta$$

```
C    TOLLMIEN-KUETHE SOLUTION BY ITERATION
       DIMENSION F(27),DFDPH(27),PH(27),PHD(27)
       DIMENSION VDRN(3),YR(3),UN(3)
C    VRAT=U(E)/U(I),     PHE=PHI(E),     PHI=PHI(I)
C     INDEX=1 FOR CONTINUATION OF CALCULATION FOR ANOTHER VALUE OF VRAT
C                     OTHERWISE CALCULATION STOPS
C     VDR=(U-U(E))/(U(I)-U(E)),        YR=(PHI-PHI(E))/(PHI(I)-PHI(E))
C1    READ IN STARTING VALUES
      1 READ(5,100)VRAT,PHI,PHE,INDEX
        WRITE(6,99)VRAT
        WRITE(6,97)
        WRITE(6,98)PHI,PHE
        SQ3=SQRT(3.)
        VDRN(1)=.9
        VDRN(2)=.5
        VDRN(3)=.1
        YR(1)=.16
        YR(2)=.47
        YR(3)=.78
C2    ITERATION LOOP FOR PHI(I)
        L=1
      2 PHED=PHE-PHI
      3 THED=SQ3*PHED/2.
        CTH=COS(THED)
        STH=SIN(THED)
        EXPH=EXP(PHED)
        EXP02=EXP(PHED/2.)/2.
        M=1
C     CALCULATION OF CONSTANTS
        D1=(PHI-1.)/3.
        DOX=D1/EXPH
        D2=(2.*PHI+1.)/3.
        D3=1./SQ3
        C=CTH*(D2+1.)+STH*(D3-SQ3*D2)
        ER=C*EXP02-VRAT-DOX
        IF(ABS(ER).LT.1.0E-06)GO TO 10
        M=M+1
        IF(M.GT.20)GO TO 50
        GRDER=-PHI/(3.*EXPH)
        PHI=PHI-ER/GRDER
        GO TO 2
C3    ITERATION LOOP FOR PHI(E)
     10 CV=CTH*(1.-D2)-STH*(D3+SQ3*D2)
        ERV=DOX+EXP02*CV
        IF(ABS(ERV).LT.1.0E-06)GO TO 11
        L=L+1
        IF(L.GT.20)GO TO 51
        GRDERV=-2.*D1/EXPH
        PHED=PHED-ERV/GRDERV
        PHE=PHED+PHI
        GO TO 3
     11 WRITE(6,497)
        WRITE(6,301)PHI,PHE,D1,D2,D3
C4   CALCULATION OF CROSS-STREAM INTEGRALS AND RATIO OF ENTRAINMENT RATES
        AB=0.5*(D2+1.)
        BB=0.5*(D3-SQ3*D2)
        A2C=AB*AB*(CTH*(CTH/SQ3+STH)+SQ3/2.)
        B2C=BB*BB*(STH*(STH/SQ3-CTH)+SQ3/2.)
        ABC=AB*BB*(SIN(2.*THED)/SQ3-COS(2.*THED))
```

```
      AC=AB*(STH-CTH/SQ3)
      BC=BB*(STH/SQ3+CTH)
      EXF02=2.*EXF02
      FINTE=SQ3*EXPH*(A2C+B2C+ABC)/4.-SQ3*D1*(AC-BC)/EXFC2-
     1    0.5*D1*D1/EXP(2.*PHED)
      FINTI=(5.*AB*AB+3.*BB*BB-2.*SQ3*AB*BB)/8.+D1*(AB+SQ3*BB-D1/2.)
      FI=D1+D2
      FE=DOX+EXF02*(D2*CTH+D3*STH)
      ENTRAT=FI/FE
      ETA=(FE-FI)/PHED
      ZETA=(ETA-VRAT)/(1.-VRAT)
      THETA=((1.+VRAT)*ETA-VRAT-(FINTE-FINTI)/PHED)/((1.-VRAT)**2)
      WRITE(6,303)
      WRITE(6,302)ETA,ZETA,THETA,ENTRAT
C5    CALCULATION OF F AND DF/DPHI FOR EQUAL INTERVALS OF PHI
      WRITE(6,310)
      DPH=.05*PHED
      DO 20 K=1,27
      PHD(K)=(FLOAT(K)-4.)*DPH
      THD=SQ3*PHD(K)/2.
      CTH=COS(THD)
      STH=SIN(THD)
      EXPH=EXP(PHD(K))
      EXF02=EXP(PHD(K)/2.)
      DOX=D1/EXPH
      F(K)=DOX+EXF02*(D2*CTH+D3*STH)
      IF(K.LT.4.OR.K.GT.24)GO TO 20
      DFDPH(K)=-DOX+EXF02*(CTH*(D2+SQ3*D3)+STH*(D3-SQ3*D2))/2.
      PH(K)=PHI+PHD(K)
   20 CONTINUE
C6    CALCULATION OF THIRD DIFFERENTIAL
      DO 21 K=4,24
      DIF1=F(K+1)-F(K-1)
      DIF2=F(K+2)-F(K-2)
      DIF3=F(K+3)-F(K-3)
      D3FDPH=(DIF2-13.*DIF1/8.-DIF3/8.)/DPH**3
      ERROR=D3FDPH+F(K)
      N=K-4
   21 WRITE(6,311)N,PH(K),PHD(K),F(K),DFDPH(K),D3FDPH,ERROR
C7    LOCATION OF POINTS FOR SPECIFIED VDR VALUES
      DO 30 L=1,3
      M=1
      UN(L)=VDRN(L)*(1.-VRAT)+VRAT
      PHDN=YR(L)*PHED
   31 THD=SQ3*PHDN/2.
      CTH=COS(THD)
      STH=SIN(THD)
      EXPH=EXP(PHDN)
      EXFC2=EXP(PHDN/2.)
      DOX=D1/EXPH
      DFDPH(L)=-DOX+EXF02*(CTH*(D2+SQ3*D3)+STH*(D3-SQ3*D2))/2.
      DUDPH=DOX+EXFC2*(CTH*(SQ3*D3-D2)-STH*(D3+SQ3*D2))/2.
      CORR=(UN(L)-DFDPH(L))/DUDPH
      IF(ABS(CORR).LT.1.0E-05)GO TO 32
      M=M+1
      IF(M.GT.20)GO TO 30
      PHDN=PHDN+CORR
      GO TO 31
   32 IF(L.NE.2)GO TO 33
```

```
      PHM=PHDN
      PHMS=(1.-VRAT)/DUDPH
       PHMSOT=PHMS/(THETA*PHED)
   33 YR(L)=PHDN/PHED
   30 CONTINUE
C8    CALCULATION OF CROSS-STREAM DIMENSIONS AND RATIOS
      YNOTH=(YR(3)-YR(1))/THETA
      YSTRI=(YR(2)-YR(1))/THETA
      YSTRE=(YR(3)-YR(2))/THETA
      WRITE(6,312)
      WRITE(6,313)YNOTH,YSTRI,YSTRE,PHM,PHMSOT
C9    CALCULATION OF VALUES FOR SPECIFIED INTERVALS OF YSTAR
      WRITE(6,314)
      DELYT=0.4
      DO 40 I=1,23
      YSTOT=FLOAT(I-11)*DELYT
      PHDI=PHM+YSTOT*THETA*PHED
      IF(PHDI.GT.0.)GO TO 40
      IF(PHDI.LT.PHED)GO TO 40
      THD=SQ3*PHDI/2.
      CTH=COS(THD)
      STH=SIN(THD)
      EXPH=EXP(PHDI)
      EXP02=EXP(PHDI/2.)
      DOX=D1/EXPH
      DFDPH(I)=-DOX+EXP02*(CTH*(D2+SQ3*D3)+STH*(D3-SQ3*D2))/2.
      DUDPH=DOX+EXP02*(CTH*(SQ3*D3-D2)-STH*(D3+SQ3*D2))/2.
      VDR=(DFDPH(I)-VRAT)/(1.-VRAT)
      DUDPT=-DUDPH*THETA*PHED
      WRITE(6,315)PHDI,YSTOT,DFDPH(I),VDR,DUDPT
   40 CONTINUE
      GO TO 12
   50 WRITE(6,400)ER
      GO TO 12
   51 WRITE(6,401)ERV
   12 IF(INDEX.EQ.1)GO TO 1
      STOP
   97 FORMAT(5X,35HINITIAL VALUES OF PHI(I) AND PHI(E)/)
   98 FORMAT(5X,2F10.4//)
   99 FORMAT(1H1,30HKUETHE SOLUTION FOR VEL RATIO=,F5.3/)
  100 FORMAT(F5.3,2F10.4,I2)
  301 FORMAT(5X,2F10.4,4X,F10.6,2F10.4/)
  302 FORMAT(1X,4F16.4//)
  303 FORMAT(1X,72HVALUES OF CROSS-STREAM INTEGRALS OF VRAT,VDR,AND VDR(
     11-VDR),AND OF FI/FE/)
  310 FORMAT(8X,3HPHI,4X,9HPHI-PHI,I,5X,1HF,7X,5HDFDPH,5X,6HD3FDPH,4X,
     1    5HERROR/)
  311 FORMAT(1X,I2,5(3X,F7.4),1PE11.1/)
  312 FORMAT(1H0,1H )
  313 FORMAT(5X,6HYNOTH=,F6.4,6X,6HYSTRI=,F6.4,6X,6HYSTRE=,F6.4,6X,
     1    4HPHM=,F7.4,6X,7HPHMSOT=,F6.4//)
  314 FORMAT(10X,21HEQUALLY-SPACED VALUES//10X,9HPHI-PHI,I,1X,
     1    10HYSTR/THETA,4X,1HU,8X,3HVDR,6X,5HDUDPT//)
  315 FORMAT(8X,F10.3,F10.2,2F10.3,F10.4)
  400 FORMAT(1X,15HR EQUALS 20,ER=,E10.3)
  401 FORMAT(1X,16HL EQUALS 20,ERV=,E10.3)
  497 FORMAT(5X,42HFINAL VALUES OF PHI(I),PHI(E),D1,D2,AND D3/)
      END
```

APPENDIX C

EXPERIMENTAL DATA PROCESSING

C.1.

A short computer programme (XPDTP) was written to carry out the required processing of the experimental readings. For each traverse, the bulk of the data to be treated consisted of:

transverse position (y - scale readings),

pitot manometer reading,

hot-wire D.C. voltage, and

hot-wire r.m.s. A.C. voltage

From these it was required principally to derive the value of the momentum thickness, θ, of the layer, and, for each point, the following values:-

velocity ratio, URAT $\equiv U/U_I$

velocity-difference ratio, VDR $\equiv (U-U_E)/(U_I-U_E)$

transverse position, y^*, measured from the position at which VDR = 0.5 (i.e., from the position of mean velocity)

transverse position ratio, YSTOT $\equiv y^*/\theta$

relative and absolute turbulence intensities, $\frac{u_r}{U}$ and $\frac{u_r}{U_I}$.

A listing of the programme is included in this Appendix. The programme was run on the PUFFT facility of the Imperial College IBM 7090/7094 computer. A description of its function follows.

C.2.

Apart from the general question of the accuracy of individual experimental measurements, which is considered elsewhere, the main cause of uncertainty in the interpretation of the experimental results arises in the assignment of values for the free-stream properties; there is also the associated problem of deciding where the outer edges of the layer are. In particular, changes in U_I and U_E will affect the value of momentum thickness θ calculated for a profile (and, indeed; of any other representative dimension used instead of θ).

In the programme, the subscripts NOI and NOE identify the points marking the edges of the layer. Three possible processing procedures for any profile are:-

1. Initially to assign tentative values to NOI and NOE, but subsequently to vary them as required to ensure that $(y_E-y_I)/\theta$ lies within prescribed limits, taking for U_I and U_E the velocities at the edges of the layer; U_I and U_E may thus change with NOI and NOE.
2. To vary NOI and NOE as in 1.), but to retain initially-prescribed values for U_I and U_E.
3. To fix NOI, NOE, U_I, and U_E initially and to retain these values unchanged.

The programme in its final form allows any of these procedures to be adopted.

C.3.

The experimental readings for each traverse are processed together. After the data is read in, the first action of the programme is to check the order, and if necessary to reverse it, so that values for the high speed stream will be printed at the left side of the print-out (for convenience in reading). In general the calculations are very simple. Some explanation is required, however, of the basis of the turbulence calculation (see next section), and of the iteration loop which varies the number of points within the boundary layer.

The basis of this sequence is the requirement that the non-dimensional width of the layer, defined as:

$$\text{DELYR} \equiv (y_E - y_I)/\theta \quad ,$$

shall lie between the limits

$$\text{DYRDES} = 8.3 + 8 \times \text{URAND} - .01\, U_E/[U_I(\text{URAND}+0.2)$$

and $$\text{DYRDSA} = 1.1 \times \text{DYRDES} \quad ,$$

where URAND is the mean of the relative turbulence intensities just outside the two edges of the layer. The expression for DYRDES is based partly on a preliminary examination of the experimental results and partly on the theoretical results from the finite-difference solutions.

In the programme, θ is calculated using a trapeizoidal integration. DELYR is then calculated and compared with DYRDES and DYRDSA. If DELYR is too small, an extra point

is added to the mixing layer profile at either the I or E boundary, the choice being determined by the gradients of the relative turbulence intensity; if DELYR is too large, a point is discarded.

C.4.

In converting the readings of the hot-wire anemometer A.C. and D.C. voltmeters to values of turbulence intensity, the calibration curves of the hot-wire probes were assumed to be of the form:

$$V^2 = V_0^2 + k\,U^n \qquad \text{(C.4-1)}$$

where k and n are constants, the latter being given the value 0.45, as recommended by Collis and Williams (reference 34).

Since equation C.4-1 holds for a range of velocity U which does not include zero, some method for determining the effective no-flow D.C. voltage, V_o, is required. The situation is complicated by the variation of both V_o and k during the life of a probe. To avoid the necessity for frequent calibration, the following procedure was adopted in the present case:-

From calibration tests for each probe the value of V_o satisfying equation C.4-1 was ascertained, and the difference between this value and the measured no-flow

D.C. voltage was calculated; this difference, $\Delta V_{o,cal}$, was assumed to be a constant for the probe, and was added to the measured no-flow voltage for each subsequent run with that probe. The use of the equation:

$$\frac{u_r}{U} = \frac{2v_r V}{n(V^2-V_o^2)} \qquad \text{(C.4-2)}$$

in which v_r is the observed root-mean-square (i.e. A.C.) voltage reading, implies that k may vary, in order to preserve the form of equation C.4-1.

```
C    XPDTP
C    EXPERIMENTAL DATA PROCESSING FOR PLANE MIXING LAYER

      DIMENSION Y(57),H(57),U(57),URAT(57),VDR(57),PROD1(57),PROD2(57),
     1 YD(57),YDR(57),V(57),VT(57),TINT(57),YS(57),HS(57),VS(57),VTS(57)
     2   ,ABTNT(57),HC(57),YSTR(57),YSTOT(57)

C    J=RUN NUMBER,ID1,D2,D3,INDICATE DATE
C
C    OBSERVATION PROCEEDS FROM STREAM 1 TO STREAM 2
C    NOP=NUMBER OF POINTS ON PROFILE
C    NO1 IS READING REFERENCE NUMBER AT STREAM 1 BOUNDARY
C    NO2 IS READING REFERENCE NUMBER AT STREAM 2 BOUNDARY
C
C    HO=MANOMETER ZERO READING
C    HF1,HF2,ARE FREE-STREAM MANOMETER READINGS
C    YO=Y-SCALE READING ON AXIS AT X=0
C    VO=NO-FLOW READING OF HOT-WIRE D.C.METER
C    NPRO=S.J.P. HOT WIRE PROBE NUMBER
C    NTRAV=TRAVERSE REFERENCE NUMBER
C    NBOX=DISA SET NUMBER
C
C    ADD 100 TO VALUE OF NTRAV FOR CHECK POINTS. IN THIS CASE VALUE OF Z
C                                          IS NOT PRINTED IN HEADING.
C
C    UNITS.  X,YS,YO-CMS.
C            HS,HF1,HF2,HO-MMS(WATER MANOMETER)
C            HBAR-MMS(MERCURY BAROMETER)
C            TWS-DEGREES CENTIGRADE
C            VS-VOLTS(DISA D.C.METER)
C            VTS-MILLIVOLTS(DISA R.M.S. METER)
C
C    IF INDEX=1,NEW HOT-WIRE CALIBRATION CONSTANTS ARE READ IN
C    IF INDEX=2,A NEW RUN NUMBER AND DATE CARD IS READ
C    IF INDEX=3,DETAILS OF THE NEXT TRAVERSE ARE READ IN
C    IF INDEX=4,THE CURRENT TRAVERSE DATA ARE REPROCESSED
C    IF INDEX=5,THE CALCULATION PROCEDURE STOPS
C    IF INDIC=0,THE PROFILE DATA ARE PROCESSED WITHOUT CHANGING NO1,NO2,
C                                                        HF1,AND HF2
C    IF INDIC=1,THE BOUNDARY POINTS NO1 AND NOE ARE VARIED UNTIL THE
C       WIDTH OF THE LAYER IS WITHIN PRESCRIBED LIMITS,WITH U(NO1) AND
C       U(NOE) AS THE FREE-STREAM VELOCITIES
C    IF INDIC=2,THE WIDTH OF THE LAYER IS VARIED,BUT THE INITIAL VALUES
C           OF UI AND UE ARE RETAINED
C
C    COLOUR CODE FOR DATA CARDS
C       GREEN-RUN NUMBER,DATE,BAROMETER
C       RED-PROFILE DATA(X,NOP,NO1,NO2,HO,HF1,HF2,ETC.)
C       YELLOW-PROFILE POINTS(Y,H,V,VT)
C
C    VDR=(U-UE)/(UI-UE)
C    THETA=MOMENTUM THICKNESS OF LAYER
C    YM=Y-VALUE FOR WHICH VDR=0.5
C    YDR=(Y-YO)/THETA          YSTR=Y-YM          YSTOT=YSTR/THETA
C
C1    READ CALIBRATION CONSTANTS FOR HOT-WIRE PROBE
     5 READ(5,50)NPROB,DVOCAL,AKCAL,ANCAL
       WRITE(6,90)NPROB,DVOCAL,AKCAL,ANCAL
C2    DATA READ-IN,AND REVERSAL OF ORDER OF PROFILE POINTS,IF REQUIRED,SO
```

```
C                    THAT HIGH-SPEED STREAM VALUES ARE AT LEFT OF PRINT-OUT
    7 READ(5,51)J,ID1,D2,D3,HBAR
      WRITE(6,99)J,ID1,D2,D3,HBAR
      WRITE(6,95)
      WRITE(6,96)
    8 READ(5,52)X,Z,NOP,H0,TWS,V0,NPRO,NTRAV,NBOX
      READ(5,53)(YS(I),HS(I),VS(I),VTS(I),I=1,NOP)
    9 READ(5,54)INDIC,INDEX,NO1,NO2,HF1,HF2,Y0
      V0=V0+DV0CAL
      U1=SQRT(HF1-H0)
      U2=SQRT(HF2-H0)
      TWR=TWS+273.
      FAC=6.75*SQRT(TWR/HBAR)
      IF(HF1.GT.HF2)GO TO 11
      UI=U2
      UE=U1
      DO 10 L=1,NOP
      I=NOP+1-L
      Y(I)=YS(L)
      H(I)=HS(L)
      V(I)=VS(L)
   10 VT(I)=VTS(L)
      NOI=NOP+1-NO2
      NOE=NOP+1-NO1
      GO TO 20
   11 DO 12 I=1,NOP
      Y(I)=YS(I)
      H(I)=HS(I)
      V(I)=VS(I)
   12 VT(I)=VTS(I)
      UI=U1
      UE=U2
      NOI=NO1
      NOE=NO2
C3   CALCULATION OF VELOCITY AND RELATIVE TURBULENCE INTENSITY.
   20 DO 19 I=1,NOP
      HC(I)=H(I)-H0
      U(I)=SQRT(HC(I))
      AU=50.*(V(I)-V0)*(V(I)+V0)/V(I)
      TINT(I)=VT(I)/(ANCAL*AU)
   19 CONTINUE
C4    ITERATION LOOP FOR CHOOSING BEST PAIR OF BOUNDARY POINTS.
      M=1
   43 VRAT=UE/UI
      VELFI=FAC*UI
      VELFE=FAC*UE
      DO 21 I=1,NOP
      URAT(I)=U(I)/UI
   21 ABTNT(I)=TINT(I)*URAT(I)
      URAND=.05*(TINT(NOI-1)+TINT(NOE+1))
      DYRDES=8.3+8.*URAND-.01*VRAT/(URAND+.02)
      DYRDSA=DYRDES*1.1
C    CALCULATION OF MOMENTUM THICKNESS.
      DO 22 I=NOI,NOE
   22 VDR(I)=(U(I)-UE)/(UI-UE)
      SUM=0.
      NOEM1=NOE-1
      DO 23 I=NOI,NOEM1
      Z=.5*(VDR(I)+VDR(I+1))
```

```
   23 SUM=SUM+(Y(I+1)-Y(I))*(Z-Z*Z)
      SUM=ABS(SUM)
      FACY=1.
      IF(Y(NOP).LT.Y(1))FACY=-1.
      DO 24 I=1,NOP
      YD(I)=FACY*(Y(I)-Y0)
   24 YDR(I)=YD(I)/SUM
      DELYR=YDR(NOE)-YDR(NOI)
      IF(INDIC.EQ.0)GO TO 26
      WRITE(6,999)NOP,M,NOI,NOE,SUM,DELYR
      IF(DELYR.LT.DYRDSA.AND.DELYR.GT.DYRDES)GO TO 26
      M=M+1
      IF(M.GT.10)GO TO 26
      DTDYI=ABS((TINT(NOI)-TINT(NOI-1))/(YDR(NOI)-YDR(NOI-1)))
      DTDYE=ABS((TINT(NOE)-TINT(NOE+1))/(YDR(NOE)-YDR(NOE+1)))
      IF(DELYR.LT.DYRDES)GO TO 41
      IF(DTDYI.GT.DTDYE)NOE=NOE-1
      IF(DTDYI.LT.DTDYE)NOI=NOI+1
      IF(INDIC.EQ.2)GO TO 43
      UI=U(NOI)
      UE=U(NOE)
      GO TO 43
   41 IF(DTDYI.GT.DTDYE)NOI=NOI-1
      IF(DTDYI.LT.DTDYE)NOE=NOE+1
      IF(INDIC.EQ.2)GO TO 43
      UI=U(NOI)
      UE=U(NOE)
      GO TO 43
   26 DO 44 I=NOI,NOE
      IF(VDR(I).GT.0.5)GO TO 44
      YM=Y(I)+(Y(I-1)-Y(I))*(.5-VDR(I))/(VDR(I-1)-VDR(I))
      GO TO 45
   44 CONTINUE
   45 DO 46 I=1,NOP
      YSTR(I)=FACY*(Y(I)-YM)
   46 YSTOT(I)=YSTR(I)/SUM
C5    PRINT-OUT OF PROCESSED DATA
      IF(NTRAV.LT.100)GO TO 28
      MTRAV=NTRAV-100
      WRITE(6,94)MTRAV,X,VRAT
      GO TO 29
   28 WRITE(6,100)NTRAV,X,VRAT,Z
   29 WRITE(6,98)VELFI,VELFE,TINT(NOI-1),TINT(NOE+1),TWS
      WRITE(6,97)V(NOI),V(NOE),V0,NPRO,NBOX
      WRITE(6,101)SUM,DELYR
      DO 30 J=1,3
      GO TO (31,32,33),J
   31 IF(NOI.EQ.1)GO TO 30
      NUM1=1
      NUM2=NOI-1
      GO TO 34
   33 IF(NOE.EQ.NOP)GO TO 30
      NUM1=NOE+1
      NUM2=NOP
      GO TO 34
   32 NUM1=NOI
      NUM2=NOE
   34 WRITE(6,102)(Y(I),I=NUM1,NUM2)
      WRITE(6,108)(HC(I),I=NUM1,NUM2)
```

```
      WRITE(6,103)(YD(I),I=NUM1,NUM2)
      WRITE(6,110)(YSTR(I),I=NUM1,NUM2)
      WRITE(6,111)(YSTOT(I),I=NUM1,NUM2)
      IF(J.NE.2)GO TO 35
      WRITE(6,106)(VDR(I),I=NUM1,NUM2)
   35 WRITE(6,105)(URAT(I),I=NUM1,NUM2)
      WRITE(6,107)(TINT(I),I=NUM1,NUM2)
      WRITE(6,109)(ABTNT(I),I=NUM1,NUM2)
      WRITE(6,200)
   30 CONTINUE
      WRITE(6,200)
      GO TO (5,7,8,9,13),INDEX
   13 STOP
   50 FORMAT(I3,3F7.4)
   51 FORMAT(I4,I5,2F3.2,F5.2)
   52 FORMAT(2F5.2,I5,3F5.2,I2,I3,I5)
   53 FORMAT(4F5.2,F10.2,3F5.2,F10.2,3F5.2)
   54 FORMAT(2I2,2I3,3F5.2)
   90 FORMAT(1X,38HCALIBRATION CONSTANTS FOR PROBE S.J.P.,I2,/5X,
     1    21HNO-FLOW VOLTAGE SHIFT,F5.2,3X,2HK=,F5.2,3X,2HN=,F5.3///)
   94 FORMAT(1H0,8HTRAVERSE,I2,5HCHECK,3X,2HX=,F4.1,2HCM,3X,4HVEL ,
     1    6HRATIO=,F5.3/)
   95 FORMAT(3X,46HRLTI DENOTES 10X 'RELATIVE TURBULENCE INTENSITY)
   96 FORMAT(3X,46HABTI DENOTES 10X ABSOLUTE TURBULENCE INTENSITY//)
   97 FORMAT(1X,5HV(I)=,F4.2,1HV,3X,5HV(E)=,F4.2,1HV,5X,13HNO-FLOW P.D.-
     1    ,F4.2,14HV(PROBE S.J.P.,I2,2H, ,12HDISA SET NO.,I3,1H),/)
   98 FORMAT(1X,5HU(I)=,F4.1,5HM/SEC,3X,5HU(E)=,F4.1,5HM/SEC,5X,
     1    8HRLTI(I)=,F4.2,3X,8HRLTI(E)=,F4.2,3X,4HTWS=,F4.0,5HDEG C/)
   99 FORMAT(1H1,10HRUN NUMBER,I4,4X,5HDATE-,I2,2F3.2,8X,10HBAROMETER ,
     1    8HREADING-,F5.1,11HMM. MERCURY/)
  100 FORMAT(1H0,8HTRAVERSE,I2,3X,2HX=,F4.1,2HCM,3X,10HVEL RATIO=,F5.3,
     1    3X,2HZ=,F4.1,2HCM/)
  101 FORMAT(1X,6HTHETA=,F5.3,2HCM,10X,14H(YE-YI)/THETA=,F5.2/)
  102 FORMAT(1X,4H    Y,1X,19F6.2)
  103 FORMAT(1X,4H   YD,1X,19F6.2)
  105 FORMAT(1X,4HURAT,1X,19F6.3/)
  106 FORMAT(1X,4H VDR,1X,19F6.3)
  107 FORMAT(1X,4HRLTI,1X,19F6.3)
  108 FORMAT(1X,4H    H,1X,19F6.2)
  109 FORMAT(1X,4HABTI,1X,19F6.3)
  110 FORMAT(1X,4HYSTR,1X,19F6.2)
  111 FORMAT(1X,4HYSOT,1X,19F6.2)
  200 FORMAT(1X,1H )
  999 FORMAT(1H0,5X,4I5,1P2E15.2)
      END
```

APPENDIX D

Copy of Reference 2

IMPERIAL COLLEGE OF SCIENCE AND TECHNOLOGY

DEPARTMENT OF MECHANICAL ENGINEERING

Exhibition Road, London, S.W.7

Equations of turbulent motion of an incompressible fluid

by

A. N. Kolmogorov

(Translation from the original Russian by D. B. Spalding)

November 1968

ON/6

"Equations of turbulent motion of an incompressible fluid"

by

A. N. Kolmogorov

(Short resumé of report delivered at Kazan during the period 26-28 January, 1942). Published in Izvestia Akademia Nauk SSSR, Seria fizicheska VI 1942, no. 1-2, pp. 56-58.

Translation from the original Russian by D. B. Spalding.

The general features of turbulent motion may be thought of in the following fashion, which accords with the ideas of Taylor and Richardson. Superimposed on the mean motion are turbulent pulsations of various length scales; these range from the order of the "external scale" of turbulence L (the "mixing length") down to a much smaller scale ("inner scale"), of the order of the distance λ at which the fluid viscosity is effective. In regions having dimensions which are small compared with L, the field of velocity is smooth. Pulsations having the largest length scales withdraw energy from the mean motion and transfer it to pulsations of smaller scale. There thus arises a "stream of energy", flowing constantly from pulsations of larger scale to those of smaller scale. Dissipation of energy, i.e. its reduction to molecular motion, proceeds in essence only through pulsations of the scale λ. A fundamental characteristic of the turbulent motion at all scales is the quantity w which stands for the rate of dissipation of energy in unit volume and time.

The properties of the motion which are most characteristic of turbulence pertain to regions which have dimensions which

are small in comparison with L. The local structure of turbulence (i.e. its structure at scales which are much smaller than L) may be taken as spatially homogeneous and isotropic. It may be studied in a way which is analogous to that in which Taylor and von Karman studied isotropic turbulence. But it is necessary to consider at the same time the moments of various orders, defined as mean values from the components of the vector difference of velocities between two different points of the volume. By reason of isotropy, these moments are functions only of the distance r between the points (for $r << L$). Thus, the moments of the second order B_{nn} and B_{tt} are mean values of the squares of the differences of velocity at two points, resolved respectively along the line joining these points and / along the directions perpendicular to it. For $r << \lambda$, these moments are proportional to r^2, but for $r >> \lambda$ (but also $r << L$) B_{nn} and B_{tt} are proportional to $r^{2/3}$ [D.A.N. SSSR XXX, 299, 1941]. The internal scale of turbulence itself is proportional to $\nu^{3/4}(\rho\,\omega)^{1/4}$, where ν is the viscosity of the fluid, and ρ is its density. These results are in good agreement with the measurements of the velocity correlations of Dryden and others.

We may submit to a rather less complete mathematical investigation the turbulent motion which is homogeneous and isotropic (in all scales), and from which a mean flow is absent; such a flow decays continuously with time. By extending the works of Taylor and von Karman, with the aid of L.G.Loitsiansky's non-linear law of conservation (Reports of TsAGI no. 440, 1939), we may show (Doh. Ak. Na. SSSR XXXI,538, 1941) that pulsations of velocity decay in inverse proportion to $t^{6/7}$. The scale of the motion L grows in proportion to $t^{2/7}$.

Starting from the above local properties of turbulence, (and with the help of some more coarsely-approximate assumptions),

we may construct the following complete system of equations to describe turbulent motion:

$$\frac{D\overline{v}_i}{Dt} = F_i - \frac{\partial}{\partial x_i}\left(\frac{\overline{p}}{\rho} + b\right) + A \sum_j \frac{\partial}{\partial x_j}\left[\frac{b}{\omega}\left(\frac{\partial \overline{v}_i}{\partial x_j} + \frac{\partial \overline{v}_j}{\partial x_i}\right)\right] , \qquad (1)$$

$$\frac{D\omega}{Dt} = -\frac{7}{11}\omega^2 + A' \sum_j \frac{\partial}{\partial x_j}\left[\frac{b}{\omega}\frac{\partial \omega}{\partial x_j}\right] , \qquad (2)$$

$$\frac{Db}{Dt} = -b\omega + \frac{A}{3}\frac{b}{\omega}\varepsilon + A'' \sum \frac{\partial}{\partial x_j}\left[\frac{b}{\omega}\frac{\partial b}{\partial x_j}\right] . \qquad (3)$$

Here D/Dt stands for the substantial derivative; F_i is the external force; $\overline{v}_i$ is the time-averaged velocity; $\overline{p}$ is the time-averaged pressure; $b \equiv \frac{1}{3}\sum_j \overline{v_j'^2}$, i.e. one third of the root-mean-square fluctuation velocity; ω is some mean "frequency", determined by $\omega = cb^{\frac{1}{2}}/L$, where c is a constant; and the symbol ε stands for $\sum_{i,j}\left(\frac{\partial \overline{v}_i}{\partial x_j} + \frac{\partial \overline{v}_j}{\partial x_i}\right)^2$. Finally, A, A' and A" are numerical constants which must be determined once and for all from the comparison of some solution of the equations with experimental data. The expression b/ω in equations (1) (2) and (3) plays the role of a "coefficient of diffusion", respectively for the mean motion, the "frequency" ω and the pulsation velocity b. The first term on the right of (3) represents two-thirds of the rate of dissipation of turbulent energy per unit mass of fluid ($\frac{2}{3}\frac{\omega}{\rho}$); and the second term represents two-thirds of the energy which given by the mean motion to the turbulent fluctuations. The ratio of the coefficients of the first terms in (1) and (2) can be determined from the previously mentioned relation of Loitsiansky. Equations (1) to (3) determine the vector of the mean velocity $\overline{v}_i$, the fluctuating velocity b and the scale of the motion L.

The solution of these equations presents great difficulties. In a limited form they may be integrated for the motion of a fluid between two moving parallel planes; the result is in

agreement with the well-known results of von Karman.

The report closes with the presentation of preliminary results of numerical integrations of equations (1) to (3) for turbulent motion in a pipe of circular cross-section.

Discussion. A. Landau remarked that A. N. Kolmogorov was the first to provide correct understanding of the local structure of a turbulent flow. As to the equations of turbulent motion, it should be constantly borne in mind, in Landau's opinion, that in a turbulent field the presence of rotation in the velocity was confined to a limited region; qualitatively correct equations should lead to just such a distribution of eddies.

P. L. Kapitsa also took part in the discussion.